THE UNIVERSITY *of* EDINBURGH

Title	In vitro studies of medial vestibular nucleus neurones
Author	Sulaiman, Mohd Roslan.
Qualification	PhD
Year	1999

Digitisation Notes:

Pages 90 – 99 are missing in the original thesis.

IN VITRO STUDIES OF MEDIAL VESTIBULAR NUCLEUS NEURONES

by

MOHD ROSLAN SULAIMAN
DVM

Thesis submitted
for the degree of Doctor of Philosophy

February, 1999

بسم الله الرحمن الرحيم

FOR

AZAHRIAH

AND

SHATIREE

DECLARATION

The studies outlined in this thesis were carried out in the Department of Physiology, University Medical School, Edinburgh, under the supervision of Dr. M. B. Dutia. All of the work was performed by myself except where otherwise stated.

ACKNOWLEDGEMENTS

There are many people who have provided a great deal of help during my time in Edinburgh. Of great importance has been the love, encouragement and prayers provided by my parents, wife, brothers and sisters. Their faith and confidence in me has been a constant source of inspiration.

I am indebted to my supervisor, Dr Mayank Dutia for his generous guidance, help and constant encouragement during my three and half years in his laboratory and who it has been a great pleasure to work with. Many thanks also to Dr Alex Johnston for his advice and efforts in reading my thesis over the last six months.

A special thanks must go to Aydin, Ustaz Ammar, Ped and to all friends both within and outside the Physiology Department for their unfailing supply of comfort and laughter.

Finally, I would also like to express thanks to my sponsor, Universiti Putra Malaysia.

PUBLICATIONS

(1). Sulaiman, MR., Dutia, MB. (1997) Effect of opioid peptides on rat medial vestibular nucleus neurones *in vitro*. J Physiol (Lond) 504P:166

(2). Sulaiman, MR., Dutia, MB. (1998) Opioid inhibition of rat medial vestibular nucleus neurones *in vitro* and its dependence on age. Exp Brain Res 122:196-202

(3). Sulaiman, MR., Niklasson, M., Tham, R., Dutia, MB. (1999) Modulation of vestibular function by nociceptin/orphanin FQ: an *in vivo* and *in vitro* study. Brain Res (in press)

(4). Sulaiman, MR., Cameron, SA., Dutia, MB. (1999) Compensatory changes in membrane properties of vestibular neurones after unilateral labyrinthectomy. J Neurophysiol. (submitted)

CONTENTS

page

ABBREVIATIONS

MVN	medial vestibular nucleus.
LVN	lateral vestibular nucleus.
SVN	superior vestibular nucleus.
IVN	inferior vestibular nucleus.
CNS	central nervous system.
δ	delta.
μ	mu.
κ	kappa.
CHO	chinese hamster ovary
DADLE	[D-Ala^2, D-Leu^5]-enkephalin.
aCSF	artificial cerebrospinal fluid.
TEA	tetraethylammonium bromide.
TTX	tetrodotoxin.
μM	micromolar.
mM	milimolar.
nM	nanomolar.
N/OFQ	nociceptin/orphanin FQ.
ORL1	opioid receptor like-1.
VOR	vestibulo-ocular reflex.
VCR	vestibulo-collic reflex
FTN	floccular target neurone.
e.p.s.p	excitatory postsynaptic potential.
i.p.s.p	inhibitory postsynaptic potential.
AHP	afterhyperpolarisation.
mV	milivolts.
GΩ	gigaohm.
pA	picoamps.
μV	microvolts.
ms	milliseconds.
V/sec	volts per second.
h	hour.
S.E.M	standard error of the mean.
I-V	current-voltage relationship.

W_T	width of spike at threshold.
W_H	width of spike half-way between threshold and peak.
A_{AHP}	amplitude of the AHP.
A_{SP}	amplitude of the spike.
cDNA	complementary deoxyribonucleic acids.
mRNA	messenger ribonucleic acids.
VC	vestibular compensation.
UL	unilateral labyrinthectomy.
SFA	spike-frequency adaptation.
ISI	interspike interval.

ABSTRACT

This thesis describes electrophysiological studies of rat medial vestibular nucleus (MVN) *in vitro* in which the actions of opioids and the opioid receptor like-1 agonist, nociceptin (orphanin FQ) were characterised. In addition the changes in the intrinsic membrane properties of the MVN neurones during behavioural recovery after unilateral vestibular deafferentation ("vestibular compensation", a model of lesion-induced plasticity in the adult brain), were investigated.

In the first part of this thesis, using agonists and antagonists selective for opioid receptor subtypes, the presence of δ- but not μ- or κ-opioid receptors was demonstrated on spontaneously active MVN neurones *in vitro*. The majority (80%) of spontaneously active MVN neurones were inhibited in dose-dependent manner by the δ-opioid receptor agonist [D-Ala^2,D-Leu^5]-enkephalin (DADLE) but not the μ-opioid receptor agonists, morphine and κ-opioid receptor agonist, U50 488H. The inhibitory actions of DADLE persisted after the blockade of synaptic transmission and were effectively antagonised by naloxone and naltrindole. In whole-cell current-clamp recordings, the DADLE-induced inhibition was accompanied by a membrane hyperpolarisation and a decreased cell input resistance. In voltage clamp experiments, DADLE induced an outward current that was reduced but not abolished by tetraethylammonium bromide (TEA). The degree of DADLE-induced inhibition was dependent on post-natal age, such that the responses to DADLE were smaller in younger animals and increased significantly with age. These findings resolved an earlier conflict in the literature and clarified the actions of opioids on vestibular function.

In the second part, the effect of nociceptin / orphanin FQ (N/OFQ), the recently discovered endogenous ligand for the opioid receptor like-1 (ORL1) receptor was examined on spontaneously active MVN neurones. It was demonstrated that N/OFQ potently inhibited the spontaneous discharge of the majority (86%) of MVN neurones. This inhibition was dose-dependent, persisted in low Ca^{2+}, Co^{2+} aCSF, and was insensitive to antagonism by naloxone but was effectively antagonised by the selective

ORL1 receptor antagonist [Phe$^1\psi$(CH_2-NH)Gly^2]nociceptin(1-13)NH_2. Whole-cell recordings showed that N/OFQ caused membrane hyperpolarisation and decreased in input resistance in the MVN neurones. Both N/OFQ and DADLE inhibited the spontaneous discharge of the majority of MVN neurones, while a minority of neurones were selectively responsive either to N/OFQ or to DADLE, but not both. In addition, co-administration of N/OFQ and DADLE to neurones that were responsive to both agonists, resulted in an inhibitory response that was the same as or smaller than the inhibition induced by either agonist alone, indicating occlusion in the MVN neurones in response to the activation of the δ- and ORL1 receptors by the agonists.

In the final part of this thesis, the changes in intrinsic membrane properties and the action potential firing characteristics of identified "Type A" and "Type B" MVN neurones in the rostral region of the MVN were studied during the early stage of vestibular compensation (4h after unilateral labyrinthectomy, UL). It was shown that the electrophysiological properties of Type A MVN neurones were unchanged following UL. By contrast, marked changes occurred in the membrane excitability and action potential firing characteristics of a specific sub-population of rostral Type B MVN neurones, indicating that changes in the intrinsic membrane properties of this sub-population of MVN neurones may be important cellular mechanism during behavioural recovery after vestibular lesions.

INTRODUCTION

In recent years, with the development of *in vitro* electrophysiological techniques individual neurones in the mammalian central nervous system (CNS) have been demonstrated to possess many different intrinsic membrane properties as well as receptors for numerous transmitter and neuromodulator substances, which endow them with complex integrative functions (Llinas, 1988). The vestibular system has been used for several decades as a good model to investigate the organisation and physiology of sensorimotor networks. The adoption of *in vitro* electrophysiological methods by vestibular neuroscientists has led to insights into the intrinsic properties, neurotransmitter receptors and the mechanisms of vestibular plasticity (Darlington *et al.*, 1995).

The vestibular system is a sensorimotor system that plays a major role in the control of posture and movement by the generation of vestibulo-ocular reflexes (VOR) and vestibulo-collic reflexes (VCRs). The VORs serve to stabilise the visual field on the surface of retina during locomotion through command signals to the eye muscles which result in eye movements that are equal and opposite to head movements (Wilson and Melvill-Jones, 1979; Dutia, 1989; Berthoz *et al.*, 1992; Dieterich and Brandt, 1995), while VCRs give rise to the reflex excitation of the appropriate group of neck muscles to resist and counteract the head displacement, thus stabilising the head on the trunk (Wilson and Melvill-Jones, 1979; Dutia, 1989; Berthoz *et al.*,., 1992; Wilson *et al.*, 1995). These reflexes are initiated in the peripheral vestibular organs where information about head movements and the orientation of the head with regard to gravity is transduced into neural signals in the vestibular VIIIth nerve. These signals are transmitted into the vestibular nuclei in the brainstem and then to the oculomotor and abducens nuclei which control eye movements, as well as to the neck motoneurone pools. Therefore, these reflexes are critical for the stabilisation of gaze during head movement and maintenance of the head posture in relation to the trunk.

The vestibular nuclei, sometimes collectively called the vestibular complex, consist of four main nuclei namely medial (MVN), lateral (LVN), superior (SVN) and inferior (IVN) nuclei. Anatomical studies have demonstrated that most of the primary afferent input from different peripheral vestibular organs terminates in distinct areas

of the four vestibular nuclei and each of these nuclei is connected with other areas of the CNS. Afferent input from the semicircular canals projects mainly to the MVN, SVN and IVN, while the afferent inputs from the utriculus and sacculus terminate mainly in the LVN and IVN. The SVN and the MVN are part of the VOR circuitry and play an important role in co-ordination of the head, neck and eye movements. They project to cervical motoneurone pools, abducens nuclei, inferior olivary complex, reticular formation as well as cerebellum. The IVN is a relay nucleus of the spino-vestibular pathway and projects primarily to the cerebellum. The LVN plays a major part for the vestibulo-spinal reflexes and projects extensively to all segments of the spinal cord. In addition, these nuclei are interconnected bilaterally and ipsilaterally (Wilson and Melvill-Jones, 1979; Carpenter, 1988; Buttner-Ennerver, 1992, Shinoda *et al.*, 1993).

Among the four principal vestibular nuclei, the MVN is the largest and the most easily distinguished in freshly dissected brainstem by its colour and shape on the dorsal floor of the brainstem. The MVN therefore has recently proven to be an attractive target for the *in vitro* electrophysiological studies of vestibular neurones. Here, in this thesis, I describe electrophysiological studies of rat MVN neurones *in vitro* using extracellular and intracellular whole cell patch recording techniques, in which the action of opioids and N/OFQ were studied, and the electrophysiological properties of MVN neurones during the early stage of vestibular compensation were investigated.

CHAPTER 1

POSTSYNAPTIC INHIBITORY ACTION OF OPIOIDS ON RAT MEDIAL VESTIBULAR NUCLEUS NEURONES *IN VITRO* AND ITS DEPENDENCE ON AGE

1.1 LITERATURE REVIEW

1.1.1 THE MEDIAL VESTIBULAR NUCLEUS AND ITS CONNECTIONS

Afferent innervation of the MVN

Labyrinthine innervations

Early *in vivo* electrophysiological studies in the cat demonstrated that the MVN neurones were mono-synaptically and poly-synaptically activated by electrically stimulating the vestibular afferent fibres originating from the ipsilateral vestibular labyrinth (Precht and Shimazu, 1965; Shinoda and Yoshida, 1974). Subsequently, Wilson *et al.,* (1967) showed that neurones which were mono-synaptically activated by vestibular nerve stimulation were concentrated mainly in the rostral third of the MVN. Anatomical studies have demonstrated that innervation of primary afferents from the ipsilateral semicircular canals, primarily the horizontal canal, appeared particularly dense at the rostral area of the MVN (Stein and Carpenter, 1967; Gacek, 1969; Korte and Friedrich, 1979; Carleton and Carpenter, 1984; Sato *et al.*, 1989), consistent with the findings that neurones in the rostral region of the MVN respond to angular acceleration of the head in both the horizontal and vertical planes (Shimazu and Precht, 1965; Markham, 1968; Jones and Milsum, 1970; Curthoys and Markham, 1971).

Studies in the MVN of normal monkeys, cats, guinea pigs, gerbils and rats have identified two types of horizontal semicircular canal related neurones, Type I and Type II neurones, with Type I neurones outnumbering Type II neurones (Precht and Shimazu, 1965; Shimazu and Precht, 1965, 1966; Precht *et al.*, 1966; Shimazu, 1983; Hamann and Lannou, 1988; Smith and Curthoys, 1988a, 1988b; Newlands and Perachio, 1990a, 1990b). Both types of MVN neurones discharge spontaneously even with the head absolutely stationary, at frequency sometimes greater than 80 impulses/sec, and show a bi-directional response. Type I MVN neurones increase their discharge frequency with acceleration of the head around an earth-vertical axis in the ipsilateral direction (i.e., toward the side of the neurone being recorded). Their discharge frequency decreases when the head is accelerated in the opposite direction (contralateral direction). Other neurones, Type II MVN neurones, respond in exactly the opposite pattern to Type I MVN neurones (i.e., decreased their discharge frequency with ipsilateral acceleration and show an

increase with contralateral acceleration) because Type I neurones are excited directly by ipsilateral horizontal canal primary afferents, whereas Type II neurones are excited by contralateral horizontal canal afferents via commissural pathways between the VN. Type II neurones are inhibitory neurones and act to silence Type I neurones (Fig. 1.1.1.1). MVN neurones also receive projections from otolith organs (Stein and Carpenter, 1967; Gacek, 1969), with neurones responded to stimulation of the utricular nerve and to forward and backward tilting. Otolith-responsive neurones are distributed throughout the MVN (Peterson, 1970). The afferent inputs from semicircular canals to the MVN are functionally excitatory and mediated by excitatory amino acid neurotransmitters, glutamate and/or aspartate acting on mainly non-NMDA receptors (Raymond *et al.*, 1984; de Waele *et al.*, 1990; Doi *et al.*, 1990; Capocchi *et al.*, 1992; Carpenter and Hori, 1992; Yamanaka *et al.*, 1997).

Intrinsic and commissural connections

The Golgi studies of Ramón y Cajal (1909) and Lorente de Nó R (1933) suggested the presence of ipsilateral intrinsic vestibular connections, which were later experimentally demonstrated by use of the axonal degeneration technique (Ladpli and Brodal, 1968). Recent studies using anterograde and retrograde labelling techniques have demonstrated extensive internuclear connectivity within the VN, with the SVN topographically and reciprocally connected to the IVN and MVN, and LVN reciprocally connected to MVN. Apart from the connections between the individual subnuclei, it has also been demonstrated the rostral and caudal MVN are reciprocally connected (Pompeiano *et al.*, 1978; Epema *et al.*, 1988).

Using HRP retrograde labelling techniques a commissural connection between the MVN and contralateral MVN, SVN and IVN has been demonstrated, mostly dense between the MVNs of the two sides (Rubertone *et al.*, 1983; Ito *et al.*, 1985; Epema *et al.*, 1988). Shimazu and Precht (1966) showed that when the contralateral vestibular nerve is electrically stimulated, field potentials could be recorded in the ipsilateral VN. This response could be abolished following a midline incision that interrupted the commissural fibres, thus confirming that the labyrinth influences the activity of the contralateral VN through the commissural fibres. In mammals, stimulation of the contralateral vestibular nerve is predominantly inhibitory on the ipsilateral side (Shimazu and Precht, 1966; Precht *et al.*, 1973;

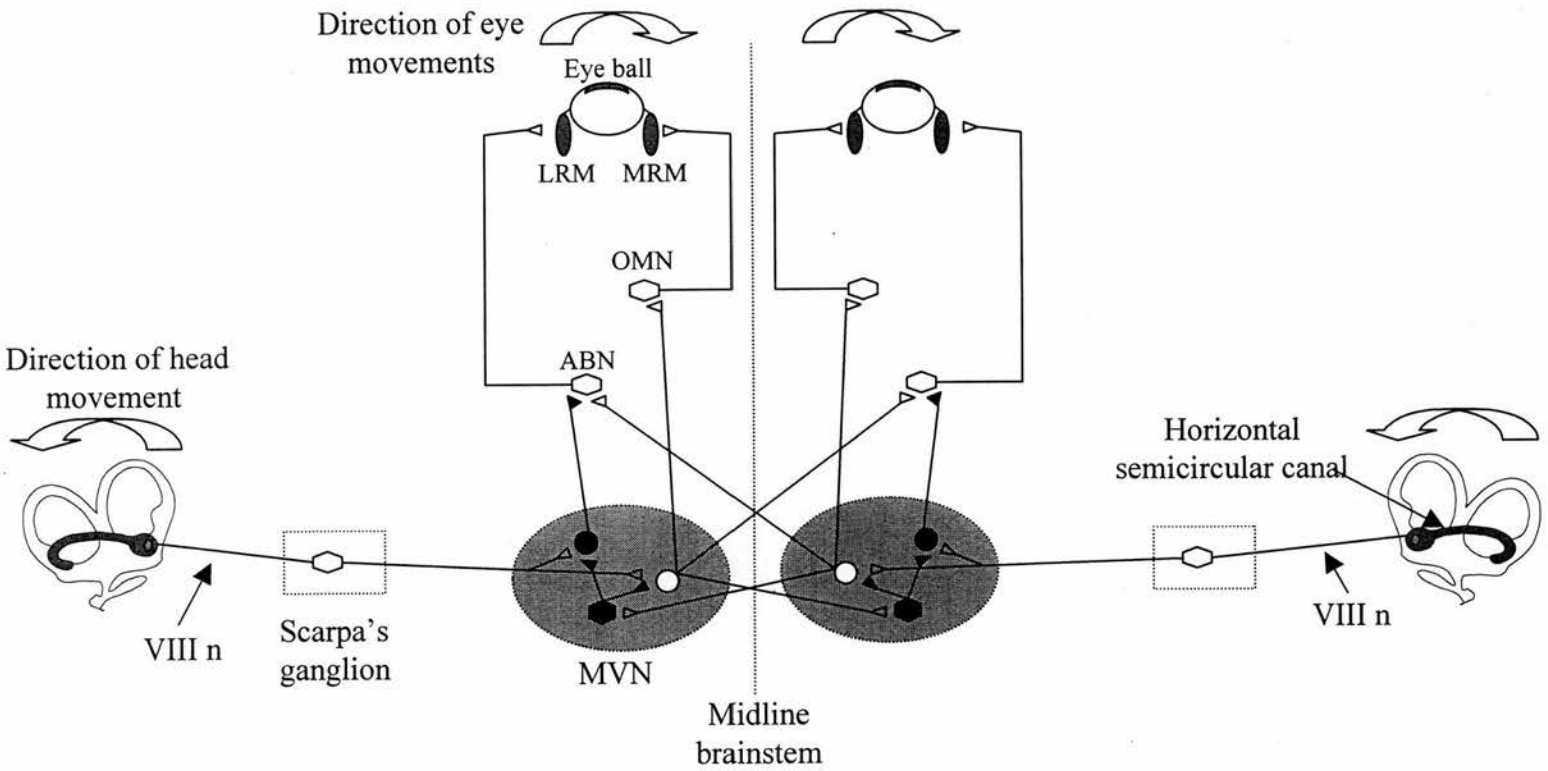

Figure 1.1.1.1 ; Simplified schematic diagram of some neuronal networks of the medial vestibular nucleus (MVN).

The type I MVN neurones (◯) increase their discharge frequency for horizontal angular acceleration to the ipsilateral side, and type II MVN neurones (⬡) increase their discharge frequency for horizontal angular acceleration to the contralateral side. LRM, lateral rectus muscle; MRM, medial rectus muscle; OMN, oculomotor nucleus; ABN, abducens nucleus; VIIIn, vestibulo-cochlear nerve. [□ excitatory; ■ inhibitory]

(Adapted from Smith and Darlington, 1996)

Kasahara and Uchino, 1974), whereas in amphibians it is mainly excitatory (Cochran *et al.*, 1987; Knopfel, 1987; Dieringer, 1995).

Cerebellar, brainstem and other afferent innervations

The MVN receives extensive afferent projections from the cerebellum. The area of the cerebellum that projects to MVN is known as the vestibulo-cerebellum, and consists of the flocculus, nodulus, uvula, paraflocculus and fastigial nuclei. Immunohistochemical tracing studies showed that floccular fibres terminate mainly in the rostral area of the ipsilateral MVN (Langer *et al.*, 1985; Umetani, 1992), while the nodulus fibers terminate in the caudal area of the ipsilateral MVN (Brodal, 1974, (Langer *et al.*, 1985). The fastigial nuclei project to the MVN on both sides, the rostral part projecting to the ipsilateral MVN and caudal to the contralateral MVN (Ito *et al.*, 1985). The Purkinje neurones of the flocculus and nodulus have an inhibitory action on MVN neurones (Baker *et al.*, 1972; Fukuda *et al.*, 1972). The rostral MVN neurones that receive inhibitory fibres from the flocculus have been termed floccular target neurones (FTN), and are involved in the three-neurone arc of the VOR (Sato *et al.*, 1988; Lisberger *et al.*, 1994; Stahl and Simpson, 1995). In contrast, the fastigial nucleus has a facilitatory influence on MVN neurones (Ito *et al.*, 1970; Shimazu and Smith, 1971). Through these connections the floccular cortex, which receives convergent vestibular, visual and oculomotor information, is involved in controlling vestibular related motor activities. It has also been suggested to play an important role in long term plasticity of the VOR gain as well as lesion-induced plasticity in vestibular neurones (Lisberger *et al.*, 1994; Kitahara *et al.*, 1997).

A number of brainstem nuclei are known to send their projections to the MVN. Anatomical studies using horseradish peroxidase (HRP) labelling techniques demonstrated that the MVN received afferent projections from the interstitial nucleus of Cajal (Pompeiano and Walberg, 1957; Carpenter *et al.,* 1970) and from the nucleus prepositus hypoglossi (Pompeiano *et al.,* 1978). Pontine and medullary reticular formation also sends descending fibres to the MVN (Grottel and Jakielska-Bukowska, 1993). Immunohistochemical studies have demonstrated that MVN neurones also receive innervation from the caudal part of the dorsal nucleus of the raphe (Kawasaki and Sato, 1981), from inferior olive (Balaban, 1984) and a nonadrenergic input from locus coeruleus (Schuerger and Balaban, 1993).

Efferent projections from the MVN

Vestibulo-ocular projections

Physiological and anatomical studies have indicated that the vestibular nuclei particularly MVN and SVN provide the largest efferent projections to the oculomotor nuclei, which ascend in the medial longitudinal fasciculus (MLF). (Fig.1.1.1.2; Tarlov, 1970a, 1970b; Gacek, 1974, 1977; Furuya and Markham, 1981; Babalian *et al.*, 1997). The six extraocular muscles of each eye are innervated by motoneurones in the oculomotor, trochlear and abducens nuclei via IIIrd, IVth and VIth cranial nerves (Fig.1.1.1.2.1; Tarlov and Tarlov, 1971; Gacek, 1974; Graf and Ezure, 1986).

The motoneurones of the abducens and the trochlear nucleus innervate the ipsilateral rectus muscle and the contralateral superior oblique respectively. The remaining four muscles, the superior, inferior, inferior oblique and medial rectus are innervated by the oculomotor nucleus. The MVN projects to the abducens and oculomotor nuclei bilaterally, but only ipsilaterally to the trochlear nucleus (Fig.1.2.1.2; Wilson and Melvill Jones, 1989). It has been shown that electrical stimulation of the vestibular nerve evokes a disynaptic excitatory post-synaptic potentials (e.p.s.p) in the contralateral abducens motoneurones, and a disynaptic inhibitory postsynaptic potentials (i.p.s.p) is evoked in ipsilateral abducens motoneurones. Stimulation of the rostral region of the MVN evokes similar but monosynaptic potentials in the abducens nucleus. Thus, the anatomical and electrophysiological results indicate that the vestibulo-ocular pathway originating in the semicircular canal relays in the rostral region of the MVN, which then projects to the oculomotor nuclei (Buttner-Ennever, 1992; Buttner-Ennever and Buttner, 1992).

Spino-vestibular projections

The lateral (LVST) and medial vestibulospinal tracts (MVST) provide the major descending outflows from the vestibular nuclei to the spinal cord. The LVST originates in the LVN and IVN and projects to all segments of the spinal cord, terminating mainly in the extensor muscle motoneurone pools (Brodal *et al.*, 1962; Brodal, 1974). The MVN is the main source of the MVST and projects primarily to the ventral horn of the cervical spinal cord from C1 to C6 (Nyberg-Hensen, 1964;

Wilson *et al.*, 1967). Peterson *et al.,* (1978) reported that the caudal vestibulospinal tract originates in the LVN and parts of the MVN and IVN.

Vestibulo-cerebellar projections

Anatomical studies using HRP labelling techniques demonstrated that primary vestibular nerve afferents terminate as mossy fibres in the flocculus, nodulus and uvula, particularly in the ipsilateral half of the cerebellum (Carleton and Carpenter, 1984) and in the fastigial nucleus (Kotchabhakdi and Walberg, 1978). Secondary vestibular axons originating mainly from the caudal part of the MVN, project to the floculli in both sides, uvula and nodulus (Rubertone *et al.*, 1983; Barmack *et al.*, 1992; Kitahara *et al.*, 1997). In agreement with the anatomical studies, monosynaptic evoked field potentials are recorded in the nodulus and flocculus following electrical stimulation of the vestibular nerve and vestibular nuclear afferents (Shinoda and Yoshida, 1975). These authors also demonstrated that afferents from the rostral area of the MVN reach the vestibulocerebellum.

Other efferent projections originating from the MVN include projections to the contralateral MVN and to other vestibular nuclei (Rubertone *et al.,* 1983; Ito *et al.,* 1985; Epema *et al.,* 1988), to the contralateral inferior olive (Balaban and Beryozkin, 1994), to the pontine and medullary recticular formation (Ladpli and Brodal, 1968; Tarlov, 1969) and to the thalamus (Doi *et al.,* 1997)

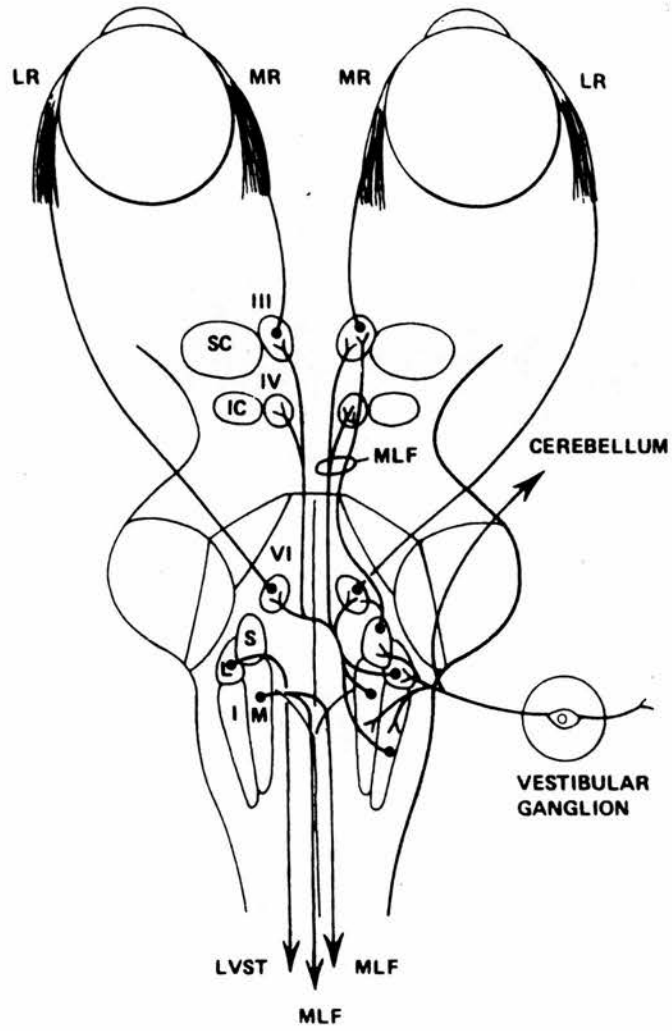

Figure 1.1.1.2 : Schematic illustration of the main projections arising from the vestibular nuclei

The origins of the descending projections are illustrated on the left side of the diagram and the origins of the ascending projections on the right side. Only the connections to the medial (MR) and lateral (LR) rectus muscles which control horizontal gaze are shown. III, oculomotor nucleus; SC, superior colliculus; IV, trochlear nucleus; IC, inferior colliculus; MFL, medial longitudinal fasciculus; VI, abducens nucleus; S, superior vestibular nucleus; L. lateral vestibular nucleus; I, inferior vestibular nucleus; M, medial vestibular nucleus; LVST., lateral vestibulo-spinal tract.

(Adapted from Gilman and Newman, 1992)

1.1.2 *IN VITRO* ELECTROPHYSIOLOGICAL STUDIES OF MEDIAL VESTIBULAR NUCLEUS NEURONES

The 'brainstem slice' preparation, first used by Joel Gallagher and his colleagues (1985), has become a widely used *in vitro* electrophysiological preparation to study the brainstem vestibular nucleus complex (VNC) particularly the medial vestibular nucleus (MVN). Considering the large number of slice studies that have been conducted, the similarities in the *in vitro* MVN neurone resting activity are remarkable. In all cases, with no input from the peripheral vestibular apparatus or other areas of the CNS that are active in the intact animal, the MVN neurones recorded in the brainstem slices of rats and guinea pigs display regular spontaneous discharge rates (Gallagher *et al.*, 1985; Ujihara *et al.*, 1988; Darlington and Smith, 1989; Ujihara *et al.*, 1989; Darlington *et al.*, 1990; Phelan *et al.*, 1990; Serafin *et al.*, 1990, 1991a, 1991b, 1992, 1993; Smith *et al.*, 1990; Darlington *et al.*, 1992; Dutia *et al.*, 1992; Gallagher *et al.*, 1992; Phelan and Gallagher, 1992; Johnston *et al.*, 1993, 1994; Dutia *et al.*, 1995; Johnston and Dutia, 1996; Cameron and Dutia, 1997; Ris and Godaux, 1998). In rat brainstem slices, the spontaneous discharge rates of MVN neurones range from 0.5 - 60 spikes/sec, on average between 10 and 20 spikes/sec, similar to those observed *in vivo* (Hamann and Lannou, 1988).

It has been established by a number of *in vitro* studies that this regular spontaneous neuronal discharges persist even when synaptic transmission is blocked by perfusion with low Ca^{2+} / high Mg^{2+} or low Ca^{2+} / Co^{2+} aCSF (Gallagher *et al.*, 1985, 1992; Gacek *et al.*, 1988; Ujihara *et al.*, 1988; Doi *et al.*, 1990; Carpenter and Hori, 1992; Dutia *et al.*, 1992; Lin and Carpenter, 1993, 1994), and that these MVN neurones have intrinsic, pacemaker-like ionic conductances which are highly sensitive to membrane potential, and generate their spontaneous discharges independently from synaptic inputs (Serafin *et al.*, 1990, 1991a, 1991b; Johnston *et al.*, 1994). This characteristic known as "autorhythmicity" has also been observed in many other CNS neurones such as inferior olive and thalamus (Llinas, 1988). However, the exact ionic conductances that contribute to the autorhythmicity of MVN neurones *in vitro* is still unclear. Some components of the spontaneous discharge activity observed in these neurones *in vitro* may be due to synaptic input

within the slice, since spontaneous e.p.s.ps have been observed in some preparations (Lewis *et al.*, 1989; Kinney *et al.*, 1994).

The membrane properties of MVN neurones were first examined by Gallagher *et al.,* (1985) in a transverse slice preparation of a rat brainstem, and at least two subtypes of neurone were identified within the MVN, characterised on the basis of the after-hyperpolarisation potential (AHPs) profiles following their spontaneous action potentials. One group showed a single AHP, which was possibly due to a Q-type current, while the other group showed a double AHP and a voltage-dependent rectification, which may be due to a K^+ rectifier (Gallagher *et al.*, 1985, 1992).

Serafin and colleagues (1991a,b) subsequently identified and divided guinea pig MVN neurones into three types based on their action potential shapes and intrinsic membrane properties *in vitro* (Serafin *et al.*, 1990, 1991a, 1991b). Type A neurones (about 30% of the neurones sampled) were characterised by a broad action potential, a single deep AHP, an A-type rectification and small, high threshold Ca^{2+} spikes, while type B neurones (about 50% of the neurones sampled) were characterised by a narrower action potentials, an early fast AHP and delayed slow AHP, large, high-threshold Ca^{2+} spikes and Ca^{2+} plateau potentials. The majority of type B neurones had Na^+ plateau potentials and some had low-threshold Ca^{2+} spikes. Type C neurones (about 20% of the neurones sampled) were heterogeneous group with intermediate action potential shapes and therefore could not be readily included into the other two types.

Johnston and colleagues (1994) confirmed the classification of rat MVN neurones using intracellular recordings from horizontal brainstem slice preparations. The neurones were classified as either type A or type B neurones based on their averaged action potential shape profiles. Type A neurones (33% of the 123 neurones sampled) had a single deep AHP that appeared to be mediated by a tetraethylammonium (TEA)-sensitive K^+ conductance (presumably I_K) and an apamin-insensitive Ca^{2+}-activated K^+ conductance (presumably I_c). Type B neurones (67% of the neurones sampled) had an early fast AHP and delayed slow AHP. The early fast AHP was mediated by a TEA-sensitive K^+ conductance while the delayed

slow AHP was mediated by apamin-sensitive K^+ conductance (I_{AHP}). The spontaneous discharge activity of type B neurones appeared to be regulated mainly by interactions between a persistent Na^+ conductance and the hyperpolarisation mediated by I_{AHP}. About 30% of type B neurones also had an additional inward Ca^{2+} conductance. The two types of MVN neurones were distributed throughout the rostrocaudal extent of the MVN and no Type C neurones were found (Johnston *et al.*, 1994).

1.1.3 PHARMACOLOGY OF THE CENTRAL VESTIBULAR SYSTEM

The pharmacological properties of vestibular neurones have begun to emerge only in the past decade. Different approaches including behavioural, biochemical and electrophysiological methods have been employed to study the pharmacology of the vestibular system. Numerous neurotransmitters, neuropeptides and receptors have been identified in this system.

Glutamate

Immunohistochemical and receptor binding studies have shown that all main types of glutaminergic receptors, namely ionotropic glutamate receptors (NMDA, kainate, AMPA) and metabotropic glutamate receptors (mGluRs) and their subtypes were densely present in the vestibular nuclei (for reviews see Raymond *et al.*, 1988; de Waele *et al.*, 1995). These studies are in accordance with *in vitro* electrophysiological studies, which consistently demonstrated that MVN neurones were highly sensitive to the glutaminergic receptor agonists and antagonists. It has been shown that majority of MVN neurones in the rat (Gallagher *et al.*, 1985; Lewis *et al.*, 1989), guinea pig (Smith *et al.*, 1990; Carpenter and Hori, 1992; Serafin *et al.*, 1992; Smith and Darlington, 1992) and frog (Cochran *et al.*, 1987) were depolarised by NMDA receptor agonists and that this response can be blocked by NMDA receptor antagonists.

Using intracellular recordings, Vibert *et al.,* (1992) demonstrated that bath application of the ionotropic glutamate receptor agonists, NMDA, kainate, AMPA and the metabotropic glutamate receptor agonist, trans-ACPD caused excitation and membrane depolarisation in all MVN neurones tested. These effects persisted when synaptic transmission was blocked in a high Mg^{2+}, low Ca^{2+} solution, suggesting that these effects were mediated via postsynaptic receptors. The existence of postsynaptic metabothropic glutamate receptors on MVN neurones was then confirmed by Darlington and Smith (1995). Recently, using whole-cell patch-clamp recording from rat MVN neurones, *in vitro*, Kinney *et al.,* (1993) have reported that a metabotropic-receptor antagonist blocked e.p.s.ps evoked by stimulation of vestibular VIIIth nerve or the medial longitudinal fasciculus.

Gaba and Glycine

Immmunohistochemical and In situ hybridisation studies have shown the existence of receptors for the inhibitory amino acids γ-amino-butyric acid (GABA) and glycine on MVN neurones (Holstein *et al.*, 1992; Li *et al.*, 1994; Zanni *et al.*, 1995). Existence of these receptors was consistent with the results of *in vivo* and *in vitro* electrophysiological experiments. Using *in vivo* electrophysiological recordings, Precht *et al.,* (1973) first demonstrated that the brainstem commissural inhibition between the bilateral MVN could be blocked by either $GABA_A$ or glycine receptor antagonists, indicating that both $GABA_A$ and glycine receptors mediate commissural inhibition of type I MVN neurones. In contrast, Furuya *et al.,* (1992) also using *in vivo* recordings, indicated that commissural inhibition between the bilateral MVN was mediated by $GABA_A$ receptors rather than by $GABA_B$ or glycine receptors.

Extracellular recordings from guinea pig (Smith *et al.*, 1991) and rat (Dutia *et al.*, 1992) brainstem slices, *in vitro* demonstrated that most MVN neurones were inhibited by GABA through both $GABA_A$ and $GABA_B$ receptors. The effect of GABA on MVN neurones was further assessed by intracellular studies. Vibert *et al.,* (1995a,c) using intracellular recording from guinea pig brainstem slices demonstrated that spontaneously active MVN neurones were inhibited and hyperpolarised both by $GABA_A$ and $GABA_B$ agonists in the presence of high Mg^{2+} low Ca^{2+} solution or in presence of TTX indicating the presence of postsynaptic $GABA_A$ and $GABA_B$ receptors on MVN neurones. Similarly, Lapeyre and de Waele (1995) showed that bath application of glycine caused dose-dependent inhibition of spontaneously active MVN neurones. This action was blocked by strychnine and persisted in high Mg^{2+}, low Ca^{2+} medium, indicating postsynaptic strychnine-sensitive glycinergic receptors.

Dopamine

Gallagher *et al.,* (1992) have demonstrated that microdrop application of dopamine results in excitation and membrane depolarisation of rat MVN neurones, *in vitro.* Subsequently, using intracellular recording technique *in vitro*, Vibert *et al.,* (1995) indicated the presence of D_2 receptors on guinea pig MVN neurones. They showed that both dopamine and the selective dopamine D_2 agonists, piribedil and

quinpirole caused depolarisation of MVN neurones, while a selective D_1 receptor agonist SKF 38393 had no effect. However, when synaptic transmission was blocked using low Ca^{2+}, high Mg^{2+} aCSF, the depolarisation effect of the D_2 agonist was reversed to hyperpolarisation, indicating that the activation of postsynaptic D_2 receptors may induce hyperpolarisation but D_2 receptor agonist may induce depolarisation through presynaptic inhibition.

Histamine

The hypothesis that histamine may be involved in regulating vestibular function results in fact from the development of antihistamine agents that have been used in humans for clinical treatment of motion sickness and vertigo. Anatomical studies in the rat (Panula *et al.*, 1989; Steinbusch, 1991), guinea pig (Airaksinen and Panula, 1988), rabbit (Iwase *et al.*, 1993) and cat (Tighilet and Lacour, 1996; Tighilet and Lacour, 1997) confirmed that the whole vestibular complex is innervated by histaminergic fibres from the tuberomammilary nucleus of the posterior hypothalamus and both H_1 and H_2 binding sites were also detected in the MVN (for a review see, de Waele *et al.*, 1995). Early, *in vivo* electrophysiological studies reported that histamine caused a decrease in the firing rate of the majority of vestibular neurones (Kirsten and Sharma, 1976; Satayavivad and Kirsten, 1977). The inhibitory action of histamine was blocked by H_2 receptor antagonist, metiamide but not by H_1 receptor antagonist, diphenhydramine (Satayavivad and Kirsten, 1977).

By contrast, *in vitro* electrophysiological recordings in rat brainstem slices demonstrated that in most cases, application of histamine results in excitation and membrane depolarisation (Phelan *et al.*, 1990; Wang and Dutia, 1995). In another study, using intracellular recording techniques, it has been indicated that 95% of guinea pig MVN neurones were depolarised by histamine and that this response was due to activation of postsynaptic H_2 receptors (Serafin *et al.*, 1993). However, the excitatory actions of histamine on the rat MVN neurones could be mediated by both H_1 and H_2 receptors (Wang and Dutia, 1995). This dissimilarity could be due to species differences in either the anatomical distribution or the pharmacological properties of H_1 receptors.

Acetylcholine

Recent immunocytochemical, *In situ* hybridisation and receptor autoradiographic studies have indicated the localisation of the acetylcholine and acetylcholine-related enzymes (choline acetyltransferase and acetylcholineesterase) in neurones of the VNC and also demonstrated high density of both muscarinic and nicotinic cholinergic receptors in the MVN (Zanni *et al.*, 1995). *In vitro* electrophysiological studies reported that both carbachol and muscarine cause dose-dependent increase in the firing rates (Ujihara *et al.*, 1988; Ujihara *et al.*, 1989; Dutia *et al.*, 1990; Carpenter and Hori, 1992) and membrane depolarisation (Phelan and Gallagher, 1992) of the MVN neurones, that was blocked by atrophine, an antagonist at the muscarinic acetylcholine receptors. The effects of carbachol and muscarine persisted during the blockade of synaptic transmission, indicating that they were produced postsynaptically (Ujihara *et al.*, 1989; Phelan and Gallagher, 1992). These results are consistent with earlier *in vivo* experiments which demonstrated that application of acetylcholine results in an increase in the discharge rates of MVN neurones, an effect that was antagonised by the muscarinic antagonist, atrophine (Kirsten and Sharma, 1976; Ito *et al.*, 1981).

Opioid peptides

Numerous immunohistochemical studies have demonstrated the presence of enkephalinergic neurones and terminals in the vestibular nuclei of the brainstem with the highest density of enkephalinergic neurones found particularly in the MVN (Zanni *et al.,* 1995, Nomura *et al.,* 1984, Finley *et al.,* 1981, Pearson *et al.,* 1980, Beitz *et al.,* 1987). These findings are supported by the results of receptor autoradiographic investigations, which demonstrated moderate levels of δ-opioid receptor mRNAs in the medial vestibular nucleus (Mansour *et al.,* 1994). The effects of opioids on MVN neurones have been the subjects of several electrophysiological studies. However the present evidence relating to the physiological effects of opioids on the firing rates and membrane properties of vestibular neurones is conflicting. Using single unit electrophysiological recording techniques *in vitro*, Kawabata *et al.,* (1990) demonstrated that iontophoretically applied enkephalin inhibited the resting discharge rate and response to natural vestibular stimulation of Type I MVN neurones in the chloralose-anaesthetised cat. They also showed that

Type II MVN neurones were not affected by ionthophorectically applied enkephalin By contrast, studies by Carpenter and Hori (1992) and Lin and Carpenter (1994) reported that the spontaneously active rat MVN neurones in a slice preparation *in vitro* were excited both by morphine and ala-leu-enkephalin, implicating both μ and δ subtypes of opiate receptors in this response, respectively. The excitatory effect of the opioid on these neurones was probably due to direct depolarisation rather than to disinhibition, since blockade of $GABA_A$ receptors with bicuculline did not alter the effect of the agonists. Furthermore, the excitation persisted after blockade of synaptic transmission in low-Ca medium, indicating that the opioid receptors are located postsynaptically (Lin and Carpenter 1994).

Recently, in situ hybridisation and immunohistochemical studies have demonstrated the presence of ORL1 (opioid receptor like-1) mRNA and ORL1 receptors in MVN neurones (Anton *et al.,* 1996, Houtani *et al.,* 1996). However the action of nociceptin on MVN neurones is still unknown.

1.1.4 OPIOID PEPTIDES

A brief history of opioid receptor ligands

The opiates have their basis in more than 5000 years of medicinal use of mekonion from the leaves and fruits of the plant or opium (from "opos," the Greek word for juice) from the liquid, which is obtained from the unripe seed capsule of poppy, *Papaver somniferum* and drying exudate. The analgesic and anti-diarrhoea properties of opium were already recognised by the Sumerians, who inhabited the Euphrates delta, who cultivated poppies and isolated opium. They called opium "gil," the lord of joy, and the poppy "hul gil" plant of joy. It appears that opium spread from Sumeria to the remainder of the Old World including Assyria, Babylonia and Egypt. The therapeutic use of opium was discussed by Hippocrates, Dioscorides and Galen. Thus, "opium," "laudanum," "pulvis Doveri" and "paregoric" have been used for centuries in western medicine. The nature of the mood changes also produced by opium has been the basis for its non-medicinal use and abuse. In particular, opium eating and smoking replaced the consumption of alcoholic drinking in Islamic countries, such as Arabia, Turkey and Iran. As early as the eighth century AD, Arab traders brought opium to India and China and it was also consumed as a favourite substance of pleasure. Between the tenth and thirteenth centuries opium has spread from Asia Minor to all parts of Europe. Starting in the sixteenth century, manuscripts can be found describing drug abuse and tolerance in Turkey, Egypt, Germany and England.

A German chemist, Friedrich Sertüner in 1806, isolated the active component in opium and called it morphine (from "Morpheus," the Greek word for the god of dreams), which was then used in therapy. Unfortunately, morphine has just as much potential for abuse as opium. This prompted a great deal of effort to develop a safer, more efficacious, non-addicting. Subsequently, in 1898, heroin (diacetylmorphine) was synthesised and claimed to be more potent than morphine and free from abuse liability. This was the first of such claims for novel opioids. However, to date, none has proven valid (for a review see Brownstein, 1993). Heroin carries ten times the potency of morphine, giving a short lasting but extremely rapid and intense euphoria. Furthermore, heroin possesses far greater addictive potential and remains the most notorious and abused of the opiate-derived

drug. Intense research over the last two decades to understand the processes underlying opiate tolerance, dependence and addiction led to discovery of the opioid peptides.

Opioid peptides

Evidence for the existence of endogenous ligands for opiate receptors was first suggested by Terenius and Wahlström (1975) and Hughes and Kosterlitz (1975). Subsequently, Hughes and his collaborators successfully isolated and characterised the sequence of two endogenous opioid pentapeptides Tyr-Gly-Gly-Phe-Met and at lower concentration Tyr-Gly-Gly-Phe-Leu from the pig brains, and they called them methionine [Met]-enkephalin and leucine [Leu]-enkephalin, respectively (Hughes *et al.*, 1975). These were the first opioid peptides isolated from the mammalian central nervous system. Both [Met] and [Leu]-enkephalin have been shown to have potent opiate agonist activity when tested on mouse vas deferens and guinea pig ileum. Soon after this discovery, it became apparent that the sequence of [Met]-enkephalin was found on the amino terminal (N-terminal) of another molecule, beta (β)-endorphin, a fragment of beta-lipotropin that had been isolated and sequenced from pituitary extract (Bradbury *et al.*, 1976; Li *et al.*, 1976). Following these initial discoveries many other endogenous opioid peptides were discovered, including dynorphin A (Goldstein *et al.*, 1979, 1981) and α-neo-endorphin (Kangawa *et al.*, 1981) which were structurally related to enkephalin.

All these endogenous opioid peptides have in common an N-terminal extension of either [Met]-enkephalin or [Leu]-enkephalin sequence (Fig.1.1.4.1), for instance, β-endorphin is a N-terminal extension of [Met]-enkephalin and dynorphin and α-neo-endorphin are N-terminal extensions of [Leu]-enkephalin. Because of the structural similarities of these peptides, it was postulated that β-endorphin is the precursor of [Met]-enkephalin and that dynorphin or α-neo-endorphin is the precursor of [Leu]-enkephalin. However, neither β-endorphin nor dynorphin or α-neo-endorphin was the precursor of [Met] or [Leu]-enkephalin, respectively. The discovery of these opioid peptides has suggested that the opioid peptides might make up a family of neuropeptides. Although it was appreciated that these neuropeptides must be synthesised in precursor form, there was no clear

PEPTIDES	STRUCTURES
	1 5 10 15 20 25 30
[Met]-enkephalin	Try-Gly-Gly-Phe-Met
[Leu]-enkephalin	Try-Gly-Gly-Phe-Leu
ENK-7	Try-Gly-Gly-Phe-Met-Arg-Phe
ENK-8	Try-Gly-Gly-Phe-Met-Arg-Gly-Leu
Peptide E	Try-Gly-Gly-Phe-Met-Arg-Arg-Val-Gly-Arg-Pro-Glu-Trp-Trp-Met-Asp-Tyr-Gln-Lys-Arg-Tyr-Gly-Gly-Phe-Leu
α–endorphin	Try-Gly-Gly-Phe-Met-Thr-Ser-Glu-Lys-Ser-Gln-Thr-Pro-Leu-Val-Thr
β–endorphin	Try-Gly-Gly-Phe-Met-Thr-Ser-Glu-Lys-Ser-Gln-Thr-Pro-Leu-Val-Thr-Leu-Phe-Lys-Asn-Ala-Ile-Ile-Lsy-Asn-Ala-Try-Lys-Lsy-Gly-Glu
γ–endorphin	Try-Gly-Gly-Phe-Met-Thr-Ser-Glu-Lys-Ser-Gln-Thr-Pro-Leu-Val-Thr-Leu
α–neo-endorphin	Try-Gly-Gly-Phe-Leu-Arg-Lys-Pro-Lys
Dynorphin A(1-17)	Try-Gly-Gly-Phe-Leu-Arg-Arg-Ileu-Arg-Pro-Lys-Leu-Lys-Trp-Asp-Asn-Gln
Dynorphin (1-8)	Try-Gly-Gly-Phe-Leu-Arg-Arg-Ileu
Dynorphin B (Rimorphin)	Try-Gly-Gly-Phe-Leu-Arg-Arg-Gy-Phe-Lys-Val-Val-Thr

Figure 1.1.4.1 : Structure of endogenous opioid peptides

Alignment of the amino acid sequence of the endogenous opioid peptides. Amino acid residues homology between opioid peptides are boxed.

Abbreviations: ENK, enkephalin; Ala, alanine; Arg, arginine; Asn, asparagine; Asp, aspartate; Cys, cysteine; Gln, glutamine; Gly, glycine; His, histidine; Ile, isoleucine; Leu, leucine; Lys, lysine; Met, methionine; Phe, phenylalanine; Pro, proline; Ser, serine; Thr, threonine; Trp, tryptophan; Try, tyrosine; Val, valine.

(Source, Simon E., 1986)

consideration on the number of opioid precursors. It later become clear by a number of distinct techniques and approaches.

Immunohistochemical studies, initiated in the 70's and completed in the 80's revealed the extensive distribution of opioid circuits in mammalian central nervous system (for reviews see Cuello, 1983; Khachaturian *et al.*, 1985). From these studies, three distinct classes of opioid circuits were identified, [Met] and [Leu] circuits, β-endorphin circuits and dynorphin A or α-neo-endorphin circuits. These studies suggested that a given neurone synthesises only one class of opioid and there were three distinct opioid precursors.

In other studies using immunoprecipitation analysis (Mains *et al.*, 1977), cell free translation studies (Roberts and Herbert, 1977) and peptide microsequencing (Chretien and Seidah, 1981), several groups independently proposed that the pituitary hormone ACTH and opioid peptide, β-endorphin were synthesised via a common precursor. This precursor has been referred to as proACTH/endorphin or pro-opiomelanocortin (POMC). Nakanishi *et al.*, (1979) using a complementary DNA (cDNA) technique, succeeded in sequencing POMC mRNA and confirmed the common precursor hypothesis. Following this, the proenkephalin A (PENK, (Noda *et al.*, 1982b), and pro-dynorphin or pro-enkephalin B mRNA and α-neo-endorphin were sequenced (Kakidani *et al.*, 1982). It is now known that all mammalian endogenous opioids are derived from these large precursor polypeptides. The three opioid precursor polypeptides are: -

(a) Proopiomelanocortin (POMC)
(b) Proenkephalin A (PENK)
(c) Proenkephalin B or Prodynorphin (PDYN)

Structure of endogenous opioid peptide precursors

The structural organisation of mammalian opioid precursors is shown in figure 1.1.4.2. As a group these three opioid precursors display a number of similarities. They range in size from 256 to 267 amino acids, and, all have a signal sequence located at the N-terminal. The opioid peptide sequences are separated within each precursor by sets of basic amino acids. In all precursors there is

evidence of duplication of end product sequences. For example, in pro-enkephalin there six copies of the [Met]-enkephalin sequence; in Pro-dynorphin the opioid peptides, α-neo-endorphin, dynorphin A and dynorphin B, each begin with the [Leu]-enkephalin sequence. Finally, all three precursors have a cysteine-rich region located at the N-terminal. The number and location of cysteine residues in Pro-enkephalin and Pro-dynorphin is very similar.

Proopiomelanocortin (POMC)

POMC (Fig.1.1.4.2A) is a 263 residue protein which was the first neuropeptide precursor protein to be isolated from the mouse pituitary cells using double-antibody immunoprecipitation procedures by Mains *et al.*, (1977). Following this, using recombinant DNA techniques, the full nucleotide sequence of the POMC precursor was characterised from the sequence of cDNA clone of POMC mRNA by Nakanishi and his collaborators (1979).

Of the three opioid peptide precursors, POMC is unique because it contains only one copy of the opioid-defining amino acid sequence which is identical to [Met]-enkephalin; this sequence is found at the aminoterminal of the most potent endogenous opioid peptide, β-endorphin (Eipper and Mains, 1980). POMC is also unique because it also contains other biologically active hormones that are not related to opioid peptides. These include adrenocorticotropic hormone (ACTH) and the three melanocytes stimulating hormones (α, β. and γ-MSH) which are part of the stress hormonal system (Mains *et al.*, 1977; Nakanishi *et al.*, 1979). β-endorphin is the only POMC product with known analgesic activity.

Proenkephalin A (PENK)

Human (Comb *et al.*, 1982), rat (Howells *et al.*, 1984; Yoshikawa *et al.*, 1984) and bovine (Mizuno *et al.*, 1980b; Gubler *et al.*, 1982; Noda *et al.*, 1982a) pro-enkephalin cDNA were cloned and sequenced in the early 80s and they appear to be functionally identical. In contrast to the POMC precursor that contains only one opioid peptide (β-endorphin), all of known PENK active peptides are opioid in nature.

The mammalian proenkephalin contains within its structure seven peptides with methionine [Met]- or leucine [Leu]-enkephalin active core (Figure 1.1.4.2B). It is apparent that each precursor polypeptide can be processed to generate four copies of [Met]-enkephalin, a single copy of [Leu]-enkephalin, one copy of carboxyl extended heptapeptide [Met]-enkephalin-Arg^6-Phe^7 (ENK-7) and one of the octapeptide [Met]-enkephalin-Arg^6-Gly^7-Leu^8 (ENK-8); each internal opioid peptide sequence is flanked by pairs of basic amino acids that are the usual processing signal in polyhormone precursors (Douglass *et al.*, 1984; Loh *et al.*, 1984). Extended enkephalin-like peptides, such as peptides E (Kilpatrick *et al.*, 1981; Rossier, 1981), BAM-22P and BAM-12P (Mizuno *et al.*, 1980a, 1980b), are also derived from this precursor by incomplete or alternative processing.

Pro-dynorphin or Pro-neoendorphin-dynorphin (PDYN)

Kakidani *et al.*, 1982 were the first to demonstrate that pro-dynorphin has a mRNA sequence containing the sequence of three opioid peptides with aminoterminal extension of [Leu]-enkephalin. The opioid peptides that derive from pro-dynorphin include dynorphin A (Minamino *et al.*, 1980) α-neo-endorphin (Kangawa *et al.*, 1981), β-neo-endorphin (Minamino *et al.*, 1981), and dynorphin B (Fischli *et al.*, 1982; Kilpatrick *et al.*, 1982).

Biosynthesis and multiple forms of endogenous opioid peptides

Endogenous opioid peptides and other transmitters or hormones are synthesised as a large molecular protein precursors, which are processed within a given cell (neural and non-neural) to produce smaller active fragments. This process depends not only on the genetic code for the precursor, but also on the program that directs the cellular enzymes to cut out or cleave the peptide from their respective precursor. As will be discussed in brief, the separations of the peptides from its large precursor by proteolytic cleavage are called post-translational processing events, i.e. events following the translation of messenger RNA into a protein precursor. These post-translational events are capable of determining the exact mixture of peptides in a given cell. Nevertheless, the processing is not uniform, depending on the tissue examined and the physiological status of the cell. Most endogenous opioid peptides are produced from their precursor by proteolytic cleavage at double basic amino acid residues (Lys-Arg, Lys-Lys, Arg-Arg, Arg-Lys,

although there are at least two opioid peptides, dynorphin A and dynorphin B that deviate from this classical pathway in that they are produced by processing mechanism that involves cleavage at a single basic arginine residue (Fig. 1.1.4.2C; Docherty and Steiner, 1982; Weber *et al.*, 1983).

Anatomy of opioid system in the CNS

Most known endogenous opioid peptides are generated from the three precursor polypeptides which are widely distributed throughout the central nervous system (CNS). Immunocytochemical techniques and in situ hybridisation analysis have been used extensively to visualise and map the distribution of opioid peptides in particular neuronal pathways (Bloom *et al.*, 1978; Khachaturian *et al.*, 1982, 1985; Watson *et al.*, 1982a, 1982b, 1983; Lewis *et al.*, 1983; Merchenthaler *et al.*, 1986; Lantos *et al.*, 1995). Distribution maps comparing the localisation of the three opioid precursors in the CNS are shown in figure 1.1.4.3.

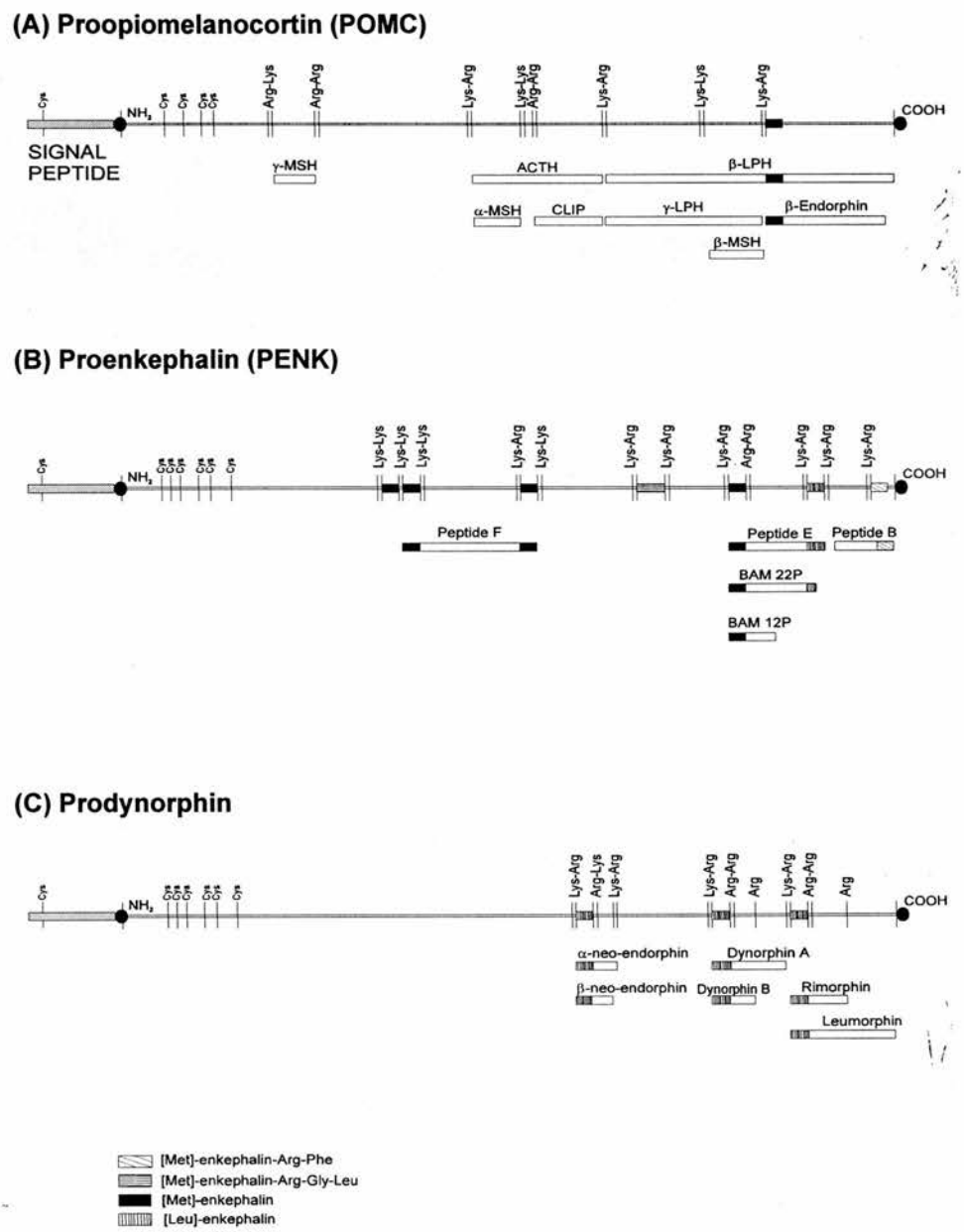

Figure 1.1.4.2 : Schematic representation of the structure of the mammalian opioid precursors.

Note that the [Met]-enkephalin appears in both POMC and PENK, while [Leu]-enkephalin is common to both PENK and prodynorphin. The paired and single basic amino acids that serve as processing sites are indicated as vertical line(s). MSH, melanotropin; ACTH, adrenocorticotropin; LPH, lipotropin; CLIP, corticotropin-like intermediate-lobe peptide.

(Adapted from Khachaturian 1985)

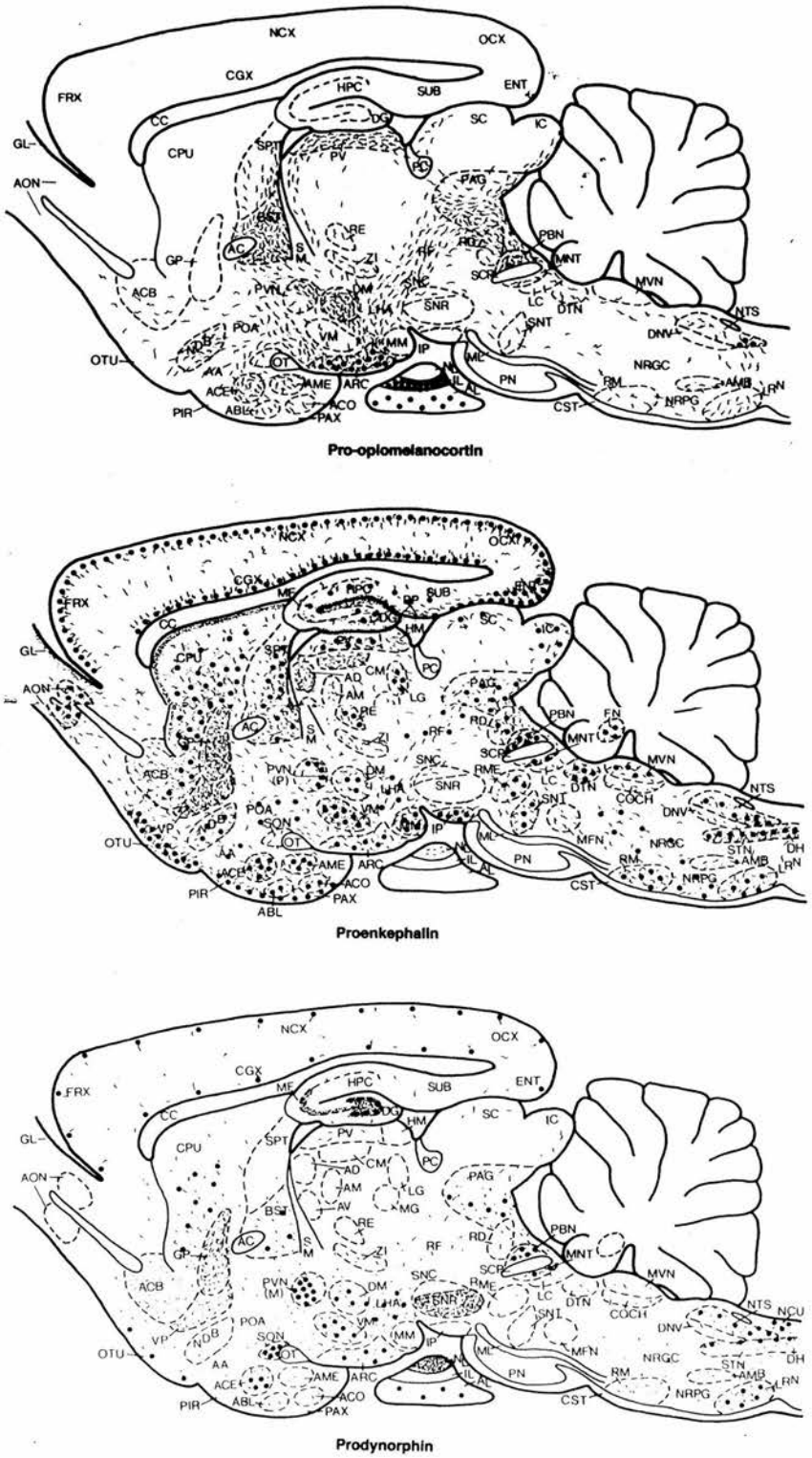

1. Pro-opiomelanocortin contains one opioid peptide (β-endorphin), one copy of ACTH, and potentially three copies of MSH, namely α-, β- and γ-MSH. In the brain, the major POMC neuronal populations resides in the arcuate nucleus, with projections to many limbic and brain stem nuclei.

2. Proenkephalin codes for several peptides containing the opioid-active core Tyr-Gly-Gly-Phe-Met (or -Leu). These include one copy of [Leu]enkephalin, four copies of [Met]enkephalin and one copy each of [Met]enkephalin-Arg-Phe and [Met]enkephalin-Arg-Gly-Leu. Peptides derived from proenkephalin are found in neuronal systems throughout the CNS, from the olfactory bulb to the spinal cord. These neurons form both local circuits and long-tract projections.

3. Prodynorphin also codes for several active opioid peptides containing the sequence of [Leu]enkephalin. These include dynorphin A, dynorphin B, and α-neoendorphin. This precursor is distributed in neuronal systems found at all levels of the neuraxis. Like their proenkephalin counterparts, the prodynorphin neurons form both short- and long-tract projections –often found in parallel with the proenkephalin systems.

In these three parasagittal maps, neuronal perikarya are shown as solid circles, and fibers-terminals as short curved lines and dots. Each map represents multiple parasagittal levels through the rat brain and was reconstructed using the rat brain atlas of G. Paxinos and C. Watson (1982, The Rat Brain in Stereotaxic Coordinates, Academic Press).

Key

AA: anterior amygdala, ABL: basolateral nucleus of amygdala, AC: anterior commissure, ACB: nucleus accumbens, ACE: central nucleus of amygdala, ACO: cortical nucleus of amygdala, AD: anterodorsal nucleus of thalamus, AL: anterior lobe of pituitary, AM: anteromedial nucleus of thalamus, AMB: nucleus ambiguus, AME: medial nucleus of amygdala, AON: anterior olfactory nucleus, ARC: arcuate nucleus, AV: bed nucleus of stria terminalis, CC: corpus callosum, CGX: cingulate cortex, CM: central-medial nucleus of thalamus, COCH: cochlear nuclear complex, CPU: caudate-putamen, CST: corticospinal tract, DH: dorsal horn of spinal cord, DG: dentate gyrus, DM: dorsomedial nucleus of hypothalamus, DNV: dorsal motor nucleus of vagus, DTN: dorsal tegmental nucleus, ENT: entorhinal cortex, FN: fastigial nucleus of cerebellum, FRX: frontal cortex, GL: glomerular layer of olfactory bulb, GP: globus pallidus, HM: medial habenular nucleus, HPC: hippocampus, IC: inferior colliculus, IL: intermediate lobe of pituitary, IP: interpeduncular nuclear complex, LC: nucleus locus coeruleus, LG: lateral geniculate nucleus, LHA: lateral hypothalamic area, LRN: lateral reticular nucleus, MF: mossy fibers of hippocampus, MFN: motor facial nucleus, MG: medial geniculate nucleus, ML: medial lemniscus, MM: medial mammillary nucleus, MNT: mesencephalic nucleus of trigeminal, MVN: medial vestibular nucleus, NCU: nucleus cuneatus, NCX: neocortex, NDB: nucleus of diagonal band, NL: neural lobe of pituitary, NRGC: nucleus reticularis gigantocellularis, NRPG: nucleus reticularis paragigantocellularis, NTS: nucleus tractus solitarius, OCX: occipital cortex, OT: optic tract, OTU: olfactory tubercle, PAG: periaqueductal gray, PAX: peri-amygdaloid cortex, PBN: parabrachial nucleus, PC: posterior commisure, PIR: piriform cortex, PN: pons, POA: preoptic area, PP: perforant path, PV: periventricular nucleus of thalamus, PVN(M): paraventricular nucleus (pars magnocellularis), PVN(P): paraventricular nucleus (pars parvocellularis), RD: nucleus raphé dorsalis, RE: nucleus reuniens of thalamus, RF: reticular formation, RM: nucleus raphé magnus, RME: nucleus raphé medianus, SC: superior colliculus, SCP: superior cerebellar peduncle, SM: stria medullaris thalami, SNC: substantia nigra (pars compacta), SNR: substantia nigra (pars reticulata), SNT: sensory nucleus of trigeminal (main), SON: supraoptic nucleus, SPT: septal nuclei, STN: spinal nucleus of trigeminal, SUB: subiculum, VM: ventromedial nucleus of hypothalamus, VP: ventral pallidum, ZI: zona incerta

Figure 1.1.4.3 : Schematic representation of the distribution of POMC, PENK and prodynorphin derived peptides in the rat CNS.

(After Khachaturian H., 1985)

1.1.5 OPIOID RECEPTORS

Endogenous opioid peptides and opiates like morphine exert their pharmacological and physiological effects on the target tissues by specifically binding to membrane-bound receptors called opioid receptors. The opioid receptors can be classified into three distinct receptor types namely mu (μ), delta (δ) and kappa (κ), which are unevenly distributed throughout central and peripheral nervous system. Each of these receptors has specific pharmacological effects and has been associated with specific functions (Simon, 1991; Lutz and Pfister, 1992; Mansour *et al.*, 1995; Dhawan *et al.*, 1996).

Opioid Receptors Multiplicity

The existence of multiple types of opioid receptor was suggested in 1965 by Portoghese based on the relationship between the molecular structure of opiate drugs and their analgesic activity. Subsequently, opioid receptors were demonstrated in the brain by radioligand binding studies showing that radiolabeled opioid drugs, selected for their high potencies, bound to brain tissues with high affinity and that this binding was stereoselective (Pert *et al.*, 1973; Simon *et al.*, 1973; Terenius, 1973; Gilbert and Martin, 1976; Martin *et al.*, 1976).

On the basis of various pharmacological effects of morphine and its derivatives (ketocyclazocine and SKF-10047) in experiments carried out in chronic spinal dog, Martin and his colleagues (1976), systematically showed the first definitive evidence supporting three opioid drug syndromes into which opioids could be divided. Furthermore, this study showed that the dependence produced by these drugs was suppressed by drugs within the same group but that abstinence symptoms would develop or might even be participated by administration of drugs from outside this group. In the light of these results, they defined the existence of three opioid receptor types, mu (μ), kappa (κ) and sigma (σ) associated with three prototypic agonists morphine, ketocylazocine and SKF 10047 (N-allynormetazocine), respectively. However, the σ receptor is no longer considered part of the opioid family since subsequent study demonstrated that the σ syndrome associated with SKF 10047 is not blocked by the general opioid antagonist naloxone (Quirion *et al.*, 1987).

After the discovery of enkephalin, Lord *et al.,* (1977) postulated another type of opioid receptor since enkephalin seemed to bind to another type of opioid receptor. Using an *in vitro* bioassay system, they found that morphine showed high potency compared to enkephalin in inhibiting the electrically induced contractions of the myentric plexus of the guinea pig illeum while in the isolated mouse vas deferens, enkephalin exhibited greater potency than morphine. This reversal in the order of agonist potency observed between the two tissues indicates that different types of opioid receptors predominate in the two systems. The major receptor present in the guinea pig ileum was then called μ to resemble Martin's μ- receptor, while the receptor in the mouse vas deferens was called delta (δ) (for *d*eferens).

The occurrence of multiple types of opioid receptor (μ, δ, κ) is now generally acknowledged, although there is some evidence to suggest that additional opioid receptors may exist. In particular, the epsilon receptor (ε, Wuster *et al.*, 1979), the zeta (ζ, Zagon *et al.*, 1991) and a high affinity binding site, lambda (λ, Grevel *et al.*, 1985), may also be parts of the opioid receptor system. The actual number of different opioid receptors is one of the major controversies of opioid receptor pharmacology. The μ-, δ- and κ-opioid receptors have been identified by their different selectivity for various naturally occurring opioid peptide and alkaloid opioid ligands, and this subdivision has been substantially supported by the development of increasingly selective synthetic ligands (for a review see Goldstein *et al.*, 1989). Some of the opioid receptor ligand agonists and antagonists are presented in 1.2.5. In addition, pharmacological studies have suggested the existence of different subtypes of the classical μ-, δ- and κ-opioid receptors (for reviews see, Lutz and Pfister, 1992; Traynor and Elliott, 1993; Dhawan *et al.*, 1996; Zaki *et al.*, 1996).

Molecular Basis of the Structure of Opioid Receptors.

Early studies suggesting the existence of multiple opioid receptor types have been extended by numerous anatomical, pharmacological, biochemical, and behavioural studies demonstrating distinct opioid receptor types in the central and peripheral nervous system.

These findings have led several investigators to isolate and purify opioid receptor proteins from cell membranes. Vigorous work in several laboratories resulted in the purification to homogeneity of μ-, δ- and κ-opioid receptor proteins

(for reviews, see Simon, 1986; Loh and Smith, 1990). However, none of these attempts revealed the structures of the proteins that were pharmacologically defined as opioid receptors primarily because of the low density of opioid receptors in tissues. Ultimately, two independent groups, Kieffer *et al.,* (1992) and Evans *et al.*, (1992) succeeded in identifying the structure of the δ-opioid receptor without purifying the protein. They cloned the cDNA encoding mouse δ-opioid receptor form NG108-15 cells by expression cloning with radiolabeled δ-opioid ligands (Evans *et al.*, 1992; Kieffer *et al.*, 1992). Subsequently, μ- (*rat*: Chen *et al.*, 1993; Fukuda *et al.*, 1993; Thompson *et al.*, 1993; Wang *et al.*, 1993; Minami *et al.*, 1994; *mouse*: Min *et al.*, 1994) and κ-opioid receptor cDNAs (*rat*: Li *et al.*, 1993; Meng *et al.*, 1993; Minami *et al.*, 1993; Nishi *et al.*, 1993; *mouse*: Yasuda *et al.*, 1993) were cloned based on their homology to the clone δ-opioid receptor. Other receptor cDNAs thought to belong to this gene family have also been cloned including isolation of a novel cDNA encoding a putative membrane receptor with high homology to the cloned classical μ, δ and κ opioid receptors (Bunzow *et al.*, 1994; Chen *et al.*, 1994; Fukuda *et al.*, 1994; Wang *et al.*, 1994; Wick *et al.*, 1994).

They revealed that the three cloned opioid receptors are members of the ever-growing family of seven transmembrane G-protein-coupled receptors, which includes other peptide receptors such as somatostatin, substance P and vasopressin as well as nonpeptide receptors. The amino acid sequences of the μ-, δ- and κ-opioid receptors are extremely homologous (approximately 70% homology) to one another at both amino acid and the nucleic acid levels, and that these similarities are highly conserved across species (≈90%). Highest homology between the receptor protein is found in regions spanning the transmembrane domains and intracellular loops. The most pronounced divergent regions of these three receptors are found at the amino (N-) and carboxyl (COOH-) termini, at the transmembrane 4 as well as extracellular loops 2 and 3. Transfection of the cloned receptors in heterologous cell lines suggests that they are negatively coupled to adenylate cyclase via G_i.

Well before the cloning of the opioid receptors, it was known that the opioid receptors are couple to G proteins and have seven transmembrane segments (Dohlman *et al.*, 1987). The evidence that the opioid receptors belong to the family of G-protein-coupled receptors includes; the binding of opioid receptor agonists, but

not the opioid receptors antagonists, is regulated by guanine nucleotides (Childers, 1991). Secondly, hydrolysis of guanine nucleotides is stimulated by opioid receptor agonists; this was originally shown in neuronal membranes, but has also been observed with purified and reconstituted μ-opioid receptor protein and G-protein (Ueda *et al.*, 1991). Finally, cellular responses to opioid receptor agonists (example, opening of K^+ channels, inhibition of adenylyl cyclase) require GTP and are blocked by pertussis toxin (Aghajanian and Wang, 1986; North *et al.*, 1987; Louie *et al.*, 1990), which ribosylates a cysteine residue in certain G proteins.

Anatomical distribution of opioid receptors

Opioid receptors consist of three distinct types namely μ-, δ- and κ-opioid receptors. Each of these receptors has a characteristic distribution in the central nervous system. Numerous autoradigraphic and *in situ* hybridisation studies have been performed to map the localisation of μ-, δ- and κ-opioid receptor binding sites and mRNAs in the central nervous system (McLean *et al.*, 1986; Mansour *et al.*, 1987; Tempel and Zukin, 1987; Mansour *et al.*, 1988, 1994, 1995). Both techniques demonstrate a distinct anatomical distribution that corresponds well to one another. These studies not only provide insight into the cellular localisation but also demonstrate the neuronal circuits they may modulate. Figure 1.1.5.1 shows schematic distribution of μ-, δ- and κ-opioid receptor mRNA expression and binding in the rat CNS (Mansour *et al.*, 1995).

Functional roles of the opioid receptors

Despite various studies of opioid actions in the brain, it is still difficult to draw a strong conclusion regarding the functional roles of the different types of opioid receptors in any neuronal system. However, significant progress has been made in several systems. Briefly, μ-opioid receptors, which are particularly enriched in the striatum, thalamus, hippocampus, the nucleus of the solitary tract, locus coeruleus and spinal cord, have been associated with analgesia, respiratory and cardiovascular functions, as well as a number of hormonal actions. δ-opioid receptors, which are expressed at high levels in many forebrain areas, including the olfactory bulb, neocortex, striatum, hippocampus and amygdala, in addition to the midbrain pontine nuclei and dorsal horns of the spinal cord, have been primarily associated with analgesia, gastrointestinal motility and thermoregulation. While the third opioid receptor type in the CNS, κ-opioid receptors are relatively high in the

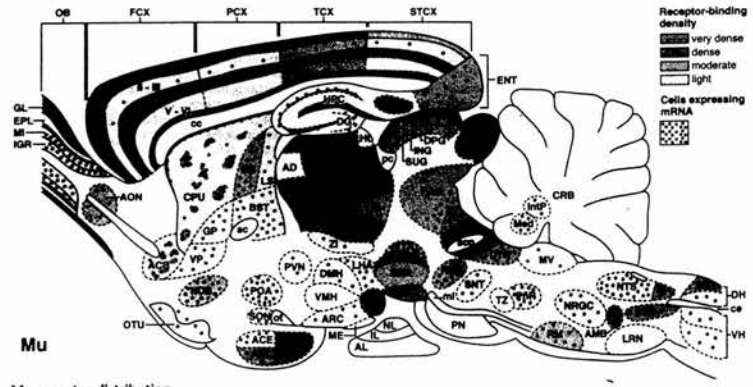

Mu-receptor distribution

A high correlation between μ-receptor mRNA expression and binding is observed in the striatal clusters and patches of the nucleus accumbens and caudate-putamen, diagonal band of Broca, globus pallidus and ventral pallidum, bed nucleus stria terminalis, most thalamic nuclei, medial and cortical amygdala, mammillary nuclei, presubiculum, interpeduncular nucleus, median raphé, raphé magnus, parabrachial nucleus, locus coeruleus, nucleus ambiguus and nucleus of the solitary tract. Differences in μ-receptor mRNA and binding distributions are observed in regions such as the neocortex, olfactory bulb, superior colliculus, spinal trigeminal nucleus and spinal cord which might be a consequence of receptor transport to presynaptic terminals.

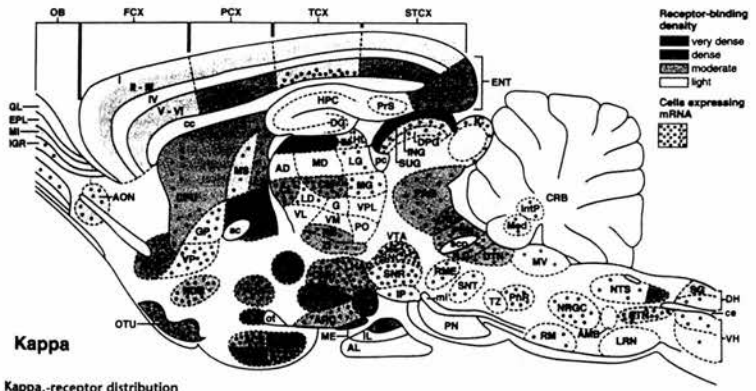

Kappa$_1$-receptor distribution

A high degree of correlation between κ_1-receptor mRNA expression and binding is observed in regions such as the nucleus accumbens, caudate-putamen, olfactory tubercle, bed nucleus stria terminalis, medial preoptic area, paraventricular, supraoptic, dorsomedial and ventromedial hypothalamus, amygdala, midline thalamic nuclei, periaqueductal gray, raphé nuclei, parabrachial nucleus, locus coeruleus, spinal trigeminal nucleus, and the nucleus of the solitary tract. Differences in the κ_1-receptor binding and mRNA distributions in the substantia nigra, pars compacta, ventral tegmental area and in the neural lobe of the pituitary might be due to receptor transport.

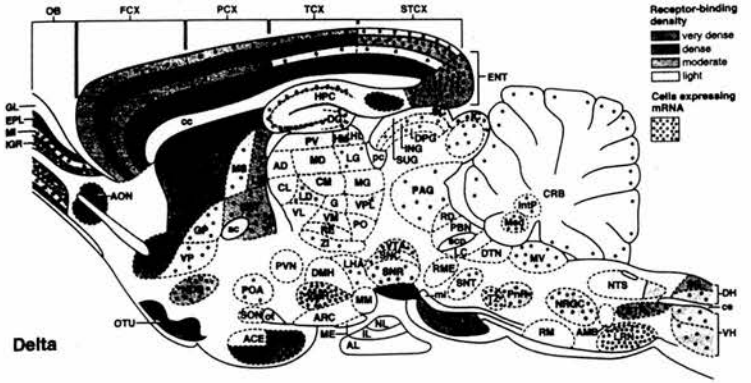

Delta-receptor distribution

A high correlation between δ-receptor mRNA expression and binding is observed in such regions as the anterior olfactory nucleus, neocortex, caudate-putamen, nucleus accumbens, olfactory tubercle, diagonal band of Broca, globus pallidus and ventral pallidum, septal nuclei, amygdala, and the pontine nuclei, suggesting local receptor synthesis. Regions of high δ-receptor mRNA expression and comparatively low receptor binding include the internal granular layer of the olfactory bulb and ventromedial nucleus of the hypothalamus. The apparent discrepancy between δ-receptor mRNA expression and δ-receptor binding in several brainstem nuclei and in the cerebellum is, in part, due to the increased sensitivity of in situ hybridization methods and high levels of nonspecific binding observed with δ-selective ligands. Differences in distributions indicative of receptor transport are observed in the substantia gelatinosa of the spinal cord, external plexiform layer of the olfactory bulb, and the superficial layer of the superior colliculus.

Abbreviations

ABL, basolateral amygdaloid nucleus; ac, anterior commissure; ACB, nucleus accumbens; ACE, central amygdaloid nucleus; ACO, cortical amygdaloid nucleus; AD, anteriodorsal thalamus; AL, anterior lobe, pituitary; AMB, nucleus ambiguus; AME, medial amygdaloid nucleus; AON, anterior olfactory nucleus; ARC, arcuate nucleus, hypothalamus; BST, bed nucleus stria terminalis; cc, corpus callosum; ce, central canal; CL, centrolateral thalamus; CM, centromedial thalamus; CPU, caudate–putamen; CRB, cerebellum; DG, dentate gyrus; DH, dorsal horn, spinal cord; DMH, dorsomedial hypothalamus; DPG, deep gray layer, superior colliculus; DTN, dorsal tegmental nucleus; ENT, entorhinal cortex; EPL, external plexiform layer, olfactory bulb; FCX, frontal cortex; G, nucleus gelatinosus thalamus; GL, glomerular layer, olfactory bulb; GP, globus pallidus; HL, lateral habenula; HM, medial habenula; HPC, hippocampus; IC, inferior colliculus; IGR, intermediate granular layer, olfactory bulb; IL, intermediate lobe, pituitary; ING, intermediate gray layer, superior colliculus; IntP, interposed cerebellar nucleus; IP, interpeduncular nucleus; LC, locus coeruleus; LD, laterodorsal thalamus; LG, lateral geqiculate thalamus; LHA, lateral hypothalamic area; LRN, lateral reticular nucleus; LS, lateral septum; MD, dorsomedial thalamus; ME, median eminence; Med, medial cerebellar nucleus; MG, medial geniculate; Mi, mitral cell layer, olfactory bulb; ml, medial leminscus; MM, medial mammillary nucleus; MS, medial septum; MV, medial vestibular nucleus; NDB, nucleus diagonal band; NL, neural lobe, pituitary; NRGC, nucleus reticularis gigantocellularis; NTS, nucleus tractus solitarius; OB, olfactory bulb; ot, optic tract; OTU, olfactory tubercle; PAG, periaqueductal gray; PBN, parabrachial nucleus; pc, posterior commissure; PCX, parietal cortex; PN, pons; PnR, pontine reticular; PO, posterior nucleus thalamus; POA, preoptic area; PrS, presubiculum; PV, paraventricular thalamus; PVN, paraventricular hypothalamus; RD, dorsal raphé; RE, reuniens thalamus; RM, raphé magnus; RME, median raphé; SC, superior colliculus; scp, superior cerebellar peduncle; SG, substantia gelatinosa; SNC, substantia nigra, pars compacta; SNR, substantia nigra, pars reticulata; SNT, sensory nucleus trigeminal; SON, supraoptic nucleus; STCX, striate cortex; STN, spinal trigeminal nucleus; SUG, superficial gray layer, superior colliculus; TCX, temporal cortex; TZ, trapezoid nucleus; VH, ventral horn, spinal cord; VL, ventrolateral thalamus; VM, ventromedial thalamus; VMH, ventromedial hypothalamus; VP, ventral pallidus; VPL, ventroposteriolateral thalamus; VTA, ventral tegmental area; and ZI, zona incerta.

Figure 1.1.5.1 : Schematic representation of μ-, κ- and δ-opioid receptor mRNA expression in the rat CNS.

(After Mansour *et al.*, 1995)

nucleus accumbens, hypothalamus, amygdala, and parallel the μ- distribution in the brainstem and spinal cord, have been strongly associated with analgesia and maintaining water balance as well as other neuroendocrine functions and behaviours (for a review see, Akil *et al.*, 1993).

Opioid peptides-receptors relationship

The three opioid receptor systems in the central nervous system can be stimulated by one or more of the endogenous and exogenous opioid peptides (table 1.1.5.1). Endogenous opioid peptides are derived from three separate precursor molecules as a result of post-translational enzymatic processing. POMC is the precursor from which β-endorphin is derived; PENK gives rise to [Met]- and [Leu]-enkephalin; and PDYN serves as the precursor for dynorphin and its related peptides. This multiplicity in both systems raises questions as to the relationship between the various opioid peptides and opioid receptors. A great deal of work has been carried out to demonstrate and to analyse actions of opioids with respect to the particular receptors and ligands involved (for a review see Corbett *et al.*,1993).

β-endorphin, a POMC-derived peptide product, binds equally well to μ- and δ-receptors and possibly to ε-receptor (Shook *et al.*, 1988). Likewise, PENK products, [Met]- and [Leu]-enkephalin have the highest affinity for δ-opioid receptors, but can also bind to μ-opioid receptors (Davis *et al.*, 1985). Prodynorphin products, such as β-neoendorphin and dynorphin A, have high affinity for κ-opioid receptors (Chavkin *et al.*, 1982). However shorter prodynorphin products (dynorphin A(1-8), α-neoendorphin) appear to bind well to other opioid receptors, particularly in the rat brain where there is predominance of μ and δ-opioid receptors (Quirion and Pert, 1981; Wuster *et al.*, 1981; Schulz *et al.*, 1982).

The three opioid receptor subtypes also represent targets for exogenous opioid peptides. Many peptides and alkaloid like compounds showed high affinity and selectivity for the various opioid receptors, and have become available in recent years. As indicated in table 1.1.5.1, morphine and synthetic peptides, DAGO and DAMGO have a high affinity and selectivity for the μ-opioid receptor (Handa *et al.*, 1981), thus representing exogenous μ-opioid receptor ligands. On the other hand, synthetic peptides such as DPDPE and U69593 are highly selective for δ- and κ-

opioid receptors, respectively (Mosberg *et al.*, 1983; Lahti *et al.*, 1985). In addition, several opioid receptor antagonists have been synthesised. Naloxone, naltrexone and nalmefene are "non-selective" antagonists in that they interact not only with μ-opioid receptors, but also interact with δ- and κ-opioid receptors, despite with lower affinity in case of naloxone and naltrexone (DeHaven-Hudkins *et al.*, 1990). Other antagonists that exhibit high selectivity for μ-, δ- and κ-opioid receptors are indicated in table 1.1.5.1.

TABLE 1.1.5.1

PEPTIDE LIGANDS FOR OPIOID RECEPTORS

OPIOID RECEPTOR TYPE	ENDOGENOUS LIGANDS	EXOGENOUS LIGANDS	ANTAGONISTS	
			NON-SELECTIVE	SELECTIVE
μ	β–endorphin	Morphine DAGO DAMGO	Naloxone Naltrexone Nalmefene	CTOP CTAP
δ	Enkephalins	DPLPE DPDPE DELTROPHIN		ICI 174864 Naltrindole β-Funaltrexamine
κ	Dynorphin	U50 488H U69593		Nor-binaltrophimine

CTOP: D-Phe-Cys-Tyr-D-Trp-Orn-Thr-Pen-Thr-NH_2; **CTAP:** D-Phe-Cys-Tyr-D-Trp-Arg-Thr-Pen-Thr-NH_2; **DAGO:**Tyr-D-Ala-Gly-MePhe-Gly-ol; **DAMGO:**Try-D-Ala-Gly-MePhe-$NH(CH_2)_2$-OH;
DELTROPHIN: Tyr-D-Ala-Phe-Asp-Val-Val-Gly-NH_2; **DPLPE:** Try-D-Ala-Gly-Phe-D-Leu; **DPDPE:** Try-D-Pen-Gly-Phe-D-Pen; (Pen-pencillamine)
ICI 174864: N,N-dially-Tyr-Aib-Aib-Phe-Leu;(Aib: Aminoisobutyrate) **Naltrindole:** 17-cyclopropylmethyl-6,7-dehydro-4,5-epoxy-3,14-dihydroxy-6,7,2',3'-indolmorphinan;
Nor-binaltrophimine: 17,17'-*bis*(cyclopropylmethyl)-6,6',7,7'-tetradehydro-4,4',5,5'-diepoxy-6,6'-(imino)(7,7'-bimorphinan)-3,3',14,14'-tetrol hydrochloride hydrate;
U50 488H: *trans*-(+)-3,4-dichloro-*N*-methyl-[2-(1-pyrrolidinyl)cyclohexyl] benzeneacetamide methanesulphonate; **U69593:** 5α,7α,8β-(-)-*N*-methyl-N-[7-(1-pyrrolidinyl)-1-oxaspiro(4,5)dec-8-yl]-benzeneacetamide;

(Adapted from Herz., 1997)

1.1.6 CELLULAR MECHANISMS OF ACTION OF OPIOIDS

The biological effects of opioids begin with the binding of agonist to their endogenous receptors and end with series of cellular responses. Within this, a series of complex transduction steps takes place, which translates the action of receptor binding into biological responses. It has now been shown that all three opioid receptor types are coupled to G-proteins, and many of these transductions utilise this coupling protein to activate all three of the well recognised effector systems; i.e. adenylate cyclase, calcium channels and potassium channels.

Adenylate cyclase

Coupling of the opioid receptors to the inhibitory system of adenylate cyclase has been studied in transformed cell lines and in brain membranes (for a review see, Childers, 1993). The hybridoma cell line NG108-15, consisting of mouse neuroblastoma N18TG-2 and rat glioma C6Bu-1, has been an excellent model system to study the mechanisms of opioid receptor coupling to adenylate cyclase (Sharma *et al.*, 1975,1977; Traber *et al.*, 1975). The pharmacological characteristics of these opioid sites correspond to δ-opioid receptor types (Chang *et al.*, 1978, 1981). Other transformed cell types, including N4TG1, N1E-115 and N18TG2 cells, also have been identified as expressing the δ-opioid receptor type as well as δ-inhibited adenylyl cyclase (Gilbert and Richelson, 1983). In all of these cell lines, opioids inhibit both basal and prostagladin E_1-stimulated adenylate cyclase activity. Incubation of NG108-15 cells with pertussis toxin abolishes the inhibition of adenylate cyclase by opioids (Burns *et al.*, 1983; Hsia *et al.*, 1984), suggesting that G_i (or G_o) protein is coupled to these opioid receptors to exert their inhibitory activity.

The coupling of μ and δ opioid receptors to the inhibitory system of adenylate cyclase has been demonstrated also in the brain using membrane preparations derived from several brain regions including striatum (Collier and Roy, 1974), thalamus (Childers, 1993) and preaqueductal gray (Fedynyshyn and Lee, 1989). The inhibition of adenylate cyclase activity by κ-opioid receptor agonists has been demonstrated in membranes from rat spinal cord neurones (Attali *et al.*, 1989) and in the guinea pig cerebellum (Konkoy and Childers, 1989).

The cloned μ-, δ- and κ-opioid receptors expressed in COS or CHO cell lines are also coupled to the inhibitory system of adenylate cyclase (Evans *et al.*, 1992; Chen *et al.*, 1993; Meng *et al.*, 1993; Wang *et al.*, 1993; Yasuda *et al.*, 1993). The

inhibitory effects of opioid agonists on this system in the CHO cells expressing μ-, δ- and κ-opioid receptors are blocked by pertusis toxin, indicating that G_i ($_o$) were required for the inhibitory effect.

Calcium (Ca^{2+}) channels

One of the cellular events that underlies the effect of opioids in reducing cellular excitability and neurotransmitter release is the inhibition of voltage-dependent Ca^{2+} channels (for reviews see, North, 1986, 1987; Grudt and Williams, 1995). It has been shown that opioid receptor agonists for μ-, δ- and κ-opioid receptors can inhibit Ca^{2+} currents in various preparations, including a human neuroblastoma cell line (Seward *et al.*, 1991), dorsal root ganglion cells (Macdonald and Werz, 1986; Gross and Macdonald, 1987; Schroeder *et al.*, 1991), and guinea pig submucosal neurones (Shen and Surprenant, 1990; Surprenant *et al.*, 1990). This inhibition of Ca^{2+} currents by opioid receptors is blocked by pertussis toxin (Surprenant *et al.*, 1990; Seward *et al.*, 1991), indicating the involvement of G_i- and/or G_o-proteins. Hescheler *et al.,* (1987) revealed that G_o is more effective than G_i in reconstituting the inhibitory actions on Ca^{2+} channels in the cells pretreated with pertussis toxin.

The cloned κ-opioid receptor expressed in PC12 cells couples with the Ca^{2+} channel system to inhibit Ca^{2+} conductance through N-type channels (Tallent *et al.*, 1994). Functional coupling between the cloned κ-opioid receptor and N-type channels has been identified in *Xenopus* oocyte system. The κ-opioid agonist U50488H inhibited Ca^{2+} channels in *Xenopus* oocytes co-injected with *in vitro* transcribed mRNAs encoding the κ-opioid receptor and α1-and β-subunits of the Ca^{2+} channel (Kaneko *et al.*, 1994).

Potassium (K^+) channels

Another cellular event, which is thought to be an important effect of opioids in reducing cellular excitability and neurotransmitter release is the membrane hyperpolarisation caused by an increase in K^+ conductance (for reviews see, North, 1986, 1993; Grudt and Williams, 1995). Activation of μ-, δ- and κ-opioid receptors leading to an increase in K^+ conductance has been observed in neurones from various regions of the mammalian nervous system such as locus coeruleus and submucosal plexus (North *et al.*, 1987), hippocampus (Wimpey and Chavkin, 1991) as well as substantia gelatinosa neurones (Grudt and Williams, 1993). The K^+

channels that are activated have many properties of the inward rectifier family of channels. This increased in inwardly rectifying K^+ conductance caused by activation of opioid receptors are sensitive to pertussis toxin, indicating mediation through G_i- and /or G_o-proteins (Tatsumi *et al.*, 1990). Opioid receptors are also commonly coexpressed on cells with other G-protein coupled receptors, such as α_2-adrenoceptors, muscarinic acetylcholine M_2, somatostatin and $GABA_B$ receptors, whose activation also opens K^+ channels. Indeed, Shen *et al.,* (1992) demonstrated that all three opioid receptors could couple to a single K^+ channel in an excised patch of membrane.

The increased in K^+ conductance by the activation of opioid receptors has been confirmed using *Xenopus* oocytes system, in which the cloned μ-, δ- and κ-opioid receptor and G-protein-activated K^+ channel are co-expressed (Chen and Yu, 1994; Ikeda *et al.*, 1995; Kovoor *et al.*, 1995). They showed that these increases of K^+ conductance were also blocked by pertussis toxin.

1.2 AIMS OF STUDY

Electrophysiological studies in various areas of the mammalian central nervous system have shown that activation of opioid receptors predominantly results in an inhibition of the neuronal firing of action potentials. The inhibitory actions of opioids occur either directly through membrane hyperpolarisation which is associated with the potentiation of potassium conductances in the post-synaptic neurones (for reviews see, Duggan and North, 1983; McFadzean, 1988; Grudt and Williams, 1995) or through activation of presynaptic opioid receptors which, when activated result in a reduction of excitatory neurotransmitter release from pre-synaptic nerve terminals (Bixby and Spitzer, 1983; Von Kugelgen *et al.*, 1985; Pan *et al.*, 1990). The particular opioid receptor subtype associated with the inhibition mediated by an increase in membrane potassium conductances has been reported elsewhere as a μ-opioid receptor in rat locus coeruleus neurones (Williams and North, 1984; Wimpey and Chavkin, 1991) and neurones of the dorsomotor vagal nucleus (Travagli *et al.*, 1995), δ-opioid receptor in rat dentate gyrus of the hipocampus (Piguet and North, 1993) and κ-opioid receptor in guinea-pig substantial gelatinosa neurones (Grudt and Williams, 1993).

Numerous immunohistochemical studies have demonstrated the presence of enkephalinergic neurones and terminals in the vestibular nuclei of the brainstem with the highest density of enkephalinergic neurones found particularly in the medial vestibular nucleus (MVN; Pearson *et al.*, 1980; Finley *et al.*, 1981; Nomura *et al.*, 1984; Beitz *et al.*, 1987; Zanni *et al.*, 1995). Together with these findings is the result of receptor autoradiographic investigations, which demonstrated the presence of opioid receptor sites in the vestibular nuclei complex (Pearson *et al.*, 1980; Wamsley, 1983; Zanni *et al.*, 1995) and moderate levels of δ-opioid receptor mRNAs have been observed in the medial vestibular nucleus (Mansour *et al.*, 1994; Mansour *et al.*, 1995).

The effects of opioids on MVN neurones have been the subject of several electrophysiological studies. However the present evidence relating to the physiological effects of opioids on the firing rates and membrane properties of vestibular neurones is conflicting. Using single unit extracellular recording

techniques *in vivo*, Kawabata *et al.,* (1990) demonstrated that iontophoretically applied enkephalin inhibited the resting discharge rate and response to natural vestibular stimulation of Type I MVN neurones. By contrast, Carpenter and Hori (1992) and Lin and Carpenter (1994) reported that the majority (30% of neurones sampled) of tonically active rat MVN neurones recorded in a slice preparation *in vitro* were excited both by morphine and ala-leu-enkephalin, implicating a role for both μ and δ subtypes of opiate receptors in this response. A minority of MVN cells were inhibited by morphine and enkephalin, while other cells showed biphasic responses to these agonists where the brief excitatory effects were followed by a longer-lasting inhibition more typical of that seen in other neuronal cell types. These effects were obtained in response to 1-sec iontophoretic application of the agonists to the slice, and persisted after blockade of synaptic transmission in low-Ca medium and during blockade of $GABA_A$ receptors using bicucullin, indicating that the opioid receptors were postsynaptic and that the excitation produced by opioid agonists, morphine and enkephalin was due to direct depolarisation rather than to disinhibition (Lin and Carpenter, 1994).

While the actions of opioids in the mammalian central nervous system are predominantly inhibitory, the physiological evidence thus disagrees as to the functional effects of opioids in the mammalian MVN neurones as to whether their effect are inhibitory or excitatory. However, an excitatory neuronal response to opioids has been reported in the Renshaw cells of the spinal cord (Duggan *et al.*, 1976; Hill *et al.*, 1976) and in the cerebral cortex (Satoh *et al.*, 1974). Moreover, none of these findings have shown that the opioid-induced response was a direct excitation of the neuronal membranes or whether it was not due to disinhibition. An important objective of the experiments described here was therefore to clarify the opioid actions on MVN neurones and to determine their mechanisms of action using extracellular and intracellular whole-cell patch clamp recording techniques.

1.3 METHODS

Preparation of the Horizontal Slices of the Dorsal Brainstem *In Vitro*

Experimental animals.

Animal care and experimental procedures were carried out in accordance with the UK legislation for the humane care and the use of laboratory animals. Male Sprague-Dawley rats (Bantin and Kingman, Hull, UK) weighing between 60 to 180g were used throughout the study. They were housed with littermates of 10-15 per cage in an environmentally controlled animal facility: - constant room temperature of 21-23°C, relative humidity of 50-60%, 12 hours light/12 hours dark cycle, with food and water available *ad libitium*. The rats were kept for at least 2-3 days upon arrival, before being used for experiment, in order to accustom them to handling and to minimise the effects of non-specific stress.

Slice preparations.

Prior to decapitation, animals were anaesthetised with halothane (Fluothane, May and Baker Ltd., UK) by inhalation. The anaesthetic was administered by placing the animal in a small Perspex box containing a piece of halothane-soaked cotton wool. A sufficient level of anaesthesia was determined by a lack of reflex responses to a paw or tail-tip pinch. While under anaesthesia, the animal was decapitated using a small animal guillotine and rapid craniotomy was performed:

With a pair of scissors the scalp was removed, including the external ears and the neck muscles. With fine bone ronguers the occipital bone was then removed, exposing the cerebellum. The parietal and frontal bone were divided by a cut in the midline and the cranium was lifted away from the brain by carefully inserting blunt-ended forceps or scissors. The dura was cut and peeled to the edges of the skull with fine scissors. The head was then tilted sideways, and the intact brain was gently lifted up with a fine spatula, hence exposing the cranial nerves. These were also cut close to their point of exit from the brain. Finally, the whole brain was gently rolled into a beaker containing approximately 100ml of ice-cold (4°C), oxygenated (95% O_2 / 5% CO_2) artificial-cerebrospinal fluid (aCSF; for composition see solutions and chemicals). After about a minute in the beaker, the brain was then placed on its rostral surface on a cold dissecting stage which

comprised of a piece of filter paper moistened in ice-cold oxygenated aCSF placed on the surface of an upturned petri dish on ice.

The cerebrum was removed and the brainstem extending from the inferior colliculi to the obex was blocked with a sharp razor blade. The cerebellum was then removed by gently lifting it away from the brainstem with the blunt edge of scalpel blade and cutting through the cerebral penduncles, consequently exposing the MVN. The MVN were easily recognised from surrounding structures by their darker grey area and oval shape on the dorsal floor of the brainstem, symmetrically located on the floor of the fourth ventricle. During these procedures, the brain tissue was kept moist by periodic bathing with aCSF, which was also kept on ice and continuously oxygenated. Slices were cut on a motorised vibrating tissue chopper, Vibroslice made by Campden Instruments, London, UK.

The block of brainstem containing the MVN was cemented on the stage of the Vibroslice stage with cynoacrylate glue. The stage was positioned in the Vibroslice reservoir and filled with ice-cold oxygenated aCSF. Horizontal slices containing entire rostro-caudal length of the MVN were cut by advancing the reservoir in the horizontal direction. After removal of superficial layers of the dorsal brainstem about 100-200 μm, 1-2 slices were cut through the MVN at 300-400μm thickness. They were immediately removed to a small petri dish of ice-cold oxygenated aCSF. Finally, the slice was bisected along the midline to obtain 2 preparations containing the individual nucleus of the left and right side.

Maintenance of the Slice in the Chamber.

Following the slicing procedure, a single slice containing the MVN was quickly transferred to a Haas type interface recording chamber (Haas *et al.*, 1979) as illustrated in figure 1.3.1, which located in a Faraday cage and supported on an optical table isolator (Intracel, UK). The slice was positioned on the fine nylon mesh on the ramp surface of the recording chamber which sat above a thermostatically controlled water reservoir at the temperature of 33 ± 0.2 °C. The water bath was gently bubbled with 95% O_2 / 5% CO_2 to produce a continuous stream of gas saturated with water vapour which flowed over the slice through a small port at the head of the recording chamber.

A peristaltic pump (Miniplus 2, Gilson) was used to drive the oxygenated aCSF through the water bath to the recording chamber at the rate of approximately 1.8ml/min via PVC tubing (Bore: 1.5mm; Wall:1.0mm). Hence, the slice was maintained at the interface between a thin layer of flowing pre-warmed oxygenated aCSF and a layer of flowing 95% O_2 / 5% CO_2 gas saturated with water vapour. It took about one and half minutes for the aCSF flow into the recording chamber to exchange completely. The whole procedure from decapitation to the placement of the slice in the recording chamber lasted about 15 minutes and the slice was incubated for at least an hour prior to recording.

Solutions and Chemicals.

The following solutions and chemicals were used in this study: -

Artificial cerebrospinal fluid (aCSF) and modified low Ca^{2+}/high Mg^{2+} aCSF.

The normal physiological artificial cerebrospinal fluid (aCSF) (Llinas and Sugimori, 1980) used for preparing the brain slices and initial filling of the recording chamber was prepared fresh at the beginning of experiment and had the following composition (in mM); Sodium Chloride (NaCl) 124, Potassium Chloride (KCl) 5, Potassium dihydrogen orthophosphate (KH_2PO_4) 1.2, Magnesium sulphate ($MgSO_4$) 1.3, Calcium Chloride ($CaCl_2$) 2.4, Sodium bicarbonate ($NaHCO_3$) 26, D-glucose 10, and continuously bubbled with 95% O_2 / 5% CO_2.

A modified low Ca^{2+}/high Mg^{2+} aCSF (Lin and Carpenter, 1994; Lu *et al.*, 1995) was used in series of experiments to eliminate chemical synaptic transmission by reducing the concentration of Ca^{2+} and increasing the concentration of Mg^{2+} to 0.1mM and 6.3mM respectively.

Opioid agonists and antagonists

For the pharmacological experiments on opioids, 1.0 mM stock solution of opioid agonists and antagonists were made in distilled water, divided into small aliquots of 1.0ml and frozen at -20 °C until required. Opioid agonists and antagonists used in this experiment were obtained from various sources. The selective δ-opioid receptor agonists, [D-Ala^2, D-leu^5]-enkephalin (DADLE) and [D-

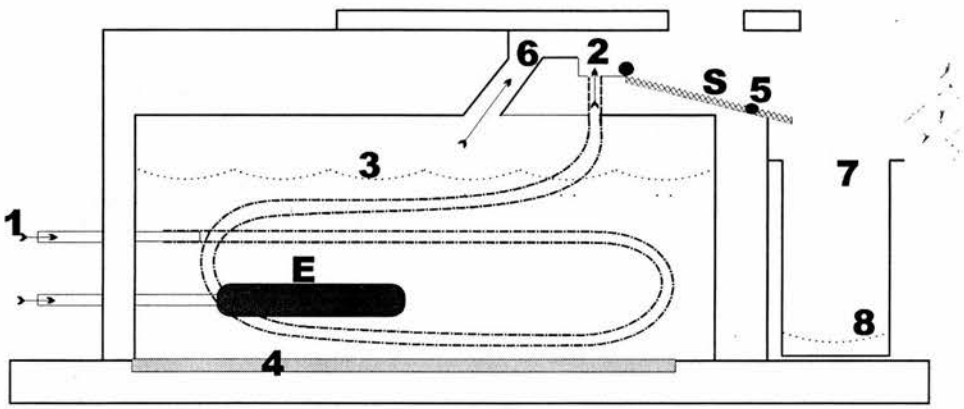

Figure 1.3.1 : Haas-type interface recording chamber

300 μm thick MVN slice (**S**) is placed on the nylon mesh on the ramp surface of the chamber and superfused with prewarmed (33 ± 0.2°C) oxygenated (95% O_2, 5% CO_2) aCSF supplied via the inlet PVC tubing (**1**) and entering the chamber at **2**. The water bath (**3**), filled with distilled water to the level indicated by the dashed line, is heated by thermoplate (**4**) and maintained at 33 ± 0.2°C by probe (**5**) connected to themoregulator. The heated distilled water is bubbled with a gas mixture (95% O_2, 5% CO_2) through water bath at **E**, and the water vapour produced enter the slice through an outlet in the ceiling of the chamber (**6**). aCSF is drained from the chamber by the cotton wick (**7**) and enter the collecting beaker at **8** and sucked out by the outlet PVC tubing to the waste reservoir.

Pen^2,Pen^5]-enkephalin (DPLPE); the selective κ-opioid receptor agonist, U50,488H and the highly selective μ-opioid receptor agonist, [D-Ala^2 ,N-Me-Phe^4, Gly^5-ol]-enkephalin (DAGO) were purchased from Sigma (UK). The μ-opioid receptor agonist, morphine was obtained from The Royal Infirmary, Edinburgh, UK. The non-selective opioid receptor antagonist, naloxone and the highly selective δ-opioid receptor antagonist, naltrindole were purchased from Research Biochemical International (Semat, UK).

DADLE is known to be a selective agonist at the δ-opioid receptor, having a K_i of 2.1 nM at δ receptors compared to a K_i of 14 nM at μ-receptors and 16000 nM at κ receptors (James and Goldstein 1984, Corbett *et al.*, 1993). The highly selective δ-opioid receptor, DPLPE has K_i value of 2.8 nM at δ-receptors compared to K_i of 710 nM at μ-receptors and >15000 nM at κ-receptors (Mosberg *et al.*, 1983; Corbett *et al.*, 1993). The arylacetamide U50,488H is a highly selective κ-opioid receptor agonist synthesized by the Upjohn Company and has a K_i of 0.69 nM at κ-receptors compared to a K_i of 435 nM at μ-receptors and 9200 nM at δ-receptors (Lahti *et al.*, 1982; Corbett *et al.*, 1993). The alkaloid morphine has approximately 50-fold higher affinity for μ-opioid receptors than for δ-opioid receptors with K_i of 1.8 nM at μ-receptors compared to 90 nM at δ-receptors and 317 nM at κ-receptors. The enkephalin analogue DAGO which is commonly used selective μ-opioid receptor agonist has the K_i of 1.9 nM at μ-opioid receptors compared to 345 nM at δ-receptors and 6090 nM at κ-receptors (Handa *et al.*, 1981; Corbett *et al.*, 1993).

Ion channel blockers

Two different ion channel blockers purchased from Sigma, UK, were used in this study: -

(1) Tetrodotoxin (TTX) was used at the concentration of 0.5 - 1.0 μM to block voltage-gated sodium channels, and

(2) Tetraethylammonium bromide (TEA) was used at the concentration of 20 mM to block voltage-gated potassium channels.

Both TTX and TEA were dissolved in distilled water to give a stock solution of 0.5mM and 1.0 M, respectively and stored into small aliquots of 1.0 ml and kept frozen until required.

Aliquot of opioids and ion channel blockers were thawed and diluted to their final concentration in the appropriate volume of oxygenated aCSF immediately prior to use, placed in the 10ml or 20ml syringes connected to the inflow of the interface chamber and applied to the slice by switching the perfusion inlet tube to the desired solution by means of 3-way taps so that the perfusion rate did not change. All opioid agonists were applied to the slice for a period of 60 seconds whereas opioid antagonists and ion channel blockers were applied continuously for at least 5-20 minutes before the next application of agonists.

Electrophysiological Recordings

There were two kinds of electrophysiological recording techniques conducted throughout this study. Extracellular recording technique was performed in the first part of the study in order to clarify the normal physiological actions of different type of opioid peptides on the spontaneously active MVN neurones as well as to determine the subtype of opioid receptor involved. In the second part of the study, current and voltage clamp experiments were conducted using whole-cell patch-clamp recording technique to investigate the mechanism of action of opioid peptides on the membrane currents of rat MVN neurones.

Recording set-up.

Conventional electrophysiological equipment was used for recording, storage and analysis of electrophysiological data. The electrophysiological system is illustrated diagrammatically in figure 1.3.2. A high input impedence amplifier, Axoclamp 2A (Axon Instruments, Foster City, CA City, USA), amplified the signals from the electrodes with an output bandwidth filter upper limit set at 3 or 10kHz. The currents and voltage (x10 gain) outputs from the Axoclamp 2A amplifier were simultaneously displayed on a 20 MHz digital storage oscilloscope (HM 205-3, Hameg, German) and monitored continuously. The voltage output was also sent to a NeuroLog system (Digitimer, UK) and to a CED 1401 Plus interface and a DigiData 1200 interface (Axon Instruments, Foster City, CA, USA) connected to an IBM-compatible computer.

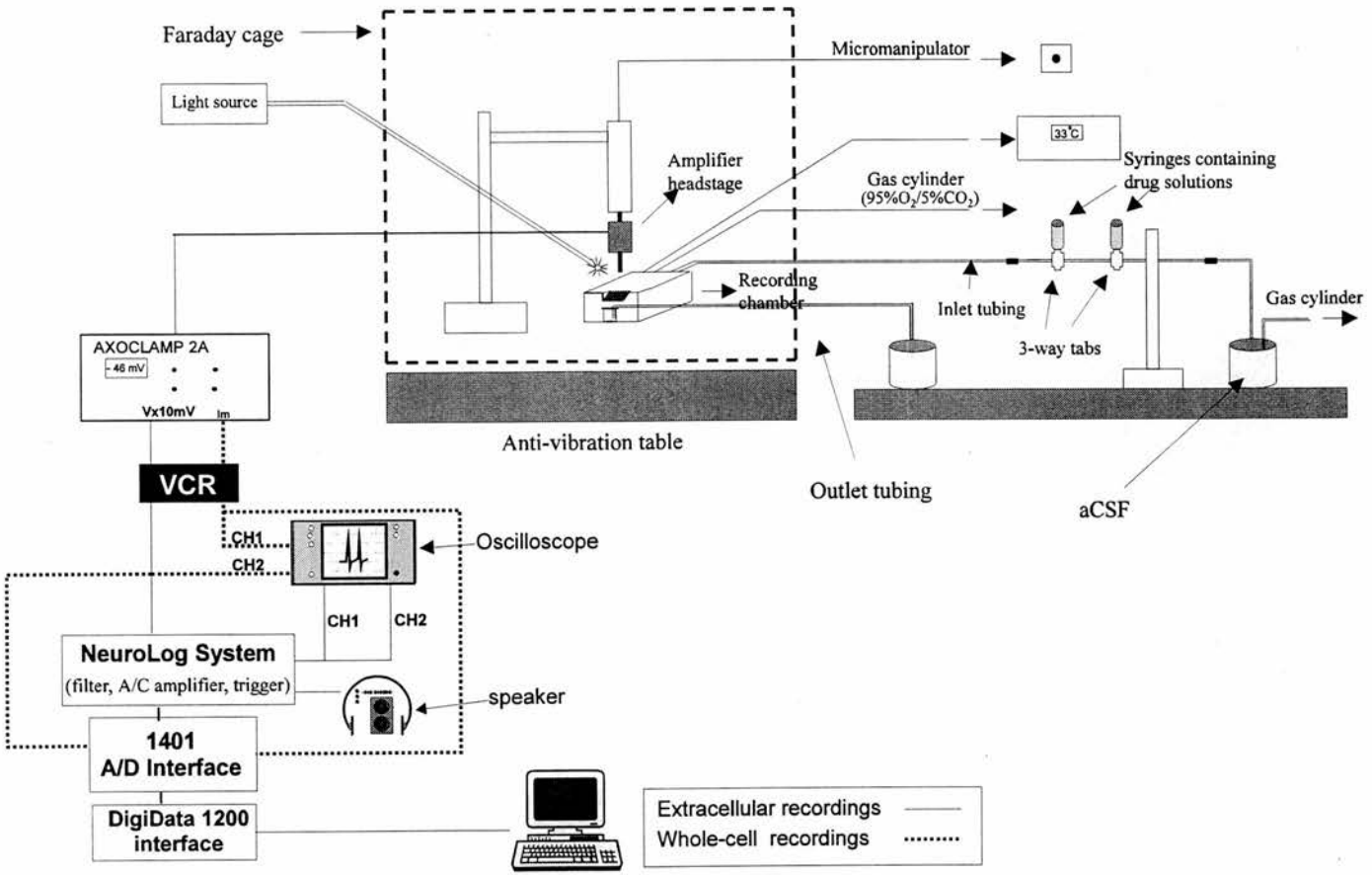

Figure 1.3.2 : Schematic representation of the electrophysiological equipment for extracellular and whole-cell recordings

The NeuroLog system consisted of a filter module (low frequency cut-off 500Hz and high frequency cut-off 5000Hz), an audio amplifier module, a high gain AC amplifier set at a gain of 1000 and a spike discriminator/triggering module. Prior to entering the DigiData 1200 interface, both current and voltage signals were amplified with a gain of x10 and x2 respectively by a conditioning amplifier to optimise digitisation of the signals. In intracellular whole-cell patch clamp experiments, current commands were generated either by the computer using pCLAMP 6.0.2 software from Axon instruments (Foster city, CA, USA) or by a Digitimer D4030 pulse generator (Digitimer, UK). All experimental data were stored for off-line analysis on the computer hard disk and also recorded on VHS video cassettes using a VR-10B digital recorder (Instrutech Corp, USA) and as a hardcopy on Gould TA 240 (GOULD instrument systems ltd, UK) chart recorder.

Recording electrodes and electrode-filling solutions

Extracellular and intracellular whole-cell patch-clamp recordings of spontaneously active MVN neurones were made using filamented standard-wall borosilicate glass microelectrodes (1.5mm outer, 0.86mm inner diameter; Clark Electromedical Instruments, UK). They were fabricated in three stages on a Flaming / Brown horizontal programmable microelectrode puller, Model-P87 (Sutter Instruments, UK) and had tips that were 1-2 μM in diameter. The extracellular microelectrodes were back-filled with 2M sodium gluconate (resistance 10 - 20 MΩ), while for the intracellular whole-cell patch-clamp microelectrodes, they were back-filled with filling solution that is different from extracellular filling solution and containing (mM) 145 potassium gluconate, 2 $MgCl_2$, 5 K_2ATP, 0.1 ethylene glycol-bis (β-amino-ethyl-ether)-*N,N,N,'N'*-tetraacetic acid (EGTA), and 5 *N*-2-hydroxyethylpiperazine-*N'*-2-ethanesulfonic acid (HEPES; pH 7.2, osmolarity adjusted to 290 mosmol, after Kinney *et al.*, 1994) immediately before being used. The intracellular filling solution used through out this study was designed such a way to mimic the intracellular milieu of the MVN neurones. An important consideration in this regard is Ca^{2+} concentration, although it is generally known that the free Ca^{2+} concentration is low inside the cells. EGTA is the most widely used buffer for Ca^{2+}. K_2ATP is used in the filling solution in order to prevent channel 'rundown' due to dialysis of intracellular ATP (Forscher and Oxford, 1985). The filling solution was also buffered at a pH between 7.1 –7.3 with HEPES and stored

frozen in 1 ml aliquots. The microelectrode resistance ranged from 5 to 20 MΩ when filled with internal filling solution.

The microelectrode was then inserted into a Perspex microelectrode holder and the solution was contacted by a silver/silver chloride wire in the holder that was linked to the unity gain headstage of the Axoclamp 2A amplifier. The slice was illuminated with fibre optics and location of MVN was visualised using a binocular-dissecting microscope (Carl Zeiss, Germany). The microelectrode was first lowered and advanced with 3-axis coarse manipulator until it was positioned under visual guidance over the MVN slice and then was further advanced into the slice in 2 μM steps with a Burleigh inchworm controller, PZ-550 (Burleigh Instruments Incorporated, USA).

Extracellular Recordings.

Single extracellular action potentials of the tonic discharge of MVN neurones were made using 2M sodium gluconate containing microelectrodes. The microelectrode was advanced into the MVN tissue as described in above and monitored continuously on the oscilloscope for the appearance of spontaneous extracellular action potentials. The spontaneous extracellular action potentials normally appeared over and above the background noise and increased in amplitude as the microelectrode approached the neurone. Figure 1.3.3 shows an example of extracellular action potentials recorded from a tonically active MVN neurone.

In order to prevent neurone injury or excitation of neurone by the microelectrode and at the same time to obtain a high signal-to-noise ratio with an extracellular action potential, the microelectrode tip position was carefully adjusted backward or forward using manipulator control so that sufficient amplitude of extracellular action potentials could be discriminated and digitised. The amplified and filtered extracellular action potentials were fed to a spike discriminator/triggering module of the NeuroLog System and continuously monitored on the oscilloscope. Proper triggering of the extracellular action potentials were obtained by setting the discriminator level greater than that of the background noise but below than that of the peak of the extracellular action potentials. The pulses that were triggered each

time an extracellular action potential crossed the triggering level were fed to a CED 1401 interface linked to a IBM-compatible. The spontaneous discharge rate of MVN neurones was displayed on-line in the form of frequency histogram (spikes/sec) with the histogram bin width of 1000ms. The program (SCAP 90) was written by Dr. MB Dutia.

The effect of opioid peptides on neuronal activity of medial vestibular nucleus were assessed as follows; After obtaining a stable recording from a single neurone for at least 5 minutes, opioid peptides were applied to the slice and the responses were assessed by observing the changes in discharge rate. Neurones were considered as having been excited or inhibited when their discharge rate showed either an increase or decrease of more than 10% compared with that recorded during 5 minutes control period.

Intracellular Whole-Cell Patch-Clamp Recordings

The effect of opioid peptides on medial vestibular neurones was also studied with the use of the "blind" whole cell recording technique (Blanton *et al.*, 1989; Coleman and Miller 1989). The electrophysiological recordings were carried out in the whole cell current-clamp configuration using recording equipment set up as described above except that the output signals from the high input impedence amplifier, Axoclamp 2A were not delivered to the filter, high gain AC amplifier and the spike discriminator/triggering module of the NeuroLog System. In addition, the side port of Perspex microelectrode holder was connected to 1.0 m PVC tubing (Altec, UK; Bore: 1.5mm, Wall: 1.0mm) for mouth pressure application.

The techniques for establishing a gigaOhm (GΩ) seal in the blind technique is described below and illustrated schematically in figure 1.3.4. Positive pressure was applied to the back of microelectrode by gentle blowing into the PVC tubing that was connected to the side port of the microelectrode holder and closed by means of three-ways tap to retain the positive pressure. This was done in order to prevent clogging of the microelectrode tip during movement through the tissue. The microelectrode was then slowly lowered into the MVN tissue. Offset potential between the reference electrode (Ag/AgCl wire) and the microelectrode was zeroed using the calibrated offset potentiometer control on the Axoclamp 2A amplifier when

the microelectrode touched the tissue. The bridge balance was compensated using a calibrated potentiometer. This gave a measurement of electrode resistance, and this was monitored on the oscilloscope throughout the recording by injecting intermittent 100 ms, -1.5nA DC current pulses using the DC current command control of the amplifier. The microelectrode was then slowly advanced into the tissue in 2 μM steps.

The presence of a cell was indicated by the presence of extracellular action potentials and an increase in resistance by 20-40% of its original amplitude. The positive pressure was then released, thus resulting in a further increase in the resistance if the electrode was indeed contacting a cell. The distance of microelectrode tip to the cell can be gauged by the speed of rebound decrease in the resistance following repeated positive pressure applications by gently blowing into the side-port tube. The closer the cell the faster the rebound. Gentle suction frequently results in the formation of a cell-attached patch. The GΩ seal (1-3 GΩ) usually formed rapidly, within 15 seconds and took a few minutes to improve and stabilise. After formation of GΩ seal between the electrode and the cell membrane, whole cell recording configuration was then achieved by application of additional suction to rupture the membrane patch.

Data Analysis and Presentation

All experimental data from extracellular recordings were continuously displayed on a storage oscilloscope, analysed on-line using Scap90 program and stored on the computer hard disk for off-line analysis. Current command protocols and membrane voltage during whole-cell recordings were continuously observed on a storage oscilloscope and were plotted directly on a Gould TA 240 chart recorder paper (GOULD Instrument Systems Ltd. UK) as well as being digitised and stored for later analyses using pCLAMP software ver. 6.0.2 (Axon Instruments, Inc, USA). Neurones obtained from whole-cell recording were accepted for analysis if they had a stable resting membrane potential, an overshooting action potential of greater than 40 mV amplitude and input membrane resistance of greater than 100 MΩ. Discharge rate histograms of extracellular firing rate and figures of whole-cell recordings were constructed for publication from selected data files using CorelDraw version 5.0 software (Corel Inc, Canada). Numerical results in this study

are expressed as mean values ± S.E of mean. Student's *t* test was used for statistical comparison between groups based on the estimation of the mean and standard deviation of the samples, after confirming that the samples were drawn from normally distributed populations (Sigmastat, Jandel Scientific, Germany), with $P < 0.05$ being the criterion for statistical significance.

The experimental protocol involved measuring the following parameters: -

The resting membrane potential

Since most neurones of MVN are tonically active, it was not possible to record a "resting" membrane potential (RMP) of these neurones. However, the measurement for the RMP was taken as the membrane potential value displayed on the digital voltmeter display of the Axoclamp amplifier. This was the time-averaged value of the cell membrane potential (Johnston *et al.*, 1994). The resting membrane potential was corrected by subtracting the offset value read directly from the voltmeter display of the Axoclamp 2A amplifier after withdrawing the microelectrode from the neurone at the end of the recording. The RMP value during whole cell configuration was taken when there was no depolarising or hyperpolarising DC current injected through recording electrode.

The spontaneous discharge rate

The measurement of spontaneous discharge rate of tonically active MVN neurones was made by recording the spontaneous action potentials at 'resting' membrane potential (i.e with no current being injected into the cell) for 15 seconds using the Fetchex program and was calculated automatically using Fetchan program, of the PCLAMP software suite.

The membrane input resistance

The membrane input resistance before, during and after drug responses was determined from the current-voltage (I-V) curves. The I-V relationships were obtained by injecting a series of constant depolarising and hyperpolarising current step commands of 40 pA increments from – 460 pA that were applied for 200 ms duration. In all measurements the membrane potential of the spontaneously active MVN neurones was hyperpolarised 10 or 20 mV below the threshold for action

potential generation by applying continuous negative current through the recording microelectrode, in order to stop the spontaneous resting discharge.

The averaged action potential shape

These procedures were adapted from the previous study of MVN neurones *in vitro* by Johnston et al 1994. The action potential shape of the spontaneously active MVN neurone was obtained by digitising the intracellularly recorded membrane potential at 40 kHz for a period of two seconds while the cell at its 'resting' membrane potential (i.e. when neither positive nor negative DC current was injected through recording microelectrode). The time of occurrence of the peak of each spontaneous action potential was located in the digitised data, and the membrane potential over a 20 ms window around each of these times was averaged to give an action potential shape synchronised to the peak of the spike (Fig. 1.3.5).

Since the membrane potential in spontaneously active MVN neurones was always gradually depolarising before the discharge of an action potential, it was not possible to make an objective measurement of the firing threshold from the averaged spike shape itself. Instead the averaged action potential shape was differentiated twice and the firing threshold was taken to be the membrane potential at the point when the second derivative became greater than 2 times its own noise level (Johnston *et al.*, 1994). The action potential rise time was measured as the time from the firing threshold to the peak of the averaged action potential and the fall time was measured as the time to return from the peak to the threshold level (see fig. 1.3.5). The amplitudes of the after-hyperpolarisation were also measured with respect to the firing threshold. The action potential width was measured both as the width at threshold (W_T) and as the width at half-height (W_H).

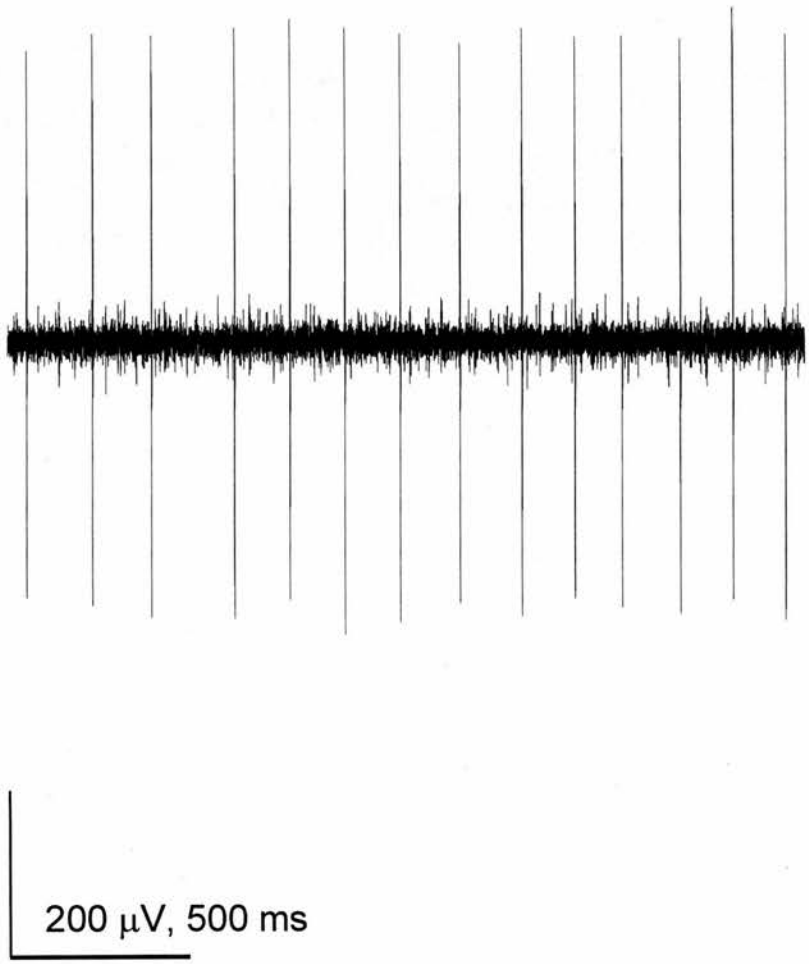

Figure 1.3.3 : An example of an extracellular recording of the action potentials fired by a spontaneously active MVN neurone in a dorsal brainstem slice preparation.

Legend 1.3.4 : Whole-cell patch-clamp techniques (blind patch)

Schematic representation of procedures for obtaining whole-cell recordings. (A and B) Neurones are detected by monitoring the microelectrode resistance as its lowered through the slice. Cell contact occludes the microelectrode tip, causing an increase in microelectrode resistance. The application of gentle pressure removes the obstruction, restoring the microelectrode resistance. (C) If the microelectrode is against a cell, then the resistance will increase when the pressure is released because of elastic recoil of the cell. The speed of recoil is used to gauge the closeness of the microelectrode's tip and cell membrane. (D) Application of gentle suction at this stage results in the formation of gigaOhm seal. (E) Further suction breaks the membrane within the microelectrode giving the whole-cell configuration.

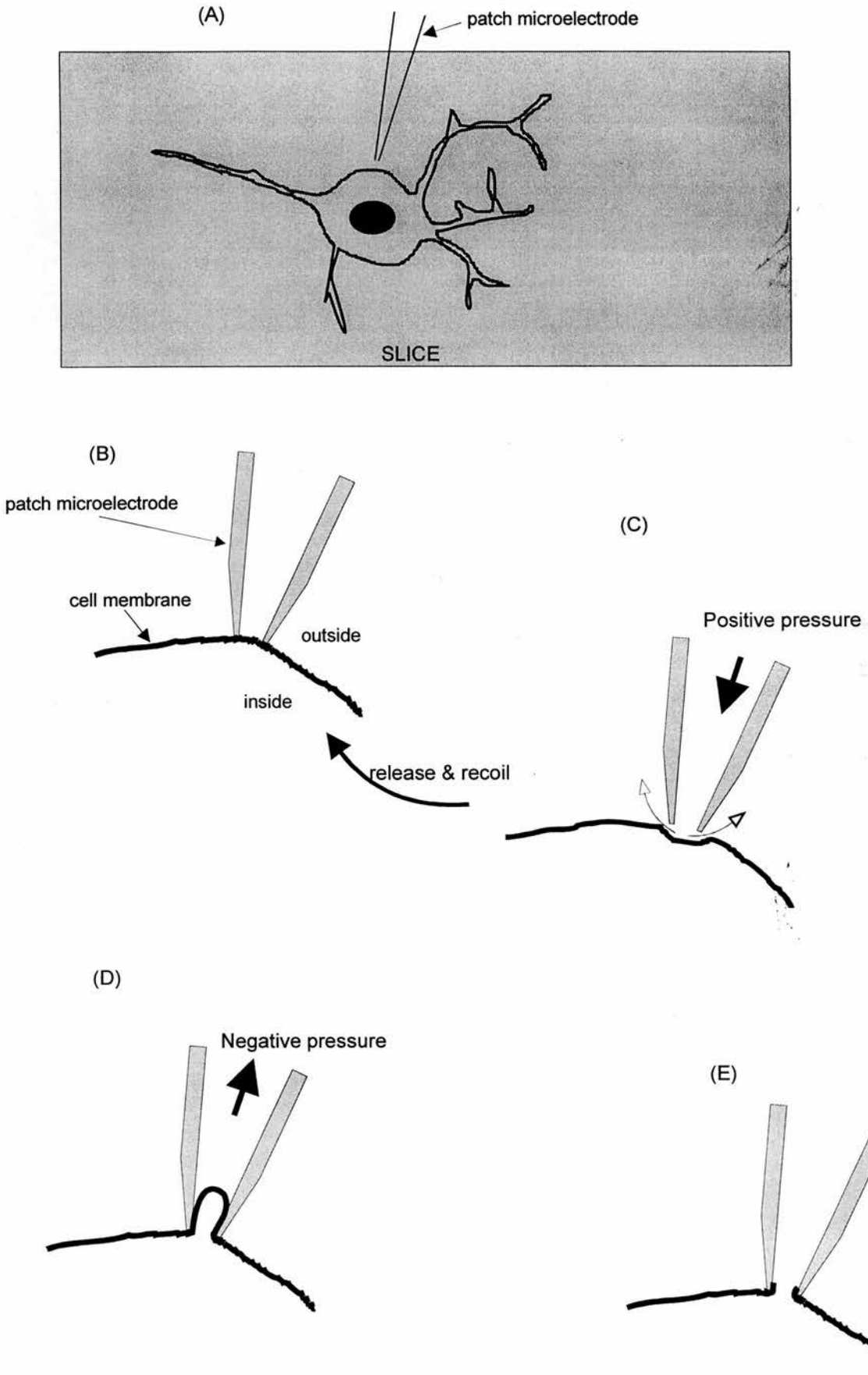

Figure 1.3.4 : Schematic diagram of procedure for obtaining whole-cell patch-clamp

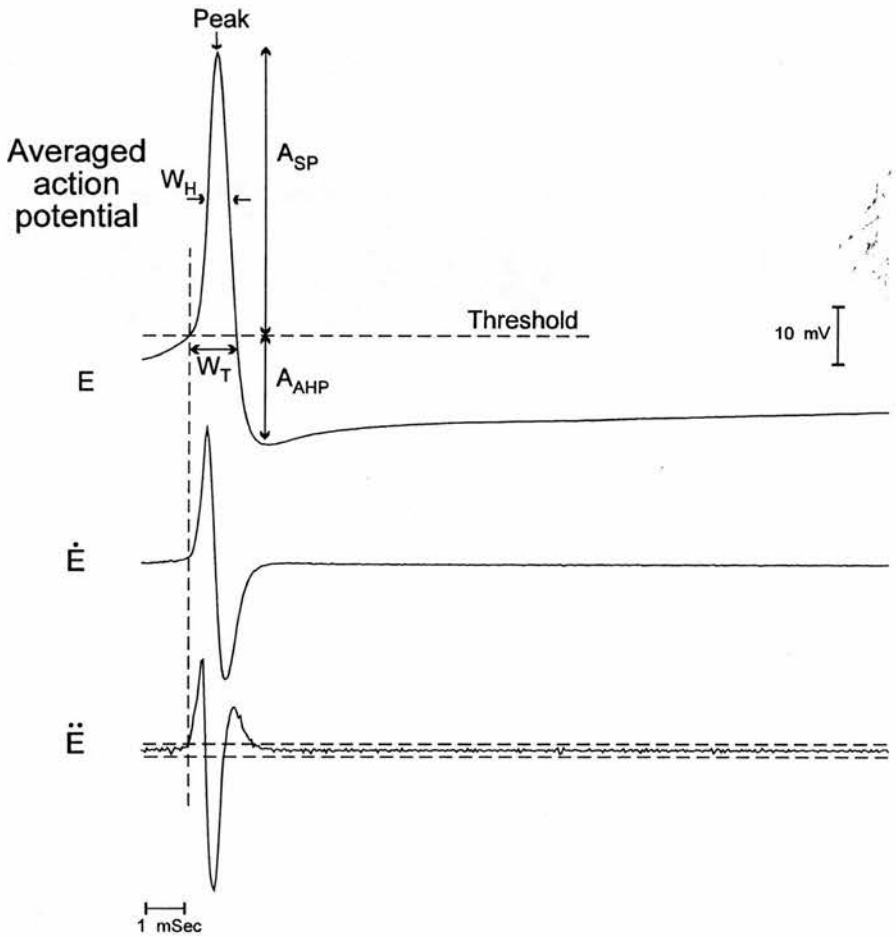

Figure 1.3.5 : Analysis of the average action potential shape

Upper trace, Averaged action potential shape (E) obtained by averaging the membrane potential over a 20ms window synchronised to the peak of each successive spike in the resting discharge of one MVN neurone, with 1.25 ms pre-trigger period (see text). Middle and lower traces, first (Ė) and second (Ë) differentials of the averaged spike shape, calculated by taking simple differences between successive points. Horizontal dashed lines in the lower panel indicate the level corresponding to twice the noise amplitude in the last 5 ms of this trace. The vertical dashed line indicates where the second differential becomes greater than this level, and the corresponding points in the averaged spike shape (upper trace) which is taken as the onset of the rising phase of the action potential (firing threshold). W_T, spike width at firing threshold; W_H, spike width midway between firing threshold and peak; A_{AHP}, amplitude of AHP with reference to firing threshold; A_{SP}, spike amplitude. Rise time was measured as the time from firing threshold to peak, and fall time as the time from peak to firing threshold.

(Adapted from Johnston *et al.*, 1994)

1.4 RESULTS

Stable extracellular recordings lasting up to 3 hours were obtained from a total of 127 spontaneously active neurones within the medial vestibular nuclei in horizontal slices of the dorsal brainstem from 45 rats. Consistent with the previous studies (Dutia *et al.*, 1992, Wang and Dutia, 1995), all neurones recorded in this study showed steady and regular resting discharge rates ranging from 7.0 to 41.4 spikes/sec, with a mean discharge rate of 21.3 ± 0.6 spikes/sec (mean ± S.E.M).

Opioid inhibition and opioid receptor subtypes on MVN neurones

The response of the MVN neurones to bath application of the selective δ-opioid receptor agonist [D-Ala^2, D-leu^5]-enkephalin (DADLE, 1-100 μM), the μ-opioid receptor agonist morphine (1-100 μM), and the selective κ-opioid receptor agonist, U50,488H (1-100 μM) were examined systematically. The results are summarised in table 1.4.

Bath application of DADLE produced a dose-dependent, long-lasting inhibition, seen as a decrease in the spontaneous discharge rate of 102/127 (80%) of the MVN neurones, the remaining 25 neurones (20%) being unresponsive to DADLE at doses up to 100 μM. The maximum inhibitory effect of DADLE was seen within 1-2 min of the peptide reaching the recording chamber, and complete recovery of the firing rate to the control level was normally seen within 15-30 min after washing out of DADLE with normal aCSF medium, (Figs. 1.4.1.1 – 1.4.1.6). The inhibitory effects evoked by DADLE were reproducible with repeated application of the peptide. Figures 1.4.1.1 and 1.4.1.2A show representative examples of the effect of successively increasing concentrations of the peptide.

To determine whether DADLE affects the MVN neurones directly or through presynaptic actions, modified low Ca^{2+}, high Mg^{2+} aCSF medium was used. This medium is essentially known to eliminate all synaptic transmission through blockade of transmitter release at the presynaptic terminal (Lu *et al.*, 1995, Lin and Carpenter 1994). If the inhibitory effect of DADLE is mediated by activation of postsynaptic receptors on medial vestibular neurones, rather than through presynaptic actions, the inhibitory effect of DADLE should therefore be maintained even when synaptic

transmission is completely blocked. In five experiments, the inhibitory responses of MVN cells to DADLE were recorded first in normal aCSF medium and repeated subsequently in modified low Ca^{2+}, high Mg^{2+} aCSF medium (0.1mM Ca^{2+}, 6.3 mM Mg^{2+}). Two of these experiments are illustrated in figure 1.4.1.3. In all 5 MVN neurones tested in this way, the inhibitory response to DADLE persisted in low Ca^{2+}, high Mg^{2+} aCSF, and remained similar to the control response in normal aCSF, indicating that the effects of DADLE are mediated by its actions on postsynaptic opioid receptors on the MVN cells, *in vitro*.

As illustrated for two different MVN neurones in Figures 1.4.1.4 to 1.4.1.6, the inhibitory effects of DADLE were mimicked by the highly-selective δ-opioid receptor agonist [D-Pen^2, Pen^5]-enkephalin (DPLPE, 1-10 μM, n = 10 cells). As illustrated for two representative neurones in figures 1.4.1.5 and 1.4.1.6, perfusion with non-selective opioid antagonist, naloxone (10 mM, Fig. 1.4.1.5B) and highly selective δ-opioid receptor antagonist, naltrindole (10-100 nM, Fig. 1.4.1.6B), which themselves had no direct effect on the discharge rate of MVN neurones, effectively antagonised the inhibitory effects of DADLE and DPLPE in all 6 MVN cells where this was tested.

By contrast, as illustrated in figures 1.4.1.2C and 1.4.1.4B the μ-opioid receptor agonist morphine (up to 100 μM) had no effect on the discharge rate of any of the 33 MVN neurones tested. In addition, the highly selective μ-opioid receptor agonist, [D-Ala^2,N-Me-Phe^4,Gly^5-ol]-enkephalin (DAGO, 1-10 μM), also had no effect on the discharge rate of any of the six MVN cells tested (Fig. 1.4.1.4B). The κ-opioid receptor agonist U50488H (up to 100 μM) also had no effect on the tonic discharge rate of all 30 MVN cells tested (e.g. Fig. 1.4.1.2B and 1.4.1.4B). These results strongly indicate the presence of δ-opioid receptors and not μ and κ-opioid receptors on rat MVN neurones.

Excitatory effects of opioids on MVN neurones

Weak excitatory responses were seen at high concentrations (30 and 100 μM) of the DADLE in only two MVN neurones, which are illustrated in figure 1.4.1.7. Neither of these MVN cells responded to lower doses of DADLE. Since these

TABLE 1.4

SUMMARY OF NEURONAL ACTIVITY CHANGES IN RESPONSE TO BATH APPLICATION OF OPIOID AGONISTS ON MVN NEURONES.

Opioid agonists	EXCITATION	INHIBITION	NO EFFECT
DADLE (n = 54 neurones)	0	48 (89%)	6 (11%)
Morphine (n = 17 neurones)	0	0	17 (100%)
U50 488H (n = 15 neurones)	0	0	15 (100%)

DADLE, [D-Ala^2, D-Leu^5]enkephalin; **U50 488H,** *trans*-(+)-3,4-dichloro-*N*-methyl-*N*-[2-(1-pyrro-lidinyl)-cyclohexyl]-benzeneacetamide methane sulphonate.

Legend 1.4.1.1 : Dose-dependent inhibition of a medial vestibular nucleus (MVN) neurone.

Discharge rate histograms showing a dose-dependent inhibition of a single MVN neurone to three different concentrations (3 μM - 30μ M) of the selective δ-opioid receptor agonist [D-Ala^2, D-Leu^5]-enkephalin (DADLE). In this neurone bath application of DADLE caused a dose-dependent, long-lasting inhibition of the spontaneous discharge rate. In this and the following figures, the bars above the data indicate the 60-sec period of application of the agonists, corrected for the lag-time in the inlet tubing

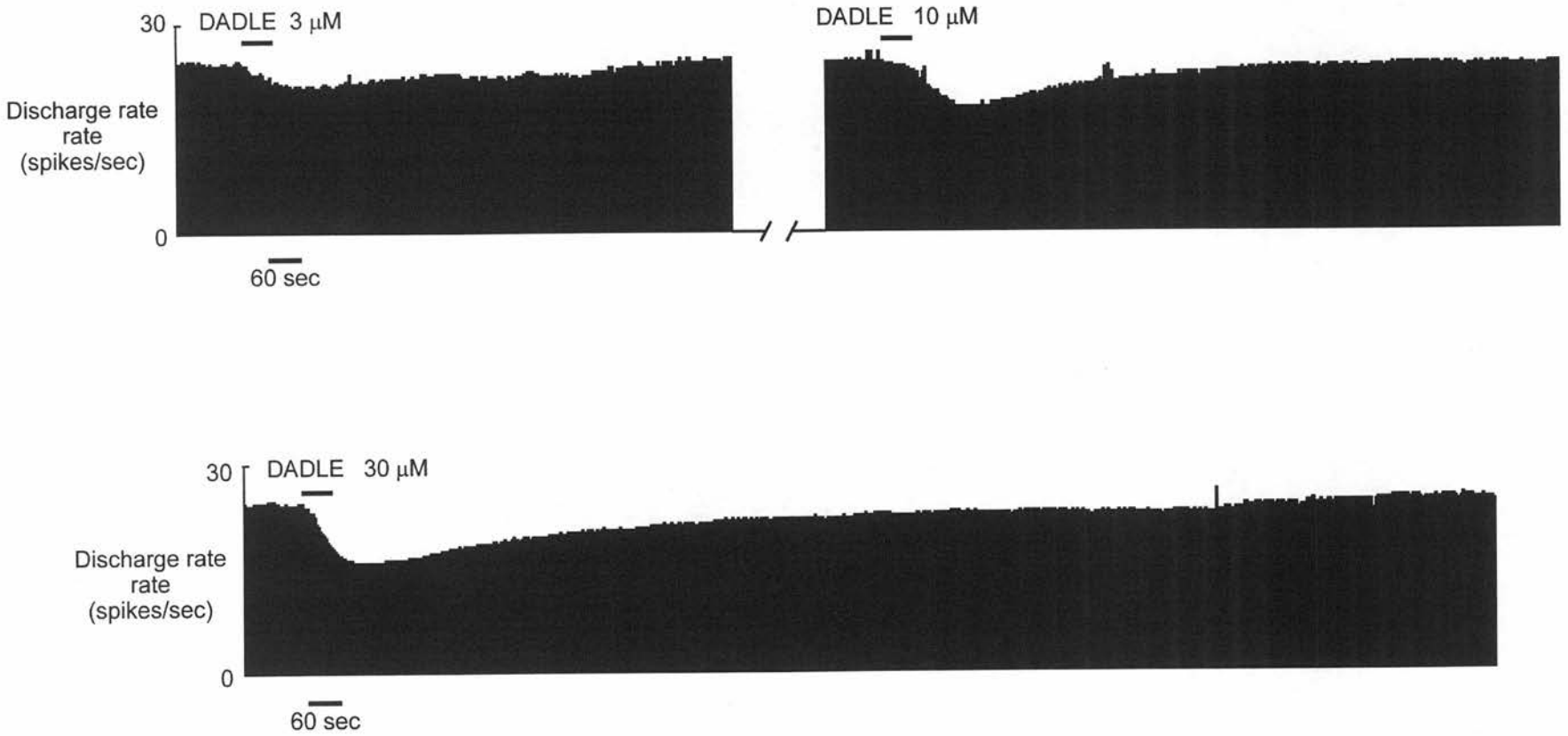

Figure 1.4.1.1 : Dose-dependent inhibition of a single MVN neurone

Legend 1.4.1.2 : Inhibition induced by selective δ-, but not μ- or κ-opioid receptor agonist.

Discharge rate histograms illustrating the response of a single MVN neurone to the selective δ-opioid receptor agonist, DADLE, the μ-opioid receptor agonist, morphine and the selective κ-opioid receptor agonist, U50 488H. During the periods indicated by the bars, the superfusion solution was changed to the one, which contained the substance indicated. (A) Another example of dose-dependent, long-lasting inhibition of the spontaneous discharge rate evoked by DADLE. (B and C) examples of lack of effect of the κ- and μ-opioid receptor agonists on the discharge rate of this MVN neurone.

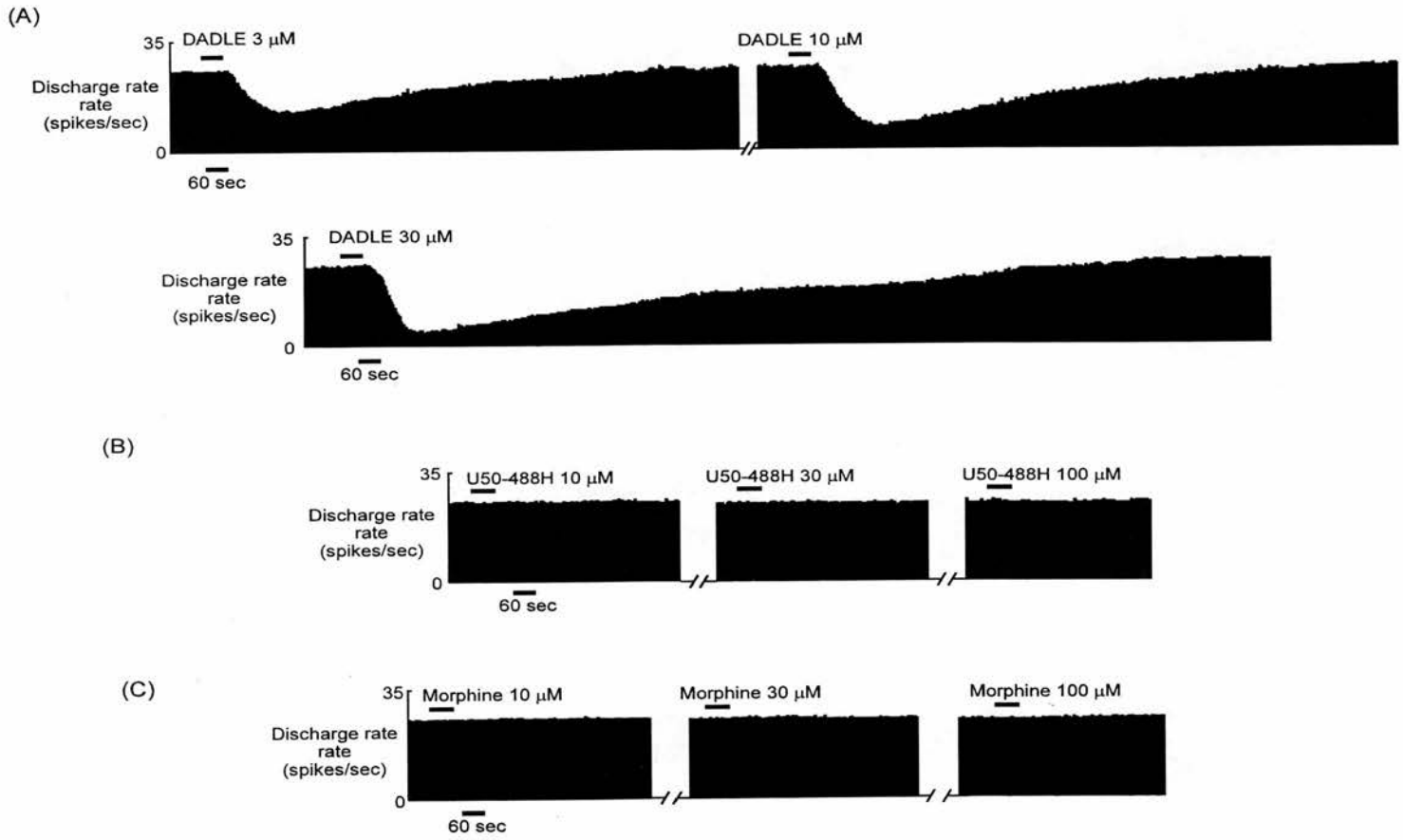

Figure 1.4.1.2 : Inhibition induced by selective δ-, but not μ- or κ-opioid receptor agonist

Legend 1.4.1.3 : Persistence of DADLE-induced inhibition during elimination of synaptic transmission.

Discharge rate histograms showing the response of two typical tonically-active MVN neurones to a 60 sec test pulse of the selective δ-receptor agonist DADLE in normal aCSF (A and C) and in low Ca^{2+}, high Mg^{2+} aCSF (B and D). Note the early increase in the tonic discharge rate of the cell after about 1 minute in the modified aCSF (arrows), indicating the blockade of synaptic transmission in the slice which in these cells presumably removed an endogenous net inhibitory influence on the tonic discharge rates of these cells

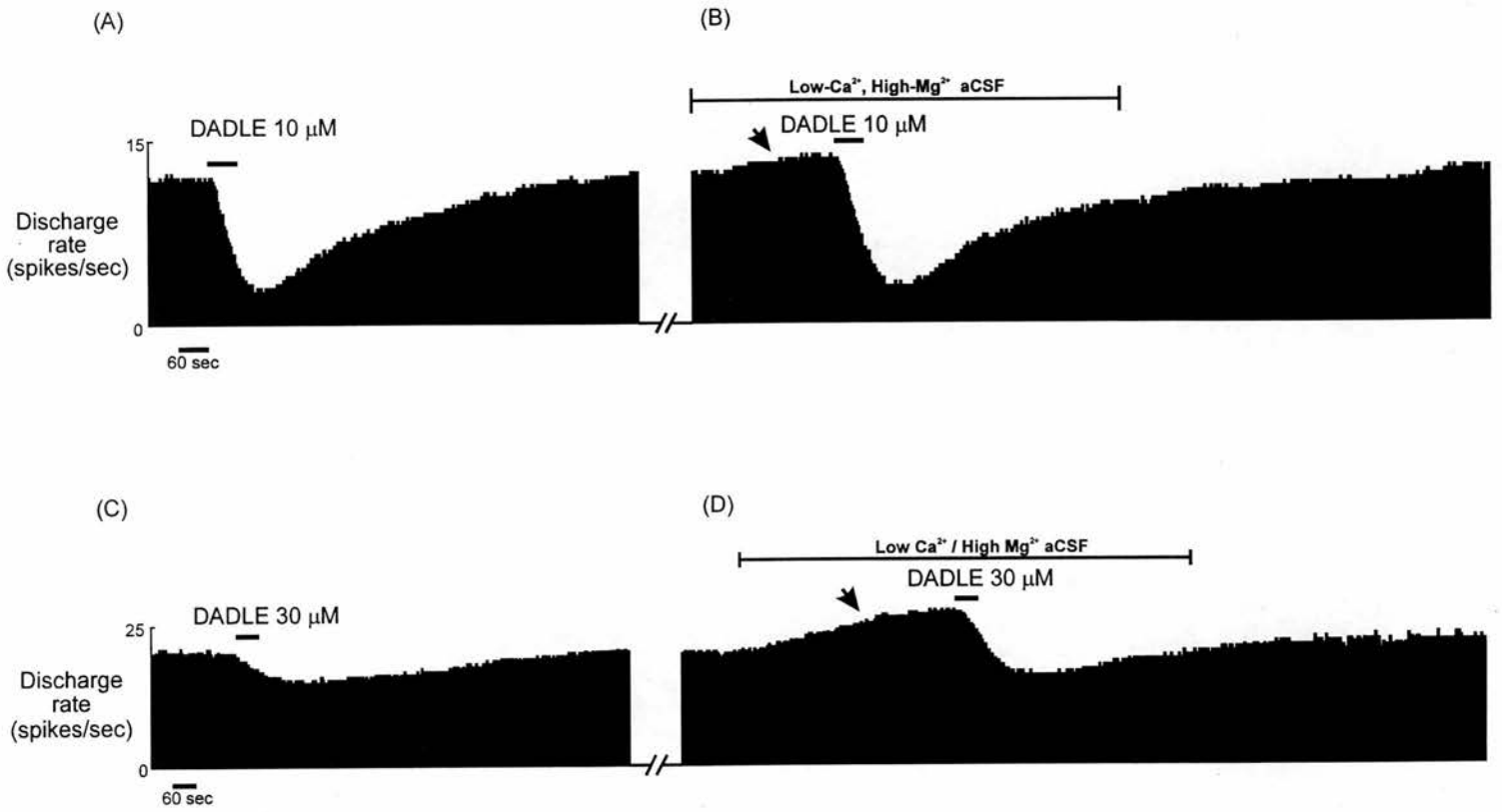

Figure 1.4.1.3 : Persistence of DADLE-induced inhibition during elimination of synaptic transmission by perfusion with low Ca2+, high Mg2+

Legend 1.4.1.4 : Comparison of the effects of various opioid peptide agonists on the spontaneous discharge rate of a single MVN neurone.

(A) DADLE-induced inhibition of MVN neurone was mimicked by highly selective δ-opioid receptor agonist [D-Pen^2, Pen^5]-enkephalin (DPLPE). (B) The κ-opioid receptor agonist U50,488, the μ-opioid receptor agonist morphine and highly selective μ-opioid receptor agonist [D-Ala^2 ,N-Me-Phe^4, Gly^5-ol]-enkephalin (DAGO) had no effect on the discharge rate of this MVN neurone.

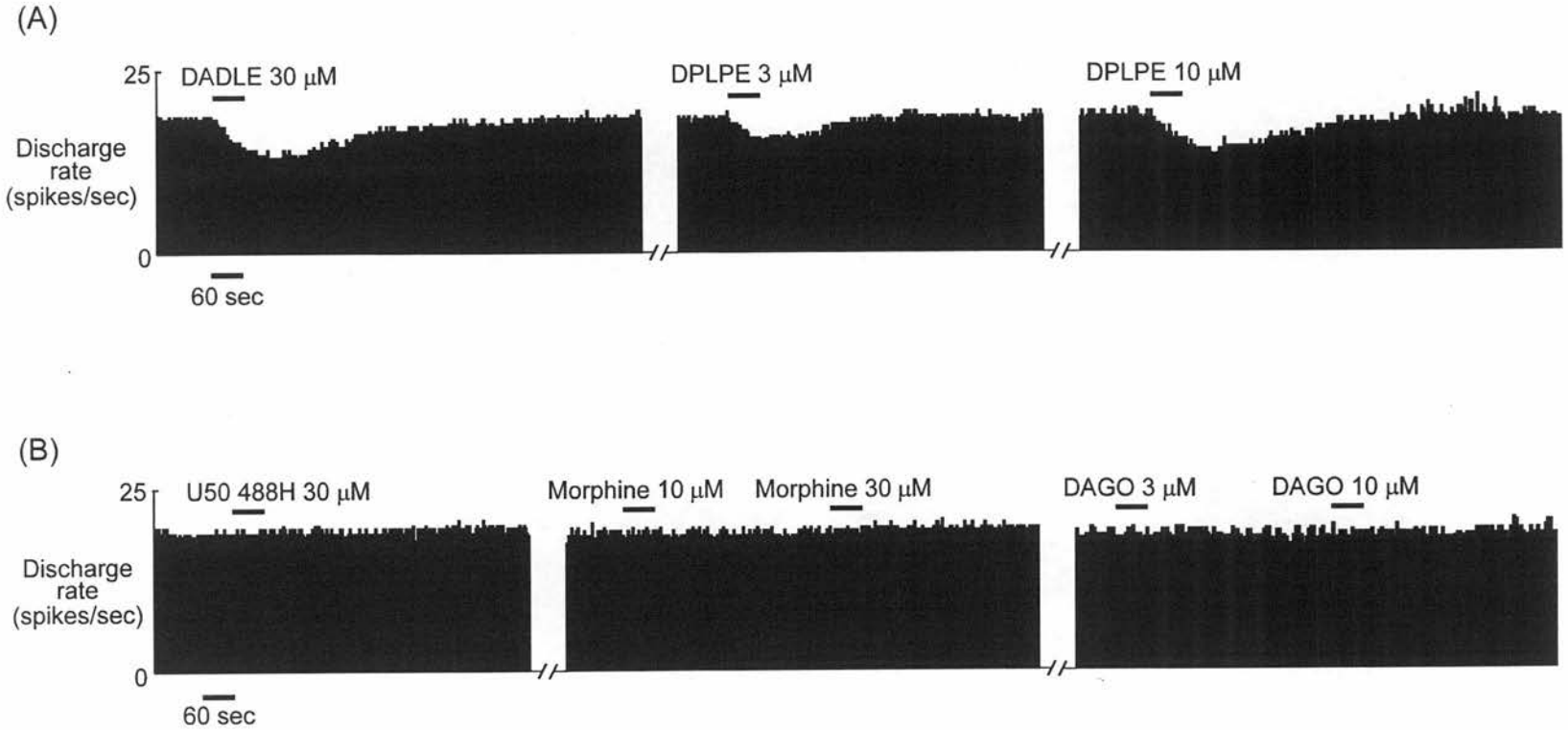

Figure 1.4.1.4 : Comparison of the effect of various opioid peptide agonists on the spontaneous discharge rate of a single MVN neurone

Legend 1.4.1.5 : Naloxone antagonism of DADLE and DPLPE induce inhibition on tonic discharge rate of a single MVN neurone.

(A) DADLE (10 μM) and DPLPE (3 μM)-induced inhibition of MVN in normal aCSF. (B) Non selective opioid receptor antagonist, naloxone (10mM) equilibrated with the slice for 10 minutes inhibited the response of DADLE and DPLPE.

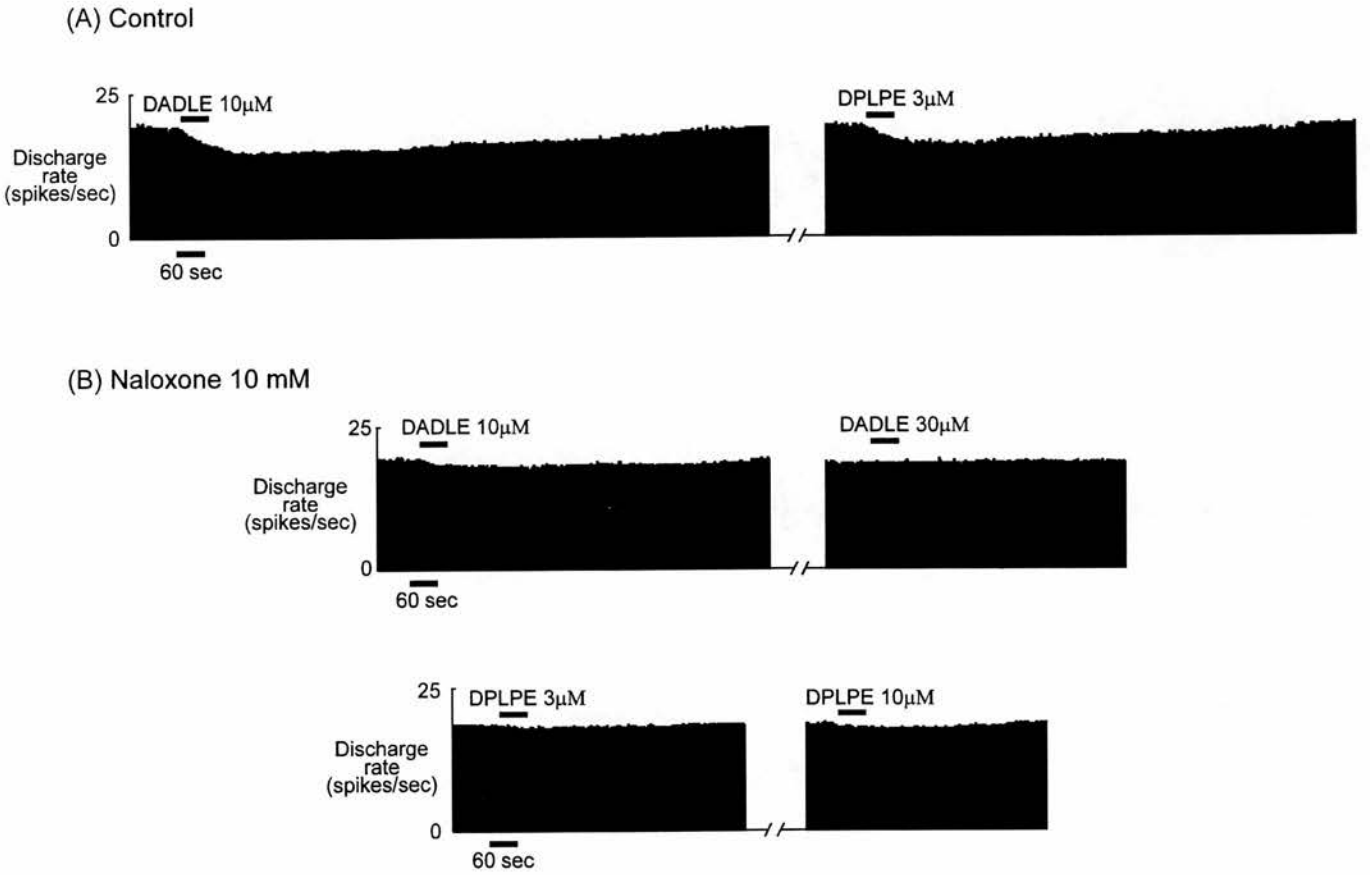

Figure 1.4.1.5 : Naloxone antagonism of DADLE and DPLPE-induced inhibition of spontaneous discharge rate of a single MVN neurone

Legend 1.4.1.6 : Antagonism by naltrindole of DADLE and DPLPE induce inhibition.on tonic discharge rate of a single MVN neurone.

(A) Inhibitory effects of DADLE and the highly-selective δ-agonist DPLPE on the tonic discharge of an MVN neurone. (B) The highly selective δ-opioid receptor antagonist, naltrindole (100 nM, equilibrated with the slice for 10 minutes) effectively antagonised the inhibitory responses to DADLE and DPLPE, seen as the reduced responses to DADLE and DPLPE in the presence of the antagonist.

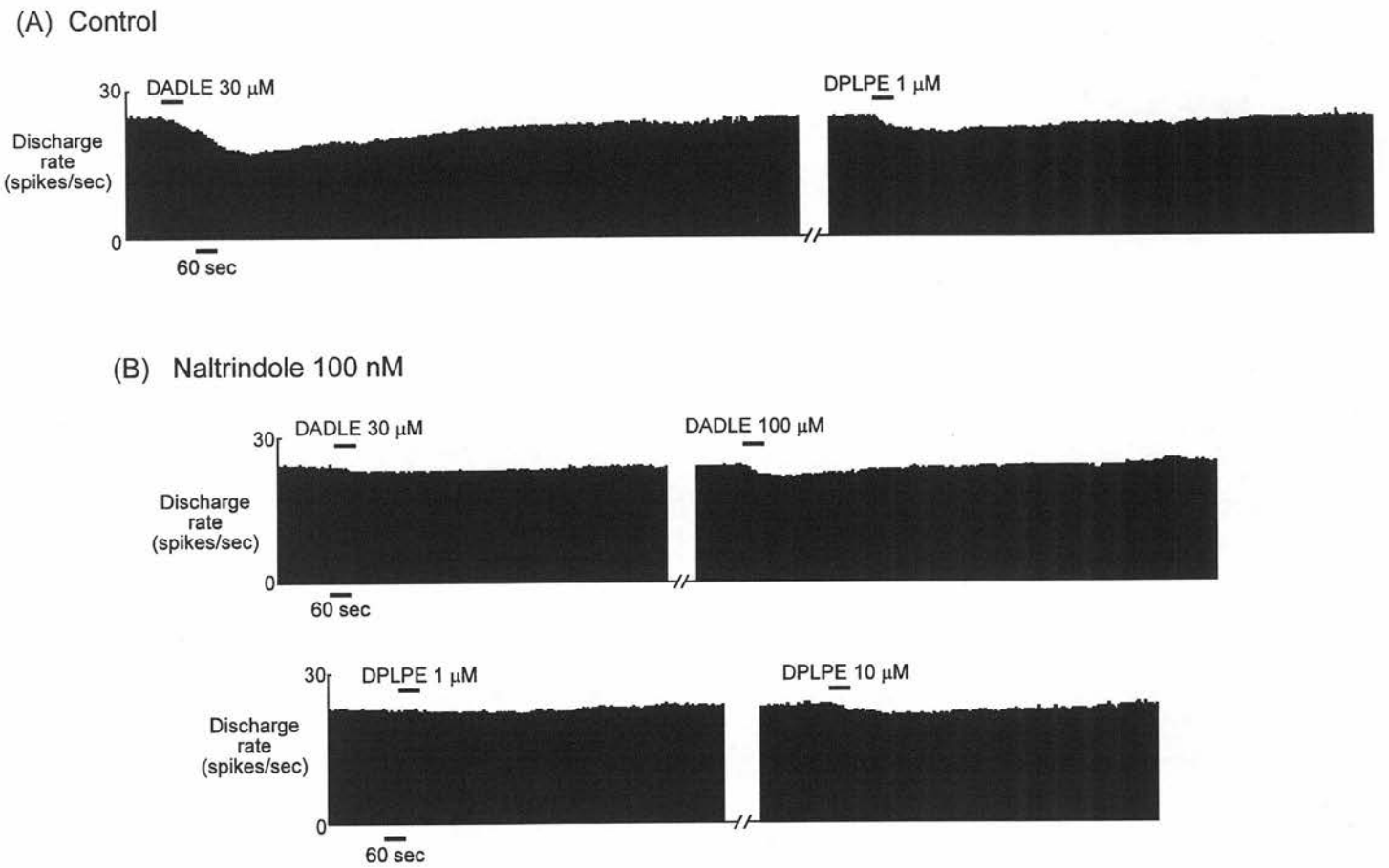

Figure 1.4.1.6 : Antagonism by naltrindole of DADLE and DPLPE-induced inhibition on spontaneous discharge rate of a single MVN neurone.

Legend 1.4.1.7 : Weak, excitatory responses to high doses of DADLE seen in two different MVN neurones.

(A) A small delayed excitation following the application of DADLE. (B) A small long-lasting excitation following the application of DADLE. Neither neurone responded to lower concentration of DADLE [10 - 30 μM for the cell in (A) and for the cell in (B)]

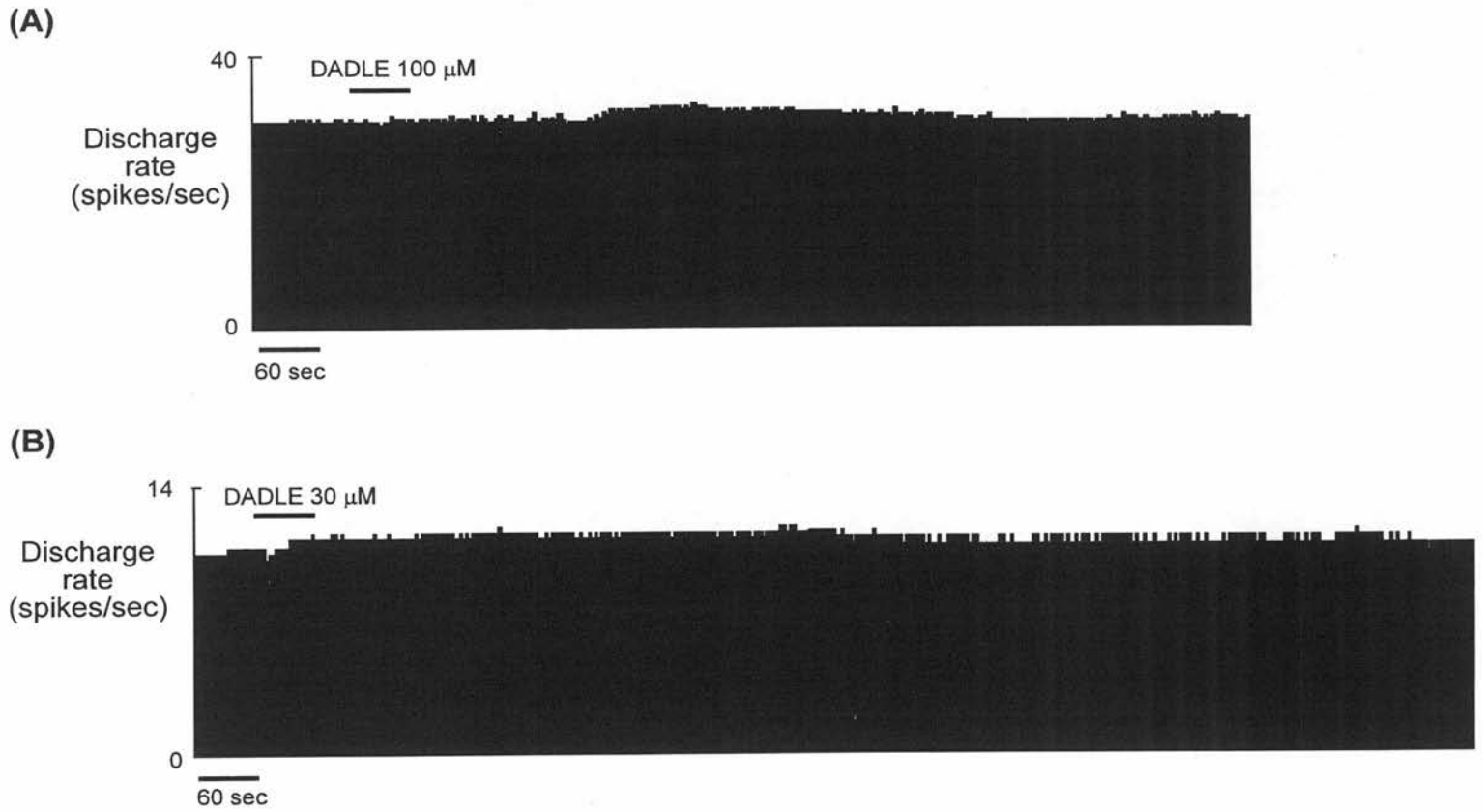

Figure 1.4.1.7 : Weak, excitatory responses to high doses of DADLE in two different MVN neurones.

excitatory effects were too small to be considered significant (less than 5% change relative to the control resting discharge rate); they were not investigated further. It is likely that these small excitations are secondary to the inhibitory effect of DADLE on other cells, which are synaptically connected to them.

Effects of DADLE on membrane properties of MVN neurones

In 19 further experiments, intracellular whole-cell patch recordings were obtained from MVN neurones and the effects of DADLE on the membrane potential and intrinsic conductances were investigated. The 19 MVN neurones had a mean resting membrane potential of –45 ± 0.6 mV, steady resting spontaneous activity of 23.5 ± 0.9 spikes/sec, spontaneous action potentials of greater than 40 mV in amplitude and the membrane input resistance was in the range 100 to 250 MΩ. From the averaged action potential shapes taken from tonically active MVN neurones over a period of 2-secs, two main distinct neuronal cell types were identified, namely Type A and Type B MVN neurones (Johnston *et al.*, 1994). Figure 1.4.1.8 shows examples of average action potential shapes in 2 different types of spontaneously active MVN neurones. Of the 19 MVN neurones, 6 (32%) cells had a single deep after-hyperpolarisation (AHP) following their spontaneous action potential and were characterised as Type A cells, while the remaining 13 (68%) neurones were characterised as Type B cells as they showed an early fast AHP and a delayed slow AHP (Serafin *et al.,* 1991, Johnston *et al.,* 1994). The membrane properties of both Type A and Type B MVN neurones are summarised in figure 1.4.1.9. Except for the properties of AHP described, there were no other differences in the membrane properties of type A and type B neither in their resting membrane potential, input resistance nor their steady resting spontaneous activity.

Bath perfusion of DADLE (3-100 μM) caused a membrane hyperpolarisation and inhibition of the tonic discharge in 18/19 (95%) of the MVN neurones tested. Five of these neurones are illustrated in figures 1.4.2 to 1.4.2.3 In some of these experiments the extracellular K^+ concentration was reduced to 2.0 mM ("low-K^+ aCSF"), in order to increase the prominence of K^+ mediated effects on membrane conductance. In low-K^+ medium, the neurone shown in figure 1.4.2 showed a marked membrane hyperpolarisation (arrow) and cessation of its tonic firing following the application of DADLE. The membrane hyperpolarisation gradually

reversed with the return of resting activity over the following seven minutes. As indicated by the smaller voltage responses to the hyperpolarising current pulses applied every 10-sec (downward deflections in Fig. 1.4.2), the DADLE induced inhibition was accompanied by a decreased input membrane resistance or an increase in the cell membrane conductance. A decreased in input membrane resistance is more clearly seen in the neurones illustrated in figures 1.4.2.1 and 1.4.2.2, where depolarising and hyperpolarising current pulses were applied before the application of DADLE (control) and during the maximal DADLE-induced inhibition, at a manually-clamped holding potential of -60 mV. From the slopes of the regression lines fitted to the steady-state membrane current/voltage relationships the apparent input resistance of these cells were seen to decrease in the presence of DADLE (Figs. 1.4.2.1C and 1.4.2.2C).

In 4 MVN neurones the membrane current evoked by DADLE was recorded under voltage-clamp configurations, also in low-K^+ aCSF and in the presence of TTX (1μM, Figs. 1.4.2.3), in order to eliminate the spontaneous Na^{2+} spikes. Bath application of DADLE for 60-seconds induced a dose-dependent outward current in all 4 neurones tested in this way. Each of these neurones was then exposed to 20 mM potassium channel antagonist, TEA in order to determine if voltage-activated potassium currents contributed to this outward current. As illustrated for 2 neurones in figure 1.4.2.3, the outward current evoked by DADLE after 15 minutes exposure to TEA became smaller in amplitude but was not abolished, indicating that the inhibition and membrane hyperpolarisation of MVN neurones evoked by DADLE involves the potentiation of TEA-sensitive potassium conductances in the cell membrane.

Age-related effects of DADLE on MVN neurones

In the course of these experiments it became apparent that the degree of inhibition of the tonic discharge of the MVN neurones evoked by DADLE tended to be greater in slices prepared from older animals. This was quantified by expressing the frequency of discharge during the maximal inhibitory effect of DADLE as a percentage of the control (pre-DADLE) resting discharge rate, for each neurone. Figure 1.4.2.4A shows the mean percentage inhibition (± S.E.M) induced by a standard dose of 30 μM DADLE in all the MVN cells tested, as a function of the

body weight of the animal which was recorded before the preparation of the slice. The inhibitory effects of DADLE were relatively small in the youngest animals used here, and increased significantly with age. As shown in figure 1.4.2.4B, there was no systematic change in the mean *in vitro* resting discharge rates of the MVN cells over the age range used in these experiments. Figure 1.4.2.5 illustrating the percentage of responsive MVN neurones at different ages to bath application of DADLE.

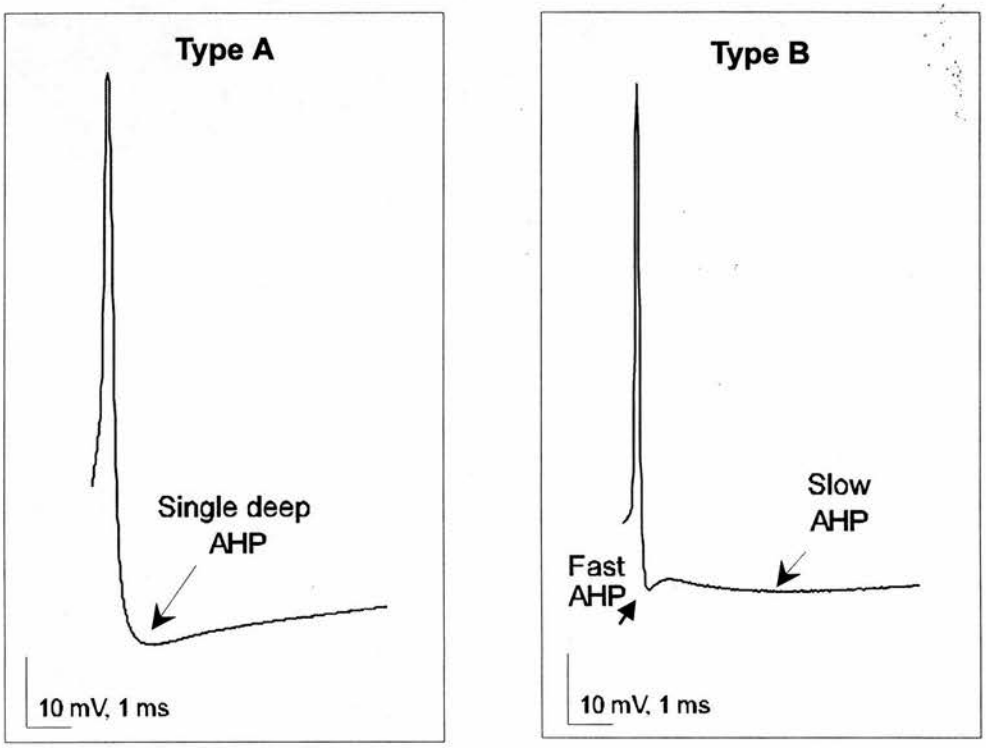

Figure 1.4.1.8 : Averaged action potential shapes of Type A and Type B MVN neurones

Two main distinct neuronal types from two different spontaneously active MVN neurones, Type A and Type B.

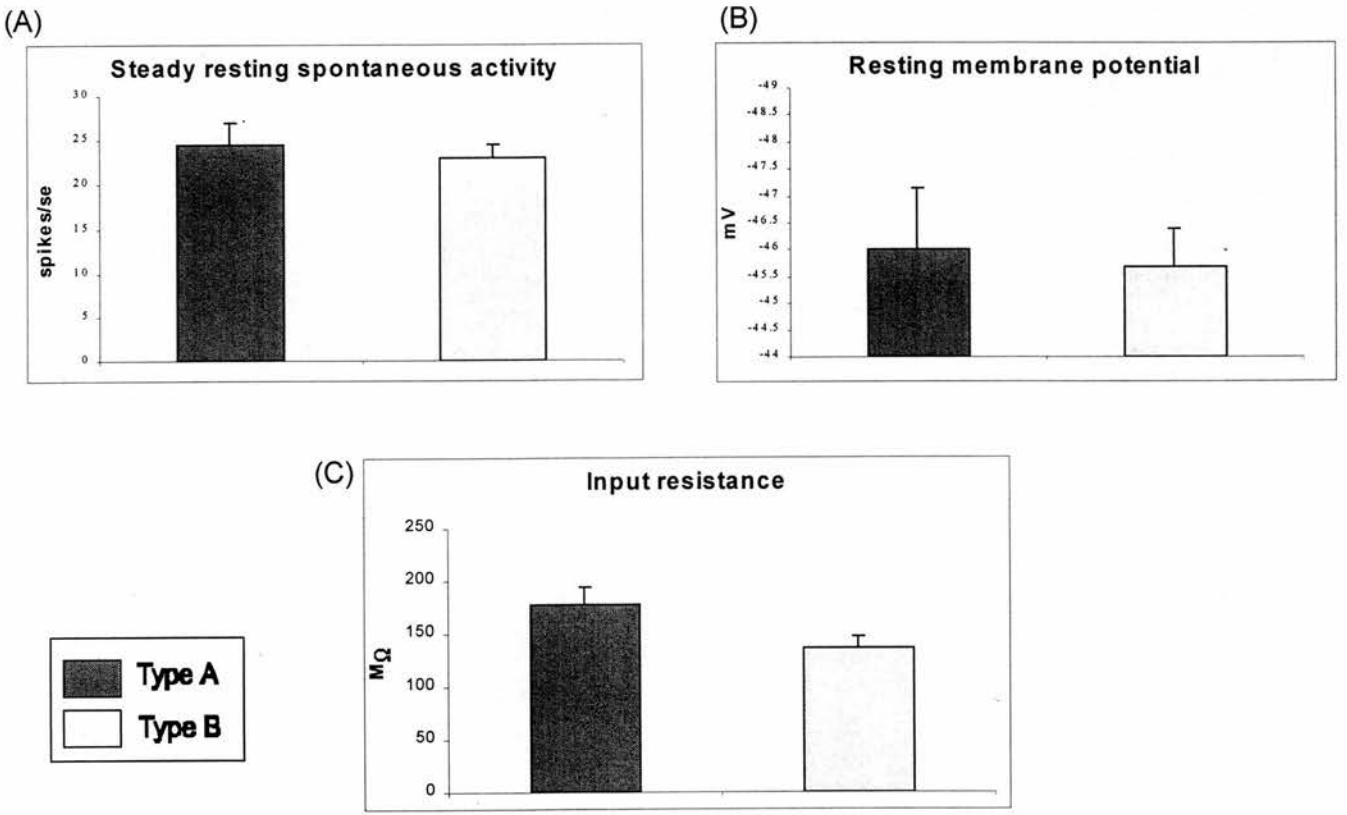

Figure 1.4.1.9 : Basic membrane properties of Type A and Type B MVN neurones

Histograms showing the overall mean (±S.E.M) of basic membrane properties of identified Type A and Type B neurones.

Figure 1.4.2 : DADLE-induced hyperpolarisation of MVN neurone.

Whole-cell patch-clamp recordings of MVN neurone illustrating the mechanisms involved in DADLE-induced inhibition. In this experiment, the external K^+concentration in the aCSF was reduced to 2.0mM. DADLE induced pronounce membrane hyperpolarisation (arrow) and cessation of spontaneous discharge. This was accompanied by an increased in membrane conductance, as indicated by the smaller voltage responses to the periodic hyperpolarising current pulses applied to the neurone (downward deflection in the trace).

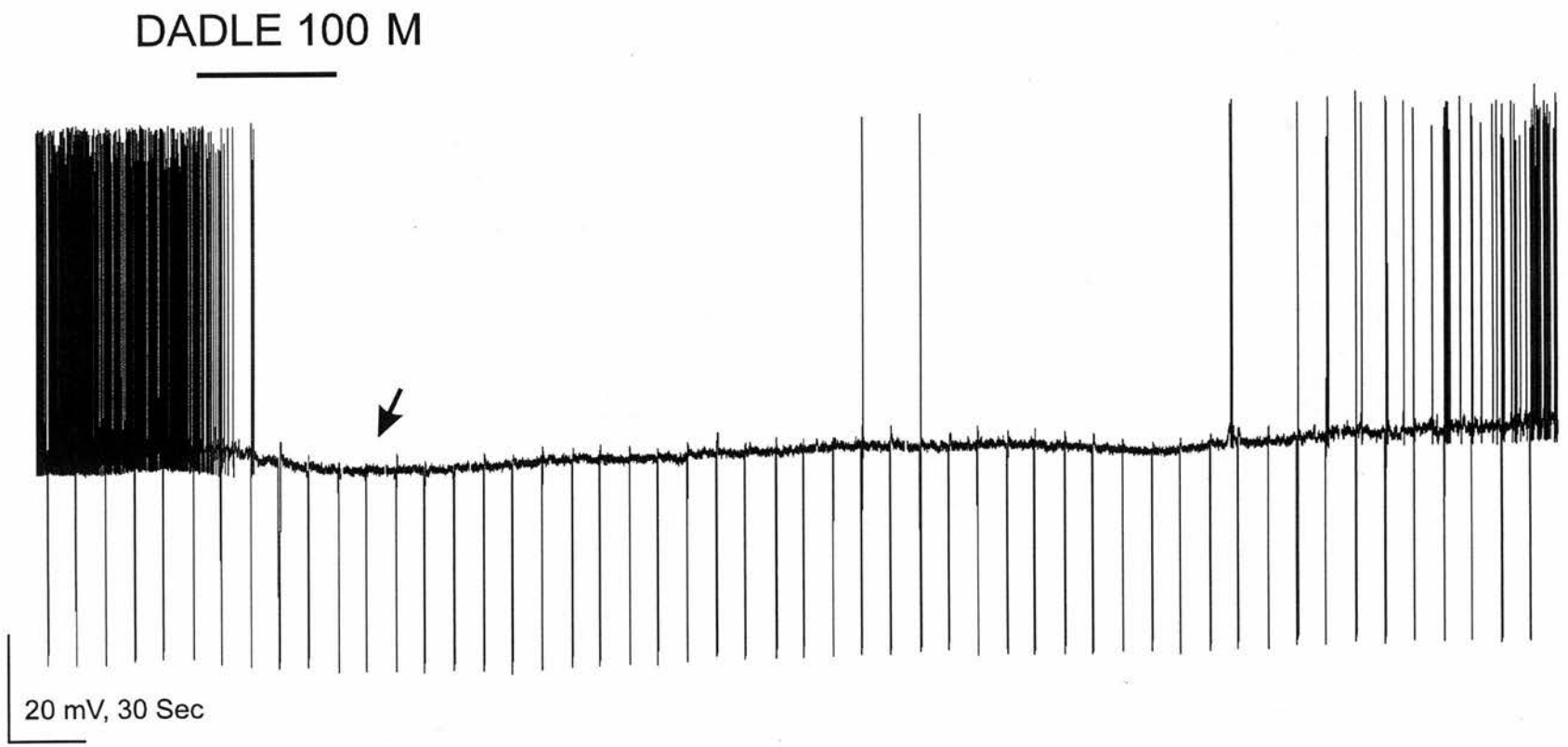

Figure 1.4.2 : DADLE-induced hyperpolarisation of MVN neurone

Legend 1.4.2.1 : Effect of DADLE on membrane input resistance of MVN neurone.

Voltage-current relationships (raw data) of an MVN neurone tested with DADLE. Left figure (A) was sampled first in normal aCSF (control) and the right figure (B) during the maximum inhibitory effect of DADLE. Graded series of constant depolarising and hyperpolarising current pulses (0.04 nA increments from -0.46 nA) were applied for 200 ms (as shown in the figures) to the recording electrode at a manually clamped holding potential of -60 mV. Decreased in membrane input resistance was indicated by smaller voltage responses at all potential tested during maximum inhibitory effect of DADLE. (C) The change in slope of the regression lines of the steady-state current-voltage (I-V) relationship obtained from (A) and (B) showed that the slope of the I-V curve decreased significantly from 175 MΩ in normal aCSF to 63 M Ω in the presence of DADLE, indicating a decreased in input resistance. Arrow head indicates where measurements were made.

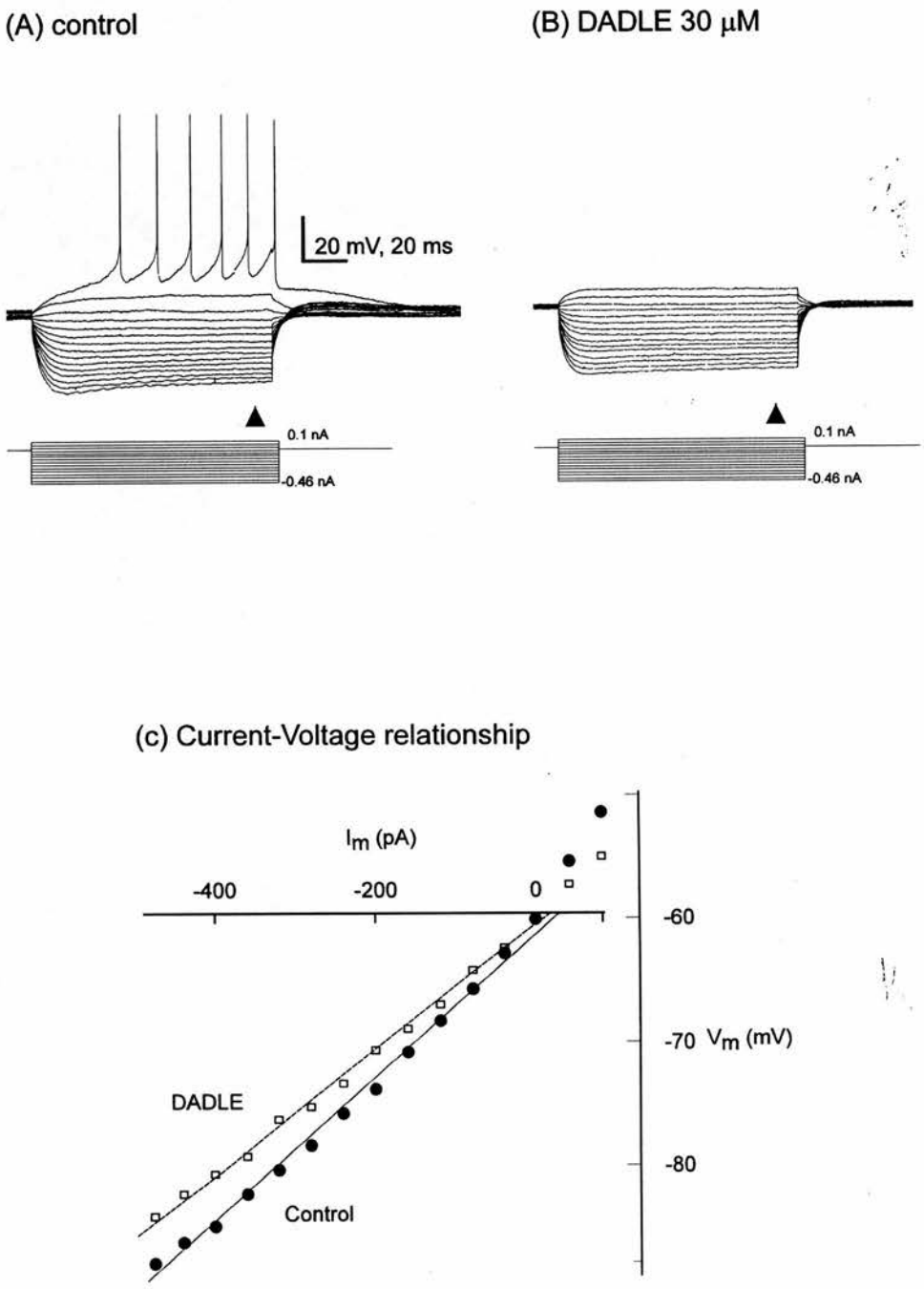

Figure 1.4.2.1 : Effect of DADLE on membrane input resistance.

Legend 1.4.2.2 : Effect of DADLE on membrane input resistance of MVN neurone.

Another example of voltage-current relationships (raw data) of MVN neurone to DADLE. Response of membrane voltage to a graded series of a constant depolarising and hyperpolarising current pulses (bottom) in normal aCSF (A) and during (B) maximum effect of DADLE. (C) I-V curves obtained from (A) and (B). The slope of the I-V curves is reduced from 125 MΩ in control to 97 MΩ in the presence of DADLE, indicating a decrease in membrane input resistance.

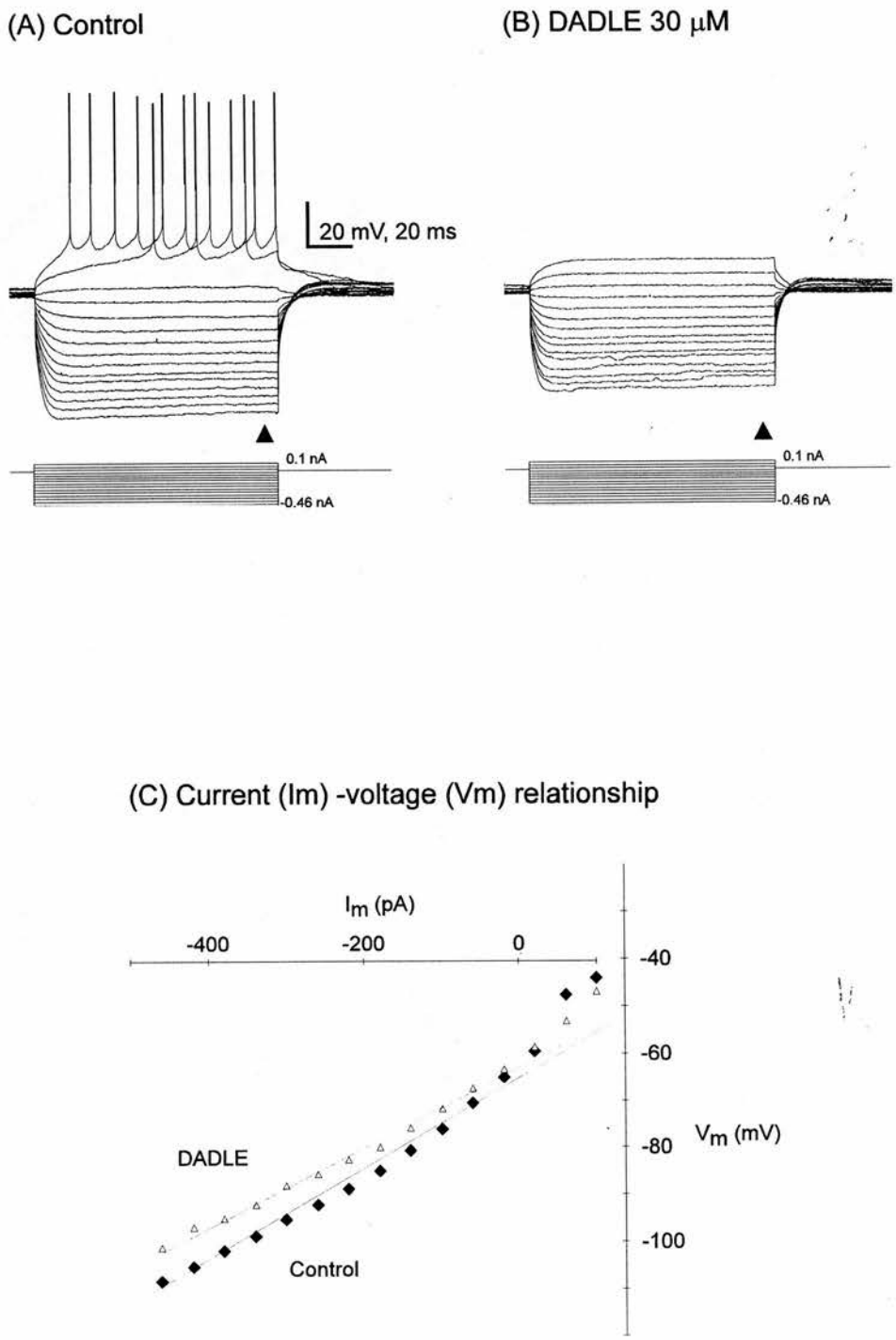

Figure 1.4.2.2 : Effect of DADLE on membrane input resistance.

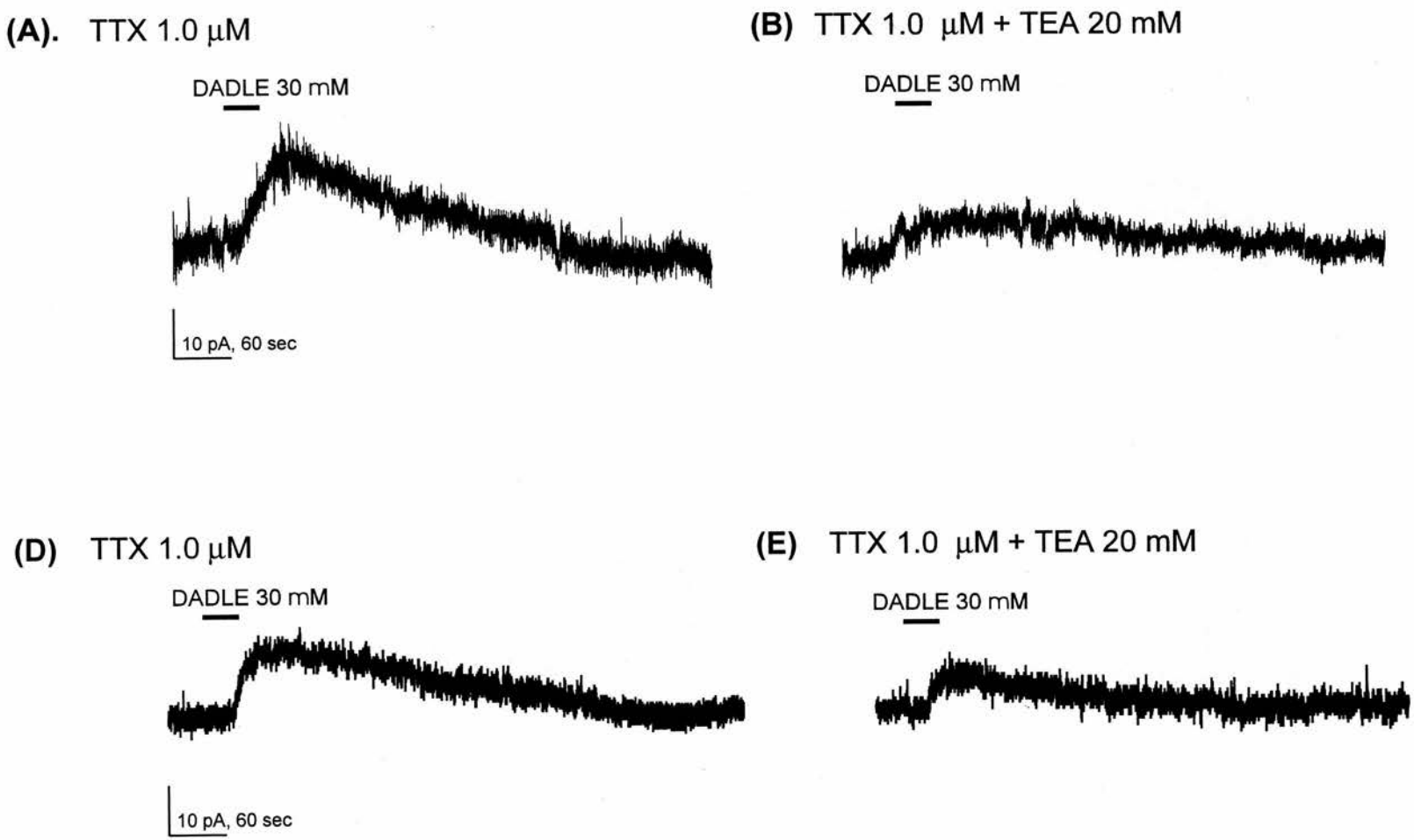

Figure 1.4.2.3 :. Membrane current of DADLE-induced hyperpolarisation of MVN neurones.

Whole-cell patch clamp recordings of membrane current of two different MVN neurones, voltage-clamped at a potential of -60 mV in low K+ aCSF containing TTX. Exposure to DADLE induced an outward membrane current, which was reduced but not abolished in the presence of TEA.

Legend 1.4.2.4 : Age-related inhibition of DADLE

Mean (± S.E.) inhibitory responses to a dose of 30 μM DADLE (upper graph), and the resting control discharge rates (lower graph), of all the MVN neurones tested, plotted as a function of the body weight of the animal before sacrifice. Percentage inhibition was calculated as the maximal inhibitory effect of DADLE expressed as a fraction of the control (pre-DADLE) resting discharge rate. The approximate age of the animal is also indicated assuming a weight gain of 50 g per week. Note that there is no systematic change in the intrinsic tonic discharge rates of the MVN cells over the age range used in these experiments, while the efficacy of the opioid-induced inhibition is relatively small in young animals and increases with age (significant linear regression, $R2 = 0.94$).

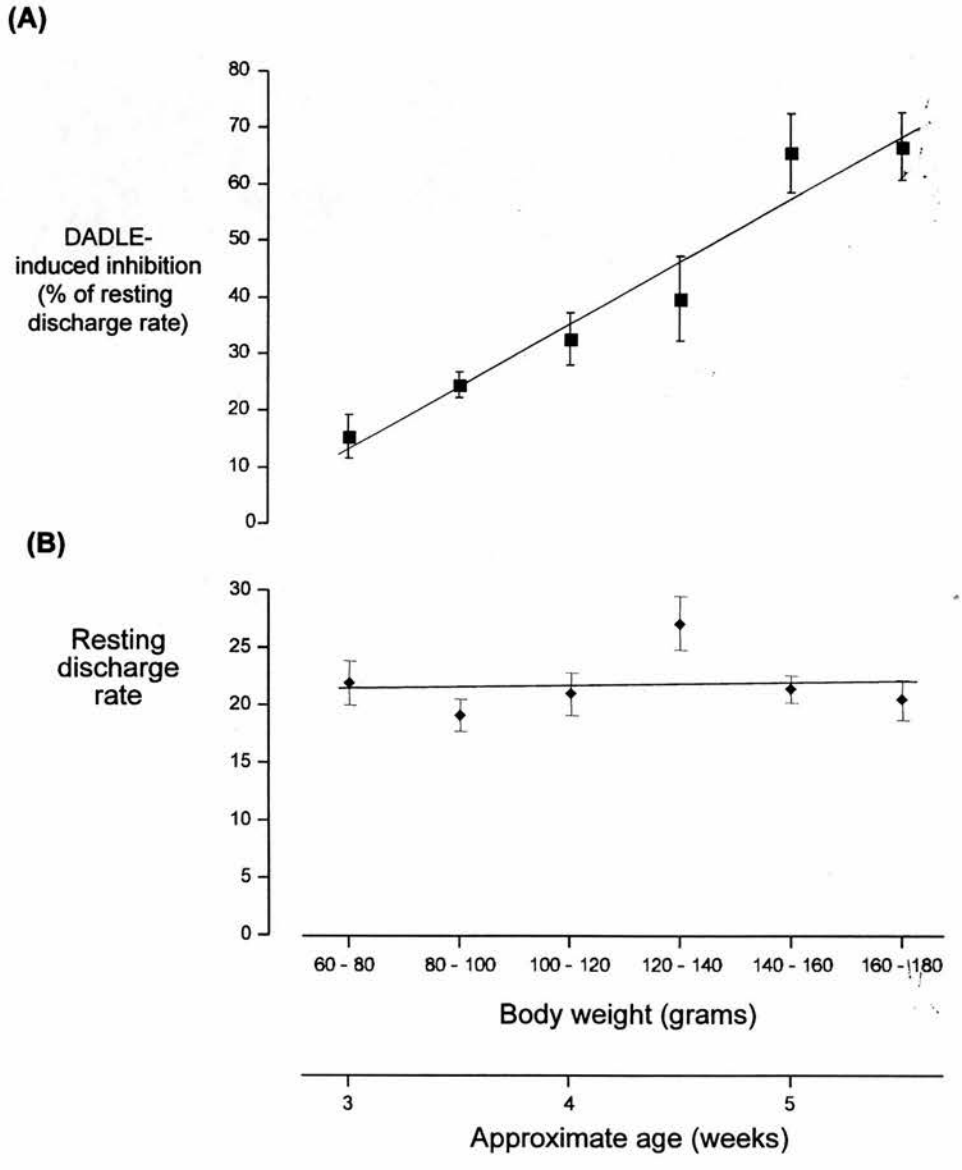

Figure 1.4.2.4 : Age-related inhibition of DADLE.

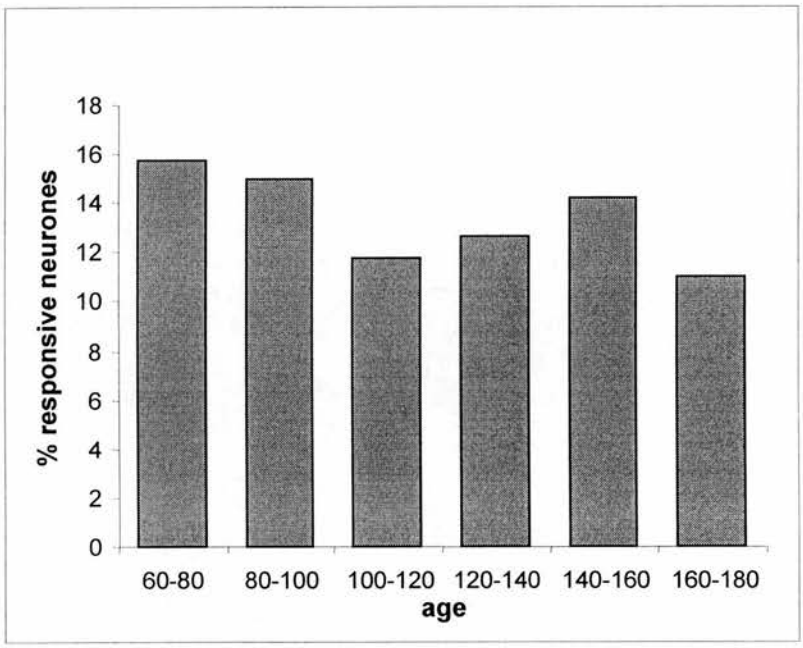

Figure 1.4.2.5 : Percentage of responsive neurones.
Histogram showing the percentage of responsive MVN neurones at different ages to bath application of DADLE.

1.5 DISCUSSION

This study examined opioidergic actions in the medial vestibular nucleus (MVN) neurones in brainslice preparations of the dorsal brainstem. The study using both extracellular and intracellular whole-cell patch-clamp techniques demonstrated that activation of δ-opioid receptors by [D-Ala^2, D-leu^5]-enkephalin (DADLE) dose-dependently inhibited the spontaneous discharge rate of the majority (80%) of neurones in the rat MVN. This effect was mediated by an increase in a TEA-sensitive potassium conductance on the postsynaptic cell membrane. These findings are in agreement with the results from other brain areas, which have found that the functional effects of opioids on neurones are predominantly inhibitory (for review see part 1.1.6)

DADLE-mediated postsynaptic inhibition

In contrast to its predominantly inhibitory effect on neuronal activity in many areas of the brain, enkephalin appears to be facilitatory on rat (Madison and Nicoll, 1988) and guinea pig (Caudle and Chavkin, 1990) hippocampal pyramidal cells. This effect might be due to inhibition of local inhibitory interneurones by enkephalin leading to a facilitatory response at the pyramidal cell. The excitatory effect of enkephalin on hippocampal pyramidal neurones appears to be the result of suppression of GABAergic i.p.s.ps, which unmasks the underlying e.p.s.ps. Excitatory opioid actions in the central nervous system may therefore be indirect effects resulting in disinhibition. Although, there is evidence that enkephalin can modulate presynaptic release of neurotransmitter and synaptic activity (McFadzean, 1988; Schlosser *et al.*, 1995; Vaughan and Christie, 1997), the inhibitory effects of DADLE on the discharge rate of MVN neurones in the present study were likely to be due to a specific interaction through postsynaptic opioid receptors since the inhibition was TTX-insensitive and persisted during blockade of synaptic transmission in modified low Ca^{2+}(2 mM), high Mg^{2+}(6 mM) aCSF medium, which eliminate both spontaneous and evoked postsynaptic potentials.

The inhibitory effect of DADLE was reversibly antagonised by the non-selective opioid antagonist, naloxone and the highly selective δ-opioid receptor antagonist, naltrindole. However, the present study does not address the possibility

of additional, presynaptic modulatory effects of opioids in the vestibular nuclei, as the experiments were carried out on single medial vestibular nuclei isolated from their normal afferent and efferent projections. It can therefore be concluded that DADLE inhibited the discharge rate of MVN neurones directly through post-synaptic opioid receptors.

The results of this study are consistent with the findings of Kawabata et al (1990), who demonstrated that iontophoretically applied met-enkephalin inhibited the discharge rate of cat MVN neurones *in vivo*. However, the results are in contrast to those of Carpenter and Hori (1992) and Lin and Carpenter (1994), who observed that the majority of spontaneously active rat MVN neurones were excited both by morphine and enkephalin *in vitro*. In the experiments of the present study there were only weak excitatory effects by opioid agonists seen in two MVN neurones in response to high doses of DADLE. The observed responses were less than a 10% change in the discharge rate. Although these responses were not investigate in any detail, they are likely to be disinhibitory effects caused by the action of DADLE on other MVN cells synaptically connected to the recorded neurones. It is possible that the differences between the present results and those of Lin & Carpenter and Carpenter & Hori could be due to a difference between the strains of rats used in the two studies (Wistar vs Sprague Dawley). However, it is more likely that the difference may arise from methodological considerations. In the present study bath application of known concentrations of the agonists were used which were equilibrated to the pH of the perfusing aCSF, while the study by Lin and Carpenter drugs were applied in rather acidic solution at high concentration by brief (1 sec) iontophoretic current injection.

Opioid receptor on MVN neurone is the δ-type

Although DADLE is known to be selective for δ-opioid receptors, it also has considerable affinity for the μ-opioid receptor. Postsynaptic inhibition induced by DADLE via δ-opioid receptors has previously been reported for rat locus coeruleus neurones (Williams *et al.*, 1982) and through μ-opioid receptors for dorsomotor vagal nucleus neurones in slices of rat medulla oblongata (Duan *et al.*, 1990). However, the present study demonstrated that the inhibitory effect evoked by

DADLE was specifically due to its direct activation on δ-opioid receptors rather than μ- or κ- opioid receptors.

The evidence indicating the presence of δ-opioid receptors in MVN neurones is as follows:- First, the discharge rate of the majority (80%) of MVN neurones was inhibited by the selective δ-opioid receptor agonist, DADLE, while the μ-opioid receptor agonist, morphine, and the κ- opioid receptor agonist, U50 488H at a concentration up to 300 μM were without effect on the discharge rate of any of the 33 and 30 neurones tested, respectively. These data indicate that μ- and κ-opioid receptors were not involved in the inhibitory action of the MVN neurones. Second, DPLPE which has previously been shown to be more highly selective opioid peptide analogue than DADLE at the δ-opioid receptor (Mosberg *et al.*, 1983) mimicked the inhibitory effect of DADLE in all MVN neurones tested, while DAGO, a highly selective μ-opioid receptor agonist failed to elicit a response in any MVN neurones tested. Third, the highly selective δ-opioid receptor antagonist, naltrindole effectively attenuated the inhibitory action of both DADLE and DPLPE. Hence, these data confirm the presence of δ-opioid receptors but not μ- or κ-opioid receptors in the rat MVN.

The results of the present study are supported by several immunohistochemical studies that have shown the presence of enkephalinergic neurones and fibres in the MVN (Pearson *et al.*, 1980; Finley *et al.*, 1981; Nomura *et al.*, 1984; Beitz *et al.*, 1987; Zanni *et al.*, 1995), together with the demonstration of moderate levels of δ-opioid receptors and low levels of μ- and κ-opioid receptors in the MVN (Fallon and Leslie, 1986; Mansour *et al.*, 1988, 1994). Despite the reported presence of low level of μ- and κ-opioid receptor in the MVN, in the present study no effects of μ- and κ-opioid receptor agonists were observed in any of the MVN cells tested. It is thus possible that any μ- and κ-receptor mediated effects within the MVN may be entirely pre-synaptic, a possibility that cannot be discounted on the basis of the present results.

Ionic mechanisms responsible for DADLE-induced inhibition

The ionic mechanisms underlying opioid actions were first elucidated in neurones of the rat locus coeruleus (Williams *et al.*, 1982). It is now clear that opioids directly inhibit the electrical activity of neurones in many regions of the nervous system by opening of the inwardly rectifying potassium channels, thus leading to membrane hyperpolarisation. Opioid inhibition of the neuronal firing rate resulting from a membrane hyperpolarisation have been reported for neurones of rat and guinea pig locus coeruleus (Pepper and Henderson, 1980; North and Williams, 1985; Travagli *et al.*, 1995), rat substantia gelatinosa (Yoshimura and North, 1983), rat periaqueductal gray (Chieng and Christie, 1994), rat dorsomotor vagal nucleus (Duan *et al.*, 1990) and guinea pig myenteric plexus (Morita and North, 1981).

Voltage-clamp experiments using whole-cell patch clamp recordings from MVN neurones in the present study confirmed that the inhibitory effect of the δ-opioid agonist, DADLE on the MVN cells was mediated via an increase in an outward TEA-sensitive potassium conductance in the cell membrane thereby causing membrane hyperpolarisation, similar to that reported in other regions of the rat and guinea pig nervous systems. This is consistent with the decrease in input resistance that was observed in current-clamp recordings of the I-V curves. Further experiments using selective K^+ channel blockers are necessary to determine which class of TEA-sensitive K^+ channels are involved. However, since the primary purpose of this study was to classify the discrepancies in the literature about the effects of opioids on MVN neurones, the nature of the K^+ current was not further investigated.

Age-related inhibition

The age-related increase in the opioid-induced inhibition on the MVN neurones in this study is of interest in the context of previous work in our laboratory on the development of the membrane properties, tonic discharge and electrical excitability of mouse MVN neurones over the first post-natal month (Dutia *et al.*, 1995; Johnston and Dutia, 1996). From the present results in the rat it is clear that the responsiveness of the MVN neurones to δ-receptor agonists is weak in young

animals and increases significantly with age (Fig. 1.4.1.5A). In the youngest animals used in the present experiments the mean spontaneous discharge rate of the MVN cells had already reached its adult level, as no further increases were seen over the following 2-3 weeks (Fig. 1.4.1.5B; Johnston and Dutia, 1996). Nevertheless the inhibitory responses to DADLE were still immature in the youngest animals but increased substantially over the following weeks. This may be due to continuing post-natal growth and maturation of the MVN neurones and their dendritic arbors, as this process occurs during the first post-natal month (Lannou, Precht and Cazin, 1983). Thus, δ-opioid receptors located on the dendrites may increasingly contribute to the DADLE-induced inhibition.

It has been shown that the expression of δ-opioid receptors in the rat and mouse brain begins in the first weeks after birth and gradually increases in density over the next three to four weeks to reach the adult level (McDowell and Kitchen, 1986; Negri *et al.*, 1997). Competitive binding study also revealed that in the rat brain δ-opioid receptors lag in development to the other opioid receptors and are not present until about the second postnatal week (Wohltmann *et al.*, 1982). Although such information is not available for the development of δ-opioid receptor expression in the brainstem neurones, the responsiveness of the agonist in relation to the age of the animal in the present study indicates that a similar pattern of expression of δ-opioid receptors may occur in MVN neurones. Alternatively it may reflect changes in the overall density of δ-opiate receptors on the MVN cells and in the efficacy of the intracellular second-messenger systems activated by them (for review see part 1.1.6). In either case, a fuller understanding of such age-related post-natal changes in the neurochemical responsiveness of neurones is likely to be important in the interpretation of results from other *in vitro* studies, where tissues from young animals are often employed.

In summary, the effects of the opioid peptides for μ-, δ and κ-opioid receptors on neurones of the MVN in the rat dorsal brainstem slice preparations were investigated with extracellular and intracellular whole-cell patch-clamp recording techniques. The present results strongly indicate that the activity of most MVN neurones was inhibited by activation of postsynaptically located δ-opioid receptors and that the DADLE inhibition is mediated via potentiation of a TEA-

sensitive potassium conductance. The present results also demonstrated that the inhibitory effect of DADLE increased linearly with age, in that the inhibitory effects of DADLE were smaller in young than in older animals.

CHAPTER 2

INHIBITION OF RAT MEDIAL VESTIBULAR NUCLEUS NEURONES BY NOCICEPTIN/ORPHANIN FQ, *IN VITRO*.

2.1 LITERATURE REVIEW

2.1.1 THE ORPHAN OPIOID RECEPTOR

The opioid receptor like-1 (ORL1) receptor

Opioid receptors were first discovered over two decades ago, and identification of the μ-, δ- and κ-opioid receptor subtypes was based on pharmacological grounds. Only in recent years has the complementary DNA (cDNA) sequences of these receptors been cloned, sequenced, and found to encode highly homologous protein with a primary structure typical for G protein-coupled membrane receptors (for reviews see Chapter 1, part 1.1.5).

The first opioid receptor cloned was the mouse δ-opioid receptor by Evans *et al.*, (1992) and Kieffer *et al.*, (1992). They succeeded in cloning the cDNA of the δ-opioid receptor and identified its amino acid sequence without purifying the protein. Both groups simultaneously used very similar cloning techniques to identify this receptor from hybrid NG108-15 neuroblastoma X glioma cells. Cloning of the δ-opioid receptor initiated an intense effort in search of the remaining members or 'other' members of this potentially large gene family. Subsequently the μ- and κ-opioid receptors were cloned on the basis of their homology to the cloned δ-opioid receptor in various species including mouse, rat and human. The deduced amino acid sequences for these three opioid receptors were approximately 60% identical (for reviews see Kieffer *et al.*, 1994; Minami and Satoh, 1995; Satoh and Minami, 1995)

Along with the μ-, δ- and κ-opioid receptors, a cDNA clone with a very high degree of amino acid sequence homology to the three opioid receptors has been identified by several independent research groups in rat, mouse and human. This "orphan" opioid receptor-like receptor is variously known as ORL1 for the human clone (Mollereau *et al.*, 1994), ROR-C (Fukuda *et al.*, 1994), oprl (Chen *et al.*, 1994), LC132 (Bunzow *et al.*, 1994), XOR1 (Wang *et al.*, 1994), Hyp-8-1 (Wick *et al.*, 1994) or C3 (Lachowicz *et al.*, 1995) from rat brain libraries and MOR-C (Nishi *et al.*, 1994) from a

mouse genomic library. For the purpose of this review, I shall refer to the receptor as the opioid-like orphan receptor (ORL1).

The homology of the cDNA deduced amino acid sequence of ORL1 with the μ-, δ-, and κ-opioid receptors is exceptionally high (>80% homology), particularly in the putative transmembrane helices and cytoplasmic loops. However, the degree of homology is much less in the N-terminus, the second and third extracellular loops. These homologies are highly conserved among mammalian species. Overall, the ORL1 receptor is equally homologous to the three types of opioid receptors except that its acidic second extracellular loop makes it resemble more closely the κ-opioid receptor (which binds dynorphins preferentially) than the μ- or δ-opioid receptors (Mollereau *et al.*, 1994). This homology profile would indicate that ORL1 exhibits signalling mechanisms similar to the opioid receptors, all of which inhibit adenyl cyclase, activate potassium conductances, and inhibit calcium currents (for a review see Childers, 1991).

Distribution of opioid-like orphan receptor (ORL1) in mammalian central nervous system (CNS).

An initial move to gain insight toward characterisation of the ORL1 in the CNS has been the gross anatomical investigation of ORL1 receptor mRNA expression by means of Northern blot and in situ hybridisation techniques (Bunzow *et al.*, 1994; Fukuda *et al.*, 1994; Mollereau *et al.*, 1994). These studies have shown that ORL1 mRNA is widely expressed throughout the brain and spinal cord. The highest levels of ORL1 mRNA expression were observed particularly in the paraventricular and ventromedial nuclei of the hypothalamus, in the amygdala and piriform cortex, and in the dorsal raphe nucleus and locus coeruleus of the brainstem. Moderate expression was observed in the cortex, thalamus, hippocampus, periaqueductal gray and in the dorsal and ventral horns of the spinal cord. A notable feature that distinguished the distribution of ORL1 from the μ-, δ- and κ-opioid receptor was the very low expression of ORL1 receptor mRNA in the caudate-putamen and cerebellum (Fig. 2.1.1.1)

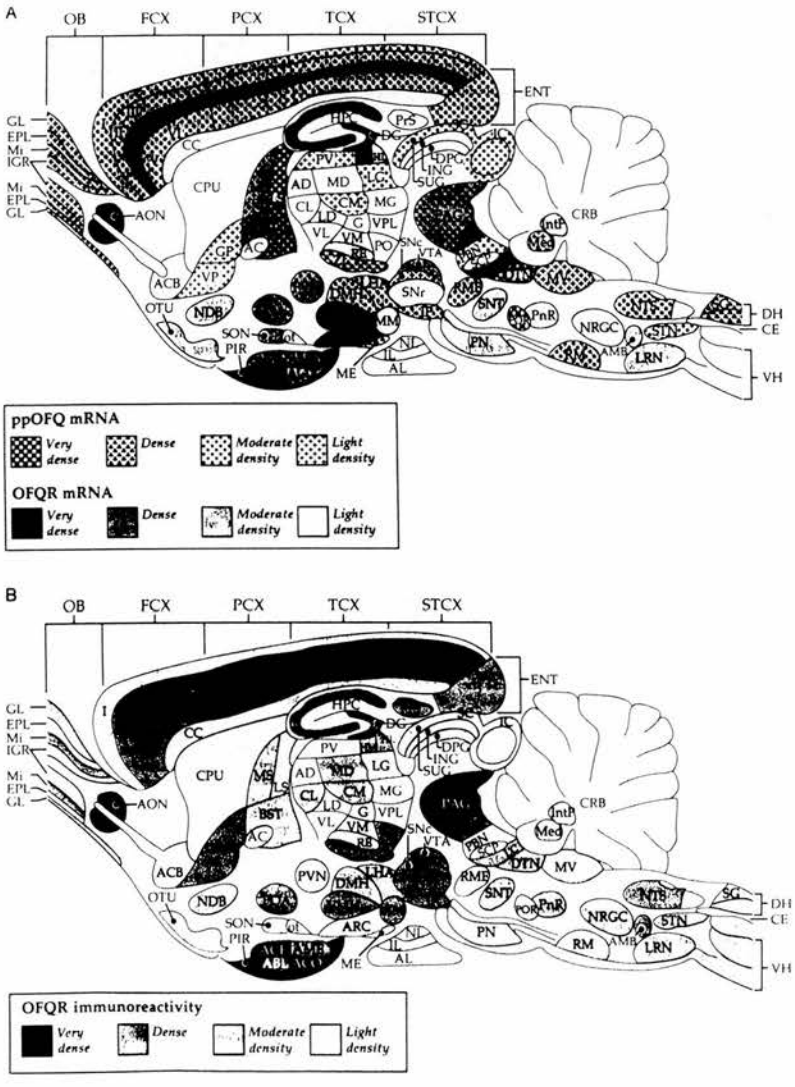

Abbreviations: I–VI, cortical layers I–VI; ABL, basolateral amygdaloid nucleus; AC, anterior commissure; ACB, nucleus accumbens; ACE, central amygdaloid nucleus; ACO, cortical amygdaloid nucleus; AD, anterodorsal thalamus; AL, anterior lobe, pituitary; AMB, nucleus ambiguus; AME, medial amygdaloid nucleus; AON, anterior olfactory nucleus; ARC, arcuate nucleus, hypothalamus; BST, bed nucleus, stria terminalis; CC, corpus callosum; CE, central canal; CL, centrolateral thalamus; CM, centromedial thalamus; CPU, caudate putamen; CRB, cerebellum; DG, dentate gyrus; DH, dorsal horn, spinal cord; DMH, dorsomedial hypothalamus; DPG, deep gray layer, superior colliculus; DTN, dorsal tegmental area; ENT, entorhinal cortex; EPL, external plexiform layer, olfactory bulb; FCX, frontal cortex; G, nucleus gelatinosus, thalamus; GL, glomerular layer, olfactory bulb; GP, globus pallidus; HL, lateral habenula; HM, medial habenula; HPC, hippocampus; IC, inferior colliculus; IGR, intermediate granular layer, olfactory bulb; IL, intermediate lobe, pituitary; ING, intermediate gray layer, superior colliculus; IntP, interposed cerebellar nucleus; IP, interpeduncular nucleus; LC, locus coeruleus; LD, laterodorsal thalamus; LG, lateral geniculate thalamus; LHA, lateral hypothalamic area; LRN, lateral reticular nucleus; LS, lateral septum; MD, mediodorsal thalamus; ME, median eminence; Med, medial cerebellar nucleus; MG, medial geniculate thalamus; Mi, mitral cell layer, olfactory bulb; MM, medial mammillary nucleus; MS, medial septum; MV, medial vestibular nucleus; NDB, nucleus diagonal band; NL, neural lobe, pituitary; NRGC, nucleus reticularis gigantocellularis; NTS, nucleus tractus solitani; OB, olfactory bulb; ot, optic tract; OTU, olfactory tubercle; PAG, periaqueductal gray; PBN, parabrachial nucleus; PCX, parietal cortex; PIR, piriform cortex; PN, pons; PnR, pontine reticular; PO, posterior nucleus thalami; POA, preoptic area; POR, perolivary region; PrS, presubiculum; PV, paraventricular thalamus; PVN, paraventricular hypothalamus; RD, dorsal raphé; RE, reuniens thalami; RM, raphé magnus; RME, median raphé; SC, superior colliculus; SCP, superior cerebellar peduncle; SG, substantia gelatinosa; SNc, substantia nigra, pars compacta; SNr, substantia nigra, pars reticulata; SNT, sensory trigeminal nucleus; SON, supraoptic nucleus; STCX, striate cortex; STN, spinal trigeminal nucleus; SUG, superficial gray layer, superior colliculus; TCX, temporal cortex; VH, ventral horn, spinal cord; VL, ventrolateral thalamus; VM, ventromedial thalamus; VMH, ventromedial hypothalamus; VP, ventral pallidus; VPL, ventroposterolateral thalamus; VTA, ventral tegmental area; and ZI, zona incerta.

Figure 2.1.1.1 : Schematic representation of N/OFQ and N/OFQ receptor expression in the rat CNS.

(After Darland *et al.*, 1998)

Using a monoclonal antibody to the N-terminus of ORL1 in order to map areas of receptor expression in the rat CNS, Anton *et al.*, (1996) produced distributions similar to the earlier ORL1 mRNA distribution observed from in situ hybridisation studies, indicating the presence of local ORL1 receptor circuitry. Following the discovery of the endogenous ligand for ORL1 receptor, Sim *et al.*, (1996) successfully mapped the ORL1 receptor in the rat cortex, amygdala, hypothalamus thalamus and brainstem that matched with the earlier studies which used agonist-induced incorporation of [^{35}S]GTPγS in brain slices.

Interaction of opioid ligands with the ORL1 receptor.

At the time of cloning of cDNA-deduced amino acid sequences of the ORL1 no endogenous ligand for this receptor had been isolated. In spite of its extensive nucleotide sequence homology to μ-, δ- and κ-opioid receptors, the ORL1 receptor binds opioid ligands and antagonists with very low affinity compared with these opioid receptors. Mollereau *et al.*, (1994) and Lachowicz *et al.*, (1994) have demonstrated that in the recombinant Chinese hamster ovary (CHO) cells expressing the ORL1 protein receptor, no specific binding of peptide or nonpeptide opioid ligands could be found.

However, the ORL1 receptor was shown to have some functional similarity to the classical opioid receptors. In stable CHO cells expressing the ORL1 receptor, the potent oripavine agonist, etorphine was found to inhibit forskolin-induced accumulation of cAMP but at a concentration three orders of magnitude higher than that required to produce the effect through the opioid receptors (Mollereau *et al.*, 1994). On the other hand, dynorphin A and dynorphin A (1-13) stimulate potassium currents in *Xenopus* oocytes co-injected with the cRNAs to the XOR1 receptor and a G protein-activated potassium channel, suggesting that dynorphins may be endogenous ligands for the ORL1 receptor (Zhang and Yu, 1995).

2.1.2 THE ENDOGENOUS LIGAND OF THE ORPHAN OPIOID RECEPTOR

A characteristic of the ORL1 receptor was that all of the known opioid receptor ligands bound with very low affinity to it suggesting the presence of unknown endogenous neurotransmitter as its natural ligand. This endogenous ligand was subsequently identified by two separate groups, Meunier *et al.*, (1995) and Reinscheid *et al.*, (1995), who used similar strategies and found it to be a heptadecapeptide.

Starting with crude whole rat brain in the case of the former group and porcine hypothalamus extracts in the latter, both groups used this assay to monitor ORL1 agonist activity through a series of biochemical fractionation steps, which ultimately led them to isolate and identify the heptadecapeptide with a sequence of amino acids that suggested a close evolutionary relationship to the existing endogenous opioid peptides, in particular dynorphin A. However, the most striking dissimilarity between this new endogenous peptide and all of the other endogenous opioid peptide lies in the N-terminal amino acid residue. While all endogenous opioid peptides derived from their separate pro-precursors have tyrosine as their N-terminal, the N-terminal amino acid of this new endogenous peptide is phenylalanine (Phe; Fig.2.1.2.1A).

In addition, the isolated peptide was shown to strongly inhibit forskolin-induced accumulation of cAMP with nanomolar binding affinity in the transfected CHO cells expressing ORL1. The maximal inhibition observed was 80-90%. When the two groups examined this isolated peptide for activity *in vivo* by injecting this peptide intracerebroventricularly (i.c.v) in the mouse brain, each group found that the peptide did not induce analgesia as expected, but rather appeared to be hyperalgesic in the hot-plate escape jumping latency (Meunier *et al.*, 1995) and tail-flick latency (Reinscheid *et al.*, 1995) tests. Meunier and colleagues named the new peptide "nociceptin", as indication of its *in vivo* pro-nociceptive properties, whereas Reinscheid and colleagues, called it "orphanin FQ" (OFQ) to designate the fact that it was an endogenous ligand for an orphan receptor and that its amino acid sequence begins with phenylalanine and ends with glutamine (F and Q, in the single-letter code). The

peptide was later identified as an endogenous ligand of the mouse ROR-C receptor and reported to induce allodynia following intrathecal administration in conscious mice (Okuda-Ashitaka *et al.*, 1996).

Nociceptin / orphanin FQ precursor

As is often the case for small peptide hormones and transmitters, nociceptin / Orphanin FQ (N/OFQ) appears to be synthesised as part of a larger polyprotein precursor. The cDNA carrying the entire coding sequence of the polyprotein precursor for N/OFQ was subsequently isolated from rat (Nothacker *et al.*, 1996), mouse (Houtani *et al.*, 1996; Pan *et al.*, 1996; Saito *et al.*, 1996) and from human brains (Mollereau *et al.*, 1996). The deduced N/OFQ precursor showed a sequence similar to the opioid peptide precursors, preproenkephalin, preprodynorphin and preproopiomelanocortin and shares characteristic structural features particularly with preprodynorphin, indicating that the precursor proteins are evolutionary related. Figure 2.1.2.1B summarises structural similarity between the N/OFQ precursor and the opioid peptide precursors. Both N/OFQ precursor and preprodynorphin contain 6 conserved cysteine residues in the amino-terminal (NH_2) region preceded by the signal peptide. These residues form disulfide bridges. Both N/OFQ and dynorphin A are found in the conserved position residing near the carboxyl terminus of each precursor. The amino acid sequence of N/OFQ is flanked by the dibasic amino acids, Lys-Arg, the recognition site for several endopeptidase (Seidah *et al.*, 1992). This is consistent with the idea that the precursor of N/OFQ is proteolytically processed. There are several paired dibasic amino acids distributed throughout the N/OFQ precursor, which suggests that this large polyprotein precursor could be a source of several other bioactive peptides, just as the opioid precursors are.

Distribution of nociceptin / orphanin FQ

Following the discovery of N/OFQ as a natural ligand for ORL1 receptor, a number of groups have begun to map the detailed expression of N/OFQ in the mammalian CNS by means of in situ hybridisation and immunohistochemical techniques. Using in situ hybridisation analysis of N/OFQ precursor mRNA in the

Legend 2.1.2.1 : Comparison of N/OFQ peptide sequence and precursor structure with other opioids.

(A) Structure of N/OFQ, the endogenous agonist of the ORL1 receptor compared with those of closely related peptide agonists at classical opioid receptors. Amino acid residue homology between N/OFQ and other peptides is indicated in bold. (B) Schematic representation of the structures of the N/OFQ precursor and opioid precursors. The locations of neuropeptides as well as characteristic amino acid residues are indicated.

(A)

Nociceptin/ orphanin FQ	Phe - **Gly** - **Gly** - **Phe** - Thr - Gly - Ala - Arg - **Lys** - **Ser** - Ala - Arg - lys - Leu - Ala - **Asn** - **Gln**
Dynorphin A	Tyr - **Gly** - **Gly** - **Phe** - Leu - Arg - Arg - Ile - Arg - Pro - Lys - Leu - **lys** - Trp - Asp - **Asn** - **Gln**
β-Endorphin	Tyr - **Gly** - **Gly** - **Phe** - Met - Thr - Ser - Glu - **Lys** - **Ser** - Gln - Thr - Pro - Leu - Val - Thr - Leu - Phe - Lys - Asn - Ala - Ile - Ile - Lys - Asn - Val - His - Lys - Lys - Gly - Gln
Met-enkephalin	Tyr - **Gly** - **Gly** - **Phe** - Met
Leu-enkephalin	Tyr - **Gly** - **Gly** - **Phe** - Leu

(B)

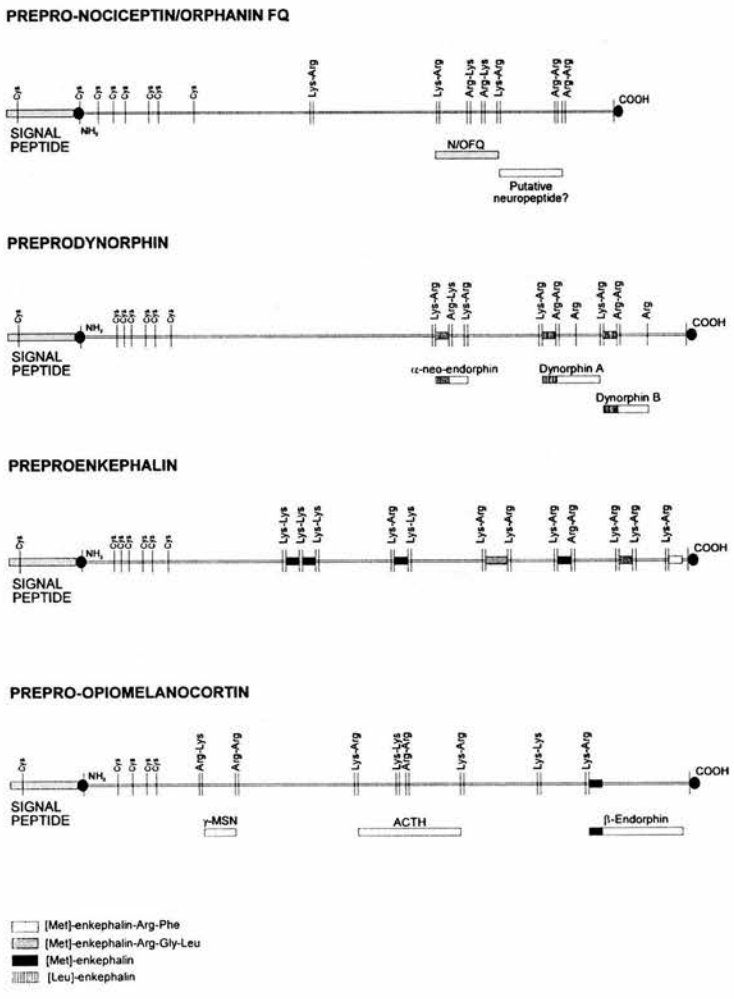

Figure 2.1.2.1 : Comparison of N/OFQ peptide sequence and precursor structure with other opioids

mouse CNS, Houtani *et al.*, (1996) observed hybridisation signals in neuronal perikarya in discrete sites of the brain and spinal cord. In the brain N/OFQ mRNA is highly expressed in the central gray, central tegmental field, nucleus of the lateral lemniscus, superior olive and spinal trigeminal nucleus of the brainstem but are absent in the caudate-putamen and cerebellum. Within the spinal cord, N/OFQ mRNA precursor is abundant in laminae I-III of the dorsal horn and lamina X.

Riedl and colleagues (1996) raised specific antibodies against the N/OFQ peptide and revealed high levels of N/OFQ immunoreactivity in the superficial dorsal horn, lateral spinal nucleus and the region dorsal to the central canal. This was subsequently confirmed by Schuligoi *et al.*, (1997) and Lai *et al.*, (1997). Schulz *et al.*, (1996) have detected high N/OFQ immunoreactivity in the sensory trigeminal complex, locus coeruleus, raphe nucleus, periaqueductal grey, amygdala, hypothalamic and septal areas. Overall, the distribution of the precursor of N/OFQ and /or N/OFQ peptides in mammalian CNS is clearly distinct from that of the classical opioid precursors and/or peptide but matches the distribution of the ORL1 receptor mRNA (Riedl *et al.*, 1996; Schulz *et al.*, 1996; Monteillet-Agius *et al.*, 1998). Figure 2.1.1.1 shows a schematic representation of N/OFQ and ORL1 receptor distribution in the rat CNS.

Cellular actions of nociceptin / orphanin FQ

The cellular actions of N/OFQ have received considerable attention and the actions induced by N/OFQ are similar to those induced by agonists acting at other receptors that are also members of the seven transmembrane domain, G-coupled receptor superfamily, particularly the classical opioid receptors. Meunier *et al.*, (1995) and Reinscheid *et al.*, (1995) have demonstrated that in CHO cells transfected with the ORL1 receptor, N/OFQ potently inhibited forskolin-stimulated adenylate cyclase and activated inwardly rectifying potassium currents (Matthes *et al.*, 1996). Ikeda *et al.*, (1997) reported that the ORL1 receptor is functionally coupled with a G-protein activated potassium channel in *Xenopus* oocytes, and that the receptor mRNA and G-protein-activated potassium channel mRNA co-exist in various neurones of the mouse

CNS. In addition they found that in hippocampal pyramidal neurones, N/OFQ induced hyperpolarising currents through activation of inwardly rectifying potassium channels. N/OFQ inhibition of neuronal electrical activity associated with activation of an inwardly rectifying potassium conductance has also been observed with N/OFQ, in rat dorsal raphe neurones (Vaughan *et al.*, 1997), rat locus coeruleus neurones (Connor *et al.*, 1996a), rat supraoptic (Doi *et al.*, 1998) and ventromedial nucleus neurones (Lee *et al.*, 1997) of the hypothalamus, rat periaqueductal gray neurones (Vaughan *et al.*, 1997), rat cardiomotor neurons in the rostral ventrolateral medulla (Chu *et al.*, 1998) and guinea pig arcuate nucleus neurones (Wagner *et al.*, 1998).

Apart from its ability to increase an inwardly rectifying potassium conductance, N/OFQ also has been shown to have the potential to modulate the function of neurones in the CNS via a number of different cellular effectors. Connor *et al.*, (1996) reported that N/OFQ inhibits N-type Ca^{2+} channel currents in SH-SY5Y human neuroblastoma cells in vitro as well as promoting the release of Ca^{2+} from intracellular stores. Connor and Christie (1998) using whole cell patch clamp technique demonstrated that N/OFQ predominantly inhibits the N-type Ca^{2+} channel current but has little effect on L- and R-type Ca^{2+} channel currents in acutely dissociated rat periaqueductal gray neurones. Previously, using the same recording techniques in freshly dissociated CA1 and CA3 hippocampal neurones, Knoflach *et al.*, (1996) demonstrated that N/OFQ modulated L-, P/Q- as well as N-type voltage-gated Ca^{2+} channels. The inhibition of Ca^{2+} entry through voltage-gated Ca^{2+} channels and the release of Ca^{2+} from intracellular stores by N/OFQ were prevented with pretreatment with pertussis (Connor *et al.*, 1996b; Knoflach *et al.*, 1996). In rat cerebrocortical slices (Nicol *et al.*, 1996), N/OFQ was shown to inhibit K^+-stimulated glutamate release and Faber *et al.*, (1996) provided indirect evidence of N/OFQ inhibition of glutamatergic transmission on the neonatal rat hemisected spinal cord preparation, suggesting a role for N/OFQ in the control of glutamatergic neurotransmission.

N/OFQ also has been found to inhibit the release of dopamine in the nucleus accumbens of the anaesthetised rat (Murphy *et al.*, 1996), tachykinin in the guinea pig

renal pelvis preparation (Giuliani and Maggi, 1996) and inhibition of acetylcholine release from parasympathetic nerves of the guinea pig trachea (Patel *et al.*, 1997) as well as release of GABA from nerve terminals of rat periaqueductal gray neurones (Vaughan *et al.*, 1997). The cellular responses induced by N/OFQ are thus features this receptor shares with the "classical" opioid receptors. However, surprisingly N/OFQ is reported to either enhance nociception (Meunier *et al.*, 1995; Reinscheid *et al.*, 1995) or to antagonise the antinociceptive effect of opioids (Mogil *et al.*, 1996a; Mogil *et al.*, 1996b).

2.2 AIMS OF STUDY

Following the successful cloning of the complementary DNA (cDNA) encoding G-proteins for the δ-, μ- and κ-opioid receptors (for a review see Chapter 1, part 1.1.5), several independent groups have isolated and cloned a fourth novel opioid receptor from mouse, rat and human brains (for a review, refer to part 2.1.1). This fourth receptor, referred to hereafter as the opioid receptor-like receptor (ORL1) has very high structural homology with the classical opioid receptors. However it did not bind all of the known opioid ligands with the expected high affinity. This receptor was therefore considered as an "orphan" member of the opioid receptor family.

The putative endogenous ligand for the ORL1 receptor was subsequently identified and was discovered to be a heptadecapeptide (17-amino-acid peptide) with a sequence of amino acids most closely related to the existing endogenous opioid peptide, in particular dynorphin A. The peptide was termed "nociceptin" by Meunier *et al.*, (1995) and "orphanin FQ" by Reinscheid *et al.*, (1995). A noticeable difference between nociceptin/orphanin FQ (N/OFQ) and the other endogenous opioid peptides is located on the N-terminal amino acid residue. All of the known endogenous opioid peptides have tyrosine as their N-terminal amino acid while N/OFQ contains phenylalanine.

At the cellular level the responses induced by N/OFQ are similar to those induced by agonists of the classical opioid receptors including the inhibition of neuronal activity via activation of inwardly rectifying K^+ channels (Vaughan and Christie 1996, Connor *et al.*, 1996, Lee *et al.*, 1997, Vaughan *et al.*, 1997, Doi *et al.*, 1998, Wagner *et al.*, 1998) and the modulation of a variety of voltage-dependent Ca^{2+} currents (Connor *et al.*, 1996a, 1996b, Knoflach *et al.*, 1996, Connor and Christie 1998). Surprisingly, in spite of these similarities, N/OFQ and the ORL1 receptors appear to be anatomically and pharmacologically distinctive from the classical opioid system.

Neurones expressing N/OFQ mRNA and ORL1 receptor transcripts have been demonstrated in many brain regions including the MVN of the brainstem (Mollereau *et al.*, 1994, Bunzow *et al.*, 1994, Fukuda *et al.*, 1994, Lachowicz 1994, Anton *et al.*, 1996, Houtani *et al.*, 1996, Darland *et al.*, 1998). While the effects of

opioid peptides on MVN neurones have been recently demonstrated (Kawabata *et al.*, 1990, Lin and Carpenter 1994, Carpenter and Hori 1992, Sulaiman and Dutia 1998), the actions of nociceptin on vestibular neurones are presently unknown. The aim of this study, therefore was to examine the actions of N/OFQ on the spontaneously active MVN neurones in the horizontal brainslice preparation of the rat dorsal brainstem *in vitro* and compare the responses produced by N/OFQ to those obtained with the classical δ-opioid receptor agonist, DADLE (Sulaiman and Dutia, 1998).

2.3 METHODS

The horizontal MVN slices were prepared from Sprague Dawley rats weighing between 60 – 120g. The procedures used in the preparation of the animal, maintenance of the horizontal slices of the MVN *in vitro* and recording techniques used in this study are similar to that outlined in the methods section of Chapter 1 (part 1.3).

Drugs and Chemicals

N/OFQ and its selective antagonist, [Phe$^1\psi$(CH_2-NH)Gly^2] Nociceptin (1-13) NH_2 (Guerrini, *et al.*, 1998) were obtained from Tocris Cookson (UK). Both compounds were dissolved in distilled water to make a stock solution (0.1 mM) and subsequently stored in small aliquots at -20°C. The δ-opioid receptor agonist, [D-ala^2, D-leu^5]-enkephalin, the peptidase inhibitor bestatin, and the non selective opioid antagonist naloxone hydrochloride were purchased from Sigma (UK). The inactive derivative of N/OFQ, [des-phe^1]-nociceptin was obtained from Phoenix Pharmaceutical Inc. (USA). Stock solutions of these drugs were also made up in distilled water, divided into small aliquots and stored frozen at -20°C. The aliquots were thawed and diluted to working concentrations by using oxygenated aCSF immediately before use. Drugs were applied to the MVN slice by changing the perfusion medium to one that differed only in its content of drug by means of three-way taps (Dutia, *et al.*, 1992). Peptide agonists were applied to the slice for a period of 60 seconds while peptide antagonists were applied continuously for at least 20 minutes before the application of the agonists

2.4 RESULTS

In the course of this study, stable extracellular recordings were made from a total of 57 spontaneously active MVN neurones in horizontal slices of the dorsal brainstem in vitro. These neurones had a mean resting discharge of 19.7 ± 0.7 spikes/sec which is similar to that of previous studies (Dutia *et al.*, 1992; Wang and Dutia, 1995).

Postsynaptic inhibition of MVN neurones by N/OFQ

The effects of N/OFQ at concentration of 0.1–1.0 μM were tested on 57 spontaneously active MVN neurones. Bath application of N/OFQ resulted in an inhibition of the discharge rate in 49 of 57 neurones (86%), while the remaining neurones were unresponsive. The N/OFQ-induced inhibition was dose-dependent. As illustrated for two neurones in figures. 2.4.1.1 and 2.4.1.2, the inhibitory effect of N/OFQ was seen rapidly after the drug reached the slice and full recovery occurred over the 5-15 minutes after the end of the 60-second exposure to the peptide.

The inhibitory effect induced by N/OFQ persisted in the presence of modified low Ca^{2+}/ Co^{2+} aCSF medium (n = 3 neurones) (Llinas and Sugimori, 1980), that abolished synaptic neurotransmission. As shown in the example in figure 2.4.1.3, the spontaneous discharge rate of the MVN neurones increased in this modified aCSF, but the inhibitory effects of N/OFQ were similar to those in normal aCSF, suggesting a direct action of N/OFQ on the postsynaptic receptor of the recorded neurones.

Protease inhibitor on N/OFQ action and the effect of [des-Phe^1]-nociceptin

In order to confirm that the inhibitory action of N/OFQ was due to the peptide itself and not any possible products of its degradation following proteolysis within the slice tissue, in three further experiments bath applications of N/OFQ were conducted in the continuous presence of the peptidase inhibitor, bestatin (20 μM). This procedure did not alter the inhibitory response of the MVN neurones to N/OFQ or alter their discharge rates in the presence of bestatin. In addition, as the example in figure. 2.4.1.2, bath application of the inactive analogue of N/OFQ, [des-phe^1]-nociceptin (1 - 3μM) had no effect on the spontaneous discharge rate of the MVN

neurones, and did not interfere with the action of N/OFQ when co-applied with N/OFQ.

N/OFQ-induced inhibition of the MVN neurones mediated via ORL1 receptors

In 18 of the 57 MVN neurones, the effects of N/OFQ and the selective δ-opioid receptor agonist [D-Ala^2, D-Leu^5]-enkephalin (DADLE) over a dose range of 3-30 μM were systematically tested. The effects of N/OFQ and DADLE are summarised as in table 2.4. Of these, 11/18 neurones (61%) were inhibited both by N/OFQ and DADLE, while 5/18 neurones (28%) were inhibited only by DADLE and did not respond to N/OFQ up to a dose of 30 uM. Conversely, in 2/18 cells (11%) nociceptin induced a dose-related inhibition but DADLE was ineffective (Fig. 2.4.1.4).

In 6 other neurones, which were inhibited both by N/OFQ and DADLE application of non-selective opioid receptor antagonist, naloxone at a concentration of 10 μM reversibly blocked the inhibitory effect of DADLE while the inhibitory effect of nociceptin remained unaffected (Fig. 2.4.1.5). By contrast, a selective antagonist of the ORL1 receptor, [Phe^{1}ψ(CH$_2$-NH)Gly^2]nociceptin(1-13)NH$_2$ at a concentration of 30nM-100nM effectively blocked the inhibitory action of N/OFQ but not that of DADLE (Fig. 2.4.1.6). The effect of [Phe^{1}ψ(CH$_2$-NH)Gly^2]nociceptin(1-13)NH$_2$ on the action of N/OFQ was reversible.

Interaction between N/OFQ and DADLE

The similarity between the effect of ORL1 receptor agonist, N/OFQ and the δ-opioid receptor agonist, DADLE suggests that both agonists may activate the same ionic conductance. If this were the case, it would be expected that the maximum conductance change evoked by the agonists at the two receptors would be the same and any combination of agonists should produce inhibition which never exceed this maximum. In 4 further experiments on neurones that were responsive to both agonists, concomitant application of nociceptin (1μM) and DADLE (10μM) produced an inhibition which was either the same as, or somewhat smaller than, the inhibition caused by nociceptin alone (Figs. 2.4.1.5B and 2.4.1.7). This finding indicates that occlusion rather than summation occurs between the receptor-messenger systems activated by the two peptides in MVN cells.

Effects of N/OFQ on membrane properties of MVN neurones

The effects of N/OFQ (1 - 3μM) were also tested on eight MVN neurones recorded intracellularly, of which four were classified as Type A neurones and four as Type B neurones. All neurones included in this study had apparent input membrane resistance exceeding 100 MΩ and action potential amplitude larger than 60 mV. The mean RMP and spontaneous discharge rates of the two subtypes of MVN neurones were not different (Type A: -44.5 ± 1.0 mV and 27.0 ± 1.6 spikes/sec, respectively. n = 4; Type B: -45.3 ± 0.9 mV and 25.4 ± 1.7 spikes/sec, n = 4).

In all neurones (Type A and Type B) exposure to N/OFQ by bath perfusion for 1 min, caused a marked decrease of the spontaneous discharge rate (a decrease of more than 10% of control) accompanied by a detectable membrane hyperpolarisation as shown by the example in figure 2.4.1.8. During N/OFQ–induced hyperpolarisation, the input membrane resistance decrease from the control value by more than 20%, measured as voltage deflections produced by injecting depolarising and hyperpolarising current pulses through recording electrode (Fig. 2.4.1.9).

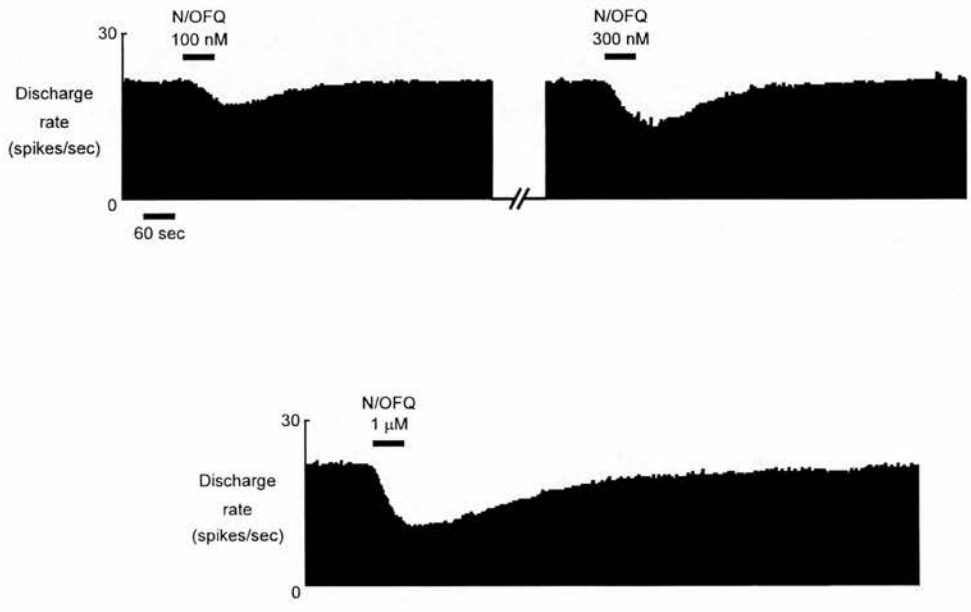

Figure 2.4.1.1 : Dose-dependent inhibitory effect of N/OFQ

Discharge rate histograms from extracellular recordings showing dose-dependent inhibition relationship of a single spontaneously active MVN neurone to successively increasing concentration of N/OFQ (0.1-1μM). In this and subsequent figures, the perfusion of solution was changed to one containing agonists at the given dose during the duration indicated by the solid horizontal bar above the traces.

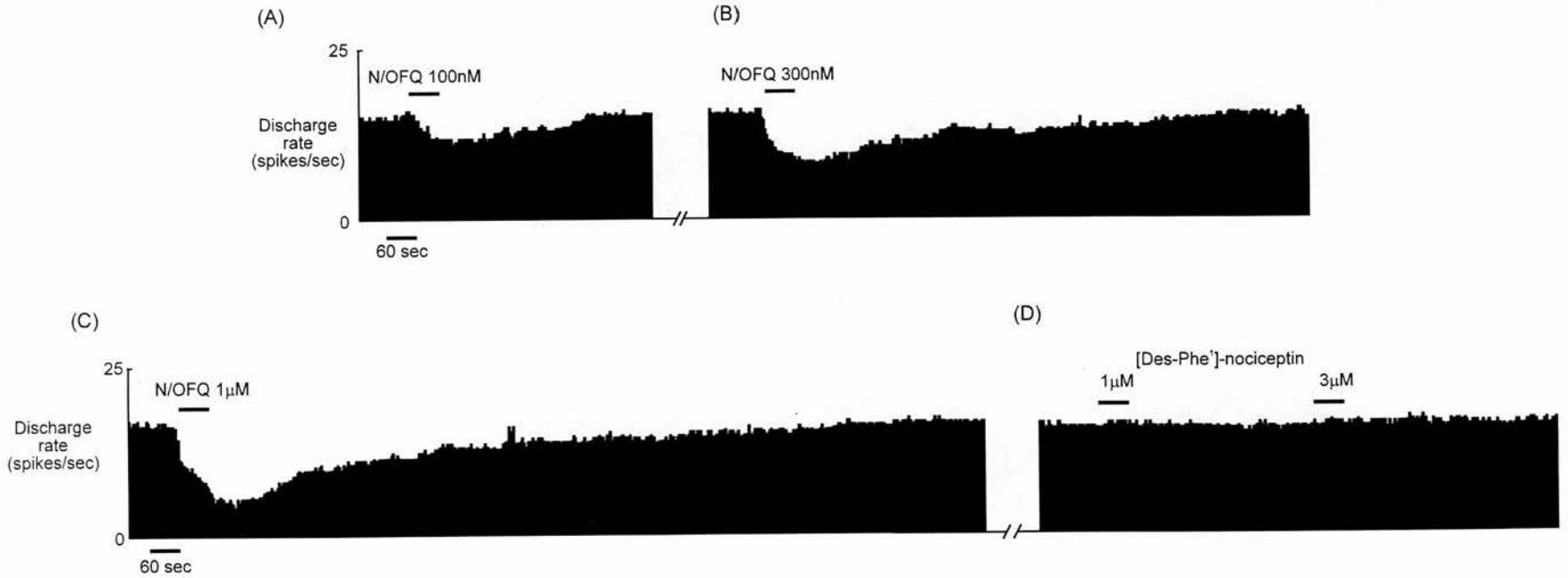

Figure 2.4.1.2 : Effect of N/OFQ and its active analogue on MVN neurone

(A-C) Example of a single MVN neurone that was inhibited in dose-dependent manner by various doses of N/OFQ.

(D) Lack of response of this neurone to inactive analogue of N/OFQ, [des-Phe1]-nociceptin.

Legend 2.4.1.3 : Persistence of N/OFQ-induced inhibition during blockade of synaptic neurotransmission.
Recordings from two different MVN neurones (A) and (B) are shown. The neurones that have been previously inhibited by N/OFQ in normal aCSF were inhibited by the peptide at the same dose in modified low Ca^{2+}, Co^{2+} aCSF. The arrows indicates the early increased in the discharge rate of the neurones in modified aCSF indicating the blockade of synaptic transmission.

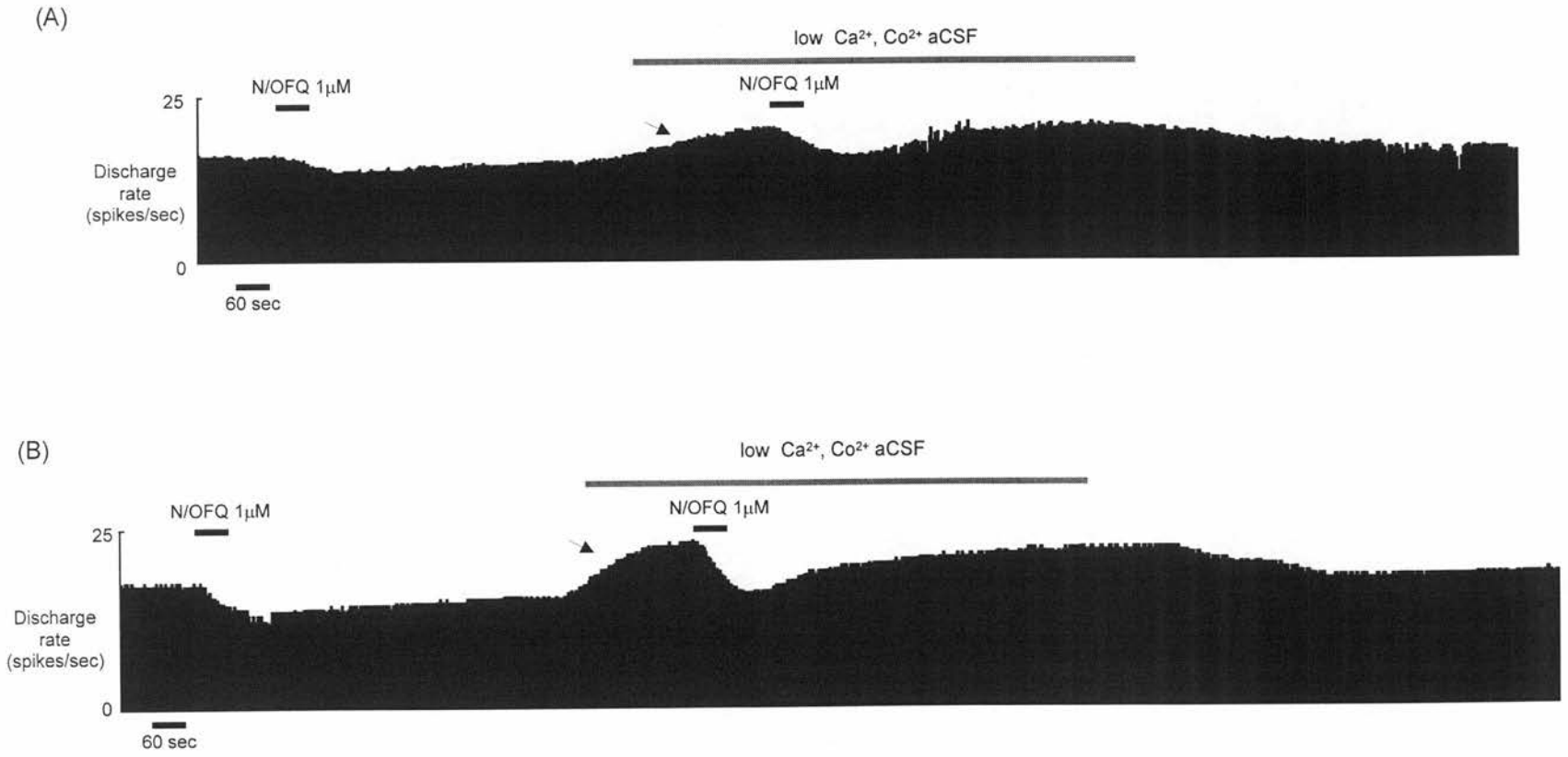

Figure 2.4.1.3 : Persistence of N/OFQ-induced inhibition during blockade of synaptic neurotransmission.

TABLE 2.4

COMPARISON EFFECTS OF N/OFQ AND DADLE ON MVN NEURONES

Nociceptin/orphanin FQ (N/OFQ)	[D-Ala^2, D-Leu^5]enkephalin (DADLE)	
Inhibition	Inhibition	11
Inhibition	No effect	2
No effect	Inhibition	5
No effect	No effect	0

(n = 18 neurones)

Legend 2.4.1.4 : Comparison effects of N/OFQ and DADLE on the MVN neurones

Examples of discharge rate histograms showing the effects of N/OFQ and DADLE on three different MVN neurones. (A) N/OFQ had no effect, while DADLE caused decrease in discharge rate. (B) N/OFQ caused decrease in discharge rate but not DADLE (C) Both agonists produced inhibition in this neurone.

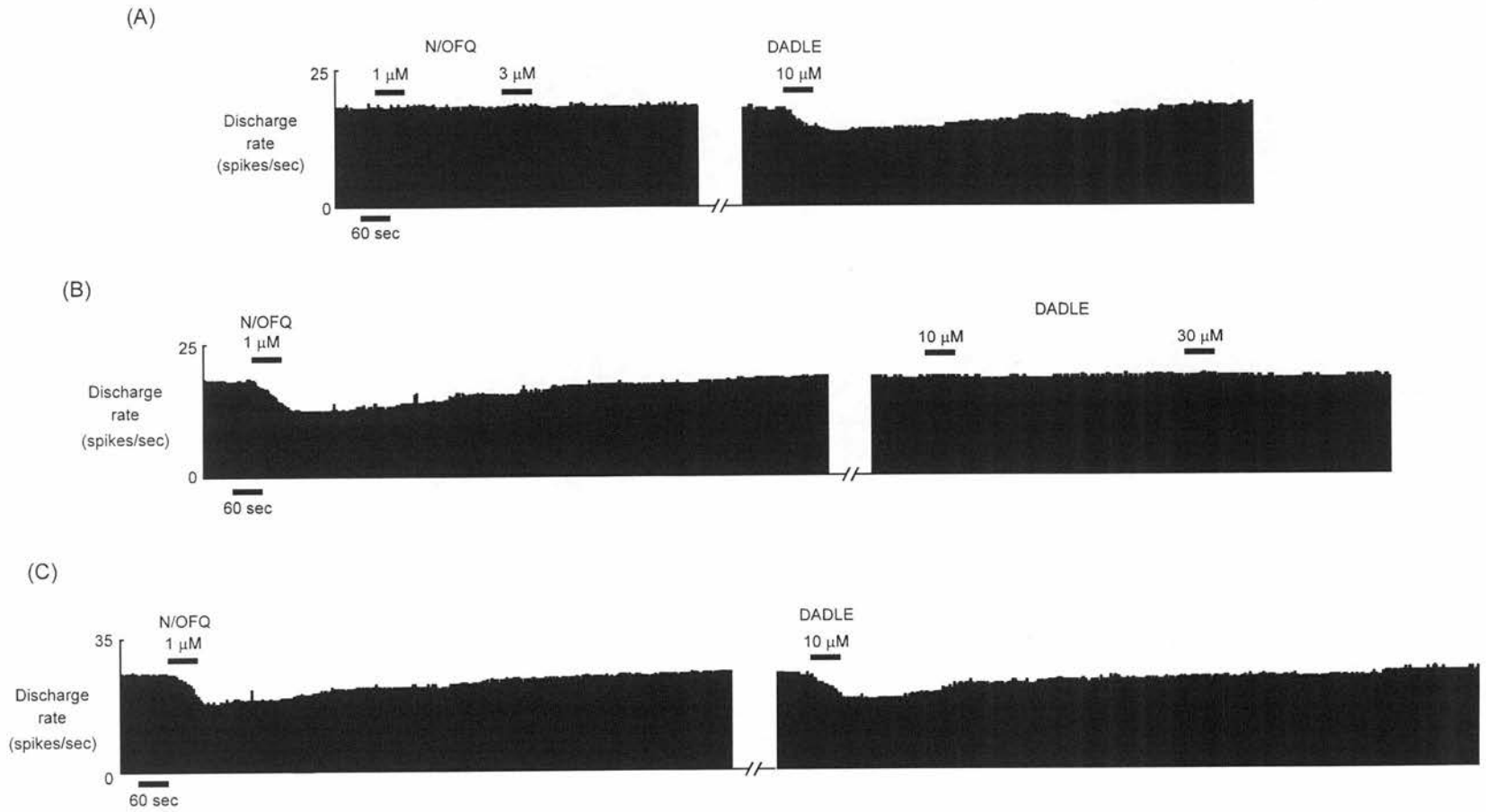

Figure 2.4.1.4 : Comparison of effects of N/OFQ and DADLE on the MVN neurones

Legend 2.4.1.5 : Interaction between N/OFQ and DADLE , and effect of naloxone

Recording from a single MVN neurone illustrating (A) the inhibitory effect of both N/OFQ and DADLE. (B) Co-application of N/OFQ and DADLE caused inhibition that is smaller than the inhibition caused by N/OFQ alone. (C) Non-selective opioid receptor antagonist, naloxone failed antagonise the inhibitory effect of N/OFQ but effectively reversed the inhibitory effect of DADLE.

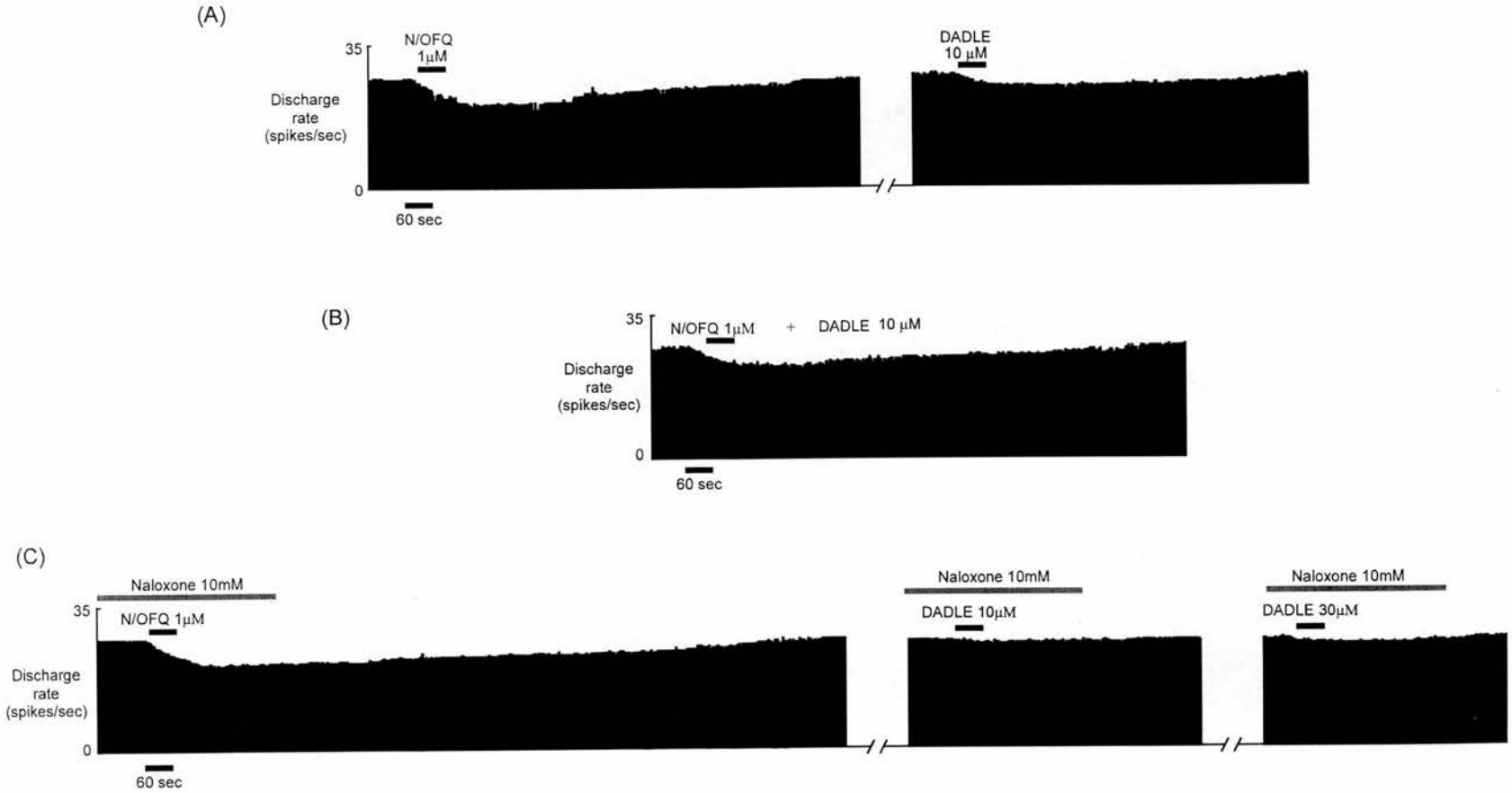

Figure 2.4.1.5 : Interaction between N/OFQ and DADLE, and effect of naloxone

Legend 2.4.1.6 : Antagonism by selective ORL1 receptor antagonist of N/OFQ-induced inhibition.

(A) Dose-dependent inhibition induced by N/OFQ and DADLE in control medium. Note that 1 mM N/OFQ is required to cause complete inhibition of the spontaneous discharge rate of this neurone. (B) After 15 minutes perfusion with selective ORL1 receptor antagonist. In this medium, 3 μM N/OFQ is required to produce similar inhibition as in normal medium and ORL1 receptor antagonist failed to antagonise the effect of DADLE.

(A) control

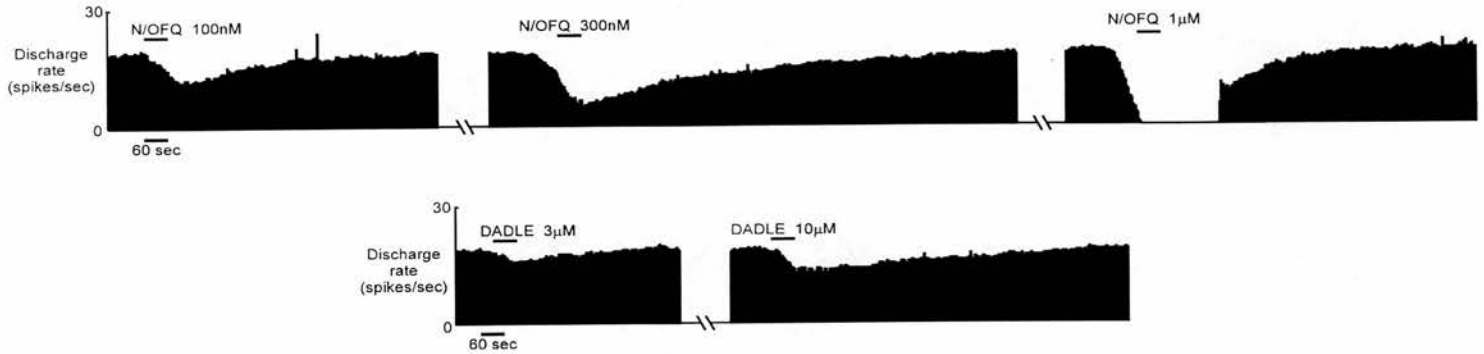

(B) 30nM [Phe$^1\psi$(CH$_2$-NH)Gly^2]nociceptin(1-13)NH$_2$

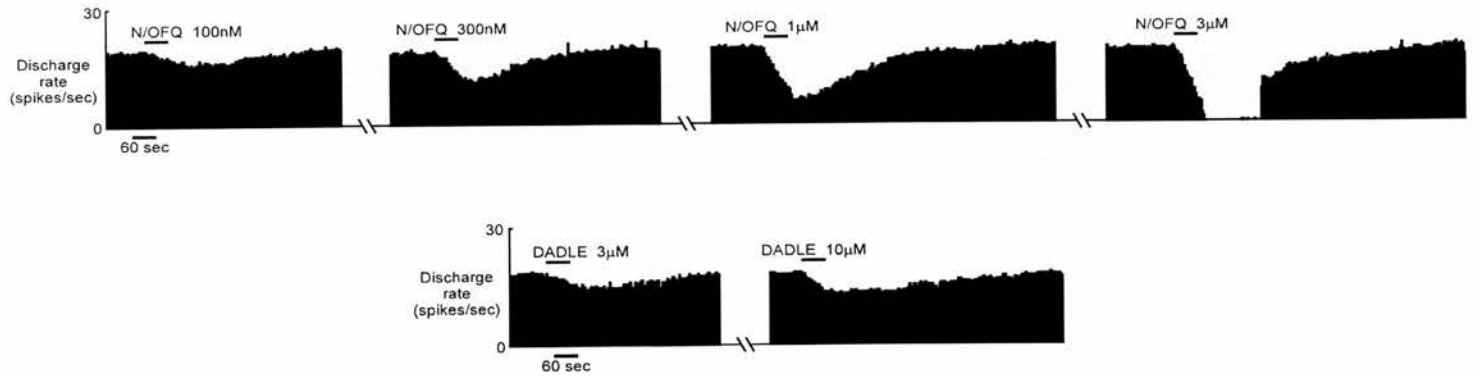

Figure 2.4.1.6 : Antagonism by selective ORL1 receptor antagonist.

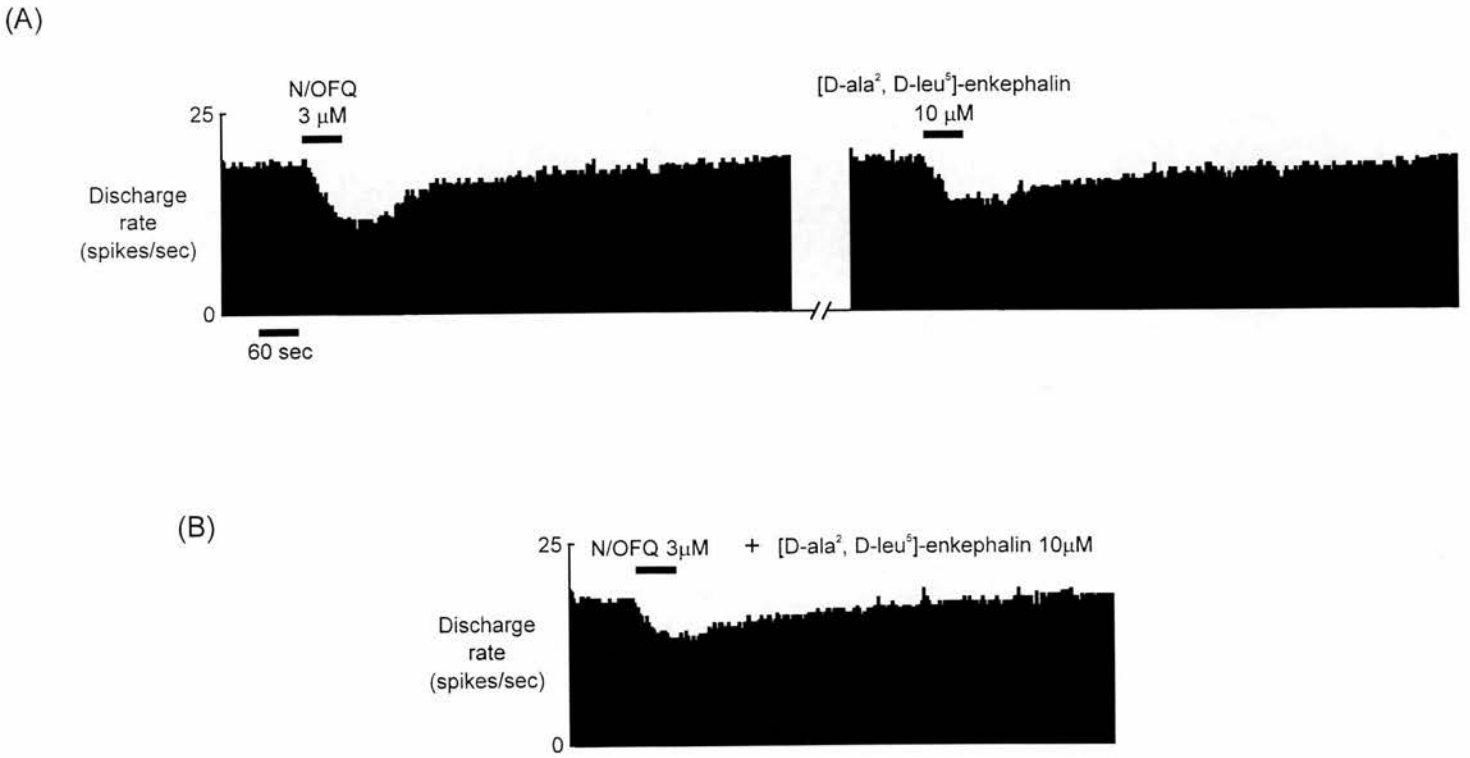

Figure 2.4.1.7 : Interaction between N/OFQ and DADLE

(A) Inhibitory effects of a single MVN neurone with N/OFQ (44% inhibition) and DADLE (27%). (B) Co-application of both agonists produced inhibition (24%) which is smaller than the inhibition caused by N/OFQ or DADLE alone.

Legend 2.4.1.8 : Whole-cell patch-clamp recordings of MVN neurone

(A) Inhibition of the spontaneously active MVN neurones by N/OFQ (1μM). This was accompanied by membrane hyperpolarisation (arrow). (B) Firing rate of the same neurone as in (A).

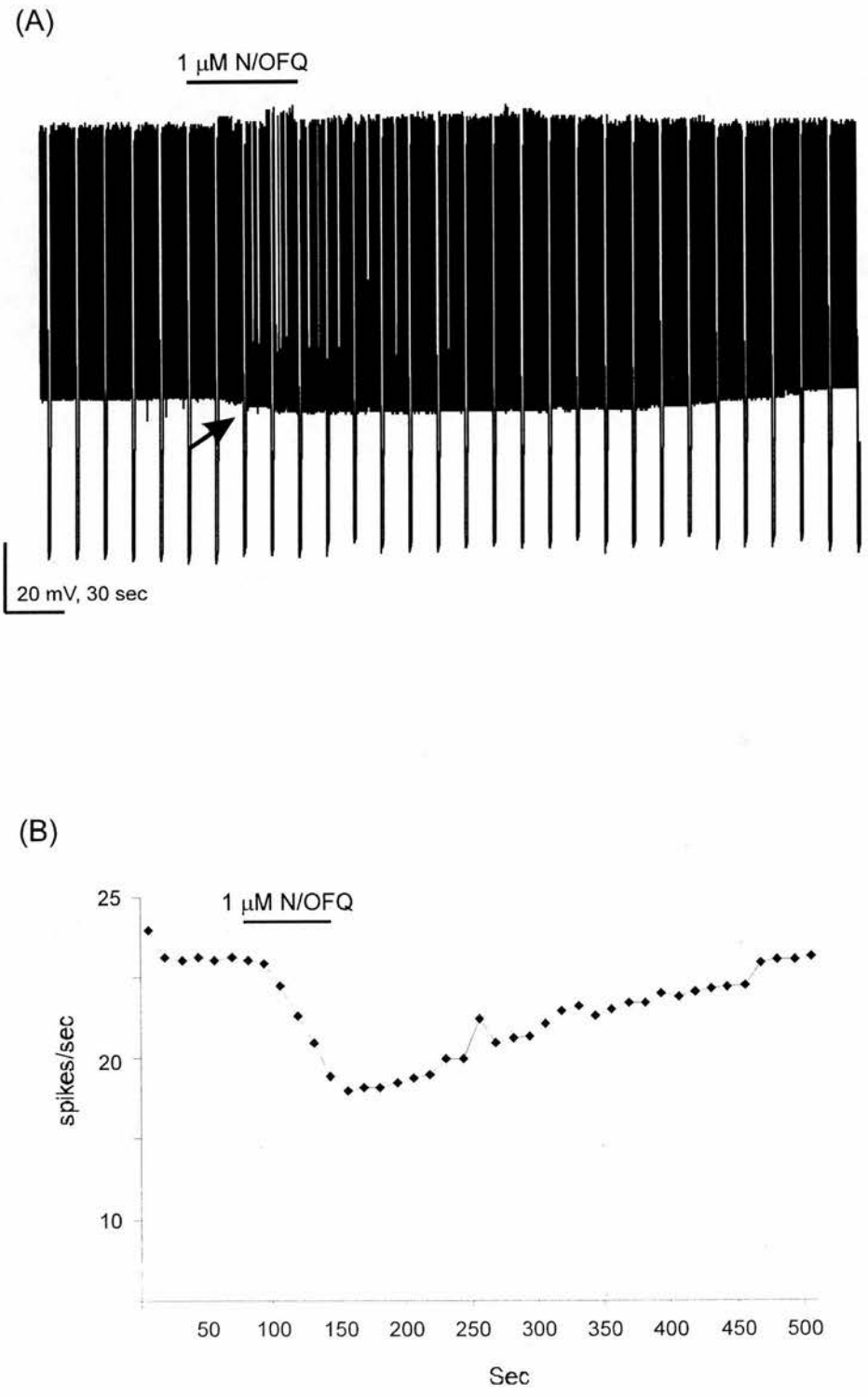

Figure 2.4.1.8 : Whole-cell patch-clamp recordings from MVN neurone

Legend 2.4.1.9 : Effects of N/OFQ on membrane input resistance

Example of voltage-current relationship (raw data) of MVN neurone to N/OFQ. Response of membrane voltage to a graded series of a constant depolarising and hyperpolarising current pulses (bottom) in normal aCSF (A) and during maximum effect of N/OFQ (B). Arrow indicates where measurements were made. (C) The slope of I-V curves is reduced from 104 MΩ in control to 87 MΩ in the presence of N/OFQ, indicating a decrease in membrane input resistance. The membrane potential was held at -60 mV.

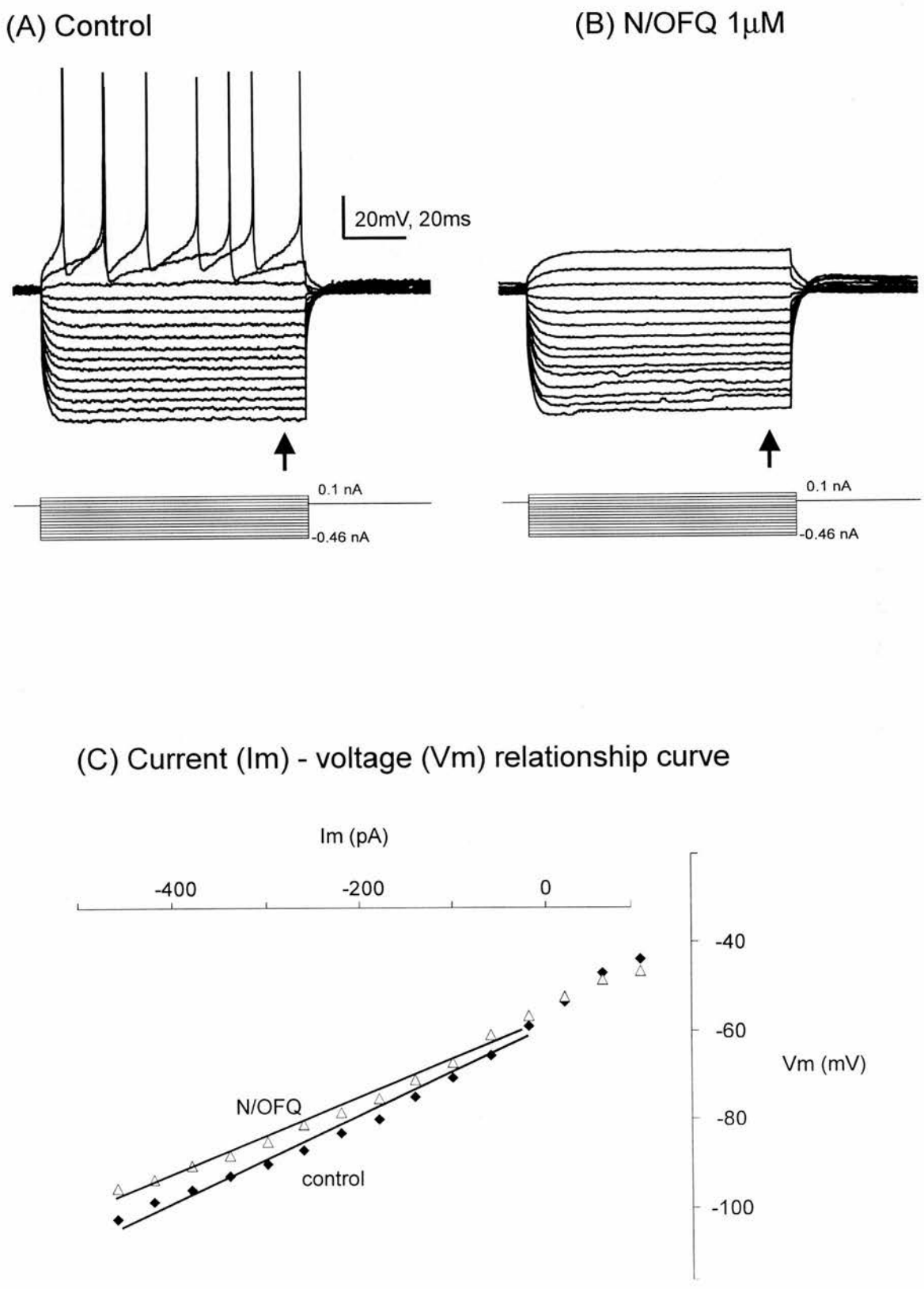

Figure 2.4.1.9 : Effect of N/OFQ on membrane input resistance of MVN neurone

2.5 DISCUSSION

Postsynaptic inhibition of N/OFQ on MVN neurones

In the present study, it has been demonstrated that bath application of the endogenous ORL1 receptor ligand, N/OFQ dose dependently inhibited the ongoing discharge rate of over 80% of spontaneously active MVN neurones in slices of the rat dorsal brainstem *in vitro*. The minimum concentration of N/OFQ required for the inhibition *in vitro* was 100 nM. These results are consistent with the reported in situ hybridisation and immunohistochemical studies indicating the presence of low to moderate level of ORL1 receptor mRNA (Anton *et al.*, 1996; Darland *et al.*, 1998) in the MVN. The inhibition of MVN neurones resulting from activation of ORL1 receptors is similar to that reported in the rat substantia gelatinosa neurones (Lai *et al.*, 1997), supraoptic nucleus neurones (Doi *et al.*, 1998) and cardiomotor neurones in the rostral ventrolateral medulla (Chu *et al.*, 1998). It is presumed that as in those other regions, the inhibitory effect of nociceptin seen in these study results from an increased membrane potassium conductance.

The inhibitory effect of N/OFQ was likely to be mediated through direct activation of receptors located on the postsynaptic neurone as the inhibition effect persisted after blockade of synaptic transmission in modified low Ca^{2+}/Co^{2+} aCSF medium (Llinas and Sugimori, 1980). In addition, the peptidase inhibitor, bestatin did not increase the potency of the inhibitory effect of N/OFQ indicating that the effects were due to the peptide itself and not any possible products of its degradation. The functional importance of phe^1 moiety in the binding of N/OFQ to the ORL1 receptor was also demonstrated, as [des-phe^1]- nociceptin did not alter the discharge rate of any MVN neurones tested and a combination of N/OFQ with [des-phe^1]-nociceptin did not interfere with the inhibitory effect of N/OFQ (Dooley and Houghton, 1996; Doi *et al.*, 1998).

N/OFQ-induced inhibition of the MVN neurones mediated via ORL1 receptors

In Chapter 1, it has been demonstrated that δ- but not μ-, or κ-opioid receptors are present on spontaneously active MVN neurones in vitro and that the inhibitory action of δ-opioid receptors was due to an increase in a TEA-sensitive potassium conductance in the cell (Sulaiman and Dutia, 1998). In the present study, N/OFQ acts via an interaction with the ORL1 receptor to inhibit the discharge rate of

MVN neurones and not via a δ-opioid receptor mediated mechanism, since the majority of MVN neurones were inhibited both by nociceptin and δ-opioid receptor agonist, DADLE, while a minority of MVN neurones were inhibited either by nociceptin or DADLE. Furthermore bath application of the non-selective opioid receptor antagonist, naloxone did not diminish the effect of N/OFQ but effectively antagonised the response of DADLE. Conversely application of the selective ORL1 receptor antagonist, [Phe$^1\psi$(CH_2-NH)Gly^2]nociceptin(1-13)NH_2 reversibly antagonised the effect of N/OFQ but had no effect on the responses to DADLE. These findings are consistent therefore with an inhibitory action of N/OFQ on rat MVN neurones through its direct activation of the ORL1 receptor. This is supported by the fact that the potency of N/OFQ was comparable to that found by others at the ORL1 receptor both in the CNS and also in heterologous expression systems (Matthes *et al.*, 1996; Vaughan and Christie, 1996; Vaughan *et al.*, 1997). These results also indicate that both ORL1 and δ-opioid receptors are co-expressed on the majority of rat MVN neurones.

Interaction between N/OFQ and DADLE

Co-existence of μ-opioid receptors, somatostatin receptors, α-adrenoceptor and ORL1 receptors have been shown for rat locus coeruleus neurones (Connor *et al.*, 1996). Agonists of these receptors act on their distinct receptor to activate the same population of potassium channels. In this study, it has been found that both δ-opioid and ORL1 receptors act on distinct receptors to affect the same conductance (presumably a K^+ conductance) because co-application of nociceptin and DADLE produced an inhibition which was similar to the inhibition that was caused by nociceptin or DADLE alone. This finding indicates that occlusion rather than summation occurs between the receptor-messenger systems activated by the two peptides in MVN neurones.

Ionic mechanisms of N/OFQ-induced inhibition

Recent studies on other neurone types have demonstrated that N/OFQ-induced hyperpolarisation is associated with activation of a K^+ conductance, through G-proteins coupled to the ORL1 receptor (for a review, refer to part 2.1.1). In this study the membrane hyperpolarisation and decrease in input resistance seen in MVN neurones in response to N/OFQ is in agreement with such actions on K^+

conductances, though further voltage clamp experiments are necessary to confirm the conductance(s) involved.

The functional importance of N/OFQ pathways in modulating vestibular reflexes *in vivo* will be an interesting area of future research. In parallel experiments to the *in vitro* study described in this chapter, our collaborators in Linköping, Sweden carried out an analysis of the effects of intracerebroventricular (i.c.v.) injection of N/OFQ on the VOR in the alert rat (Sulaiman *et al.*, 1999, in press). They showed that low concentration of N/OFQ i.c.v., which did not cause general behavioural effects, caused a significant decreased in the gain of the VOR. This was accompanied by a significant increase in the time-constant of post-rotatory nystagmus, indicating that the "velocity-storage" mechanism in the brainstem was significantly potentiated by N/OFQ. Although these *in vivo* results probably involve the effects of N/OFQ on many other sites in addition to MVN neurones (e.g. cerebellar flocculus), these *in vivo* and *in vitro* results show that N/OFQ has a role in modulating vestibular function, which has now to be explored in more detailed in future work.

CHAPTER 3

ELECTROPHYSIOLOGICAL PROPERTIES OF NEURONES IN THE RAT MEDIAL VESTIBULAR NUCLEUS FOLLOWING UNILATERAL LABYRINTHECTOMY

3.1 LITERATURE REVIEW

3.1.1 VESTIBULAR COMPENSATION

Vestibular compensation a model of lesion-induced plasticity

In all classes of vertebrates, surgical removal of the peripheral vestibular receptors of one ear (unilateral labyrinthectomy, UL) or transection of the VIIIth cranial nerve results in the loss of excitatory input to the vestibular nucleus complex ipsilateral to the lesion, resulting in an imbalance in neuronal activity between the two sides of the brainstem. Since many of the vestibular neurones project directly to the motoneurones controlling the ocular and skeletal musculature, the imbalance in neuronal activity on the lesioned and intact sides of the vestibular nuclei is believed to generate the characteristic syndrome of severe oculomotor and postural symptoms, including spontaneous ocular nystagmus, roll- and yaw-tilt of the head, contralateral limb extension and ipsilateral limb flexion, barrel-rolling and circular walking, that is consistent among all vertebrate species (for reviews see Smith and Curthoys, 1989; Curthoys and Halmagyi, 1995; Dieringer, 1995; Vibert *et al.*, 1997). Remarkably, over time, many of the severe symptoms following UL gradually disappear or decrease in a process of behavioural recovery known as "vestibular compensation" (VC). Since the peripheral vestibular receptors do not regenerate and neurones in Scarpa's ganglion do not undergo functional recovery following UL, the phenomenon of VC has been attributed to plasticity in the central vestibular pathways, and is regarded as an attractive model for studying lesioned-induced plasticity in the adult mammalian central nervous system (CNS).

The severe symptoms following UL are divided into two categories, "static" and "dynamic" symptoms, depending upon their relationship to head movement. Static symptoms occur in the absence of head movement and include spontaneous ocular nystagmus, deviation of the eyes towards the lesioned side, roll- and yaw-tilt of the head. Dynamic symptoms such as impaired gain and phase of the vestibulo-ocular and vestibulo-spinal reflexes occur as a result of head movement (Fisch, 1973; Maioli *et al.*,

1983). Although, the exact time-course of vestibular compensation varies among species, it is the static symptoms which undergo a remarkable degree of compensation while the dynamic symptoms compensate more slowly and compensation is normally incomplete (Curthoys and Halmagyi, 1995).

Behavioural changes following unilateral labyrinthectomy (UL).

Static symptoms

In mammals, the most prominent ocular motor effect immediately after UL is a spontaneous nystagmus, with quick phases directed away from the lesioned side, and slow phases directed toward the lesioned side (for reviews see Smith and Curthoys, 1989; Curthoys and Halmagyi, 1995; Vibert *et al.*, 1997). In non-mammalian species such as frogs and probably in all amphibians, the spontaneous nystagmus of the eyes is absent. Instead the eyes undergo a tonic deviation toward the side of the lesioned labyrinth (Precht and Dieringer, 1985; Dieringer, 1995). The recovery period of the spontaneous nystagmus after UL varies among species, from a few hours for the rat (Hamann and Lannou, 1988) and guinea pig (Curthoys *et al.*, 1988), to a few days for the cat (Maioli *et al.*, 1983; Maioli and Precht, 1985) and monkey (Fetter and Zee, 1988), to about a week for humans (Cass *et al.*, 1992).

UL also causes severe disturbances in maintaining the posture of the head and eyes, which has been referred as the ocular tilt reaction. The ocular tilt reaction consists of roll- and yaw-tilt of the head, skew deviation of the eyes, ipsilateral flexion and contralateral extension of the forelimbs, circling and rolling toward the lesioned side (for reviews see Halmagyi *et al.*, 1979; Curthoys *et al.*, 1988, 1991; Curthoys and Halmagyi, 1995). Changes in maintained head posture after UL are more prominent in species such as guinea pigs (Curthoys *et al.*, 1988; De Waele *et al.*, 1989), rats (Sirkin *et al.*, 1984; Hamann and Lannou, 1988), cats (Xerri and Lacour, 1980; Cass and Goshgarian, 1991) and monkeys (Fetter and Zee, 1988) than in human (Halmagyi *et al.*, 1979). In the former four species, UL results in both roll- and yaw- head tilts, while in humans the head tilt is moderate. As mentioned earlier, recovery of postural abnormalities induced by UL varies among species. It may take several hours in rats

(Sirkin *et al.*, 1984; Hamann and Lannou, 1988), days in guinea pigs (Smith *et al.*, 1986b; Smith *et al.*, 1986a) weeks in monkeys (Fetter and Zee, 1988) and months in frogs (Dieringer and Precht, 1982; Dieringer, 1995). Recovery of the postural abnormalities occurs much faster in the presence of visual input (Putkonen *et al.*, 1977; Smith *et al.*, 1986a).

UL also causes skew deviation of the eyes, in which the eye on the ipsilateral side to the lesion is held lower in the orbit than the eye on the intact side (Halmagyi *et al.*, 1979; Curthoys *et al.*, 1991; Wolfe *et al.*, 1993). In species such as guinea pigs, rabbits, rats and horses, the eye on the side of the lesion deviates down and the eye on the contralateral side deviates up, while in humans the eye on the lesioned side moves down and the eye on the opposite side remains in its normal position (Baarsma and Collewijn, 1975; Halmagyi *et al.*, 1979; Dieringer and Precht, 1982; Sirkin *et al.*, 1984; Curthoys *et al.*, 1991).

Dynamic symptoms

The dynamic symptoms following UL include a disruption of the vestibularly mediated ocular motor and postural reflexes, which are evoked by head movement. While the static symptoms caused by UL and their compensation have been known for 150 years, the dynamic symptoms were first described when measures of ocular motor and postural reflexes became available about 50 years ago (Curthoys and Halmagyi, 1995).

In mammals, UL causes severe deficits in the gain, symmetry and timing of the horizontal vestibulo-ocular reflex (VOR). Numerous studies have shown severe and permanent VOR gain asymmetry following UL in which the gain of the VOR is smaller for head rotations toward the lesioned side compared to that of head rotations towards the intact side representing an asymmetric VOR gain. Therefore, eye movements are neither sufficient in amplitude nor phase in order to compensate for head movements (Baarsma and Collewijn, 1975; Maioli *et al.*, 1983; Maioli and Precht, 1985; Cass and Goshgarian, 1991).

The dynamic symptoms improve over a period of weeks, however comparatively their compensation is much slower and more limited than in the case of the static symptoms. In all species studied, the asymmetry of the VOR gain appears to be permanent since deficits in the VOR gain can be detected many months or even years following UL (for reviews see Smith and Curthoys, 1989; Curthoys and Halmagyi, 1995).

Neuronal changes following UL

Extensive *in vivo* extracellular electrophysiological studies from brainstem vestibular relay neurones, particularly the medial vestibular nucleus (MVN) neurones have been carried out in order to examine the changes in neural activity that occur during VC (Precht *et al.*, 1966; Markham *et al.*, 1977; Ried *et al.*, 1984; Hamann and Lannou, 1988; Smith and Curthoys, 1988a, 1988b; Newlands and Perachio, 1990a, 1990b; Ris *et al.*, 1995, 1997). These studies have demonstrated the sequence of changes in the resting activity of the vestibular neurones, which correlates well with the sequence of changes in behaviour. It has been shown that immediately after UL or vestibular neurorectomy, the normally high resting discharge rate of most MVN neurones on the ipsilateral side of the lesion is largely abolished but gradually restored over time as VC advances (Fig. 3.1.1.1).

Smith and Curthoys (1988a,b) demonstrated that immediately after UL (0-8 hours) in anaesthetised guinea pigs, there is a reduction in the number of Type I neurones recorded from the MVN on the ipsilateral side to the lesion and the average resting discharge of recorded neurones is very low. Studies in alert guinea pigs also reveal that during the first 10 hours after UL, 69% of the Type I MVN neurones on ipsilateral side are silent while the remaining active neurones have a very low average resting discharge (Ris *et al.*, 1995, 1997). Conversely, recordings from MVN neurones contralateral to the lesion show an increase in the resting discharge rate of the Type I MVN neurones. These results are consistent with the recordings of single neurone activity in cats (Markham *et al.*, 1977; Ried *et al.*, 1984), gerbils (Newlands and

Perachio, 1990a) and rats (Precht *et al.*, 1966; Hamann and Lannou, 1988). The loss of neuronal activity in the Type I MVN neurones on the ipsilateral side to the lesion appears to be caused not only by the loss of excitatory drive from the lesioned ipsilateral primary vestibular afferents, but also due to an enhanced commissural inhibition from the contralateral MVN neurones, which become hyperactive due to loss of inhibitory drive from the ipsilateral side (Fig. 3.1.1.1: Smith and Curthoys, 1988a, 1988b; Curthoys and Halmagyi, 1995).

While recordings from Type 1 MVN neurones on the ipsilateral side showed an immediate decrease in the resting discharge rate and increase on the contralateral side at 0 - 8 hours post-UL, the resting discharge rate of Type II MVN neurones on the ipsilateral side was reported either to increase (Shimazu and Precht, 1965; Smith and Curthoys, 1988b) or remain the same as normal (Hamann and Lannou, 1988). On the contralateral side, the resting discharge rate of Type II MVN neurones were reported to be lower than that of normal animals (Smith and Curthoys, 1988b) or virtually absent (Ried *et al.*, 1984).

Apart from these electrophysiological studies, this early imbalance in the neuronal activity between both sides of the MVN has also been suggested by studies using other indicators of activity including 2-deoxyglucose (Patrickson *et al.*, 1985; Luyten *et al.*, 1986), c-fos expression (Kaufman *et al.*, 1992; Cirelli *et al.*, 1993; Kitahara *et al.*, 1995; Cirelli *et al.*, 1996) and recently glial fibrillary acidic protein (GFAP) mRNA expression (de Waele *et al.*, 1996).

As VC progresses, the imbalance in neuronal activity of Type I MVN neurones on both sides of the brainstem gradually improves. Recording from guinea pig MVN neurones on the ipsilateral side to the lesion showed that the resting discharge rate of Type I MVN neurones returned to normal, 52 hours after UL (Smith and Curthoys, 1988b) and a recent study in the alert guinea pig demonstrated that a resting discharge rate of Type I MVN neurones on the ipsilateral side begin to recover as early as 12 hours post-UL with complete restoration within 1 week post-UL (Ris *et al.*, 1995). The

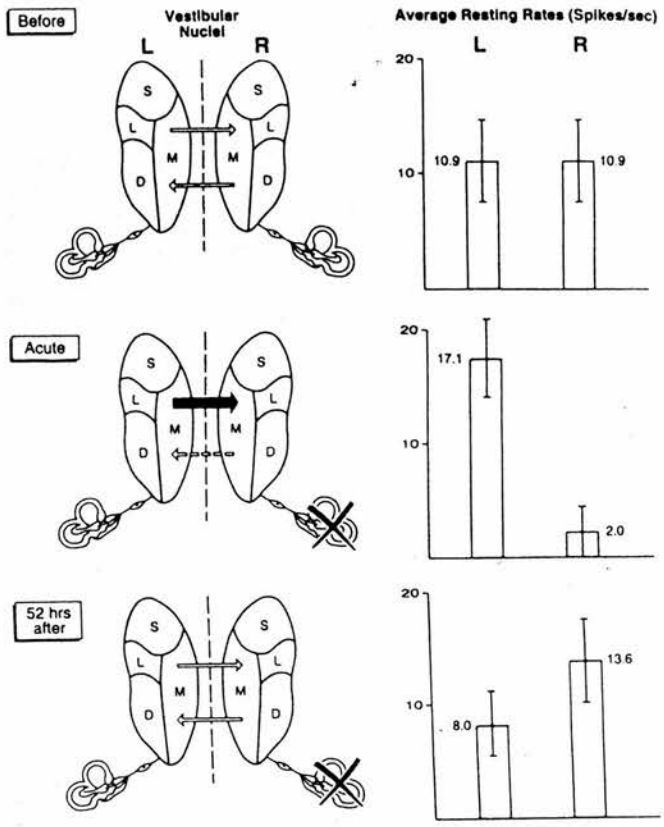

Figure 3.1.1.1 : <u>The interaction between the VN and changes in resting activity following UL</u>

Before UL, each MVN receives excitatory input from the eight nerve and exerts inhibition via the commissural fibers on the opposite MVN. The average resting discharge is equal in both nuclei. Following UL (0-8h) Type I neurones on the lesioned side (ipsilateral side) are now disfacilitated due to the loss of their excitatory input. The resting discharge of MVN neurones in the ipsilateral side drops to a low value, thus inhibition of the contralateral MVN is reduced. In turn, the contralateral MVN neurones become hyperactive and they thus exert greater inhibition on the neurones in the ipsilateral side (thick arrow). Thus the ipsilateral MVN neurones rapidly fall silent after UL, while the neurones on the contralateral side are hyperactive. However, during VC (52h after UL) the vestibular neurones on the ipsilateral side recover their resting activity, and the marked imbalance in excitability is progressively reduced.

(Adapted from Curthoys and Halmagyi, 1995)

restoration of normal spontaneous neuronal activity of Type I MVN on the ipsilateral side seems to correlate with the recovery of the initial static symptoms of UL. In guinea pigs, compensation of the static symptoms occurs within 52 hours post-UL (Smith *et al.*, 1986a). In the frog, compensation of the static postural symptoms occurs over a longer time-period, approximately 40 - 70 days post-UL and is also associated with a return of the normal resting activity to neurones in the lesioned side (Dieringer and Precht, 1979a).

Mechanisms of vestibular compensation.

Electrophysiological changes within the vestibular nuclei induced by UL, particularly restoration of spontaneous neuronal activity to Type I MVN neurones on the lesioned side have been associated with the initial rapid stage of behavioural recovery. However the mechanisms underlying the rapid restoration of spontaneous neuronal activity in these ipsilateral Type 1 MVN neurones are still largely unknown. Since the early study by Precht and his colleagues (1966) on the decerebrated cat, several hypotheses have been put forward to explain VC.

Reactive synaptogenesis

Reactive synaptogenesis, the sprouting of healthy axons to form new synapses in response to deafferentation as a possible outcome of UL in cats, was first proposed by Precht *et al.,* (1966), and has often been considered as a likely mechanism of VC. Although there is evidence for reactive synaptogenesis in the frog (Dieringer *et al.*, 1984) and cat (Korte and Friedrich, 1979; Raymond *et al.*, 1991) as early as 5 days post-UL, this cellular process appears to be too slow to account for the rapid time-course of static compensation in other mammalian species. For example, in the guinea pig and rat, neuronal activity returns within 52 h and 24h respectively. Reactive synaptogenesis is clearly too slow to explain the rapid restoration of resting discharge rate of deafferented vestibular nucleus neurones, however, it may be responsible for the long-term stability of VC (Gacek *et al.*, 1988, 1989, 1991; Raymond *et al.*, 1991).

Denervation supersensitivity

Another relatively slow developing cellular process of lesion-induced synaptic plasticity that has been suggested as a possible mechanism of VC is denervation supersensitivity. It is suggested that neurones in the VN, which have been deprived of afferent input by UL, become more sensitive to the transmitter normally released by the now silent primary afferents. This process has been suggested in other neurones to be due to either an up-regulation in the number of postsynaptic receptors or due to an increase in receptor affinity following denervation and occurs within days rather than hours (Sharpless, 1975; Wall and Devor, 1981; Ulas *et al.*, 1990). As far as the VN is concerned, there is no convincing evidence so far to support the denervation supersensitivity hypothesis. Although several studies have suggested that the return of resting discharge rate in the ipsilateral MVN neurones may be associated with an up-regulation of NMDA receptors (Smith and Darlington, 1988; Darlington and Smith, 1989; de Waele *et al.*, 1990; Pettorossi *et al.*, 1992; Flohr and Luneburg, 1993), neither electrophysiological studies nor neurotransmitter binding studies clearly support this hypothesis (for reviews see Smith and Curthoys, 1989; Darlington *et al.*, 1991; Smith and Darlington, 1991). Furthermore the time period of VC does not correlate with the time period required for denervation supersensitivity and therefore does not support this hypothesis as mechanism of VC.

Role of vestibular commissures

Participation of vestibular commissures in the compensation process has been demonstrated in the frog. It has been demonstrated that VC in the frog is associated with an increase in efficacy of excitatory brainstem commissural input to lesioned vestibular neurones (Bienhold and Flohr, 1978; Dieringer and Precht, 1979a; Dieringer and Precht, 1979b; Galiana *et al.*, 1984; Kunkel and Dieringer, 1994; Dieringer, 1995), however, in mammals, there is no evidence in support of this hypothesis (Smith and Curthoys, 1988c; Newlands and Perachio, 1990a). The failure to find any corresponding change in commissural efficacy can most easily be explained by the fact that in mammalian species, the vestibular commissures are functionally inhibitory rather than excitatory (see Galiana *et al.*, 1984 for a discussion).

Cerebellar shutdown

Because of its important role in motor co-ordination in the normal animal, the cerebellum is believed to play a functional role in VC. Involvement of the cerebellum in VC following UL in the cat has been suggested by McCabe and Ryu (1969). They have suggested that the cerebellum is involved in VC by responding to a massive asymmetry of neuronal activity following UL. During the acute stage of post-UL, the cerebellum imposes a shutdown of the intact side in order to rebalance the asymmetry of neuronal activity between the two vestibular nuclei. This hypothesis is called "cerebellar shutdown". The authors also demonstrated that a cerebellectomy released this shutdown of neuronal activity on the intact MVN, indicating that they were previously inhibited by the cerebellum during the critical stage of compensation (McCabe and Ryu, 1969; McCabe *et al.*, 1972). The reduction of horizontal VOR gain for both directions of rotation immediately after UL supports this hypothesis (Fetter and Zee, 1988). However, cerebellar shutdown by itself is not enough to prevent spontaneous nystagmus as it occurs soon after UL. Also, other *in vivo* electrophysiological recordings in cat and other species have shown that MVN neurones in the intact side were not silenced following UL (Markham *et al.*, 1977; Hamann and Lannou, 1988; Smith and Curthoys, 1988a; Ris *et al.*, 1997)

Change in Intrinsic excitability

It has been suggested that an intrinsic capacity of the cell membrane for repetitive firing may be responsible for the regeneration of resting activity which occurs in the lateral cuneate nucleus following partial deafferentation (Kjerulf and Loeser, 1973). In the light of this work, Darlington and Smith (1996) have proposed that such a mechanism may also be functioning in the deafferented VN, since recent studies have demonstrated that the majority of MVN neurones *in vitro* exhibit a spontaneous resting discharge in the absence of synaptic drive (Darlington *et al.*, 1989, 1990; Lewis *et al.*, 1989; Serafin *et al.*, 1990, 1991a; Smith *et al.*, 1991; Dutia *et al.*, 1992) and possess endogenous pacemaker-type properties such as the persistent Na^+ conductance and low and high threshold Ca^{2+} conductances (Serafin *et al.*, 1991b; Johnston *et al.*, 1994).

The first direct evidence for a change in the intrinsic excitability of MVN neurones, which is argued may be responsible for the restoration of the resting discharge on the lesioned side of the MVN following UL was demonstrated by Cameron and Dutia (1997) in rat dorsal brainstem slices. They have shown that a significant increase in the intrinsic excitability of MVN neurones on the lesioned side occurs between 2 - 4 hours after UL. The increase in intrinsic excitability of these neurones was observed as an increase in the mean spontaneous discharge rates of the MVN neurones on the lesioned side when the MVN of the two sides are isolated *in vitro.* Thus, they are removed from the influence of the commissural inhibitory system that normally links them *in vivo.* In addition, the change in intrinsic properties of the MVN on the lesioned side is restricted to the neurones located in the rostral area of the lesioned nucleus where the vestibular nerve afferents predominantly terminate.

It has been suggested that the mechanism underlying the increase in excitability of the deafferented MVN neurones may be due to down-regulation of GABA receptors on these neurones, since it is known that the spontaneous discharge rate of MVN neurones *in vitro* is modulated by GABAergic activity and administration of GABA antagonists results in disinhibition (Dutia *et al.*, 1992). The proposed mechanism is supported by Calza *et al.,* (1992), who observed a decrease in benzodiazapine binding in the MVN on the side of lesion within 3 hours post-UL. In a recent *in vitro* electrophysiological study, Yamanaka *et al.*, (1998, in preparation) observed a marked down-regulation in the efficacy of both $GABA_A$ and $GABA_B$ receptors toward their agonists in the rostral region of the lesioned MVN after 4 hours post-UL. Hence, it is likely that the loss of excitatory input from the primary vestibular afferents is compensated by a decrease in responsiveness of the MVN neurones to inhibitory synaptic input, thus causing an increase in their intrinsic excitability.

In subsequent *in vitro* experiments, Cameron and Dutia (1998, in preparation) have shown that the increase in intrinsic excitability of the rostral MVN neurones after UL in the rat is dependent on the activation of the hypothalamo-pituitary-adrenal stress axis, particularly the activation of glucocorticoid receptors (Grs). The compensatory

increase in intrinsic excitability of MVN neurones did not occur in labyrinthectomised animals that were maintained under urethane anaesthesia for 4 - 6 hours after UL, so that they did not experience the stress that normally results from UL. In these animals, administration of the synthetic GR agonist dexamethasone at the time of UL in order to mimick the stress response, restored the compensatory increase in intrinsic excitability of the MVN neurones. Administration of dexamethasone in itself had no effect on the intrinsic excitability of MVN neurones in sham-operated animals. In conjunction with this experiment, Cameron and Dutia have also demonstrated a high level of c-Fos-like immunoreactivity in the paraventricular nucleus of the hypothalamus 1.5 - 3 hours post-UL in awake animals that experienced the oculomotor and postural symptoms of UL, indicating a strong activation of the stress axis. In addition, administration of the GR antagonist RU38486 at the time of UL abolished the increase in intrinsic excitability of rostral MVN neurones, and significantly delayed recovery of ocular nystagmus and circular walking.

3.2 AIMS OF STUDY

It is well established that surgical removal of one labyrinth of the inner ear (unilateral labyrintechtomy) or transection of vestibular nerve (neurectomy) generates severe disturbances of the vestibulo-ocular and vestibulo-spinal reflexes leading to a complex syndrome of ocular motor and postural symptoms (for details refer to part 3.1.2). However, many of these symptoms recover gradually over time in a process referred to as vestibular compensation (VC). The majority of recent studies using *in vivo* extracellular recording have concentrated on vestibular neurones in the MVN, in order to examine the changes in neural activity during VC. It is now known that following UL, the resting activity of MVN neurones on the lesioned side (ipsilateral) is severely depressed, due to the loss of excitatory input from the lesioned VIIIth nerve and presumably also because of enhanced commissural inhibition from contralateral MVN neurones, which become hyperactive due to the loss of inhibitory drive from the lesioned side. This severe imbalance in the excitability of the vestibular nuclei on the two sides is believed to cause the severe ocular and postural symptoms. During the process of VC over 2-3 days the vestibular neurones on the ipsilateral and contralateral sides restore their resting activity, and marked imbalance in excitability is progressively reduced correlated with the recovery of many ocular and postural symptoms.

Recently, using *in vitro* slices of the MVN from animals that had been labyrinthectomised at various times beforehand, Cameron and Dutia (1997) have demonstrated that neurones in the rostral region of the MVN develop a sustained, significant increase in their intrinsic excitability between 2 - 4 hours after UL. Thus, this rapid cellular response is likely to be an important initial step in the process of VC. Subsequently, Yamanaka *et al.*, (1998, in preparation) have shown that within 4 hours after UL, there is marked functional down-regulation of the efficacy of $GABA_A$ and $GABA_B$ receptors in the rostral MVN neurones and significant up-regulation of $GABA_A$ receptor efficacy in the contralateral MVN neurones. They have proposed that the down-regulation of GABAergic efficacy following UL may be responsible for the restoration of the resting activity in the ipsilateral rostral MVN neurones.

While the changes in GABAergic inhibitory efficacy in the ipsilateral rostral MVN neurones may contribute to their increase in intrinsic excitability after UL, it is possible that other compensatory changes in the intrinsic properties of these neurones also occur. *In vitro* electrophysiological studies of MVN neurones in the brainstem slice preparation have identified two distinct types of MVN neurones based on their after-hyperpolarisation (AHP). Type A exhibited a single AHP and Type B exhibited double AHP (Johnston *et al.*, 1994). In addition, it has been demonstrated that these neurones possess a variety of voltage activated conductances such as a persistent Na^+ conductance, K^+ conductance and Ca^{2+} activated K^+ conductances which contribute to a regular spontaneous discharge activity *in vitro*. It has also been proposed that changes in the intrinsic membrane properties of the MVN neurones may be important in the functional recovery following vestibular lesions (Darlington *et al.*, 1992). However, there have been no such studies so far of MVN neurones during VC after UL. Therefore, using whole-cell patch clamp recordings from MVN neurones in dorsal brainstem slice preparations taken from animals that had been labyrinthectomised 4 hours earlier, the primary aims of this study was to determine if changes occur in the intrinsic membrane properties and action potential firing of identified Type A and Type B MVN neurones in the early stage of VC, over the period in which these neurones develop the marked increase in their *in vitro* excitability.

3.3 METHODS

The intrinsic membrane properties of MVN neurones in normal and left unilateral labyrinthectomised adult rats were studied with the use of the blind whole cell recording techniques. For the purpose of analysis the MVN slice was visually divided into two regions, rostral part and caudal part (Fig. 3.3.0). Except for the following, the methods used in this part of study are similar to those described in the method sections of Chapter 1 (part 1.3). All values are presented as means ± S.E.M. Comparisons of the mean resting discharge rates, membrane properties and action potential properties of MVN neurones in different groups were performed using the Student's *t*-test (Sigma Stat, Jandel Scientific), unless otherwise stated and significance was assumed when $p<0.05$.

Anaesthesia

Avertin (tribromoethanol)

Avertin (Dyer *et al.*, 1981), anaesthetic was prepared fresh every morning according to the following recipe: 2.5g tribromoethanol (Sigma, UK) was added to 10ml of ethanol (Sigma, UK) and mixed until the tribromoethanol dissolved completely. To this solution, 1.5mls of 2-methylbutan-2-ol (Sigma, UK) was added and subsequently made up to a final volume of 125ml by the addition of normal saline (9g/l). The solution was administered intraperitoneally at a dose of 1ml/100g body weight and provided surgical anaesthesia for 30-40min.

Unilateral labyrinthectomy and behavioural observation

The procedure to perform a unilateral labyrinthectomy was as follows. Male Sprague-Dawley rats (60-130g) were anaesthetised with Avertin. A sufficient level of surgical anaesthesia was determined by a lack of reflex to a paw pinch. The surgical area was then clipped, shaved and scrubbed clean with hibisol. An incision about 4 cm long was made above the left ear with a sterile scalpel and the connecting tissue was cut using sharp surgical scissors, the middle ear was opened and the ossicles were removed. The muscles attached to the lambodial ridge were cut close to the bone and reflected to expose the temporal bone. The bony duct of the horizontal semicircular canal was then exposed by carefully drilling with a dental drill (Precision P.C.B drill, RS Components) near the point of exit of the VIIth cranial nerve. The area was kept clear with a needle attached to a suction pump.

The horizontal duct was followed anteriorly and opened near its ampullary swelling. Drilling was continued in the plane of the horizontal canal to follow the open duct into the vestibule of the inner ear. The ampulla of the anterior canal was drilled through, and the contents of the vestibular cavity were rinsed with 100% ethanol (Sigma U.K.), which was then aspirated. When bleeding had stopped, the wound was sutured and animals returned to their home cage to recover. An identical procedure was used for sham operated animals except that the horizontal canal was not opened, and no damage was inflicted on the inner ear. Success of the unilateral labyrinthectomy was determined by observing the animal following recovery from anaesthesia, which was completed within 50-60 min after induction. Unilaterally labyrinthectomised animals showed characteristic symptoms including tonic eye deviation, spontaneous ocular nystagmus, circular walking and head deviation toward the side of the lesion, extensor weakness in the ipsilateral limbs, and barrel rolling. These symptoms were absent in sham-operated animals. Horizontal slices of brainstem containing the MVN were then prepared 4 hours following surgery (see Part 1.3 of Chapter 1).

Experimental protocols are similar to that described in methods in Chapter 1, except for the following protocol:-

The spike frequency adaptation and steady-state gain.

Spike frequency adaptation (SFA) during constant depolarising current injection was determined by using the Clampex program (Pclamp Software Program, Axon Instruments) to obtain the interspike intervals (ISI) in ms. A series of constant depolarising current steps of increasing amplitude (50 pA increments from 100 pA, 200 ms duration) were injected into an identified Type A or Type B MVN neurone from a holding potential of RMP –20mV (below firing threshold). ISIs of each series were extracted from the Clampex files and converted to spikes/sec (Hz) using program written by Dr MB. Dutia with the formula 1/ISI X 1000 = Hz. Microsoft Excel ver 7.0 was used to plot the firing frequency Hz (y-axis) against current injection (x-axis) and provided a graphic depiction of SFA curves.

SFA index was measured by subtracting the first ISI (ISI_1) from 14th ISI (ISI_{14}) of the largest current injection (8th current pulse) and the steady-state gain was obtained from the ISI_{14}.(Fig. 3.3.1). The SFA index and steady-state gain plot of each neurone was achieved by plotting the SFA index and steady-state gain against resting discharge rate. Measurements of the membrane input resistance and spike frequency adaptation in control, sham-operated and lesioned animals were made at membrane potential held at -20 mV below firing threshold.

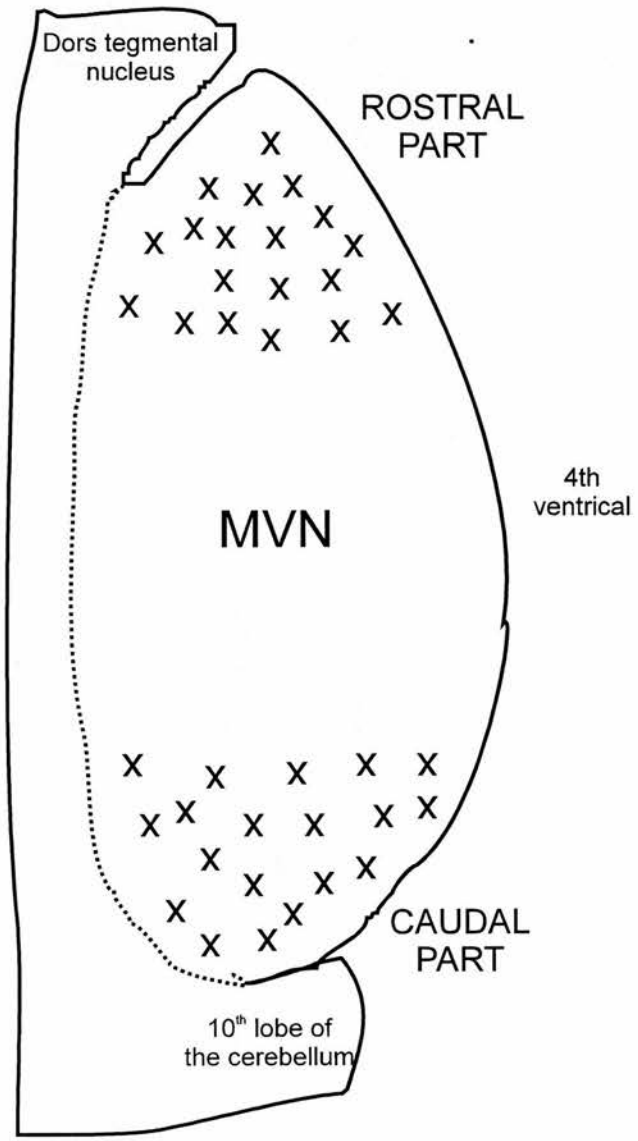

Figure 3.3.0 : Schematic representation of the MVN

Schematic representation of the horizontal slice of the left MVN showing the recording sites (X) in the rostral and caudal regions of the nucleus.

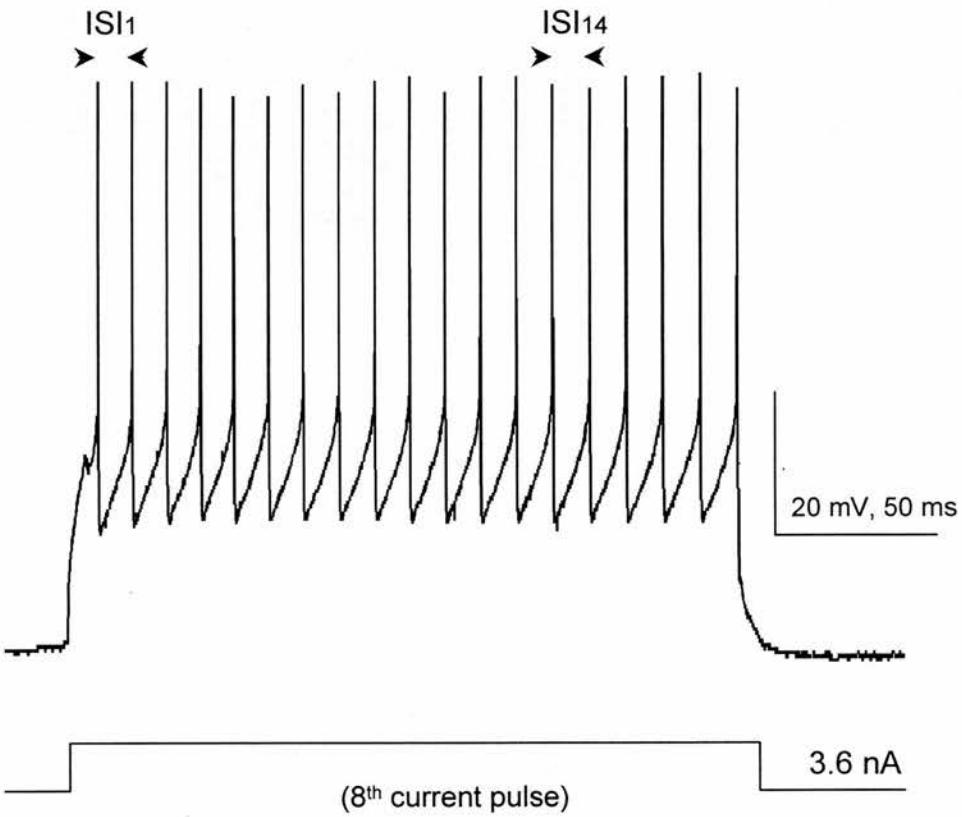

Figure 3.3.1 : Spike-frequency adaptation Index (SFA index) and steady-state gain

Firing properties of typical Type A MVN neurone in response to depolarising current injection. SFA index was measured from the difference between the first interspike interval (ISI_1) and the 14th interspike interval (ISI_{14}), while the steady-state gain was obtained from the ISI_{14} of the largest depolarising current injection (8th current pulse).

3.4 RESULTS

Data in these experiments were obtained from a total of 91 spontaneously active MVN neurones in horizontal slices of dorsal brainstem of normal, sham-operated and 4h post-UL rats, *in vitro*. The spontaneously active MVN neurones were recorded using intracellular whole cell patch clamp recording techniques and each MVN neurone was classified as either Type A or Type B based on the work of Johnston *et al.,* (1994,1998). All MVN neurones included in this study displayed a resting membrane potential (RMP) greater than –45 mV (-45.6 ± 0.5mV, mean ± S.E.M), membrane input resistances of 139.3 ± 6.1 MΩ and spontaneous action potentials larger than 60 mV in amplitude.

Electrophysiological properties of normal and sham-operated MVN neurones

Intracellular whole cell patch clamp recordings were made from a total of 25 spontaneously active MVN neurones in slices prepared from normal adult rats. Based on their averaged spontaneous action potential shapes, 9/25 (36%) of these neurones were classified as Type A MVN neurones, had a single deep post spike after-hyperpolarisation (AHP) and the remaining 16/25 (64%) were classified as Type B MVN neurones with an early fast AHP followed by a delayed slow AHP following their spontaneous action potentials (Fig. 3.4.1.1).

The mean values of the spontaneous action potential parameters obtained from averaged action potential shapes of the two MVN neurone types in normal slices are shown in Table 3.4.1. The duration of the averaged spontaneous action potential of Type A neurones, which was measured as the width at threshold (W_T) and as the width at half-height (W_H) was significantly longer than that of Type B neurones. Correspondingly, the rate of rise (measured as the rate of change of voltage from threshold to the peak of the action potential) and fall (measured as the rate of change of voltage from the peak of the action potential to return to threshold) of the action potential of Type A neurones were significantly slower than those of the Type B neurones. The membrane input resistance of Type A and Type B MVN, measured from the slope of I-V curve (Fig.3.4.1.2 and 3.4.1.3) and their resting discharge rate did not show significant difference. Thus, the proportion and averaged action potential parameters of Type A and Type B MVN neurones in this

study are similar to those obtained in the earlier studies with sharp electrodes (Johnston *et al.*, 1994; Dutia and Johnston, 1998).

As reported earlier by Serafin *et al.,* (1991) and du Lac and Lisberger (1995), Type A and Type B MVN neurones also showed a clear difference in their characteristic of action potential firing in response to long-lasting, constant depolarising current steps of increasing amplitude at a holding potential of 20 mV below RMP. As indicated in the examples in figure 3.4.1.4, Type A MVN neurones responded with an almost regular frequency through out the duration of the current injected. The spike-frequency adaptation curve (*f* - I curve) was linear (Fig. 3.4.1.5). By contrast, Type B MVN neurones fired at a higher frequency for the first few spikes of the train and then the firing frequency decayed to steady-state value (Fig. 3.4.1.6). As a result, in type B neurones, the response to current steps scaled linearly except during the initial portion of the response, thus the spike frequency adaptation curves show a secondary range (Fig 3.4.1.7, Serafin *et al.*, 1991; du Lac and Lisberger, 1995).

A further 18 MVN neurones were recorded and characterised in slices prepared from animals that had undergone a sham-operation 4 hrs previously. Of these 4/18 neurones (22%) were identified as Type A neurones and the remaining 14/18 (78%) neurones were Type B. The comparison of basic electrophysiological properties of Type A and Type B in normal and sham-operated animals are summarised in table 3.4.2. There were no significant differences found in the RMP, membrane input resistance (R_{in}), action potential characteristics and spontaneous resting discharge rates recorded from Type A and Type B of normal and sham-operated animals. As shown in the graph in Fig. 3.4.1.8, the spike frequency adaptation index (SFA index; $ISI_{14} - ISI_1$ for the largest current step) plotted against resting discharge of Type A and Type B MVN neurones for both groups also showed a linear relationship. The steady-state gain of Type A and Type B in both groups was also no different (Fig. 3.4.1.9). Therefore, the data from normal and sham-operated animals were pooled for comparison with the data obtained from UL animals.

Electrophysiological properties of MVN neurones after UL.

A total of 48 spontaneously active MVN neurones were obtained in slices prepared from adult rats that had undergone left unilateral labyrinthectomy 4 hours earlier. Whole cell patch clamp recordings were made from the neurones that were located in the rostral and the caudal regions of the MVN ipsilateral to the lesioned side. Of these, 34 MVN neurones were recorded in the rostral region of the ipsilateral nucleus, while the remaining 14 neurones were recorded in the caudal region of the ipsilateral nucleus. In this study, neurones located in the contralateral MVN were not examined.

The identification of neuronal types in both rostral and caudal regions of the ipsilateral MVN was similar to those in control. It was found that the relative proportions of Type A and Type B neurones recorded 4 hours after UL were similar to controls. Hence 6/34 (17.6%) neurones recorded in the rostral part and 4/14 neurones recorded in the caudal part were Type A neurones, while the remaining 28/34 (82.3%) rostral neurones and the remaining 10/14 (71.4%) caudal neurones were Type B.

As shown in histogram in Figure 3.4.2, there were no statistically significant differences in RMP (-45.4 ± 0.8 mV, n = 34, Type A and B neurones together) and R_{in} (153.6 ± 12.0 MΩ, Fig 3.4.2.1) in the ipsilateral rostral MVN neurones recorded 4 hours after UL compared to rostral neurones in control slices (normal and sham-operated neurones; RMP: -46.3 ± 0.6, n =28; R_{in}: 126.8 ± 8.8 MΩ, n = 28). Similarly, overall mean values for RMP (-45.1 ± 1.7 mV, n = 14) and R_{in} (153.5 ± 17.0 MΩ) did not significantly differ between neurones in the ipsilateral caudal MVN after UL and neurones in control caudal slices (RMP: -45.5 ± 0.5 mV, n = 15; R_{in}: 117 ± 8.0 MΩ).

However, it was observed that the overall mean resting discharge rate between the ipsilateral rostral MVN neurones after UL was significantly higher than that of the rostral neurones in normal and sham-operated animals (21.9 ± 1.2 spikes/sec, n = 34 neurones in UL slices vs 13.6 ± 0.9 spikes/sec, n = 28 neurones in control slices, $p < 0.05$, Student *t*-test; Fig 3.4.2.2). There was no difference in the mean resting discharge rate in the ipsilateral caudal MVN neurones after UL (14.7 ± 1.3 spike/sec, n = 14 neurones) from those of caudal MVN neurones in control

slices (14.8 ± 1.8 spikes/sec, n = 16 neurones). Hence, this result confirms the earlier report of a significant increase in intrinsic excitability of ipsilateral rostral MVN neurones within 4 hours following UL in the rat (Cameron and Dutia, 1997).

Interestingly, as shown in Fig. 3.4.2.3, comparison of the mean *in vitro* resting discharge rates of the two sub-types of MVN neurones from the population of the ipsilateral rostral MVN neurones after UL revealed that the resting discharge rate of Type A neurones (15.0 ± 1.5 spikes/sec, n = 6 neurones) was not different from that of rostral Type A neurones in pooled control (normal and sham) slices (10.9 ± 1.4 spikes/sec, n = 7 neurones). By contrast, the mean resting discharge rate of rostral Type B neurones (23.4 ± 1.2 spikes/sec, n = 28 neurones) was significant higher compared to control rostral Type B neurones (14.5 ± 1.1 spikes/sec, n = 21 neurones, $p < 0.05$, Student's *t*-test).

As indicated in figure 3.4.2.4, an analysis of the SFA index and resting discharge rate relationship showed that rostral Type B MVN neurones after UL did not form a homogenous group. Instead the SFA index values of 14/28 (50%) of the ipsilateral rostral Type B MVN neurones overlapped with those of control rostral Type B MVN neurones, and fell within the ± 99% prediction interval around the mean control regression slope. The resting discharge rate, SFA index and steady-state gains of these ipsilateral rostral Type B neurones were not different from those of control rostral Type B MVN neurones. However, the remaining 14/28 (50%) of the ipsilateral rostral Type B MVN neurones were distributed outside the ± 99% prediction interval of control regression slope, with resting discharge rates (Fig. 3.4.2.5) and SFA index that were significantly different from those of control and the other group Type B neurones. Thus of the Type B neurones in the ipsilateral rostral MVN a sub-population, which for the purpose of this thesis will be called "Type B^+ neurones", showed a marked lesion-induced plasticity and adaptation in their intrinsic membrane properties during the early stage of vestibular compensation following UL, while the other group of rostral Type B neurones after UL did not show any change in their intrinsic membrane properties ("Type B^- neurones"). Figure 3.4.2.6 to 3.4.2.9 illustrate examples of voltage traces and SFA curves of Type B^+ and Type B^- MVN neurones in response to constant depolarising current pulses.

Further analysis showed that the changes in the resting discharge rate and SFA index in of these ipsilateral rostral Type B^+ neurones were accompanied by marked changes in the parameters of their spontaneous action potentials, as seen in their averaged action potential shapes. The mean values of the spontaneous action potential parameters of the two groups of ipsilateral rostral Type B neurones after UL are shown in table 3.4.3. Following UL, the duration of the averaged spontaneous action potentials of Type B^+ MVN neurones measured at spike threshold and at half-height (W_T: 1.27 ± 0.05 ms; W_H; 0.6 ± 0.03 ms, n = 14) were significantly wider than that of Type B^- neurones after UL (W_T: 0.79 ± 0.05 ms; W_H: 0.4 ± 0.03 ms, n = 14) and rostral Type B neurones in control slices (W_T: 0.86 ± 0.05 ms; W_H: 0.4 ± 0.02 ms, n = 21, Fig 3.4.3.1A and B). Moreover, in line with the wider action potentials, both the mean rates of rise (93.8 ± 6.67 V/sec) and fall (88.5 ± 5.54 V/sec) of the action potential of Type B^+ neurones were also significantly slower than the mean rate of rise and fall of the Type B^- neurones (rise: 145.5 ± 11.91 V/sec; fall: 166 ± 14.30 V/sec) and control Type B neurones (rise: 141.5 ± 9.47 V/sec; fall : 158.9 ± 11.87 V/sec, $p < 0.05$, one way, Fig 3.4.2.8C and D). By contrast, the action potential parameters of the Type B^- neurones showed no significant changes ($p > 0.05$, one way ANOVA) in their averaged action potential shapes after UL compared to control Type B neurones.

Furthermore, it were also observed that the early fast AHP that is mediated by TEA-sensitive K^+ in Type B neurones (Johnston *et al.*, 1994) became smaller in Type B^+ neurones, while the slower, delayed AHP that is mediated by apamin-sensitive Ca^{2+}-activated K^+ conductance (Johnston *et al.*, 1994) was not affected. Figure 3.4.3.2, illustrates examples of averaged action potentials superimposed of Type B MVN neurones in control slices and slices prepared from animals 4 hours after UL. There were no change in the early fast and slow, delayed AHP in Type B-MVN neurones.

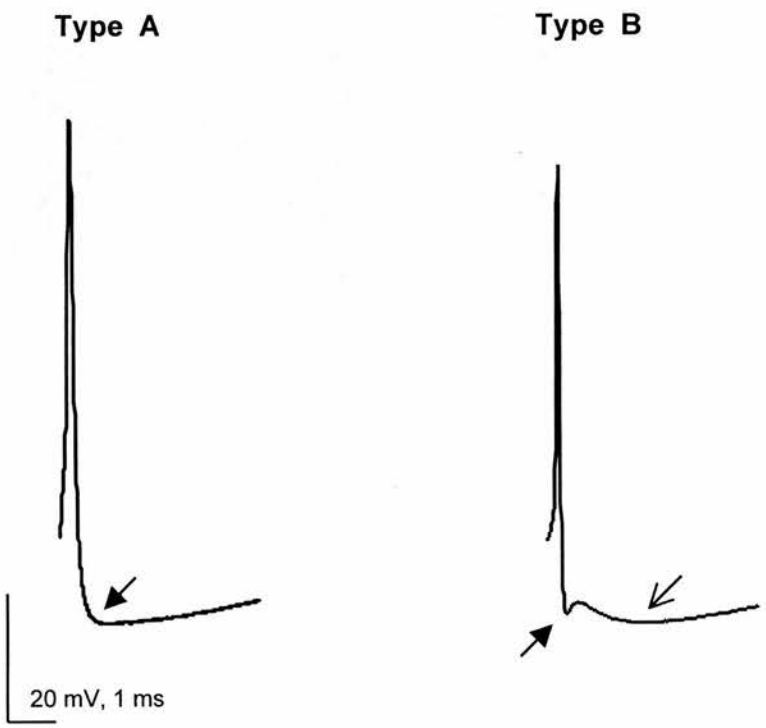

Figure 3.4.1.1 : Averaged action potential shapes of MVN neurones

Action potential averaging showing two subtype of MVN neurones, Type A and Type B. Note the single deep after hyperpolarisation in the Type A (solid arrow) and the early fast (solid arrow) followed by slow delayed (open arrow) after hyperpolarisation in the Type B neurone.

TABLE 3.4.1

COMPARISON OF ELECTROPHYSIOLOGICAL PROPERTIES OF NORMAL TYPE A AND TYPE B MVN NEURONES.

Parameters	Type A (n = 9)	Type B (n = 16)	P
AP width at threshold, ms	1.18 ± 0.09	0.80 ± 0.05	< 0.001
AP width at half-height, ms	0.56 ± 0.05	0.38 ± 0.02	< 0.001
Rate of rise, V/sec	93.9 ± 5.52	152.8 ± 10.1	< 0.001
Rate of fall, V/sec	92.9 ± 7.16	154.3 ± 9.47	< 0.001
RMP, mV	-46.1 ± 0.9	-45.5 ± 0.5	ns
R_{in}, MΩ	140.2 ± 13.31	114.8 ± 13.03	ns
Resting discharge rate, Hz	13.4 ± 2.27	14.3 ± 1.70	ns

Values are means ± S.E.M.; AP, action potential; RMP, resting membrane potential; R_{in}, membrane input resistance; ns, not significance. The P values were obtained from a Student's t-test. (n = 25)

Legend 3.4.1.2 : Response of Type A MVN neurone to current pulses

(A) Example of voltage-current relationship (I-V; raw data) of Type A MVN neurone to series of constant depolarising and hyperpolarising current pulses. (B) I-V curve obtained from (A). Input resistance of the neurone was measured from the slope of I-V curve. Arrow indicates where the measurements were made. The resting membrane potential of the neurone was held at -20 mV below firing threshold.

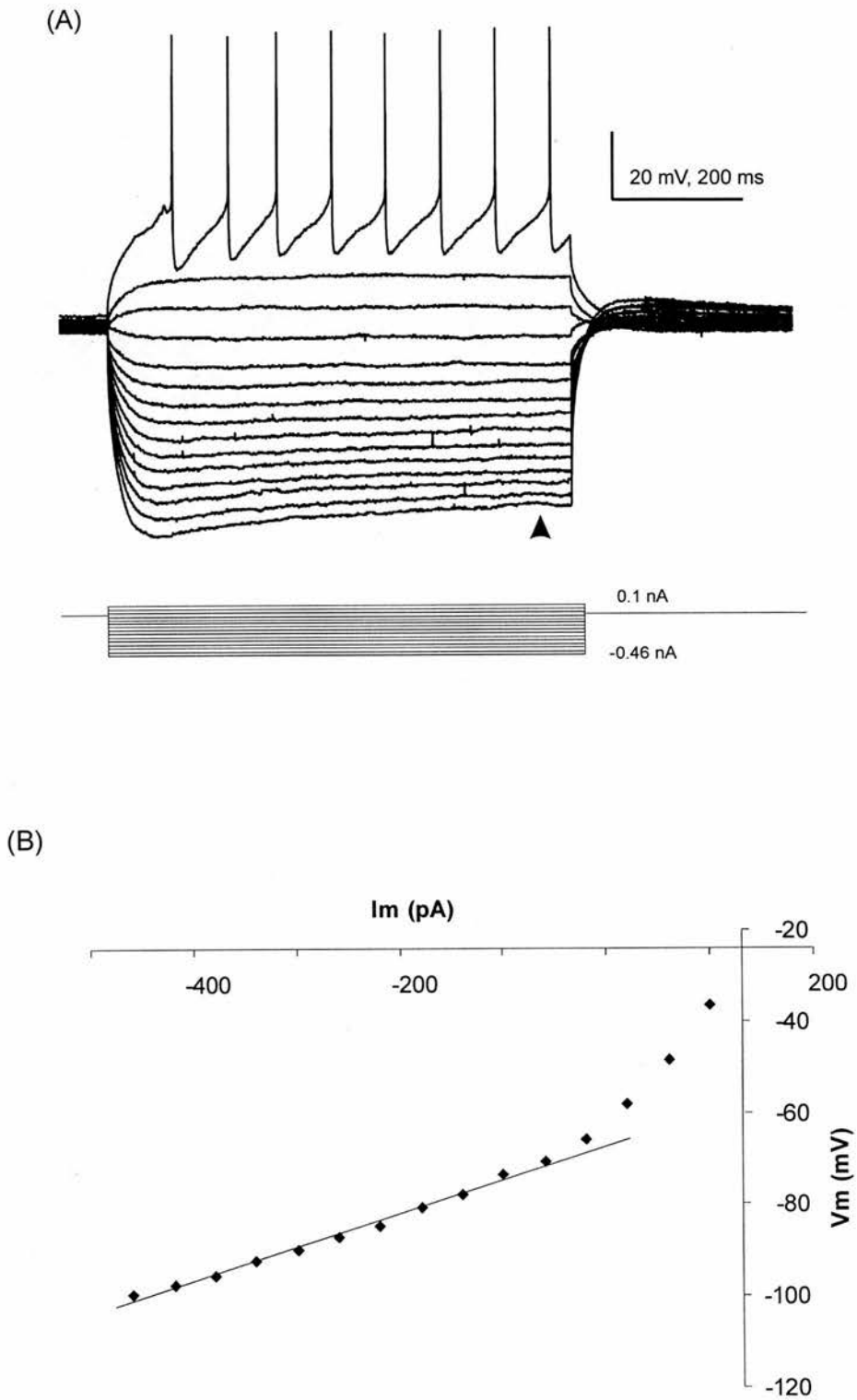

Figure 3.4.1.2 : Response of Type A neurone to current pulses.

Legend 3.4.1.3 : Response of Type B MVN neurone to current pulses

(A) Example of voltage-current relationship (I-V; raw data) of Type B MVN neurone to series of constant depolarising and hyperpolarising current pulses. (B) I-V curve obtained from (A). Input resistance of the neurone was measured from the slope of I-V curve. Arrow indicates where the measurements were made. The resting membrane potential of the neurone was held at -20 mV below firing threshold.

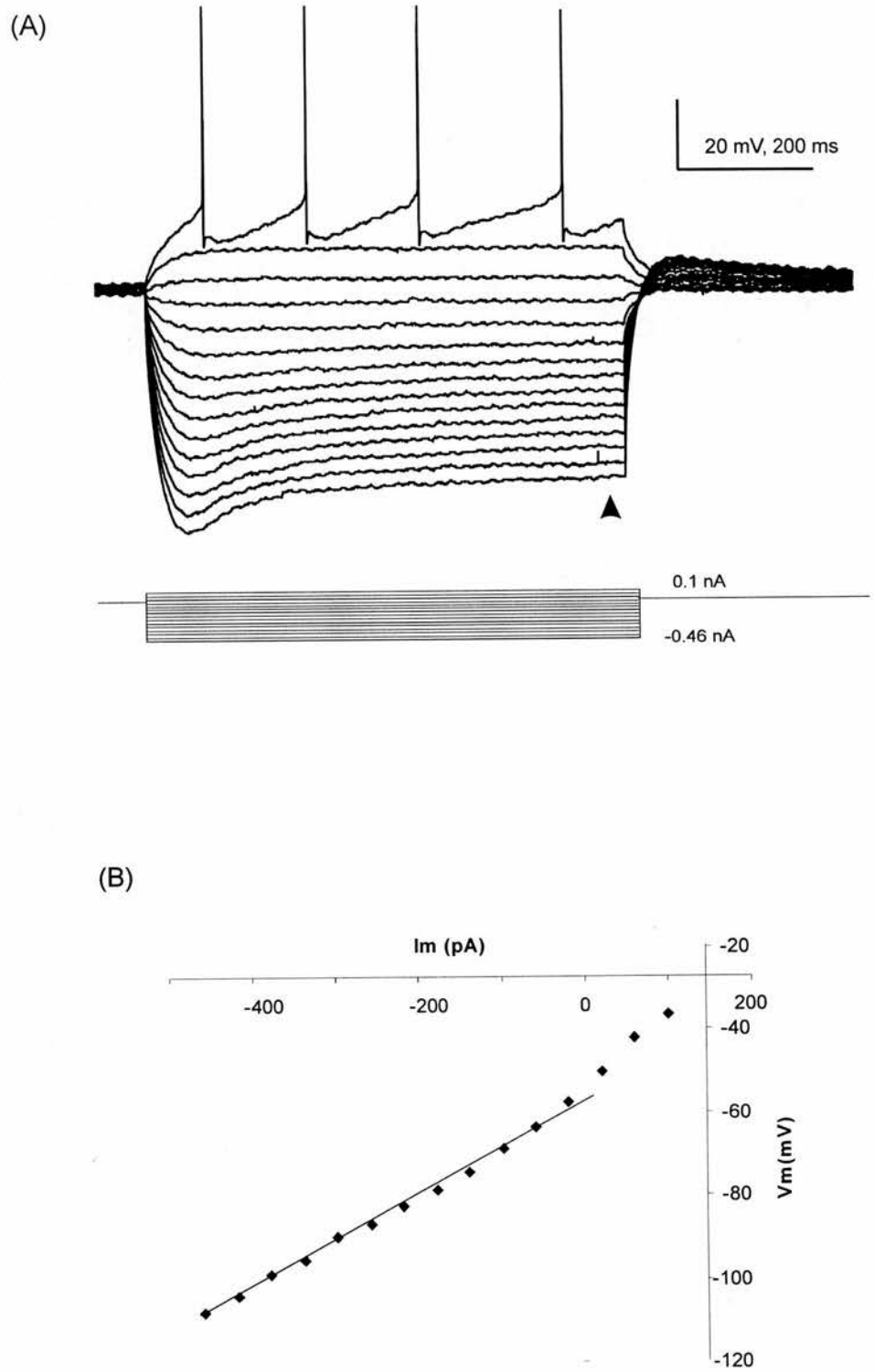

Figure 3.4.1.3 : Response of Type B neurone to current pulses.

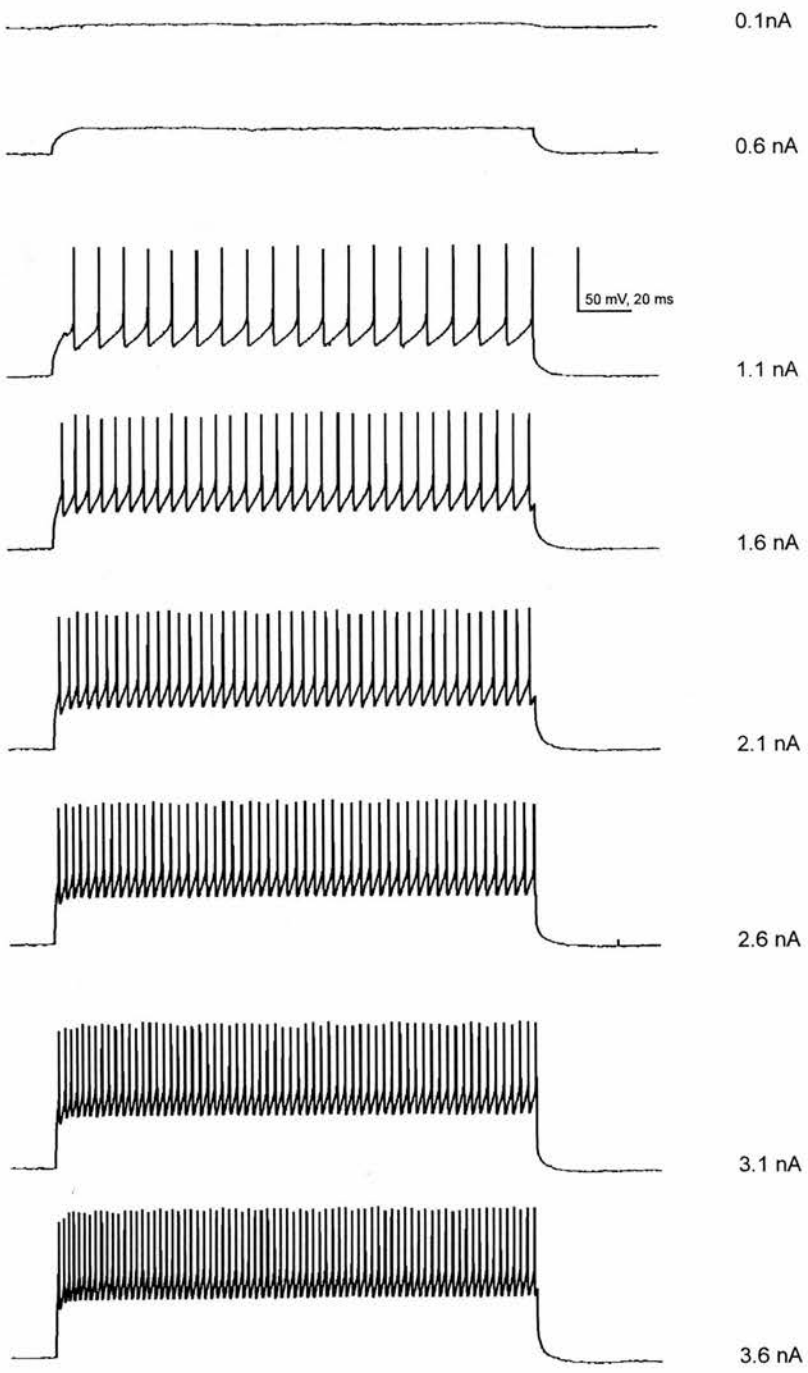

Figure 3.4.1.4 : Voltage traces of a normal Type A MVN neurone in response to depolarising current pulses of different amplitudes for duration of 200ms. The neurone displayed a regular firing frequency throughout the duration of the current injected. RMP was held at -20 mV below firing threshold.

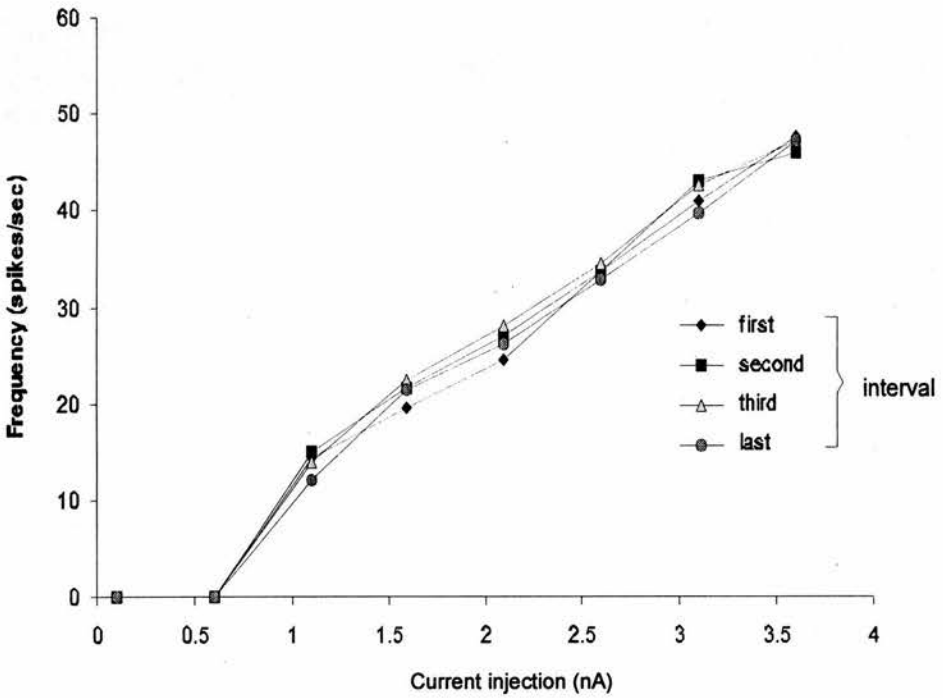

Figure 3.4.1.5 : Spike-frequency adaptation curve of normal Type A MVN neurone

Spike-frequency adaptation curve of the Type A neurone illustrated in figure 3.4.1.4, measured at different intervals showing linear relationship to the amplitude of currents injected.

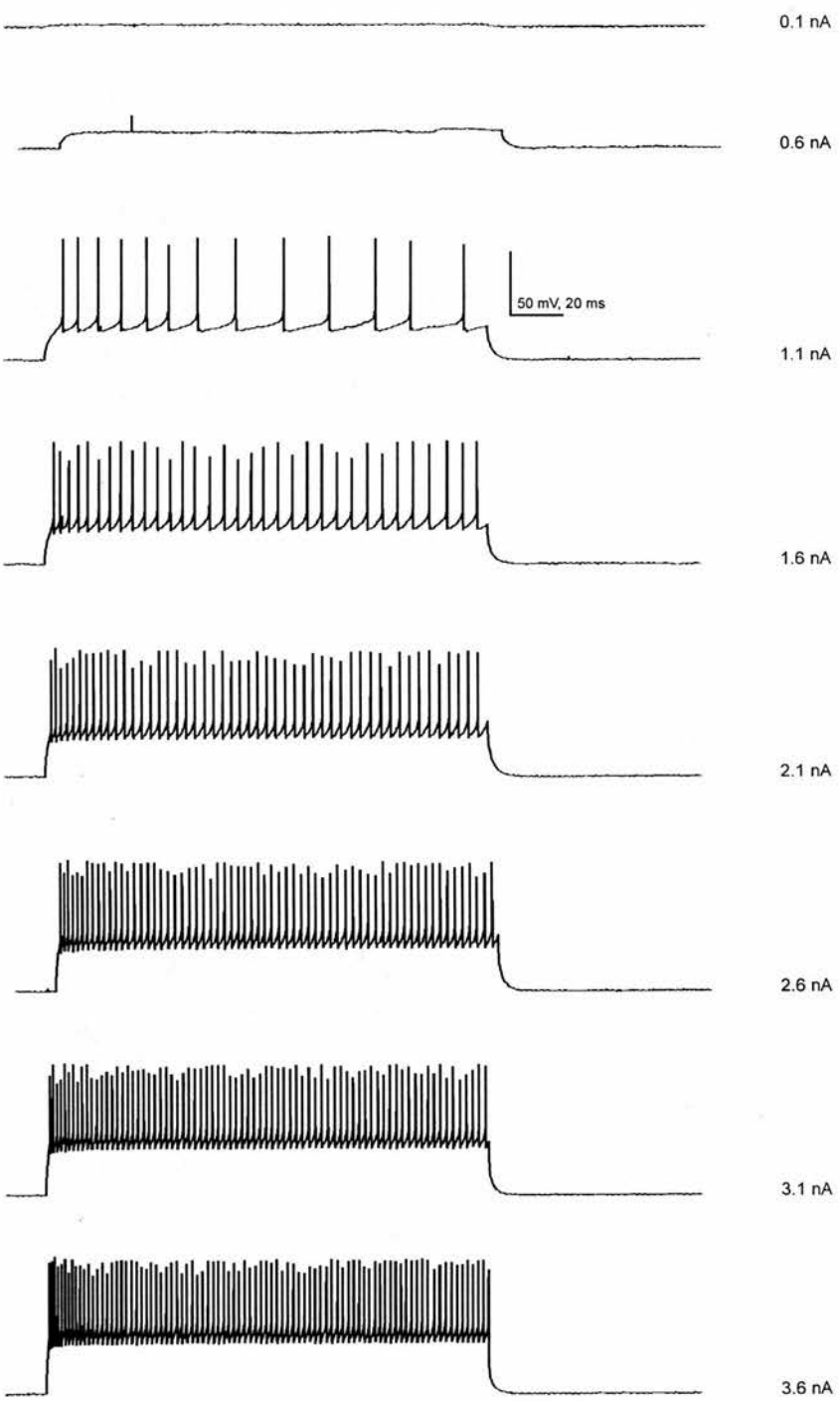

Figure 3.4.1.6 : Voltage traces of a normal Type B MVN neurone in response to depolarising current pulses of different amplitudes. The neurone displayed a higher frequency for the initial part of the spike train and then decayed to steady-state value.

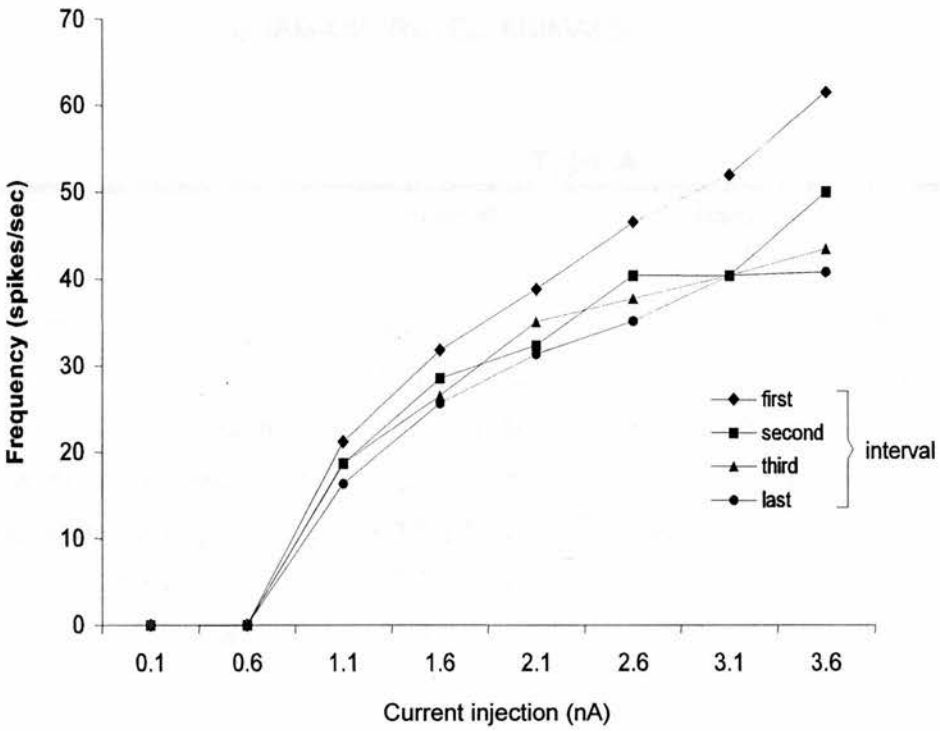

Figure 3.4.1.7 : Spike-frequency adaptation curve of normal Type B MVN neurone

Spike-frequency adaptation curve of the Type B neurone illustrated in figure 3.4.1.6, measured at different intervals showing non-linear relationship in the first interval. Notice the presence of a secondary range for the first and second intervals.

(A) Type A neurones

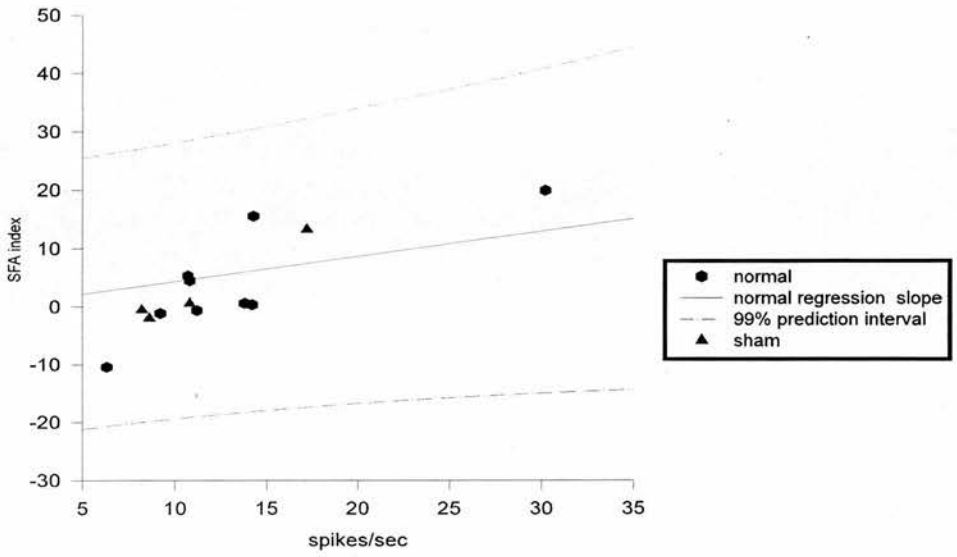

(A) Type B neurones

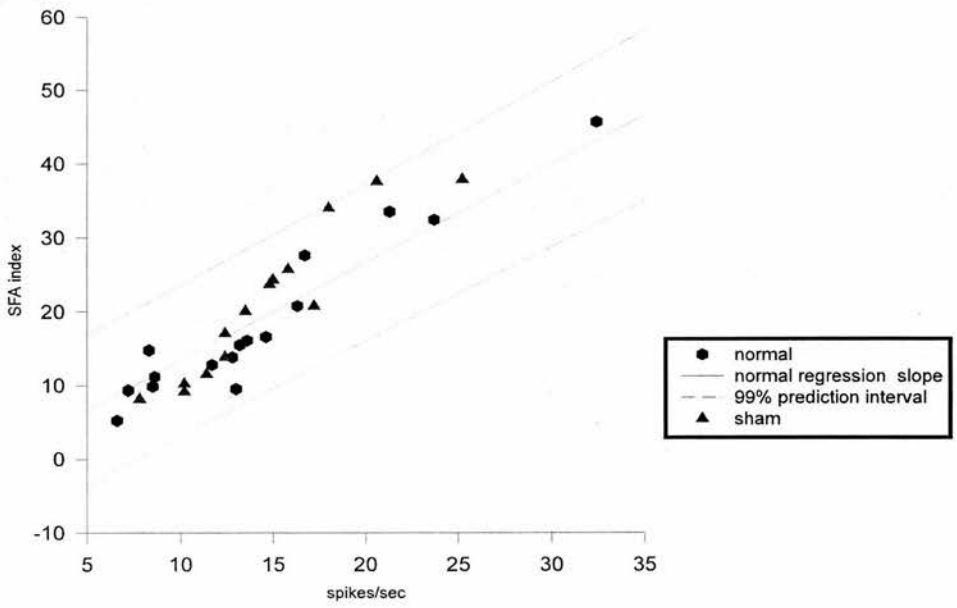

Figure 3.4.1.8 : Relationship between SFA index and resting discharge rate

Scatter graphs showing the relationship between SFA index and resting frequency of Type A and Type B MVN neurones from slices of normal and sham animals

(A) Type A neurones

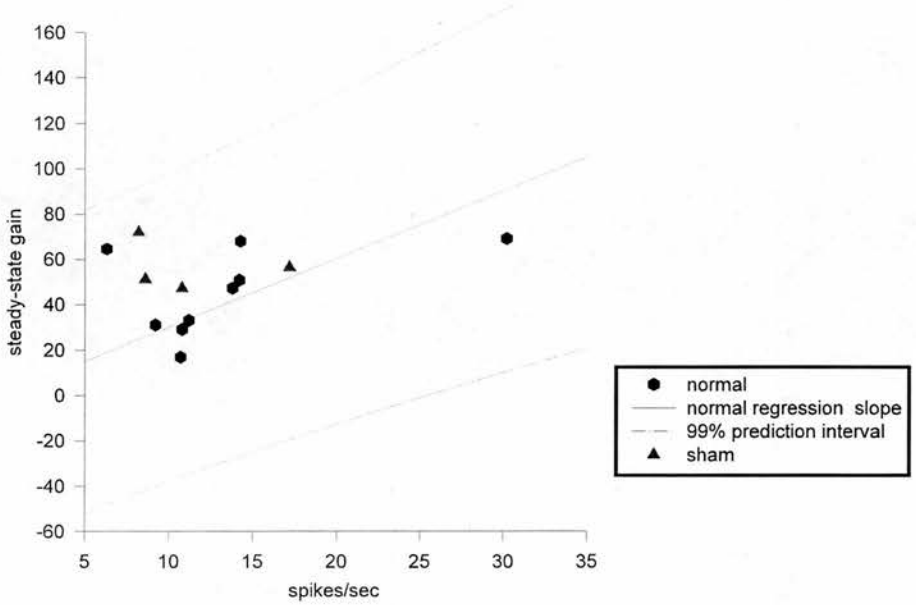

(B) Type B neurones

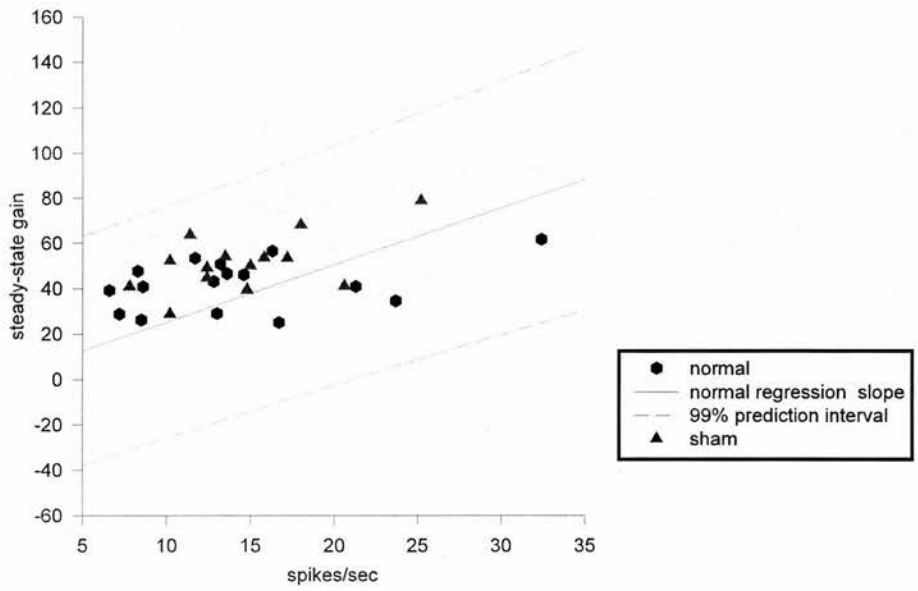

Figure 3.4.1.9 : Relationship between steady-state I-F gain and resting discharge rate

Scatter graphs showing the relationship between steady-state I-F gain and resting frequency of Type A and Type B MVN neurones from slices of normal and sham animals

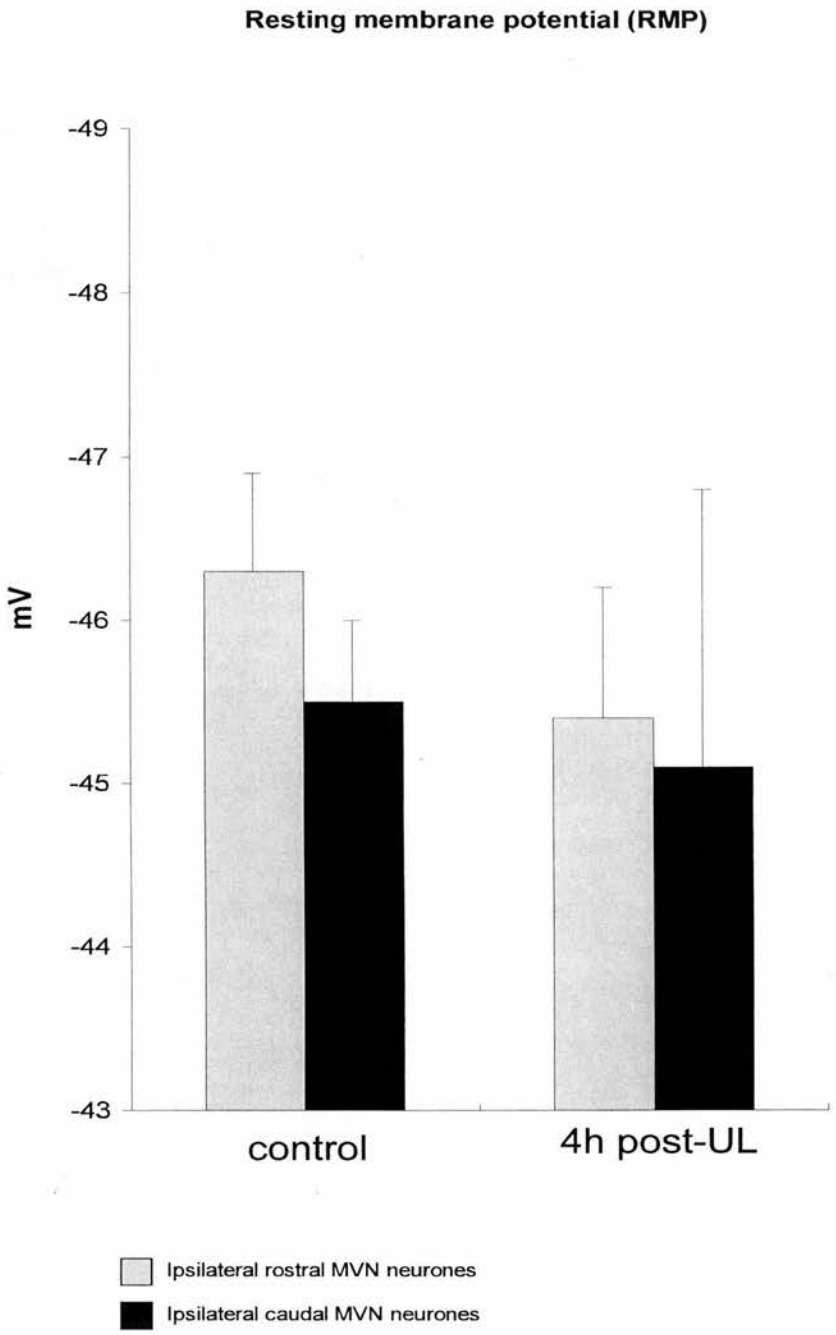

Figure 3.4.2 : Resting membrane potential of MVN neurones 4h post-UL

Histogram showing the overall mean (± S.E.M) RMP of ipsilateral rostral (open column) and ipsilateral caudal (solid column) MVN neurones in control (rostral: n=28; caudal: n=15) and 4h post-UL (rostral: n=34; caudal: n=14). There is no significant difference within groups. $P>0.05$, assessed by Student's t-test.

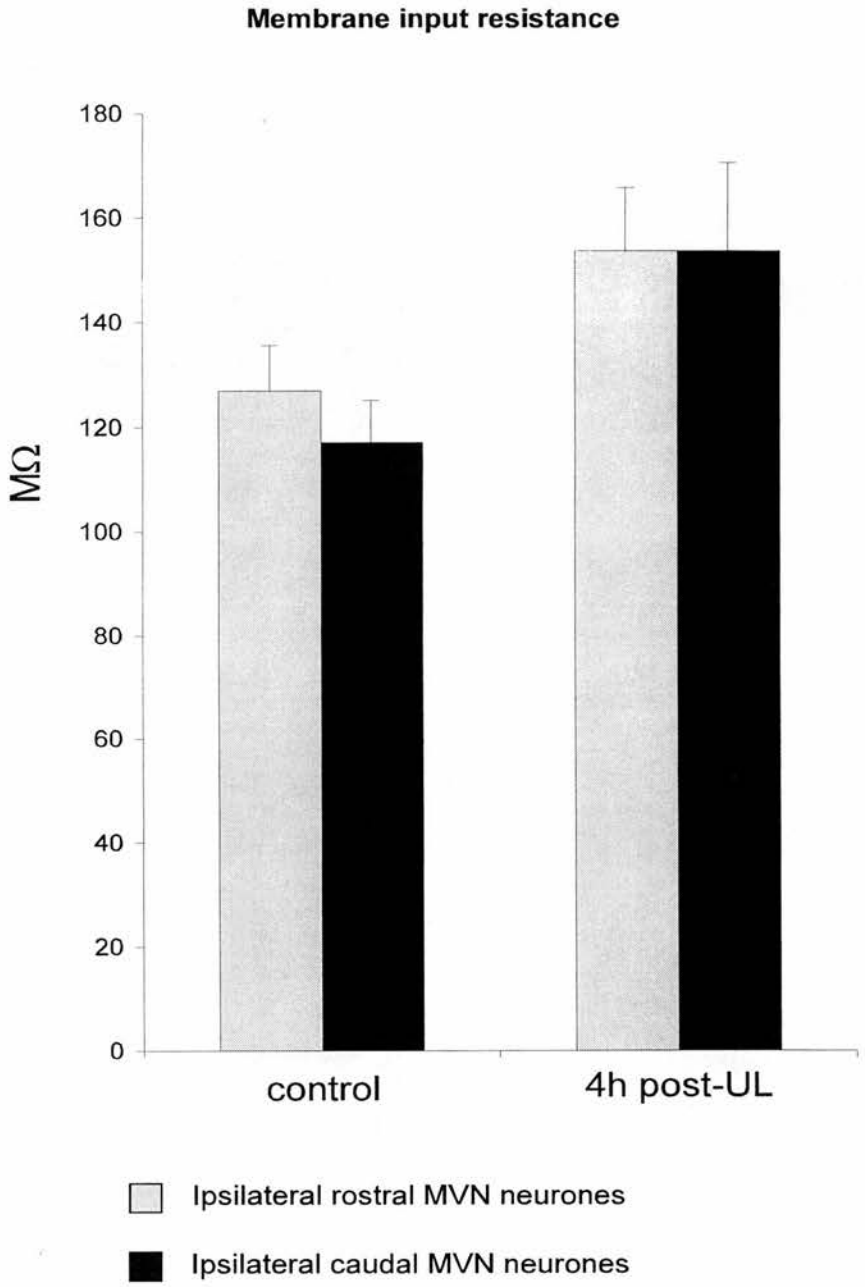

Figure 3.4.2.1 : Membrane input resistance of MVN neurones 4h post-UL

Histogram showing the overall mean (± S.E.M) membrane input resistance of ipsilateral rostral (open column) and ipsilateral caudal (solid column) MVN neurones in control (rostral: n=28; caudal: n=15) and 4h post-UL (rostral: n=34; caudal: n=14). There is no significant difference within groups. $P>0.05$, assessed by Student's t-test.

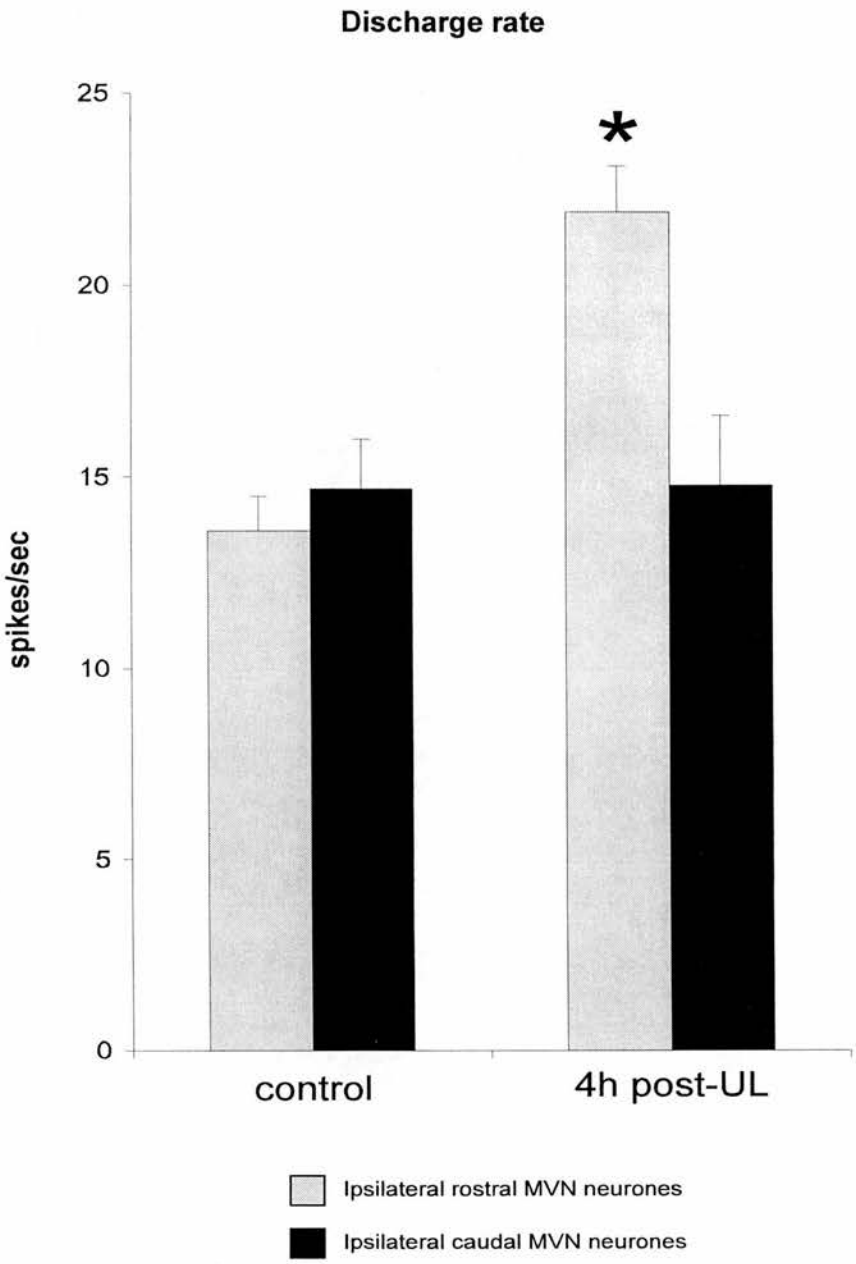

Figure 3.4.2.2 : Spontaneous discharge rate of MVN neurones 4h post-UL

Histogram illustrating the overall mean (± S.E.M) resting discharge rate of ipsilateral rostral (open column) and ipsilateral caudal (solid column) MVN neurones in control (rostral: n=28; caudal: n=15) and 4h post-UL slices (rostral: n=34; caudal: n=14). There is a significant increase in the mean resting discharge rate of MVN neurones in the ipsilateral rostral region 4h post-UL compared with control ipsilateral rostral MVN region. *$P<0.05$, assessed by student *t*-test.

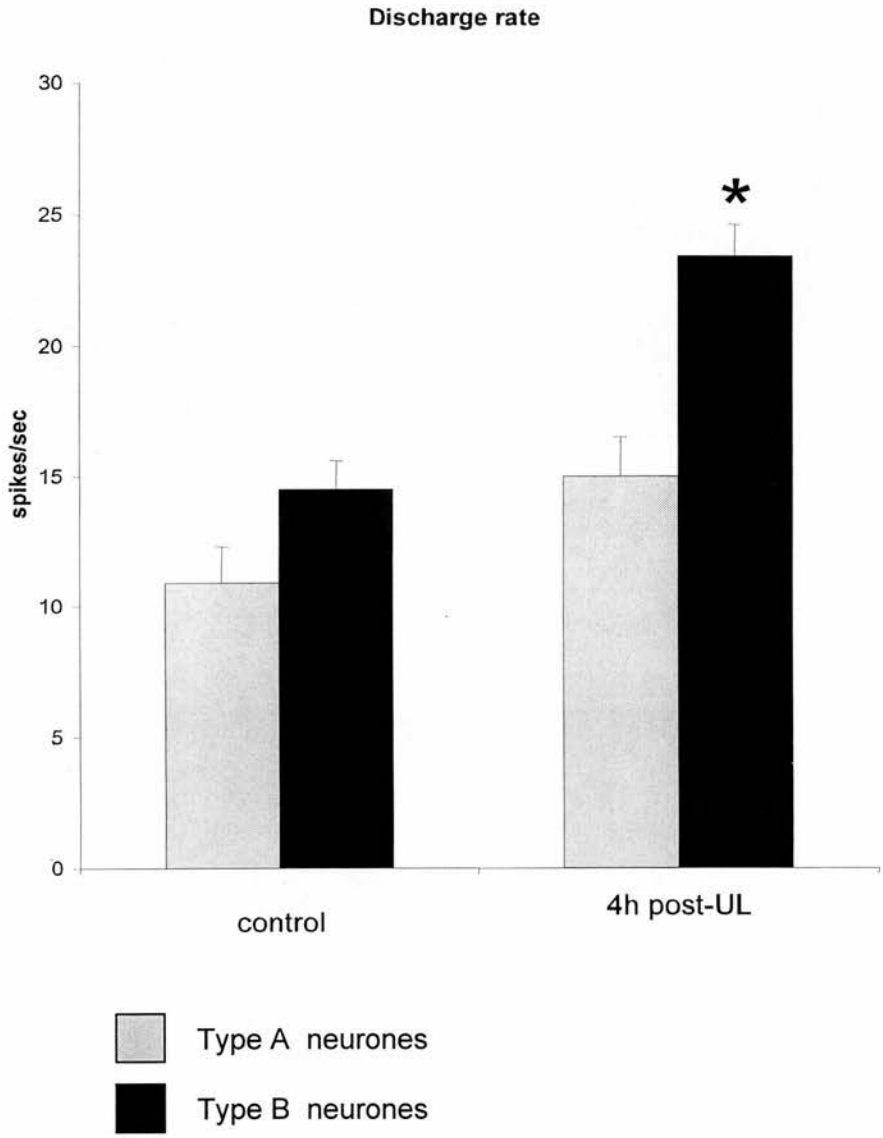

Figure 3.4.2.3 : Resting discharge rate of ipsilateral rostral Type A and Type B MVN neurones 4h after UL

Histogram illustrating the mean (± S.E.M) resting discharge rate of ipsilateral rostral Type A (open column) and ipsilateral rostral Type B (solid column) MVN neurones in control (Type A: n=7; Type B: n=21) and 4h post-UL slices (Type A: n=6; Type B: n=28). There is a significant increase in the mean resting discharge rate of Type B MVN neurones in the ipsilateral rostral region 4h post-UL compared with control Type B in the ipsilateral rostral region. * $P<0.05$, assessed by student's *t*-test.

Legend 3.4.2.4 : Relationship between SFA index, steady-state I-F gain and resting discharge rate of ipsilateral rostral Type B MVN neurones 4h after UL

(A) Scatter plots illustrating the relationship between SFA index and resting discharge rate of Type B MVN neurones in control (⬮) and ipsilateral rostral Type B MVN neurones (▲) 4h post-UL. Figure shows the regression slope of control Type B neurones and its 99% prediction interval. Notice that there are two distinct populations of Type B neurones 4h post-UL, with 50% of Type B neurones falling within (Type B-), while the remaining 50% fall outside the 99% prediction interval of control regression slope. (B) The relationship between steady-state gain and discharge rate of control Type B neurones and rostral Type B neurones post-UL.

(A)

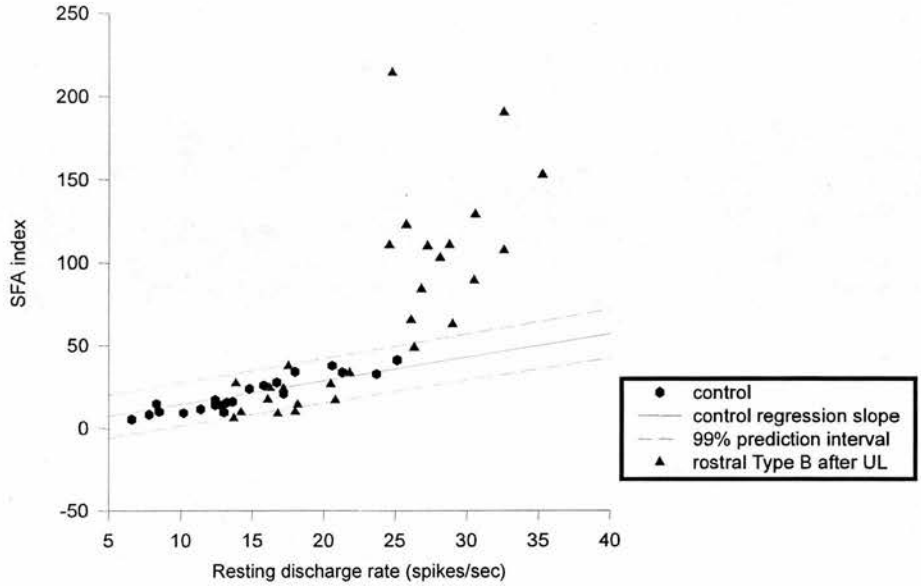

(B)

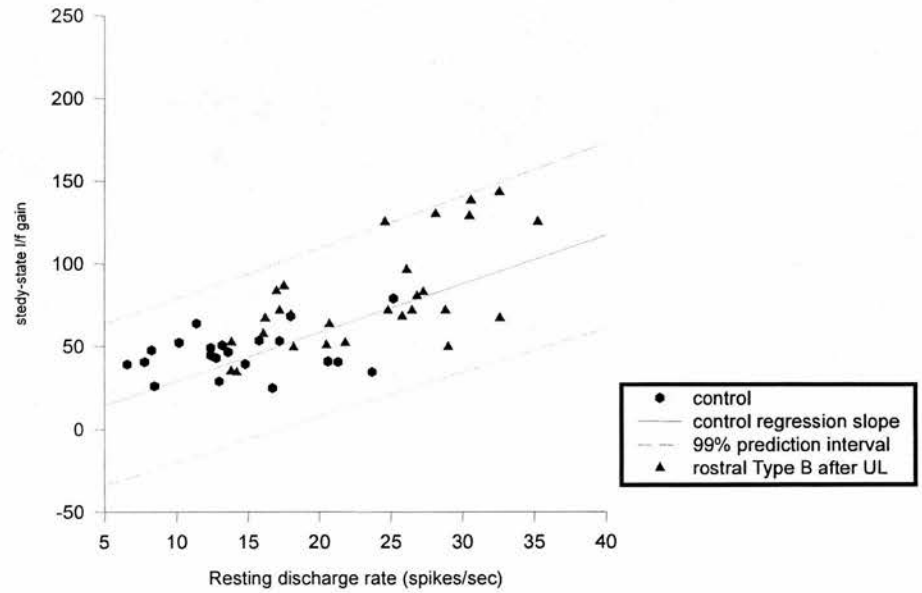

Figure 3.4.2.4 : Relationship between SFA index, steady-state I-F gain and resting discharge rate of ipsilateral rostral Type B MVN neurones 4h after UL

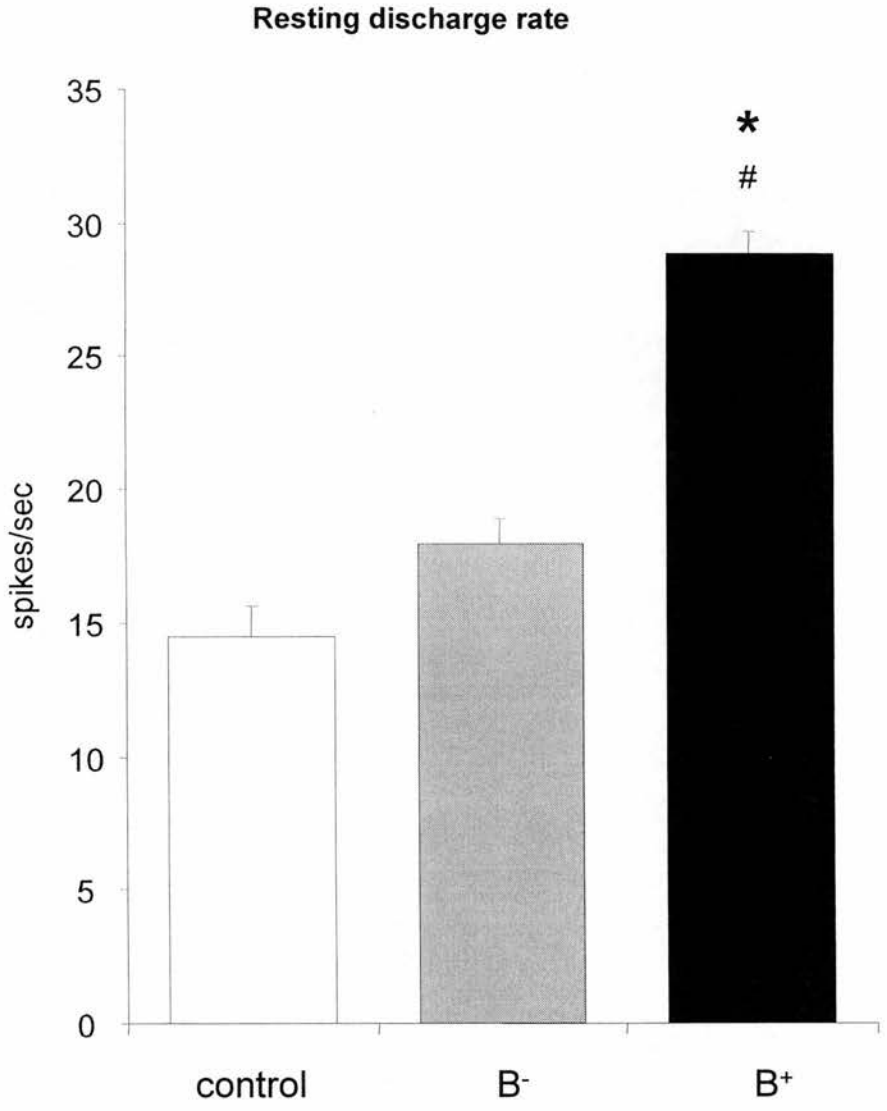

Figure 3.4.2.5 : Spontaneous resting discharge rate of rostral Type B MVN neurones in slices of control and 4h post-UL animals.

Histogram illustrating the mean (± S.E.M) of spontaneous discharge rate of rostral Type B MVN neurones in control and post-UL (Type B^+ and B^-) animals. The spontaneous discharge rate of Type B^+ neurones is significantly higher than Type B^- neurones post-UL and Type B in control animals. * $P< 0.05$ compared with Type B^-, # $P<0.05$ compared with control Type B, assessed by one way ANOVA.

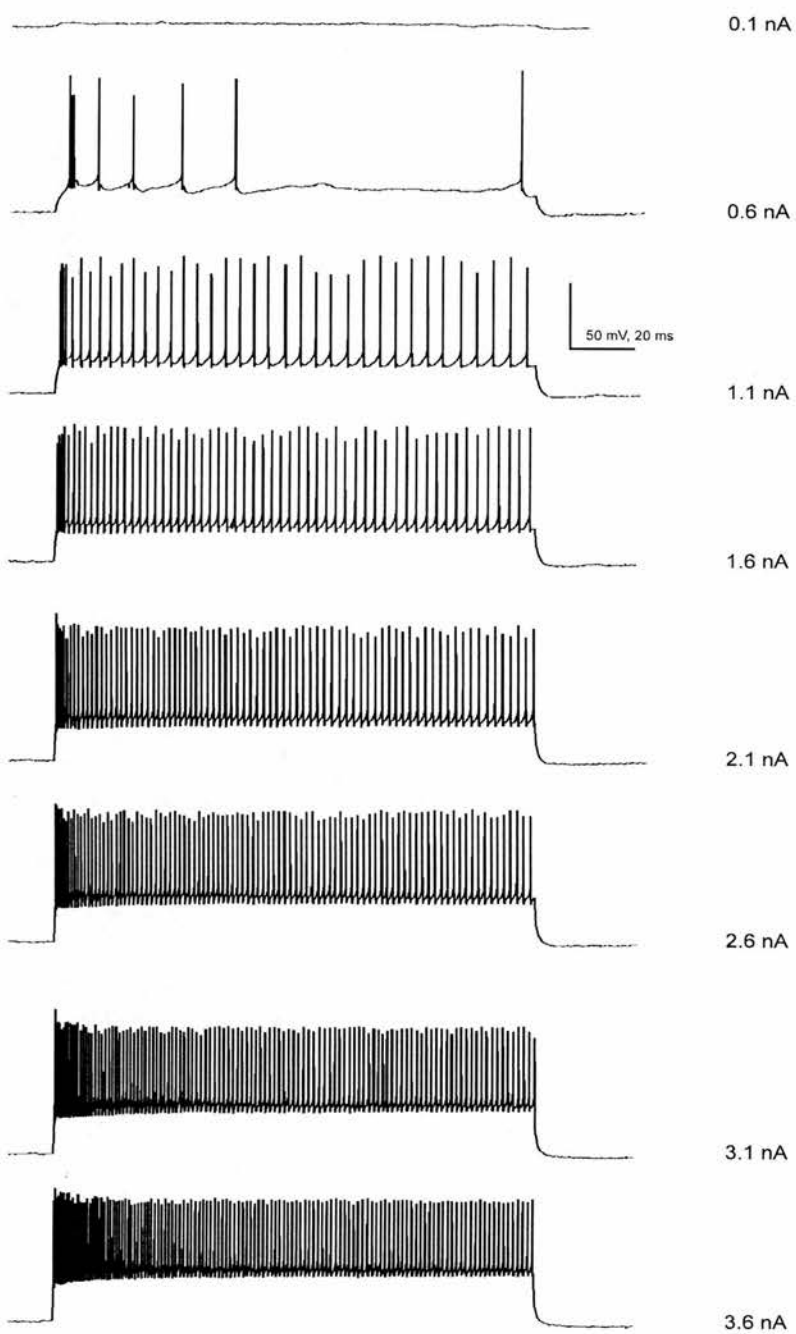

Figure 3.4.2.6 : Voltage traces of a Type B^+ MVN neurone in response to depolarising current pulses of different amplitudes. The neurone displayed a higher frequency for the initial part of the firing trains which then decayed to steady-state value (high spike-frequency adaptation).

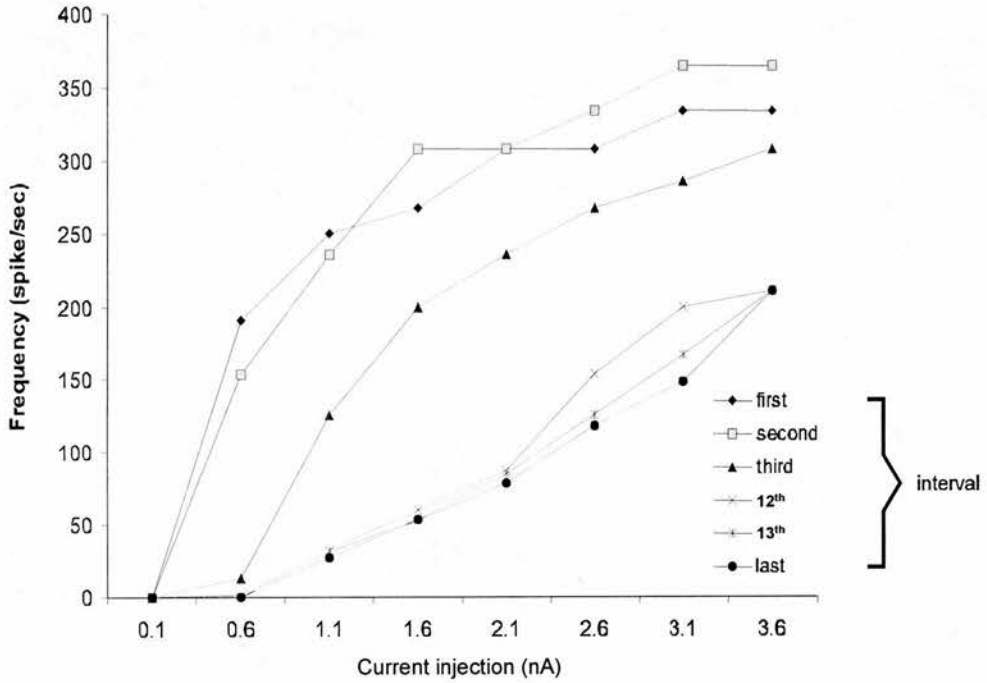

Figure 3.4.2.7 : Spike-frequency adaptation curve of Type B+ MVN neurone

Spike-frequency adaptation curve of Type B^+ neurone illustrated in figure 3.4.2.6, measured at different intervals showing non-linear relationship in the first interval. Notice the presence of a secondary range for the first three and last three intervals, which gives higher value for SFA index.

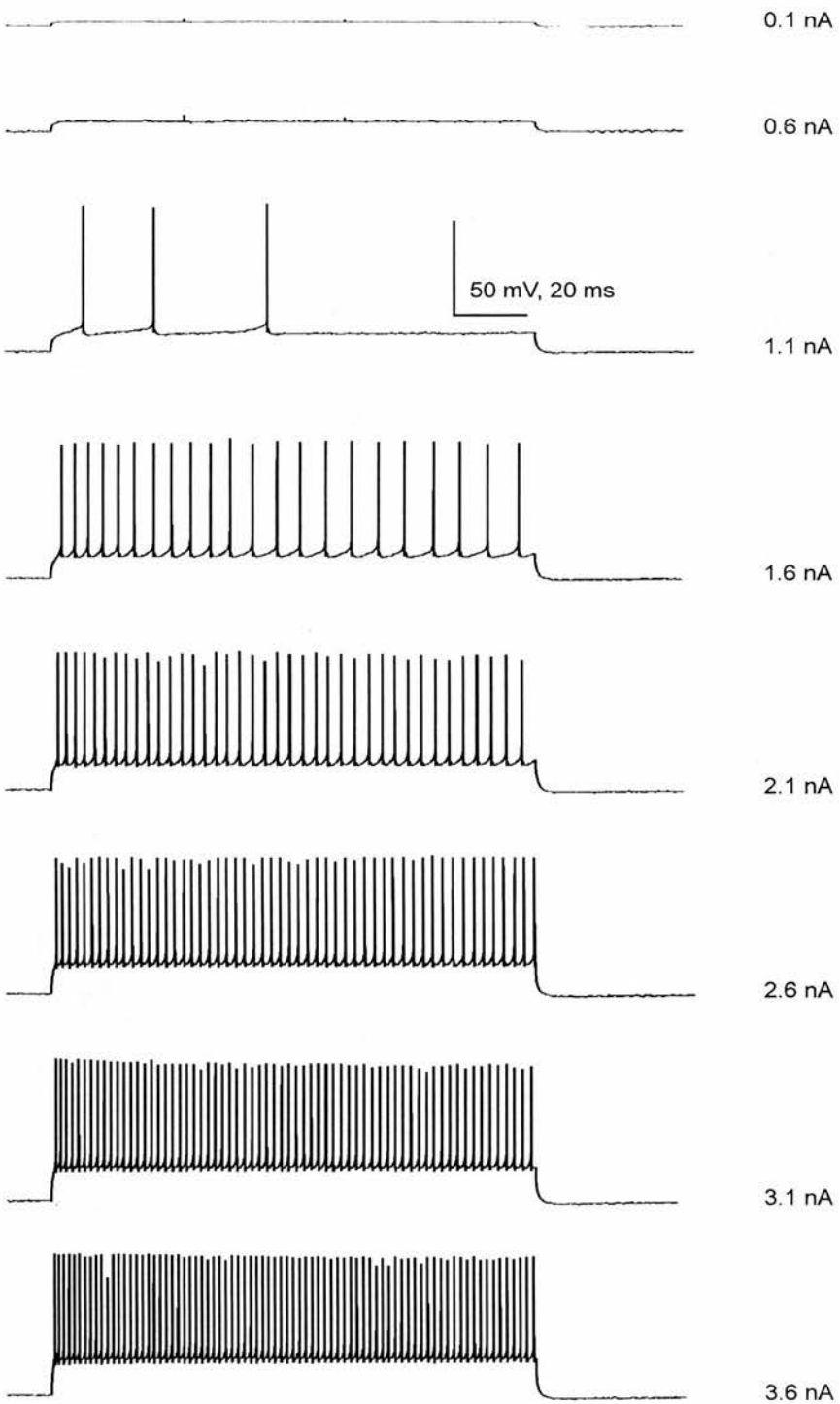

Figure 3.4.2.8 : Voltage traces of a Type B^- MVN neurone in response to depolarising current pulses of different amplitudes. The neurone displayed a higher frequency for the initial part of the firing trains but not as high as in Type B^+ and then decayed to steady-state value.

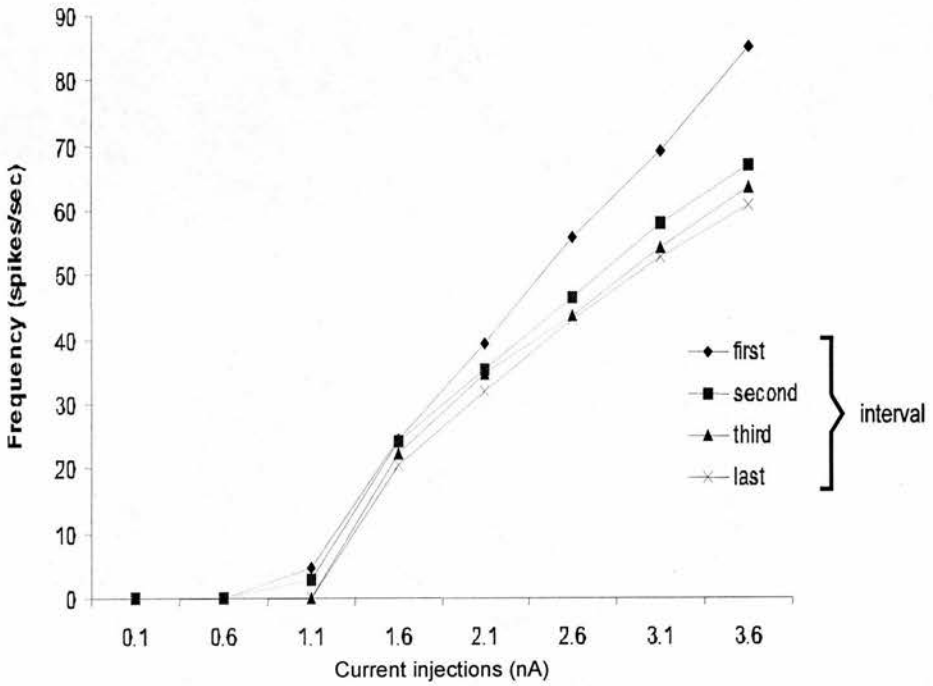

Figure 3.4.2.9 : Spike-frequency adaptation curve of Type B- MVN neurone

Spike-frequency adaptation curve of Type B- obtained from Fig.3.4.2.8, measured at different intervals showing non-linear relationship in the first interval. Notice the presence of a secondary range for the first and the second intervals.

TABLE 3.4.3

COMPARISON OF SPONTANEOUS ACTION POTENTIAL CHARACTERISTICS OF IPSILATERAL ROSTRAL TYPE B MVN NEURONES FROM CONTROL ANIMALS AND UNILATERAL LABYRINTHECTOMISED ANIMALS

		Rostral Type B after 4 hrs Unilateral Labyrinthectomy	
Parameters	Control	Type B^+	Type B^-
AP width at threshold, ms	0.86 ± 0.05	1.27 ± 0.05	0.79 ± 0.05
AP width at half-height, ms	0.40 ± 0.02	0.60 ± 0.03	0.40 ± 0.03
Rate of rise, V/sec	141.5 ± 9.47	93.8 ± 6.67	145.5 ± 11.91
Rate of fall, V/sec	158.9 ± 11.87	88.5 ± 5.54	166.0 ± 14.30
	(n = 21)	(n = 14)	(n = 14)

Values are means ± S.E.M; AP, action potential.

Legend 3.4.3.1 : Spontaneous action potential characteristics of control and 4 h after UL rostral Type B MVN neurones.

(A and B) Histogram showing the mean (±S.E.M) action potential duration of Type B MVN neurones, measured as width at threshold (W_T) and width at half-height (W_H). There is significant increase in the action potential duration of Type B^+ MVN neurones in UL animals compared to control and Type B^- neurones. (C and D) Mean of rate of repolarisation (rise) and depolarisation (fall) phase of action potential Type B MVN neurones in control and after UL animals. The rate of repolarisation and depolarisation phase of Type B^+ are significantly slower than control and Type B- MVN neurones. # $p< 0.05$ compared with control. * $p<0.05$ compared with B^- group, tested by one way ANOVA.

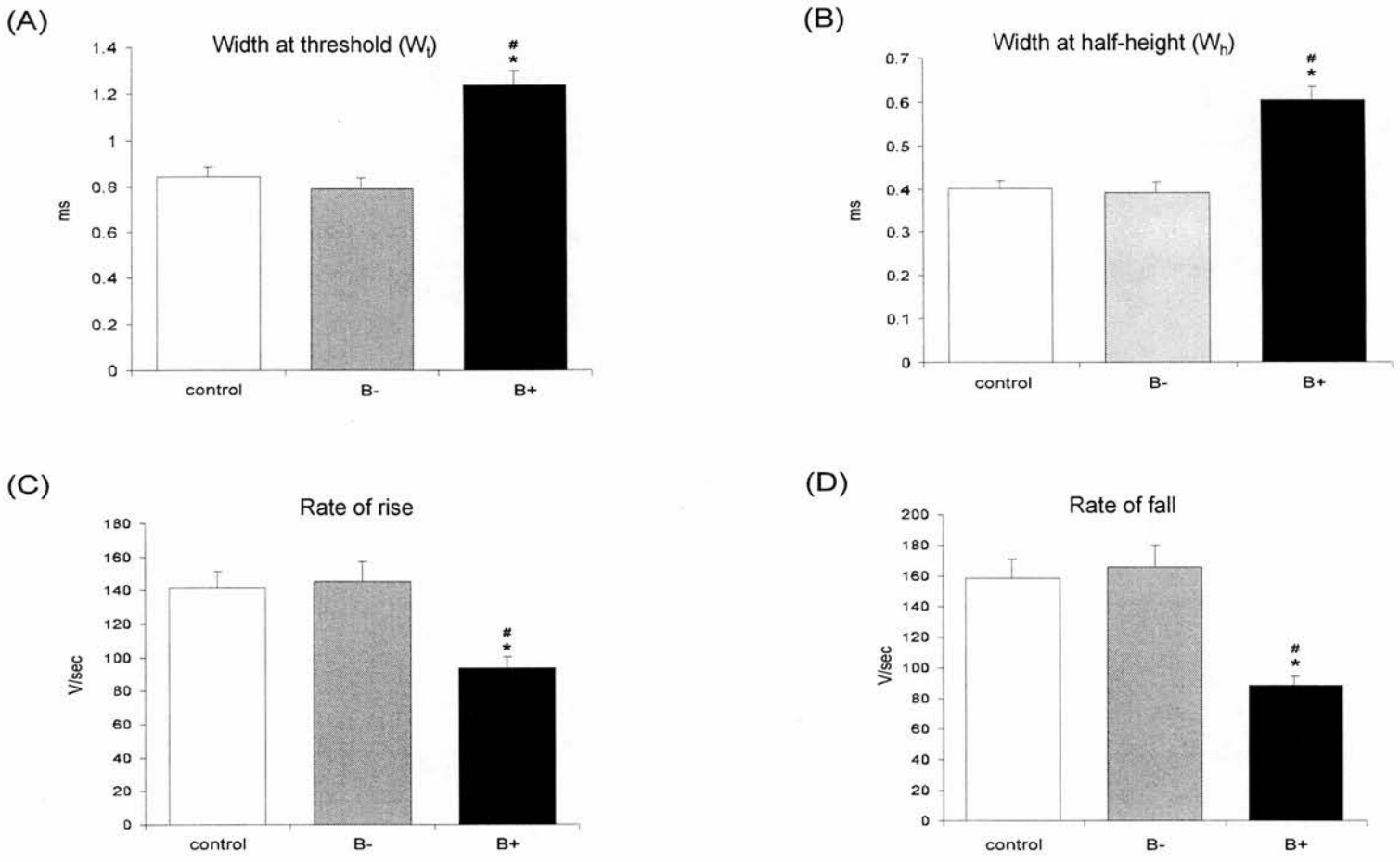

Figure 3.4.3.1 : Spontaneous action potential characteristics of Type B in control and 4h post-UL animals.

Legend 3.4.3.2 : Averaged action potential shapes superimposed from Type B MVN neurones in control and post-UL animals.

(A and B). Examples of averaged action potential shapes superimposed from Type B MVN neurone in control and 4 hrs after UL animals. Notice that absent of fast AHP in Type B^+ neurones (solid arrows), while the delayed slow AHP (open arrows) remain unchanged compared with Type B^- after UL and Type B neurones in control animals.

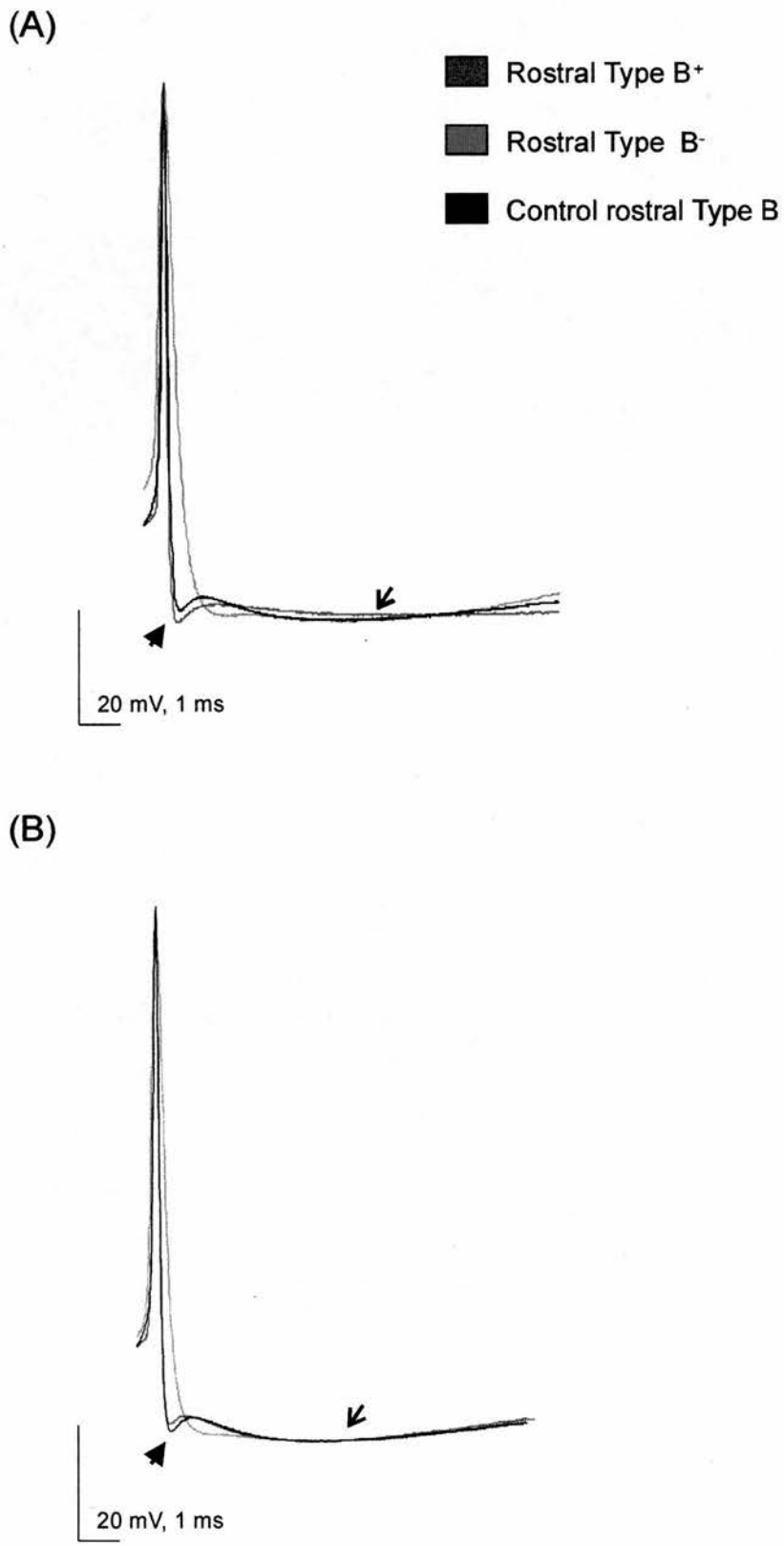

Figure 3.4.3.2 : Average action potentials superimposed from Type B MVN neurones in control and post-UL animals.

3.5 DISCUSSION

This study provides the first *in vitro* intracellular analysis of intrinsic membrane properties of vestibular neurones in the rat MVN after unilateral labyrinthectomy. The results of the study demonstrate that pronounced adaptive changes take place in the intrinsic membrane properties of a specific subpopulation of vestibular neurones in the rostral region of the MVN ipsilateral to the lesioned side. Following 4 hours after a lesion of the peripheral vestibular receptors of the left inner ear, 50% (14/28 of the sampled neurones) of the identified Type B neurones in the ipsilateral rostral MVN developed a significant increase in their intrinsically-generated *in vitro* resting discharge rate and exhibited a significant change in their spontaneous firing behaviour in response to depolarising current injection, indicated by a near two-fold increase in spike frequency adaptation index (SFA index). By contrast, the resting discharge rate and the SFA index of the remaining ipsilateral rostral Type B and ipsilateral rostral Type A as well as caudal MVN neurones were not changed after unilateral labyrinthectomy. Thus, this result indicates that the significant increase in the intrinsically-generated *in vitro* resting discharge rates of the ipsilateral rostral MVN neurones observed in the previous study by Cameron and Dutia (1997) using extracellular recordings, is attributable to a selective plastic change and adaptation in the intrinsic excitability of this sub-population of ipsilateral rostral Type B MVN neurones, which we have termed as Type B^+ neurones, while the intrinsic excitability of the remaining MVN neurones remains unchanged during the early period of vestibular compensation following UL.

There were no changes in the resting membrane potentials, apparent membrane input resistance or steady-state gain of the Type B^+ neurones after UL. However, it was observed that the increase in the intrinsic resting discharge rate and the SFA index of these Type B neurones is accompanied by a marked change in their averaged action potentials parameters. Thus, the duration of averaged spontaneous action potentials measured at spike threshold and at half-height of Type B^+ neurones were longer than those of Type B^- and control rostral Type B neurones. The rate of action potential repolarisation and depolarisation phases of Type B^+ neurones were also slower than Type B^- and control Type B neurones. Furthermore, it was also observed that the early fast AHP of Type B^+ neurones became smaller or almost invisible. The changes in all of these averaged action

potentials parameters, together with the loss of early fast AHP in Type B^+ suggesting that there is a functional down-regulation of membrane potassium conductances that are involved in the repolarisation of the action potential (Johnston *et al.,* 1994). Studies have shown that modulation of potassium current plays a major role in controlling neuronal excitability (for reviews see, Hille, 1992; Jonas and Kaczmarek, 1996; Bovill, 1997). Recent studies have indicated that potassium conductances were subjected to modulation in synaptic plasticity (Nelson and Alkon, 1991; Janigro *et al.*, 1997; Sobko *et al.*, 1998). Although, K^+ conductances in MVN neurones are not well characterised, the present findings indicate that such modulatory mechanisms may bring about the compensatory increase in the excitability of MVN neurones. However, other ionic conductances than the aforementioned K^+ conductance of MVN neurones which underlies their spontaneous action potentials may contribute to the increase resting discharge rate and SFA index as well.

Yamanaka *et al.,* (1998) showed that there was marked functional down-regulation of $GABA_A$ and $GABA_B$ receptors efficacy in the rostral ipsilateral MVN neurones within 4hrs following UL. While in the contralateral side, there was significant up-regulation of the functional efficacy of $GABA_A$ receptors. However, the selective adaptation of the electrophysiological properties of the Type B^+ neurones in the rostral MVN is in contrast to the functional down-regulation of GABA receptors which appears to occur in all rostral MVN neurones tested. It has been suggested that the down-regulation in GABAergic inhibition in the ipsilateral MVN is a key process in bringing about the restoration of the resting discharge rate of ipsilateral neurones after UL, by overcoming the disfacilitation and excessive commissural inhibition to which these neurones were subjected after the lesion (Yamanaka *et al.,* 1998). By contrast, the increase in the discharge rate and SFA index in the rostral ipsilateral Type B^+ MVN neurones after UL are more appropriate to modify the "signal processing" characteristics of these neurones during vestibular compensation. For example, the initial high frequency discharge of Type B^+ neurones during a depolarising pulse may be useful in generating spike firing in these neurones after UL. Therefore, GABA receptors down-regulation and the changes in intrinsic properties of Type B^+ neurones would therefore appear to be parallel compensatory process initiated by the vestibular deafferentation, which together result in the recovery of resting discharge in the ipsilateral MVN neurones.

There is no information at present as to the synaptic connectivity of Type A and Type B neurones in the MVN, and their roles in processing vestibular and eye-movement signals. This is a major limitation at present in understanding the significance of the changes in the properties of Type B^+ neurones seen in the present study. However, now that it is known that Type B^+ neurones show lesion-induced plasticity after UL, it should be possible to apply modern microanatomical and immunohistochemical techniques to study their characteristics and synaptic connectivity. For example, morphological reconstruction studies of identified Type A and Type B neurones after labelling with an intracellular marker (e.g. HRP) in slices could reveal whether there are differences in their size or extent of their dendritic arbors.

Nonetheless, from the location of the Type B^+ neurones in the rostral region of the ipsilateral MVN, and their frequency as observed (29%, 14/48 of total MVN neurones post-UL sampled) it is possible that these neurones may be equivalent to the flocculus target neurones (FTNs) recorded in monkeys undergoing motor learning under conditions of visual modification (Lisberger *et al.,* 1994). Projections from the cerebelar flocculus to MVN neurones have been demonstrated in the monkey (Lisberger *et al.,* 1994), cat (Sato *et al.,* 1988, Cheron 1996) and rabbit (Stahl 1991, Stahl and Simpson 1992). Lisberger *et al.*, (1994) showed that when monkey were made to wear goggles that magnified their visual field, their VOR showed an increase in gain so that a given head movement evoked a larger than normal reflex eye movement. They also showed that, in parallel with this change in the gain of the VOR, FTNs in the rostral MVN showed significant modifications in their response to visual and vestibular stimulation. It is possible that, in parallel with the recovery of resting discharge in the ipsilateral vestibular neurones after UL due to down-regulation of GABAergic inhibitory function, the large visual-vestibular mismatch that arises in the UL animals due to the imbalance in vestibular input rather than an alteration in visual feedback, may give rise to equivalent adaptive modifications in the FTNs in an effort to generate a normal VOR with the highly abnormal vestibular input. While further experiments are necessary to directly test this proposal, present findings suggest that the changes in responsiveness of FTNs observed during motor learning *in vivo* may involve not only alteration in the efficacy of cerebellar synapses but may also involve significant changes in the properties of

the postsynaptic MVN neurones as observed in this study. Direct experimental evidence for the proposal that Type B^+ neurones correspond to FTNs, may come from experiments on animals where HRP or another anterograde marker is injected into the cerebellar flocculus, some days prior to the slice experiment. In the slice experiment the identified Type B^+ neurones will be filled with another marker and the tissue would then be processed to visualise both labels. If Type B^+ neurones are FTNs, they should receive synaptic connections from the labelled cerebellar axons.

CONCLUSIONS AND FUTURE EXPERIMENTS

In conclusion, this thesis presented the results of *in vitro* electrophysiological experiments using the horizontal slices of dorsal brainstem containing the medial vestibular nucleus. These slices used are viable for periods of up to 6h or more in appropriate environments, and provide a very useful preparation in which to study the effects of neurotransmitter and neuromodulators on the tonically active neurones of the MVN. This preparation also extremely useful in studying the neuronal activity and cellular mechanisms involved in the early stages of vestibular compensation in the MVN following unilateral labyrinthectomy.

In the **first chapter**, it was demonstrated using extracellular and intracellular whole-cell patch clamp recording techniques that large majority of spontaneously active rat MVN neurones *in vitro*, were inhibited in a dose dependent manner by the δ-opioid receptor agonist, [D-Ala^2, D-Leu^5]-enkephalin (DADLE) and highly selective δ-opioid receptor agonist, DPLPE. This inhibition was effectively antagonised by the selective δ-opioid receptor antagonist, naltrindole and also persisted in the presence of modified low Ca^{2+}, high Mg^{2+} medium, suggesting that the effects of DADLE are likely to be mediated through its direct action on the postsynaptic receptors. These results confirm the presence of δ-opioid receptors on MVN neurones, consistent with the reported immunohistochemical and in situ hybridisation studies. By contrast, agonists for μ- and κ-opioid receptors failed to elicit response in any of the MVN neurones tested, although in situ hybridisation studies have demonstrated the presence of low μ- and κ-opioid receptor mRNA in the MVN. It was suggested that μ- and κ-receptor mediated effects within the MVN may be entirely presynaptic. Future investigations should aim to determine the μ- and κ-receptor mediated effects within this nucleus. For example, presynaptic modulatory effects of μ- and κ-opioid agonists on the monosynaptic excitatory postsynaptic potential (e.p.s.p) recorded with VIIIth nerve stimulation *in vitro* (Kinney *et al.*, 1994) need to be investigated. In whole cell patch clamp experiments experiments, it was shown that the inhibitory effects of DADLE were mediated by membrane hyperpolarisation associated with increased in outward K^+ conductance in the cell membrane. This finding was confirmed pharmacologically using the K^+ channel blocker, TEA. However, more selective K^+ channel blockers, and further voltage-clamp analyses are needed to characterise the K^+ conductances more fully. It was also observed

that the degree of DADLE-induced inhibition was dependent on post-natal age, in that the responses to DADLE were smaller in younger animals and increase significantly with age. It was suggested that this could be due to continuing post-natal growth and maturation of the MVN and their dendritic arbors or it could reflect changes in the overall density of δ-opioid receptors on MVN neurones. Further investigations are necessary to determine the morphological characteristics of the MVN neurones or expression binding studies of δ-opioid receptors at different postnatal age may provide information for the development of δ-opioid receptor in the MVN. The importance of opioid innervation on the post-natal development of MVN neurones can be investigated.

In the **second chapter**, the effect of N/OFQ on the spontaneously active MVN neurones was examined using extracellular and intracellular whole cell patch clamp recording techniques. It was demonstrated that N/OFQ profoundly inhibited spontaneous discharge of MVN neurones. This inhibition was dose-dependent, persisted in low Ca^{2+}, Co medium and was resistant to pharmacological blockade of naloxone, but was effectively antagonised by the selective ORL1 receptor antagonist. In addition, both N/OFQ and DADLE inhibited the spontaneous discharge of the majority of MVN neurones, while a minority of neurones was selectively responsive either to N/OFQ or to DADLE but not both. Co-administration of N/OFQ and DADLE to neurones that were responsive to both agonists resulted in occlusion rather than summation. In whole cell patch clamp experiments, it was shown that N/OFQ caused membrane hyperpolarisation and decrease in input resistance in the MVN neurones. Thus, these results indicate that N/OFQ inhibited the spontaneously active MVN neurones through its direct action via ORL1 receptors and that this inhibitory action was mediated by increased in K^+ conductances. However, further voltage clamp experiments using specific ion channel blockers are necessary to systematically determine and confirm the ionic mechanisms underlying the effects of N/OFQ on Type A and Type B neurones.

In the **final chapter**, using whole cell patch clamp recording techniques the changes in the electrophysiological properties of identified Type A and Type B MVN neurones in the rostral region of the MVN during the early stage of vestibular compensation (4h after UL) were studied. It was demonstrated that the electrophysiological properties of Type A MVN neurones were unchanged following

UL. In contrast, marked changes occurred in the membrane excitability and action potential firing characteristics of specific sub-population of rostral Type B MVN neurones, indicating that the changes in the intrinsic membrane properties of this sub-population of MVN neurones may be an important cellular mechanism during the behavioural recovery after vestibular lesions. Based on the location of this sub-population of Type B neurones, It was suggested that they might be equivalent to the flocculus target neurones (FTNs) recorded in monkey undergoing motor learning under visual modification. Further investigations are therefore required in order to explore the connectivity of this particular Type B neurones as well as voltage clamp experiments to pharmacologically isolate the ionic conductances that responsible for generation of the resting discharge after vestibular lesions.

REFERENCES

A

Akil H, Watson SJ, Young E, Lewis ME, Khachaturian H, Walker JM (1984). Endogenous opioids: biology and function. Annu Rev Neurosci 7, 223-55.

Aghajanian GK, Wang YY (1986). Pertussis toxin blocks the outward currents evoked by opiate and alpha 2-agonists in locus coeruleus neurons. Brain Res 371, 390-4.

Airaksinen MS, Panula P (1988). The histaminergic system in the guinea pig central nervous system: an immunocytochemical mapping study using an antiserum against histamine. J Comp Neurol 273, 163-86.

Anton B, Fein J, To T, Li X, Silberstein L, Evans CJ (1996). Immunohistochemical localization of ORL-1 in the central nervous system of the rat. J Comp Neurol 368, 229-51.

Attali B, Saya D, Vogel Z (1989). Kappa-opiate agonists inhibit adenylate cyclase and produce heterologous desensitization in rat spinal cord. J Neurochem 52, 360-9.

B

Baarsma EA, Collewijn H (1975). Changes in compensatory eye movements after unilateral labyrinthectomy in the rabbit. Arch Otorhinolaryngol 211, 219-30.

Babalian A, Vibert N, Assie G, Serafin M, Muhlethaler M, Vidal PP (1997). Central vestibular networks in the guinea-pig: functional characterization in the isolated whole brain in vitro. Neuroscience 81, 405-26.

Baker R, Precht W, Llinas R (1972). Cerebellar modulatory action on the vestibulo-trochlear pathway in the cat. Exp Brain Res 15, 364-85.

Balaban CD (1984). Olivo-vestibular and cerebello-vestibular connections in albino rabbits. Neuroscience 12, 129-49.

Balaban CD, Beryozkin G (1994). Organization of vestibular nucleus projections to the caudal dorsal cap of kooy in rabbits. Neuroscience 62, 1217-36.

Barmack NH, Baughman RW, Eckenstein FP, Shojaku H (1992). Secondary vestibular cholinergic projection to the cerebellum of rabbit and rat as revealed by choline acetyltransferase immunohistochemistry, retrograde and orthograde tracers. J Comp Neurol 317, 250-70.

Beitz AJ, Clements JR, Ecklund LJ, Mullett MM (1987). The nuclei of origin of brainstem enkephalin and cholecystokinin projections to the spinal trigeminal nucleus of the rat. Neuroscience 20, 409-25.

Berthoz A, Graf W and Vidal PP (1992). The head-neck sensory motor system. Oxford University Press, U.K.

Bienhold H, Flohr H (1978). Role of commissural connexions between vestibular nuclei in compensation following unilateral labyrinthectomy [proceedings]. J Physiol (Lond) 284, 178P.

Bixby JL, Spitzer NC (1983). Enkephalin reduces quantal content at the frog neuromuscular junction. Nature 301, 431-2.

Blanton MG, Lo Turco JJ, Kriegstein AR (1989). Whole cell recording from neurons in slices of reptilian and mammalian cerebral cortex. J Neurosci Methods 30, 203-10.

Bloom F, Battenberg E, Rossier J, Ling N, Guillemin R (1978). Neurons containing beta-endorphin in rat brain exist separately from those containing enkephalin: immunocytochemical studies. Proc Natl Acad Sci U S A 75, 1591-5.

Bovill JG (1997). Mechanisms of actions of opioids and non-steroidal anti-inflammatory drugs. Eur J Anaesthesiol Suppl 15, 9-15.

Bradbury AF, Smyth DG, Snell CR (1976). Biosynthetic origin and receptor conformation of methionine enkephalin. Nature 260, 165-6.

Brodal, A. (1974). Anatomy of the vestibular nuceli and their connections. In: Kornhuber HH (ed) Handbook of sensory physiology, I. Vestibular system. Springer, Berlin Heidelberg New York, pp239-352

Brodal, A., Pompeiano, O. and Walberg, F. (1962). The vestibular nuclei and their connections. Oliver and Boyd, London.

Brownstein MJ (1993). A brief history of opiates, opioid peptides, and opioid receptors. Proc Natl Acad Sci U S A 90, 5391-3.

Bunzow JR, Saez C, Mortrud M, Bouvier C, Williams JT, Low M, et al. (1994). Molecular cloning and tissue distribution of a putative member of the rat opioid receptor gene family that is not a mu, delta or kappa opioid receptor type. FEBS Lett 347, 284-8.

Burns DL, Hewlett EL, Moss J, Vaughan M (1983). Pertussis toxin inhibits enkephalin stimulation of GTPase of NG108-15 cells. J Biol Chem 258, 1435-8.

Buttner-Ennever JA (1992). Patterns of connectivity in the vestibular nuclei. Ann N Y Acad Sci 656, 363-78.

Buttner-Ennever JA, Buttner U (1992). Neuroanatomy of the ocular motor pathways. Baillieres Clin Neurol 1, 263-87.

C

Cameron SA, Dutia MB (1997). Cellular basis of vestibular compensation: changes in intrinsic excitability of MVN neurones. Neuroreport 8, 2595-9.

Capocchi G, Della Torre G, Grassi S, Pettorossi VE, Zampolini M (1992). NMDA receptor-mediated long term modulation of electrically evoked field potentials in the rat medial vestibular nuclei. Exp Brain Res 90, 546-50.

Carleton SC, Carpenter MB (1984). Distribution of primary vestibular fibers in the brainstem and cerebellum of the monkey. Brain Res 294, 281-98.

Carpenter DO, Hori N (1992). Neurotransmitter and peptide receptors on medial vestibular nucleus neurons. Ann N Y Acad Sci 656, 668-86.

Carpenter MB (1988). Vestibular nuclei: afferent and efferent projections. Prog Brain Res 76, 5-15.

Carpenter MB, Harbison JW, Peter P (1970). Accessory oculomotor nuclei in the monkey: projections and effects of discrete lesions. J Comp Neurol 140, 131-54.

Cass SP, Goshgarian HG (1991). Vestibular compensation after labyrinthectomy and vestibular neurectomy in cats. Otolaryngol Head Neck Surg 104, 14-9.

Cass SP, Kartush JM, Graham MD (1992). Patterns of vestibular function following vestibular nerve section. Laryngoscope 102, 388-94.

Caudle RM, Chavkin C (1990). Mu opioid receptor activation reduces inhibitory postsynaptic potentials in hippocampal CA3 pyramidal cells of rat and guinea pig. J Pharmacol Exp Ther 252, 1361-9.

Chang KJ, Hazum E, Killian A, Cuatrecasas P (1981). Interactions of ligands with morphine and enkephalin receptors are differentially affected by guanine nucleotide. Mol Pharmacol 20, 1-7.

Chang KJ, Miller RJ, Cuatrecasas P (1978). Interaction of enkephalin with opiate receptors in intact cultured cells. Mol Pharmacol 14, 961-70.

Chavkin C, James IF, Goldstein A (1982). Dynorphin is a specific endogenous ligand of the kappa opioid receptor. Science 215, 413-5.

Chen Y, Fan Y, Liu J, Mestek A, Tian M, Kozak CA, et al. (1994). Molecular cloning, tissue distribution and chromosomal localization of a novel member of the opioid receptor gene family. FEBS Lett 347, 279-83.

Chen Y, Mestek A, Liu J, Hurley JA, Yu L (1993). Molecular cloning and functional expression of a mu-opioid receptor from rat brain. Mol Pharmacol 44, 8-12.

Chen Y, Yu L (1994). Differential regulation by cAMP-dependent protein kinase and protein kinase C of the mu opioid receptor coupling to a G protein-activated K+ channel. J Biol Chem 269, 7839-42.

Chieng B, Christie MJ (1994). Hyperpolarization by opioids acting on mu-receptors of a sub-population of rat periaqueductal gray neurones in vitro. Br J Pharmacol 113, 121-8.

Childers SR (1991). Opioid receptor-coupled second messenger systems. Life Sci 48, 1991-2003.

Chretien M, Seidah NG (1981). Chemistry and biosynthesis of pro-opiomelanocortin. ACTH, MSH's, endorphins and their related peptides. Mol Cell Biochem 34, 101-27.

Chu X, Xu N, Li P, Wang JQ (1998). Profound inhibition of cardiomotor neurons in the rat rostral ventrolateral medulla by nociceptin (orphanin FQ). Neuroreport 9, 1081-4.

Cirelli C, Pompeiano M, D'Ascanio P, Arrighi P, Pompeiano O (1996). c-fos Expression in the rat brain after unilateral labyrinthectomy and its relation to the uncompensated and compensated stages. Neuroscience 70, 515-46.

Cirelli C, Pompeiano M, D'Ascanio P, Pompeiano O (1993). Early c-fos expression in the rat vestibular and olivocerebellar systems after unilateral labyrinthectomy. Arch Ital Biol 131, 71-4.

Cochran SL, Kasik P, Precht W (1987). Pharmacological aspects of excitatory synaptic transmission to second- order vestibular neurons in the frog. Synapse 1, 102-23.

Coleman PA, Miller RF (1989). Measurement of passive membrane parameters with whole-cell recording from neurons in the intact amphibian retina. J Neurophysiol 61, 218-30.

Collier HO, Roy AC (1974). Morphine-like drugs inhibit the stimulation of E prostaglandins of cyclic AMP formation by rat brain homogenate. Nature 248, 24-7.

Comb M, Seeburg PH, Adelman J, Eiden L, Herbert E (1982). Primary structure of the human Met- and Leu-enkephalin precursor and its mRNA. Nature 295, 663-6.

Connor M, Christie MJ (1998). Modulation of Ca2+ channel currents of acutely dissociated rat periaqueductal grey neurons. J Physiol (Lond) 509, 47-58.

Connor M, Vaughan CW, Chieng B, Christie MJ (1996a). Nociceptin receptor coupling to a potassium conductance in rat locus coeruleus neurones in vitro. Br J Pharmacol 119, 1614-8.

Connor M, Yeo A, Henderson G (1996b). The effect of nociceptin on Ca2+ channel current and intracellular Ca2+ in the SH-SY5Y human neuroblastoma cell line. Br J Pharmacol 118, 205-7.

Corbett AD, Patterson SJ, Kosterlitz HW (1993) Selectivity of ligands for opioid receptors. In: Herz A (ed) Handbook of experimental pharmacology: vol Opioids I. Springer, Heidelberg, pp 645-679.

Cuello AC (1983). Central distribution of opioid peptides. Br Med Bull 39, 11-6.

Curthoys IS, Dai MJ, Halmagyi GM (1991). Human ocular torsional position before and after unilateral vestibular neurectomy. Exp Brain Res 85, 218-25.

Curthoys IS, Halmagyi GM (1995). Vestibular compensation: a review of the oculomotor, neural, and clinical consequences of unilateral vestibular loss. J Vestib Res 5, 67-107.

Curthoys IS, Markham CH (1971). Convergence of labyrinthine influences on units in the vestibular nuclei of the cat. I. Natural stimulation. Brain Res 35, 469-90.

Curthoys IS, Smith PF, Darlington CL (1988). Postural compensation in the guinea pig following unilateral labyrinthectomy. Prog Brain Res 76, 375-84.

D

Darland T, Heinricher MM, Grandy DK (1998). Orphanin FQ/nociceptin: a role in pain and analgesia, but so much more. Trends Neurosci 21, 215-21.

Darlington CL, Flohr H, Smith PF (1991). Molecular mechanisms of brainstem plasticity. The vestibular compensation model. Mol Neurobiol 5, 355-68.

Darlington CL, Gallagher JP, Smith PF(1995). In vitro electrophysiological studies of the vestibular nucleus complex. Prog Neurobiol 45, 335-46.

Darlington CL, Smith PF (1989). The effects of N-methyl-D-aspartate antagonists on the development of vestibular compensation in the guinea pig. Eur J Pharmacol 174, 273-8.

Darlington CL, Smith PF (1995). Metabotropic glutamate receptors in the guinea-pig medial vestibular nucleus in vitro. Neuroreport 6, 1799-802.

Darlington CL, Smith PF, Gilchrist DP (1992). Comparison of the effects of ACTH-(4-10) on medial vestibular nucleus neurons in brainstem slices from labyrinthine-intact and compensated guinea pigs. Neurosci Lett 145, 97-9.

Darlington CL, Smith PF, Hubbard JI (1989). Neuronal activity in the guinea pig medial vestibular nucleus in vitro following chronic unilateral labyrinthectomy. Neurosci Lett 105, 143-8.

Darlington CL, Smith PF, Hubbard JI (1990). Guinea pig medial vestibular nucleus neurons in vitro respond to ACTH4- 10 at picomolar concentrations. Exp Brain Res 82, 637-40.

Davis TP, Porreca F, Burks TF, Dray A (1985). The proenkephalin A fragment, peptide E: central processing and CNS activity in vivo. Eur J Pharmacol 111, 177-83.

De Waele C, Graf W, Josset P, Vidal PP (1989). A radiological analysis of the postural syndromes following hemilabyrinthectomy and selective canal and otolith lesions in the guinea pig. Exp Brain Res 77, 166-82.

de Waele C, Muhlethaler M, Vidal PP (1995). Neurochemistry of the central vestibular pathways. Brain Res Brain Res Rev 20, 24-46.

de Waele C, Torres AC, Josset P, Vidal PP (1996). Evidence for reactive astrocytes in rat vestibular and cochlear nuclei following unilateral inner ear lesion. Eur J Neurosci 8, 2006-18.

de Waele C, Vibert N, Baudrimont M, Vidal PP (1990). NMDA receptors contribute to the resting discharge of vestibular neurons in the normal and hemilabyrinthectomized guinea pig. Exp Brain Res 81, 125-33.

DeHaven-Hudkins DL, Brostrom PA, Allen JT, Lesko LJ, Ferkany JW, Kaplita PV, et al. (1990). Pharmacologic profile of NPC 168 (naltrexone phenyl oxime), a novel compound with activity at opioid receptors. Pharmacol Biochem Behav 37, 497-504.

Dhawan BN, Cesselin F, Raghubir R, Reisine T, Bradley PB, Portoghese PS, et al. (1996). International Union of Pharmacology. XII. Classification of opioid receptors. Pharmacol Rev 48, 567-92.

Dieringer N (1995). 'Vestibular compensation': neural plasticity and its relations to functional recovery after labyrinthine lesions in frogs and other vertebrates. Prog Neurobiol 46, 97-129.

Dieringer N, Kunzle H, Precht W (1984). Increased projection of ascending dorsal root fibers to vestibular nuclei after hemilabyrinthectomy in the frog. Exp Brain Res 55, 574-8.

Dieringer N, Precht W (1979a). Mechanisms of compensation for vestibular deficits in the frog. I. Modification of the excitatory commissural system. Exp Brain Res 36, 311-28.

Dieringer N, Precht W (1979b). Mechanisms of compensation for vestibular deficits in the frog. II. Modification of the inhibitory Pathways. Exp Brain Res 36, 329-357.

Dieringer N, Precht W (1982). Compensatory head and eye movements in the frog and their contribution to stabilization of gaze. Exp Brain Res 47, 394-406.

Dieterich M and Brandt T (1995). The vestibulo-ocular reflex. Curr Opin Neurol 8, 83-88.

Docherty K, Steiner DF (1982). Post-translational proteolysis in polypeptide hormone biosynthesis. Annu Rev Physiol 44, 625-38.

Dohlman HG, Caron MG, Lefkowitz RJ (1987). A family of receptors coupled to guanine nucleotide regulatory proteins. Biochemistry 26, 2657-64.

Doi K, Seki M, Kuroda Y, Okamura N, Ito H, Hayakawa T, et al. (1997). Direct and indirect thalamic afferents arising from the vestibular nuclear complex of rats: medial and spinal vestibular nuclei. Okajimas Folia Anat Jpn 74, 9-31.

Doi K, Tsumoto T, Matsunaga T (1990). Actions of excitatory amino acid antagonists on synaptic inputs to the rat medial vestibular nucleus: an electrophysiological study in vitro. Exp Brain Res 82, 254-62.

Doi N, Dutia MB, Russell JA (1998). Inhibition of rat oxytocin and vasopressin supraoptic nucleus neurons by nociceptin in vitro. Neuroscience 84, 913-21.

Douglass J, Civelli O, Herbert E (1984). Polyprotein gene expression: generation of diversity of neuroendocrine peptides. Annu Rev Biochem 53, 665-715.

du Lac S, Lisberger SG (1995). Membrane and firing properties of avian medial vestibular nucleus neurons in vitro. J Comp Physiol [A] 176, 641-51.

Duan SM, Shimizu N, Fukuda A, Hori T, Oomura Y (1990). Hyperpolarizing action of enkephalin on neurons in the dorsal motor nucleus of the vagus, in vitro. Brain Res Bull 25, 551-9.

Duggan AW, Davies J, Hall JG (1976). Effects of opiate agonists and antagonists on central neurons of the cat. J Pharmacol Exp Ther 196, 107-20.

Duggan AW, North RA (1983). Electrophysiology of opioids. Pharmacol Rev 35(4), 219-81.

Dutia MB (1989). Mechanisms of head stabilisation. News in Physiological Sciences 4, 101-3.

Dutia MB, Johnston AR (1998). Development of action potentials and apamin-sensitive after-potentials in mouse vestibular nucleus neurones. Exp Brain Res 118, 148-54.

Dutia MB, Johnston AR, McQueen DS (1992). Tonic activity of rat medial vestibular nucleus neurones in vitro and its inhibition by GABA. Exp Brain Res 88, 466-72.

Dutia MB, Lotto RB, Johnston AR (1995). Post-natal development of tonic activity and membrane excitability in mouse medial vestibular nucleus neurones. Acta Otolaryngol Suppl (Stockh) 520, 101-4.

Dutia MB, Neary P, McQueen DS (1990). Effects of cholinergic agents on spontaneously active rat medial vestibular nucleus neurones in vitro. J Physiol (Lond) 425, 90P.

Dyer RG, Weick WF, Mansfield S and Corbett H (1981). Secretion of lutenizing hormone in ovarectomized adults rats treated neonatally with monosodium glutamate. J Endocrin 91, 341-346.

E

Eipper BA, Mains RE (1980). Structure and biosynthesis of pro-adrenocorticotropin/endorphin and related peptides. Endocr Rev 1, 1-27.

Epema AH, Gerrits NM, Voogd J (1988). Commissural and intrinsic connections of the vestibular nuclei in the rabbit: a retrograde labeling study. Exp Brain Res 71, 129-46.

Evans CJ, Keith DE, Jr., Morrison H, Magendzo K, Edwards RH (1992). Cloning of a delta opioid receptor by functional expression. Science 258, 1952-5.

F

Faber ES, Chambers JP, Evans RH, Henderson G (1996). Depression of glutamatergic transmission by nociceptin in the neonatal rat hemisected spinal cord preparation in vitro. Br J Pharmacol 119, 189-90.

Fallon JH, Leslie FM (1986). Distribution of dynorphin and enkephalin peptides in the rat brain. J Comp Neurol 249, 293-336.

Fedynyshyn JP, Lee NM (1989). Mu-type opioid receptors in rat periaqueductal gray-enriched P2 membrane are coupled to guanine nucleotide binding proteins. Brain Res 476, 102-9.

Fetter M, Zee DS (1988). Recovery from unilateral labyrinthectomy in rhesus monkey. J Neurophysiol 59, 370-93.

Finley JC, Maderdrut JL, Petrusz P (1981). The immunocytochemical localization of enkephalin in the central nervous system of the rat. J Comp Neurol 198, 541-65.

Fisch U (1973). The vestibular response following unilateral vestibular neurectomy. Acta Otolaryngol (Stockh) 76, 229-38.

Fischli W, Goldstein A, Hunkapiller MW, Hood LE (1982). Isolation and amino acid sequence analysis of a 4,000-dalton dynorphin from porcine pituitary. Proc Natl Acad Sci U S A 79(17), 5435-7.

Flohr H, Luneburg U (1993). Role of NMDA receptors in lesion-induced plasticity. Arch Ital Biol 131, 173-90.

Forscher P and Oxford GS (1985). Modulation of calcium channels by norepinephrine in internally perfused dialyzed avian sensory neurons. J Gen Physiol 85, 743-763.

Fukuda J, Highstein SM, Ito M (1972). Cerebellar inhibitory control of the vestibulo-ocular reflex investigated in rabbit 3rd nucleus. Exp Brain Res 14, 511-26.

Fukuda K, Kato S, Mori K, Nishi M, Takeshima H (1993). Primary structures and expression from cDNAs of rat opioid receptor delta- and mu-subtypes. FEBS Lett 327, 311-4.

Fukuda K, Kato S, Mori K, Nishi M, Takeshima H, Iwabe N, et al. (1994). cDNA cloning and regional distribution of a novel member of the opioid receptor family. FEBS Lett 343, 42-6.

Furuya N, Markham CH (1981). Arborization of axons in oculomotor nucleus identified by vestibular stimulation and intra-axonal injection of horseradish peroxidase. Exp Brain Res 43, 289-303.

Furuya N, Yabe T, Koizumi T (1992). Neurotransmitters in the vestibular commissural system of the cat. Ann N Y Acad Sci 656, 594-601.

G

Gacek RR (1969). The course and central termination of first order neurons supplying vestibular endorgans in the cat. Acta Otolaryngol Suppl 254, 1-66.

Gacek RR (1974). Localization of neurons supplying the extraocular muscles in the kitten using horseradish peroxidase. Exp Neurol 44, 381-403.

Gacek RR (1977). Location of brain stem neurons projecting to the oculomotor nucleus in the cat. Exp Neurol 57, 725-49.

Gacek RR, Lyon MJ, Schoonmaker J (1988). Ultrastructural changes in vestibulo-ocular neurons following vestibular neurectomy in the cat. Ann Otol Rhinol Laryngol 97, 42-51.

Gacek RR, Lyon MJ, Schoonmaker J (1991). Ultrastructural changes in contralateral vestibulo-ocular neurons following vestibular neurectomy in the cat. Acta Otolaryngol Suppl 477, 1-14.

Gacek RR, Lyon MJ, Schoonmaker JE (1989). Morphologic correlates of vestibular compensation in the cat. Acta Otolaryngol Suppl 462, 1-16.

Galiana HL, Flohr H, Jones GM (1984). A reevaluation of intervestibular nuclear coupling: its role in vestibular compensation. J Neurophysiol 51, 242-59.

Gallagher JP, Lewis MR, Gallagher PS (1985). An electrophysiological investigation of the rat medial vestibular nucleus in vitro. Prog Clin Biol Res 176, 293-304.

Gallagher JP, Phelan KD, Shinnick-Gallagher P (1992). Modulation of excitatory transmission at the rat medial vestibular nucleus synapse. Ann N Y Acad Sci 656, 630-44.

Gilbert JA, Richelson E (1983). Function of delta opioid receptors in cultured cells. Mol Cell Biochem 55, 83-19.

Gilbert PE, Martin WR (1976). Sigma effects of nalorphine in the chronic spinal dog. Drug Alcohol Depend 1, 373-6.

Gilman S and Newman SW (1992). Essentials of clinical neuroanatomy and neurophysiology (8^{th} ed) Davis Company, Philadephia.

Giuliani S, Maggi CA (1996). Inhibition of tachykinin release from peripheral endings of sensory nerves by nociceptin, a novel opioid peptide. Br J Pharmacol 118, 1567-9.

Goldstein A, Fischli W, Lowney LI, Hunkapiller M, Hood L (1981). Porcine pituitary dynorphin: complete amino acid sequence of the biologically active heptadecapeptide. Proc Natl Acad Sci U S A 78, 7219-23.

Goldstein A and Naidu A (1989). Multiple opioid receptors: ligand selectivity profiles and binding site signatures. Mol Pharmacol 36, 265-272.

Goldstein A, Tachibana S, Lowney LI, Hunkapiller M, Hood L (1979). Dynorphin-(1-13), an extraordinarily potent opioid peptide. Proc Natl Acad Sci U S A 76, 6666-70.

Graf W, Ezure K (1986). Morphology of vertical canal related second order vestibular neurons in the cat. Exp Brain Res 63, 35-48.

Grevel J, Yu V, Sadee W (1985). Characterization of a labile naloxone binding site (lambda site) in rat brain. J Neurochem 44, 1647-56.

Gross RA, Macdonald RL (1987). Dynorphin A selectively reduces a large transient (N-type) calcium current of mouse dorsal root ganglion neurons in cell culture. Proc Natl Acad Sci U S A 84, 5469-73.

Grottel K, Jakielska-Bukowska D (1993). The reticulovestibular projection in the rabbit: an experimental study with the retrograde horseradish peroxidase method. Neurosci Res 18, 179-93.

Grudt TJ, Williams JT (1993). kappa-Opioid receptors also increase potassium conductance. Proc Natl Acad Sci U S A 90, 11429-32.

Grudt TJ, Williams JT (1995). Opioid receptors and the regulation of ion conductances. Rev Neurosci 6, 279-86.

Gubler U, Seeburg P, Hoffman BJ, Gage LP, Udenfriend S (1982). Molecular cloning establishes proenkephalin as precursor of enkephalin- containing peptides. Nature 295, 206-8.

Guerrini R, Calo G, Rizzi A, Bigoni R, Bianchi C, Salvadori S, Regoli D (1998) A new selective antagonist of the nociceptin receptor. Br J Pharmacol 123,163-5.

H

Haas HL, Schaerer B, Vosmansky M (1979). A simple perfusion chamber for the study of nervous tissue slices in vitro. J Neurosci Methods 1, 323-5.

Halmagyi GM, Gresty MA, Gibson WP (1979). Ocular tilt reaction with peripheral vestibular lesion. Ann Neurol 6, 80-3.

Hamann KF, Lannou J (1988). Dynamic charateristics of vestibular nuclear neurones responses to vestibular and optokinetic stimulation during vestibular compensation in the rat. Acta Otolaryngology Supplement (Stockh) 455, 1-19.

Handa BK, Land AC, Lord JA, Morgan BA, Rance MJ, Smith CF (1981). Analogues of beta-LPH61-64 possessing selective agonist activity at mu- opiate receptors. Eur J Pharmacol 70, 531-40.

Herz A (1997). Endogenous opioid system and alcohol addiction. Psychopharmcology 129, 99-111.

Hescheler J, Rosenthal W, Trautwein W, Schultz G (1987). The GTP-binding protein, Go, regulates neuronal calcium channels. Nature 325, 445-7.

Hill RG, Pepper CM, Mitchell JF (1976). Depression of nociceptive and other neurones in the brain by iontophoretically applied met-enkephalin. Nature 262, 604-6.

Hille B, (1992). Ionic channels of excitable membranes (2nd ed), Sinaauer Associates Inc., Massachusetts.

Holstein GR, Martinelli GP, Cohen B (1992). Immunocytochemical visualization of L-baclofen-sensitive GABAB binding sites in the medial vestibular nucleus. Ann N Y Acad Sci 656, 933-6.

Houtani T, Nishi M, Takeshima H, Nukada T, Sugimoto T (1996). Structure and regional distribution of nociceptin/orphanin FQ precursor. Biochem Biophys Res Commun 219, 714-9.

Howells RD, Kilpatrick DL, Bhatt R, Monahan JJ, Poonian M, Udenfriend S (1984). Molecular cloning and sequence determination of rat preproenkephalin cDNA: sensitive probe for studying transcriptional changes in rat tissues. Proc Natl Acad Sci U S A 81, 7651-5.

Hsia JA, Moss J, Hewlett EL, Vaughan M (1984). ADP-ribosylation of adenylate cyclase by pertussis toxin. Effects on inhibitory agonist binding. J Biol Chem 259, 1086-90.

Hughes J (1975). Isolation of an endogenous compound from the brain with pharmacological properties similar to morphine. Brain Res 88, 295-308.

Hughes J, Smith TW, Kosterlitz HW, Fothergill LA, Morgan BA, Morris HR (1975). Identification of two related pentapeptides from the brain with potent opiate agonist activity. Nature 258(5536), 577-80.

I

Ikeda K, Kobayashi K, Kobayashi T, Ichikawa T, Kumanishi T, Kishida H, et al. (1997). Functional coupling of the nociceptin/orphanin FQ receptor with the G-protein-activated K+ (GIRK) channel. Brain Res Mol Brain Res 45, 117-26.

Ikeda K, Kobayashi T, Ichikawa T, Usui H, Kumanishi T (1995). Functional couplings of the delta- and the kappa-opioid receptors with the G-protein-activated K+ channel. Biochem Biophys Res Commun 208, 302-8.

Ito J, Matsuoka I, Sasa M, Fujimoto S, Takaori S (1981). Electrophysiologic evidence for involvement of acetylcholine as a neurotransmitter in the lateral vestibular nucleus. Otolaryngol Head Neck Surg 89, 1025-9.

Ito J, Matsuoka I, Sasa M, Takaori S (1985). Commissural and ipsilateral internuclear connection of vestibular nuclear complex of the cat. Brain Res 341, 73-81.

Ito M, Udo M, Mano N, Kawai N (1970). Synaptic action of the fastigiobulbar impulses upon neurones in the medullary reticular formation and vestibular nuclei. Exp Brain Res 11, 29-47.

Iwase M, Homma I, Shioda S, Nakai Y (1993). Histamine immunoreactive neurons in the brain stem of the rabbit. Brain Res Bull 32, 267-72.

J

James IF and Goldstein A (1984). Site-directed alkylation of multiple opioid receptors. I. Binding selectivity. Mol Pharmacol 25, 337-342.

Janigro D, Gasparini S, D'Ambrosio R, McKhann G, 2nd, DiFrancesco D (1997). Reduction of K+ uptake in glia prevents long-term depression maintenance and causes epileptiform activity. J Neurosci 17, 2813-24.

Johnston AR, Dutia MB (1996). Postnatal development of spontaneous tonic activity in mouse medial vestibular nucleus neurones. Neurosci Lett 219, 17-20.

Johnston AR, MacLeod NK, Dutia MB (1994). Ionic conductances contributing to spike repolarization and after- potentials in rat medial vestibular nucleus neurones. J Physiol (Lond) 481, 61-77.

Johnston AR, Murnion B, McQueen DS, Dutia MB (1993). Excitation and inhibition of rat medial vestibular nucleus neurones by 5-hydroxytryptamine. Exp Brain Res 93, 293-8.

Jonas EA, Kaczmarek LK (1996). Regulation of potassium channels by protein kinases. Curr Opin Neurobiol 6, 318-23.

Jones GM, Milsum JH (1970). Characteristics of neural transmission from the semicircular canal to the vestibular nuclei of cats. J Physiol (Lond) 209, 295-316.

K

Kakidani H, Furutani Y, Takahashi H, Noda M, Morimoto Y, Hirose T, et al. (1982). Cloning and sequence analysis of cDNA for porcine beta-neo- endorphin/dynorphin precursor. Nature 298, 245-9.

Kaneko S, Nakamura S, Adachi K, Akaike A, Satoh M (1994). Mobilization of intracellular Ca2+ and stimulation of cyclic AMP production by kappa opioid receptors expressed in Xenopus oocytes. Brain Res Mol Brain Res 27, 258-64.

Kangawa K, Minamino N, Chino N, Sakakibara S, Matsuo H (1981). The complete amino acid sequence of alpha-neo-endorphin. Biochem Biophys Res Commun 99, 871-8.

Kasahara M, Uchino Y (1974). Bilateral semicircular canal inputs to neurons in cat vestibular nuclei. Exp Brain Res 20, 285-96.

Kaufman GD, Anderson JH, Beitz AJ (1992). Fos-defined activity in rat brainstem following centripetal acceleration. J Neurosci 12, 4489-500.

Kawabata A, Sasa M, Ujihara H, Takaori S (1990). Inhibition by enkephalin of medial vestibular nucleus neurons responding to horizontal pendular rotation. Life Sci 47, 1355-63.

Kawasaki T, Sato Y (1981). Afferent projections to the caudal part of the dorsal nucleus of the raphe in cats. Brain Res 211, 439-44.

Khachaturian H, Lewis ME, Schafer MK, Watson SJ (1985). Anatomy of the CNS opioid systems. Trends Neurosci. 8, 111-112.

Khachaturian H, Watson SJ, Lewis ME, Coy D, Goldstein A, Akil H (1982). Dynorphin immunocytochemistry in the rat central nervous system. Peptides 3, 941-54.

Kieffer BL, Befort K, Gaveriaux-Ruff C, Hirth CG (1992). The delta-opioid receptor: isolation of a cDNA by expression cloning and pharmacological characterization. Proc Natl Acad Sci U S A 89, 12048-52.

Kieffer BL, Befort K, Gaveriaux-Ruff C, Hirth CG (1994). The delta-opioid receptor: isolation of a cDNA by expression cloning and pharmacological characterization. Proc Natl Acad Sci U S A 91, 1193.

Kilpatrick DL, Taniguchi T, Jones BN, Stern AS, Shively JE, Hullihan J, et al. (1981). A highly potent 3200-dalton adrenal opioid peptide that contains both a [Met]- and [Leu]enkephalin sequence. Proc Natl Acad Sci U S A 78, 3265-8.

Kilpatrick DL, Wahlstrom A, Lahm HW, Blacher R, Udenfriend S (1982). Rimorphin, a unique, naturally occurring [Leu]enkephalin-containing peptide found in association with dynorphin and alpha-neo-endorphin. Proc Natl Acad Sci U S A 79, 6480-3.

Kinney GA, Peterson BW, Slater NT (1994). The synaptic activation of N-methyl-D-aspartate receptors in the rat medial vestibular nucleus. J Neurophysiol 72, 1588-95.

Kirsten EB, Sharma JN (1976). Microiontophoresis of acetylcholine, histamine and their antagonists on neurones in the medial and lateral vestibular nuclei of the cat. Neuropharmacology 15, 743-53.

Kitahara T, Saika T, Takeda N, Kiyama H, Kubo T (1995). Changes in Fos and Jun expression in the rat brainstem in the process of vestibular compensation. Acta Otolaryngol Suppl (Stockh) 520, 401-4.

Kitahara T, Takeda N, Saika T, Kubo T, Kiyama H (1997). Role of the flocculus in the development of vestibular compensation: immunohistochemical studies with retrograde tracing and flocculectomy using Fos expression as a marker in the rat brainstem. Neuroscience 76, 571-80.

Kjerulf TD, Loeser JD (1973). Neuronal hyperactivity following deafferentation of the lateral cuneate nucleus. Exp Neurol 39, 70-85.

Knoflach F, Reinscheid RK, Civelli O, Kemp JA (1996). Modulation of voltage-gated calcium channels by orphanin FQ in freshly dissociated hippocampal neurons. J Neurosci 16, 6657-64.

Knopfel T (1987). Evidence for N-methyl-D-aspartic acid receptor-mediated modulation of the commissural input to central vestibular neurons of the frog. Brain Res 426, 212-24.

Konkoy CS, Childers SR (1989). Dynorphin-selective inhibition of adenylyl cyclase in guinea pig cerebellum membranes. Mol Pharmacol 36, 627-33.

Korte GE, Friedrich VL, Jr. (1979). The fine structure of the feline superior vestibular nucleus: identification and synaptology of the primary vestibular afferents. Brain Res 176, 3-32.

Kotchabhakdi N, Walberg F (1978). Cerebellar afferent projections from the vestibular nuclei in the cat: an experimental study with the method of retrograde axonal transport of horseradish peroxidase. Exp Brain Res 31, 591-604.

Kovoor A, Henry DJ, Chavkin C (1995). Agonist-induced desensitization of the mu opioid receptor-coupled potassium channel (GIRK1). J Biol Chem 270, 589-95.

Kunkel AW, Dieringer N (1994). Morphological and electrophysiological consequences of unilateral pre- versus postganglionic vestibular lesions in the frog. J Comp Physiol [A] 174, 621-32.

L

Lachowicz JE, Shen Y, Monsma FJ, Jr., Sibley DR (1995). Molecular cloning of a novel G protein-coupled receptor related to the opiate receptor family. J Neurochem 64, 34-40.

Ladpli R, Brodal A (1968). Experimental studies of commissural and reticular formation projections from the vestibular nuclei in the cat. Brain Res 8, 65-96.

Lahti RA, Von Voigtlander PF and Barsuhn C (1982) Properties of a selective kappa agonist, U50 488H. Life Sci 31, 2257-2260.

Lahti RA, Mickelson MM, McCall JM, Von Voigtlander PF (1985). [3H]U-69593 a highly selective ligand for the opioid kappa receptor. Eur J Pharmacol 109, 281-4.

Lai CC, Wu SY, Dun SL, Dun NJ (1997). Nociceptin-like immunoreactivity in the rat dorsal horn and inhibition of substantia gelatinosa neurons. Neuroscience 81, 887-91.

Langer T, Fuchs AF, Scudder CA, Chubb MC (1985). Afferents to the flocculus of the cerebellum in the rhesus macaque as revealed by retrograde transport of horseradish peroxidase. J Comp Neurol 235, 1-25.

Lannou J, Precht W, Cazin L (1983). Functional development of the central vestibular system. In: Romand R (ed) Development of the auditory and vestibular system. Academic press, London, pp 463-478.

Lantos TA, Gorcs TJ, Palkovits M (1995). Immunohistochemical mapping of neuropeptides in the premamillary region of the hypothalamus in rats. Brain Res Brain Res Rev 20, 209-49.

Lapeyre PN, De Waele C (1995). Glycinergic inhibition of spontaneously active guinea-pig medial vestibular nucleus neurons in vitro. Neurosci Lett 188, 155-8.

Lee K, Nicholson JR, McKnight AT (1997). Nociceptin hyperpolarises neurones in the rat ventromedial hypothalamus. Neurosci Lett 239, 37-40.

Lewis ME, Khachaturian H, Watson SJ (1983). Comparative distribution of opiate receptors and three opioid peptide neuronal systems in rhesus monkey central nervous system. Life Sci 33, 239-42.

Lewis MR, Phelan KD, Shinnick-Gallagher P, Gallagher JP (1989). Primary afferent excitatory transmission recorded intracellularly in vitro from rat medial vestibular neurons. Synapse 3, 149-53.

Li CH, Chung D, Doneen BA (1976). Isolation, characterization and opiate activity of beta-endorphin from human pituitary glands. Biochem Biophys Res Commun 72, 1542-7.

Li H, Godfrey DA, Rubin AM (1994). Quantitative distribution of amino acids in the rat vestibular nuclei. J Vestib Res 4, 437-52.

Li S, Zhu J, Chen C, Chen YW, Deriel JK, Ashby B, et al. (1993). Molecular cloning and expression of a rat kappa opioid receptor. Biochem J 295, 629-33.

Lin Y, Carpenter DO (1993). Medial vestibular neurons are endogenous pacemakers whose discharge is modulated by neurotransmitters. Cell Mol Neurobiol 13, 601-13.

Lin Y, Carpenter DO (1994). Direct excitatory opiate effects mediated by non-synaptic actions on rat medial vestibular neurons. Eur J Pharmacol 262, 99-106.

Lisberger SG, Pavelko TA, Bronte-Stewart HM, Stone LS (1994). Neural basis for motor learning in the vestibuloocular reflex of primates. II. Changes in the responses of horizontal gaze velocity Purkinje cells in the cerebellar flocculus and ventral paraflocculus. J Neurophysiol 72, 954-73.

Llinas R, Sugimori M (1980). Electrophysiological properties of in vitro Purkinje cell somata in mammalian cerebellar slices. J Physiol (Lond) 305, 171-95.

Llinas RR (1988). The intrinsic electrophysiological properties of mammalian neurons: insights into central nervous system function. Science 242, 1654-64.

Loh HH, Smith AP (1990). Molecular characterization of opioid receptors. Annu Rev Pharmacol Toxicol 30, 123-47.

Loh YP, Brownstein MJ, Gainer H (1984). Proteolysis in neuropeptide processing and other neural functions. Annu Rev Neurosci 7, 189-222.

Lord JA, Waterfield AA, Hughes J, Kosterlitz HW (1977). Endogenous opioid peptides: multiple agonists and receptors. Nature 267, 495-9.

Lorente de Nó R (1933). Vestibulo-ocular reflex arc. Arch Neurol Psychiat 30, 245-291

Louie AK, Bass ES, Zhan J, Law PY, Loh HH (1990). Attenuation of opioid receptor activity by phorbol esters in neuroblastoma x glioma NG108-15 hybrid cells. J Pharmacol Exp Ther 253, 401-7.

Lu YF, Hattori Y, Moriwaki A, Hayashi Y, Hori Y (1995). Inhibition of neurons in the rat medial amygdaloid nucleus in vitro by somatostatin. Can J Physiol Pharmacol 73, 670-4.

Lutz RA, Pfister HP (1992). Opioid receptors and their pharmacological profiles. J Recept Res 12, 267-86.

Luyten WH, Sharp FR, Ryan AF (1986). Regional differences of brain glucose metabolic compensation after unilateral labyrinthectomy in rats: a [14C]2-deoxyglucose study. Brain Res 373, 68-80.

M

Macdonald RL, Werz MA (1986). Dynorphin A decreases voltage-dependent calcium conductance of mouse dorsal root ganglion neurones. J Physiol (Lond) 377, 237-49.

Madison DV, Nicoll RA (1988). Enkephalin hyperpolarizes interneurones in the rat hippocampus. J Physiol (Lond) 398, 123-30.

Mains RE, Eipper BA, Ling N (1977). Common precursor to corticotropins and endorphins. Proc Natl Acad Sci U S A 74, 3014-8.

Maioli C, Precht W (1985). On the role of vestibulo-ocular reflex plasticity in recovery after unilateral peripheral vestibular lesions. Exp Brain Res 59, 267-72.

Maioli C, Precht W, Ried S (1983). Short- and long-term modifications of vestibulo-ocular response dynamics following unilateral vestibular nerve lesions in the cat. Exp Brain Res 50, 259-74.

Mansour A, Fox CA, Akil H, Watson SJ (1995). Opioid-receptor mRNA expression in the rat CNS: anatomical and functional implications. Trends Neurosci 18, 22-9.

Mansour A, Fox CA, Burke S, Meng F, Thompson RC, Akil H, et al. (1994). Mu, delta, and kappa opioid receptor mRNA expression in the rat CNS: an in situ hybridization study. J Comp Neurol 350, 412-38.

Mansour A, Khachaturian H, Lewis ME, Akil H, Watson SJ (1987). Autoradiographic differentiation of mu, delta, and kappa opioid receptors in the rat forebrain and midbrain. J Neurosci 7, 2445-64.

Mansour A, Khachaturian H, Lewis ME, Akil H, Watson SJ (1988). Anatomy of CNS opioid receptors. Trends Neurosci 11, 308-14.

Markham CH (1968). Midbrain and contralateral labyrinth influences on brain stem vestibular neurons in the cat. Brain Res 9, 312-33.

Markham CH, Yagi T, Curthoys IS (1977). The contribution of the contralateral labyrinth to second order vestibular neuronal activity in the cat. Brain Res 138, 99-109.

Martin WR, Eades CG, Thompson JA, Huppler RE, Gilbert PE (1976). The effects of morphine- and nalorphine- like drugs in the nondependent and morphine-dependent chronic spinal dog. J Pharmacol Exp Ther 197, 517-32.

Matthes H, Seward EP, Kieffer B, North RA (1996). Functional selectivity of orphanin FQ for its receptor coexpressed with potassium channel subunits in Xenopus laevis oocytes. Mol Pharmacol 50, 447-50.

McCabe BF, Ryu JH (1969). Experiments on vestibular compensation. Laryngoscope 79, 1728-36.

McCabe BF, Ryu JH, Sekitani T (1972). Further experiments on vestibular compensation. Laryngoscope 82, 381-96.

McDowell J, Kitchen I (1986). Ontogenesis of delta-opioid receptors in rat brain using [3H][D-Pen2,D- Pen5]enkephalin as a binding ligand. Eur J Pharmacol 128, 287-9.

McFadzean I (1988). The ionic mechanisms underlying opioid actions. Neuropeptides 11, 173-80.

McLean S, Rothman RB, Herkenham M (1986). Autoradiographic localization of mu- and delta-opiate receptors in the forebrain of the rat. Brain Res 378, 49-60.

Meng F, Xie GX, Thompson RC, Mansour A, Goldstein A, Watson SJ, et al. (1993). Cloning and pharmacological characterization of a rat kappa opioid receptor. Proc Natl Acad Sci U S A 90, 9954-8.

Merchenthaler I, Maderdrut JL, Altschuler RA, Petrusz P (1986). Immunocytochemical localization of proenkephalin-derived peptides in the central nervous system of the rat. Neuroscience 17, 325-48.

Meunier JC, Mollereau C, Toll L, Suaudeau C, Moisand C, Alvinerie P, et al. (1995). Isolation and structure of the endogenous agonist of opioid receptor- like ORL1 receptor . Nature 377, 532-5.

Min BH, Augustin LB, Felsheim RF, Fuchs JA, Loh HH (1994). Genomic structure analysis of promoter sequence of a mouse mu opioid receptor gene. Proc Natl Acad Sci U S A 91, 9081-5.

Minami M, Onogi T, Toya T, Katao Y, Hosoi Y, Maekawa K, et al. (1994). Molecular cloning and in situ hybridization histochemistry for rat mu- opioid receptor. Neurosci Res 18, 315-22.

Minami M, Satoh M (1995). Molecular biology of the opioid receptors: structures, functions and distributions. Neurosci Res 23, 121-45.

Minami M, Toya T, Katao Y, Maekawa K, Nakamura S, Onogi T, et al. (1993). Cloning and expression of a cDNA for the rat kappa-opioid receptor. FEBS Lett 329, 291-5.

Minamino N, Kangawa K, Chino N, Sakakibara S, Matsuo H (1981). Beta-neo-endorphin, a new hypothalamic "big" Leu-enkephalin of porcine origin: its purification and the complete amino acid sequence. Biochem Biophys Res Commun 99, 864-70.

Minamino N, Kangawa K, Fukuda A, Matsuo H, Iagarashi M (1980). A new opioid octapeptide related to dynorphin from porcine hypothalamus. Biochem Biophys Res Commun 95, 1475-81.

Mizuno K, Minamino N, Kangawa K, Matsuo H (1980a). A new endogenous opioid peptide from bovine adrenal medulla: isolation and amino acid sequence of a dodecapeptide (BAM-12P). Biochem Biophys Res Commun 95, 1482-8.

Mizuno K, Minamino N, Kangawa K, Matsuo H (1980b). A new family of endogenous "big" Met-enkephalins from bovine adrenal medulla: purification and structure of docosa- (BAM-22P) and eicosapeptide (BAM-20P) with very potent opiate activity. Biochem Biophys Res Commun 97, 1283-90.

Mogil JS, Grisel JE, Reinscheid RK, Civelli O, Belknap JK, Grandy DK (1996a). Orphanin FQ is a functional anti-opioid peptide. Neuroscience 75, 333-7.

Mogil JS, Grisel JE, Zhangs G, Belknap JK, Grandy DK (1996b). Functional antagonism of mu-, delta- and kappa-opioid antinociception by orphanin FQ. Neurosci Lett 214, 131-4.

Mollereau C, Parmentier M, Mailleux P, Butour JL, Moisand C, Chalon P, et al. (1994). ORL1, a novel member of the opioid receptor family. Cloning, functional expression and localization. FEBS Lett 341, 33-8.

Mollereau C, Simons MJ, Soularue P, Liners F, Vassart G, Meunier JC, et al. (1996). Structure, tissue distribution, and chromosomal localization of the prepronociceptin gene. Proc Natl Acad Sci U S A 93, 8666-70.

Monteillet-Agius G, Fein J, Anton B, Evans CJ (1998). ORL-1 and mu opioid receptor antisera label different fibers in areas involved in pain processing [In Process Citation]. J Comp Neurol 399, 373-83.

Morita K, North RA (1981). Clonidine activates membrane potassium conductance in myenteric neurones. Br J Pharmacol 74, 419-28.

Mosberg HI, Hurst R, Hruby VJ, Gee K, Yamamura HI, Galligan JJ, et al. (1983). Bis-penicillamine enkephalins possess highly improved specificity toward delta opioid receptors. Proc Natl Acad Sci U S A 80, 5871-4.

Murphy NP, Ly HT, Maidment NT (1996). Intracerebroventricular orphanin FQ/nociceptin suppresses dopamine release in the nucleus accumbens of anaesthetized rats. Neuroscience 75, 1-4.

N

Nakanishi S, Inoue A, Kita T, Nakamura M, Chang AC, Cohen SN, et al. (1979). Nucleotide sequence of cloned cDNA for bovine corticotropin-beta- lipotropin precursor. Nature 278, 423-7.

Negri L, Severini C, Lattanzi R, Potenza RL, Melchiorri P (1997). Postnatal development of delta-opioid receptor subtypes in mice. Br J Pharmacol 120, 989-94.

Nelson TJ, Alkon DL (1991). GTP-binding proteins and potassium channels involved in synaptic plasticity and learning. Mol Neurobiol 5, 315-28.

Newlands SD, Perachio AA (1990a). Compensation of horizontal canal related activity in the medial vestibular nucleus following unilateral labyrinth ablation in the decerebrate gerbil. I. Type I neurons. Exp Brain Res 82, 359-72.

Newlands SD, Perachio AA (1990b). Compensation of horizontal canal related activity in the medial vestibular nucleus following unilateral labyrinth ablation in the decerebrate gerbil. II. Type II neurons. Exp Brain Res 82, 373-83.

Nicol B, Lambert DG, Rowbotham DJ, Smart D, McKnight AT (1996). Nociceptin induced inhibition of K+ evoked glutamate release from rat cerebrocortical slices. Br J Pharmacol 119, 1081-3.

Nishi M, Takeshima H, Fukuda K, Kato S, Mori K (1993). cDNA cloning and pharmacological characterization of an opioid receptor with high affinities for kappa-subtype-selective ligands. FEBS Lett 330, 77-80.

Nishi M, Takeshima H, Mori M, Nakagawara K, Takeuchi T (1994). Structure and chromosomal mapping of genes for the mouse kappa-opioid receptor and an opioid receptor homologue (MOR-C). Biochem Biophys Res Commun 205, 1353-7.

Noda M, Furutani Y, Takahashi H, Toyosato M, Hirose T, Inayama S, et al. (1982a). Cloning and sequence analysis of cDNA for bovine adrenal preproenkephalin. Nature 295, 202-6.

Noda M, Teranishi Y, Takahashi H, Toyosato M, Notake M, Nakanishi S, et al. (1982b). Isolation and structural organization of the human preproenkephalin gene. Nature 297, 431-4.

Nomura I, Senba E, Kubo T, Shiraishi T, Matsunaga T, Tohyama M, et al. (1984). Neuropeptides and gamma-aminobutyric acid in the vestibular nuclei of the rat: an immunohistochemical analysis. I. Distribution. Brain Res 311, 109-18.

North RA (1986). Opioid receptor types and membrane ion channels. Trends Neusosci. 9, 114-117.

North RA (1993). Opioid actions on membrane ion channels. In: Opioid I, Vol. 104, Hand Book of Experimental Pharmacology, pp. 773-797, Herz, A. (ed.) Spinger-Verlag, Berlin, Heidelberg, New York, London, Paris, Tokyo, Hong Kong, Barcelona, Budapest.

North RA, Williams JT (1985). On the potassium conductance increased by opioids in rat locus coeruleus neurones. J Physiol (Lond) 364, 265-80.

North RA, Williams JT, Surprenant A, Christie MJ (1987). Mu and delta receptors belong to a family of receptors that are coupled to potassium channels. Proc Natl Acad Sci U S A 84, 5487-91.

Nothacker HP, Reinscheid RK, Mansour A, Henningsen RA, Ardati A, Monsma FJ, Jr., et al. (1996). Primary structure and tissue distribution of the orphanin FQ precursor. Proc Natl Acad Sci U S A 93, 8677-82.

O

Okuda-Ashitaka E, Tachibana S, Houtani T, Minami T, Masu Y, Nishi M, et al. (1996). Identification and characterization of an endogenous ligand for opioid receptor homologue ROR-C: its involvement in allodynic response to innocuous stimulus. Brain Res Mol Brain Res 43, 96-104.

P

Pan YX, Xu J, Pasternak GW (1996). Cloning and expression of a cDNA encoding a mouse brain orphanin FQ/nociceptin precursor. Biochem J 315, 11-3.

Pan ZZ, Williams JT, Osborne PB (1990). Opioid actions on single nucleus raphe magnus neurons from rat and guinea-pig in vitro. J Physiol (Lond) 427, 519-32.

Panula P, Pirvola U, Auvinen S, Airaksinen MS (1989). Histamine-immunoreactive nerve fibers in the rat brain. Neuroscience 28, 585-610.

Patel HJ, Giembycz MA, Spicuzza L, Barnes PJ, Belvisi MG (1997). Naloxone-insensitive inhibition of acetylcholine release from parasympathetic nerves innervating guinea-pig trachea by the novel opioid, nociceptin. Br J Pharmacol 120, 735-6.

Patrickson JW, Bryant HJ, Kaderkaro M, Kutyna FA (1985). A quantitative [14C]-2-deoxy-D-glucose study of brain stem nuclei during horizontal nystagmus induced by lesioning the lateral crista ampullaris of the rat. Exp Brain Res 60, 227-34.

Pearson J, Brandeis L, Simon E, Hiller J (1980). Radioautography of binding of tritiated diprenorphine to opiate receptors in the rat. Life Sci 26, 1047-52.

Pepper CM, Henderson G (1980). Opiates and opioid peptides hyperpolarize locus coeruleus neurons in vitro. Science 209, 394-5.

Pert CB, Pasternak G, Snyder SH (1973). Opiate agonists and antagonists discriminated by receptor binding in brain. Science 182, 1359-61.

Peterson BW (1970). Distribution of neural responses to tilting within vestibular nuclei of the cat. J Neurophysiol 33, 750-67.

Peterson BW, Maunz RA, Fukushima K (1978). Properties of a new vestibulospinal projection, the caudal vestibulospinal tract. Exp Brain Res 32, 287-92.

Pettorossi VE, Della Torre G, Grassi S, Zampolini M, Capocchi G, Errico P (1992). Role of NMDA receptors in the compensation of ocular nystagmus induced by hemilabyrinthectomy in the guinea pig. Arch Ital Biol 130, 303-13.

Phelan KD, Gallagher JP (1992). Direct muscarinic and nicotinic receptor-mediated excitation of rat medial vestibular nucleus neurons in vitro. Synapse 10, 349-58.

Phelan KD, Nakamura J, Gallagher JP (1990). Histamine depolarizes rat medial vestibular nucleus neurons recorded intracellularly in vitro. Neurosci Lett 109, 287-92.

Piguet P, North RA (1993). Opioid actions at mu and delta receptors in the rat dentate gyrus in vitro. J Pharmacol Exp Ther 266, 1139-49.

Pompeiano O, Mergner T, Corvaja N (1978). Commissural, perihypoglossal and reticular afferent projections to the vestibular nuclei in the cat. An experimental anatomical study with the method of the retrograde transport of horseradish peroxidase. Arch Ital Biol 116, 130-72.

Pompeiano O, Walberg F (1957). Descending connections to the vestibular nuclei: An experimental study in the cat. J Comp Neurol 108, 465-504.

Portoghese PS (1965). A new concept on the mode of interaction of narcotic analgesics with receptors. J Med Chem 8, 609-16.

Precht W, Dieringer N (1985). Neuronal events paralleling functional recovery (compensation) following peripheral vestibular lesions. Rev Oculomot Res 1, 251-68.

Precht W, Schwindt PC, Baker R (1973). Removal of vestibular commissural inhibition by antagonists of GABA and glycine. Brain Res 62, 222-6.

Precht W, Shimazu H (1965). Functional connections of tonic and kinetic vestibular neurons with primary vestibular afferents. J Neurophysiol 28, 1014-28.

Precht W, Shimazu H, Markham CH (1966). A mechanism of central compensation of vestibular function following hemilabyrinthectomy. J Neurophysiol 29, 996-1010.

Putkonen PT, Courjon JH, Jeannerod M (1977). Compensation of postural effects of hemilabyrinthectomy in the cat. A sensory substitution process? Exp Brain Res 28, 249-57.

Q

Quirion R, Chicheportiche R, Contreras PC, Johnson KM, Lodge D, Tam SW, et al. (1987). Classification and nomenclature of phencyclidine and sigma receptor sites. Trends Neurosci. 10, 444-446.

Quirion R, Pert CB (1981). Dynorphins: similar relative potencies on mu, delta- and kappa-opiate receptors. Eur J Pharmacol 76, 467-8.

R

Ramón y Cajal (1909). Histologie du système nerveux de l'homme et des vertèbrès. Maloine, Paris

Raymond J, Dememes D, Nieoullon A (1988). Neurotransmitters in vestibular pathways. Prog Brain Res 76, 29-43.

Raymond J, Ez-Zaher L, Dememes LL, Lacour M (1991). Quantification of synaptic density changes in the medial vestibular nucleus of the cat following vestibular neurectomy. Restorative. Neurological. Neuroscience 3, 197-203.

Raymond J, Nieoullon A, Dememes D, Sans A (1984). Evidence for glutamate as a neurotransmitter in the cat vestibular nerve: radioautographic and biochemical studies. Exp Brain Res 56, 523-31.

Reinscheid RK, Nothacker HP, Bourson A, Ardati A, Henningsen RA, Bunzow JR, et al. (1995). Orphanin FQ: a neuropeptide that activates an opioidlike G protein-coupled receptor. Science 270, 792-4.

Ried S, Maioli C, Precht W (1984). Vestibular nuclear neuron activity in chronically hemilabyrinthectomized cats. Acta Otolaryngol (Stockh) 98, 1-13.

Riedl M, Shuster S, Vulchanova L, Wang J, Loh HH, Elde R (1996). Orphanin FQ/nociceptin-immunoreactive nerve fibers parallel those containing endogenous opioids in rat spinal cord. Neuroreport 7, 1369-72.

Ris L, Capron B, de Waele C, Vidal PP, Godaux E (1997). Dissociations between behavioural recovery and restoration of vestibular activity in the unilabyrinthectomized guinea-pig. J Physiol (Lond) 500, 509-22.

Ris L, de Waele C, Serafin M, Vidal PP, Godaux E (1995). Neuronal activity in the ipsilateral vestibular nucleus following unilateral labyrinthectomy in the alert guinea pig. J Neurophysiol 74, 2087-99.

Ris L, Godaux E (1998). Spike discharge regularity of vestibular neurons in labyrinthectomized guinea pigs. Neurosci Lett 253, 131-4.

Roberts JL, Herbert E (1977). Characterization of a common precursor to corticotropin and beta- lipotropin: identification of beta-lipotropin peptides and their arrangement relative to corticotropin in the precursor synthesized in a cell-free system. Proc Natl Acad Sci U S A 74, 5300-4.

Rossier J (1981). Enkephalin biosynthesis, the search for a common precursor. Trends Neurosci. 4, 94-97.

Rubertone JA, Mehler WR, Cox GE (1983). The intrinsic organization of the vestibular complex: evidence for internuclear connectivity. Brain Res 263, 137-41.

S

Saito Y, Maruyama K, Kawano H, Hagino-Yamagishi K, Kawamura K, Saido TC, et al. (1996). Molecular cloning and characterization of a novel form of neuropeptide gene as a developmentally regulated molecule. J Biol Chem 271, 15615-22.

Satayavivad J, Kirsten EB (1977). Iontophoretic studies of histamine and histamine antagonists in the feline vestibular nuclei. Eur J Pharmacol 41, 17-26.

Sato F, Sasaki H, Ishizuka N, Sasaki S, Mannen H (1989). Morphology of single primary vestibular afferents originating from the horizontal semicircular canal in the cat. J Comp Neurol 290, 423-39.

Sato Y, Kanda K, Kawasaki T (1988). Target neurons of floccular middle zone inhibition in medial vestibular nucleus. Brain Res 446, 225-35.

Satoh M, Minami M (1995). Molecular pharmacology of the opioid receptors. Pharmacol Ther 68, 343-64.

Satoh M, Zieglgansberger W, Fries W, Herz A (1974). Opiate agonist-antagonist interaction at cortical neurones of naive and tolerant/dependent rats. Brain Res 82, 378-82.

Schlosser B, Kudernatsch MB, Sutor B, ten Bruggencate G (1995). Delta, mu and kappa opioid receptor agonists inhibit dopamine overflow in rat neostriatal slices. Neurosci Lett 191, 126-30.

Schroeder JE, Fischbach PS, Zheng D, McCleskey EW (1991). Activation of mu opioid receptors inhibits transient high- and low- threshold Ca2+ currents, but spares a sustained current. Neuron 6, 13-20.

Schuerger RJ, Balaban CD (1993). Immunohistochemical demonstration of regionally selective projections from locus coeruleus to the vestibular nuclei in rats. Exp Brain Res 92, 351-9.

Schuligoi R, Amann R, Angelberger P, Peskar BA (1997). Determination of nociceptin-like immunoreactivity in the rat dorsal spinal cord. Neurosci Lett 224, 136-8.

Schulz R, Wuster M, Herz A (1982). Endogenous ligands for kappa-opiate receptors. Peptides 3, 973-6.

Schulz S, Schreff M, Nuss D, Gramsch C, Hollt V (1996). Nociceptin/orphanin FQ and opioid peptides show overlapping distribution but not co-localization in pain-modulatory brain regions. Neuroreport 7, 3021-5.

Seidah NG, Day R, Benjannet S, Rondeau N, Boudreault A, Reudelhuber T, et al. (1992). The prohormone and proprotein processing enzymes PC1 and PC2: structure, selective cleavage of mouse POMC and human renin at pairs of basic residues, cellular expression, tissue distribution, and mRNA regulation. NIDA Res Monogr 126, 132-50.

Serafin M, de Waele C, Khateb A, Vidal PP, Muhlethaler M (1991a). Medial vestibular nucleus in the guinea-pig. I. Intrinsic membrane properties in brainstem slices. Exp Brain Res 84, 417-25.

Serafin M, de Waele C, Khateb A, Vidal PP, Muhlethaler M (1991b). Medial vestibular nucleus in the guinea-pig. II. Ionic basis of the intrinsic membrane properties in brainstem slices. Exp Brain Res 84, 426-33.

Serafin M, Khateb A, de Waele C, Vidal PP, Muhlethaler M (1990). Low threshold calcium spikes in medial vestibular nuclei neurones in vitro: a role in the generation of the vestibular nystagmus quick phase in vivo? Exp Brain Res 82, 187-90.

Serafin M, Khateb A, de Waele C, Vidal PP, Muhlethaler M (1992). Medial vestibular nucleus in the guinea-pig: NMDA-induced oscillations. Exp Brain Res 88, 187-92.

Serafin M, Khateb A, Vibert N, Vidal PP, Muhlethaler M (1993). Medial vestibular nucleus in the guinea-pig: histaminergic receptors. I. An in vitro study. Exp Brain Res 93, 242-8.

Seward E, Hammond C, Henderson G (1991). Mu-opioid-receptor-mediated inhibition of the N-type calcium-channel current. Proc R Soc Lond B Biol Sci 244, 129-35.

Sharma SK, Klee WA, Nirenberg M (1977). Opiate-dependent modulation of adenylate cyclase. Proc Natl Acad Sci U S A 74, 3365-9.

Sharma SK, Nirenberg M, Klee WA (1975). Morphine receptors as regulators of adenylate cyclase activity. Proc Natl Acad Sci U S A 72, 590-4.

Sharpless SK (1975). Supersensitivity-like phenomena in the central nervous system. Fed Proc 34, 1990-7.

Shen KZ, North RA, Surprenant A (1992). Potassium channels opened by noradrenaline and other transmitters in excised membrane patches of guinea-pig submucosal neurones. J Physiol (Lond) 445, 581-99.

Shen KZ, Surprenant A (1990). Mechanisms underlying presynaptic inhibition through alpha 2- adrenoceptors in guinea-pig submucosal neurones. J Physiol (Lond) 431, 609-28.

Shimazu H (1983). Neuronal organization of the premotor system controlling horizontal conjugate eye movements and vestibular nystagmus. Adv Neurol 39, 565-88.

Shimazu H, Precht W (1965). Tonic and kinetic responses of cat's vestibular neurons to horizontal angular acceleration. J Neurophysiol 28, 991-1013.

Shimazu H, Precht W (1966). Inhibition of central vestibular neurons from the contralateral labyrinth and its mediating pathway. J Neurophysiol 29, 467-92.

Shimazu H, Smith CM (1971). Cerebellar and labyrinthine influences on single vestibular neurons identified by natural stimuli. J Neurophysiol 34, 493-508.

Shinoda Y, Yoshida K (1974). Dynamic characteristics of responses to horizontal head angular acceleration in vestibuloocular pathway in the cat. J Neurophysiol 37, 653-73.

Shinoda Y, Yoshida K (1975). Neural pathways from the vestibular labyrinths to the flocculus in the cat. Exp Brain Res 22, 97-111.

Shinoda Y, Sugiuchi Y, Futami T, Ando N, Kawasaki T, Yagi J (1993). Synaptic organization of the vestibulo-collic pathways from six semicircular canals to motoneurons of different neck muscles. Prog Brain Res 97, 201-9

Shook JE, Kazmierski W, Wire WS, Lemcke PK, Hruby VJ, Burks TF (1988). Opioid receptor selectivity of beta-endorphin in vitro and in vivo: mu, delta and epsilon receptors. J Pharmacol Exp Ther 246, 1018-25.

Sim LJ, Xiao R, Childers SR (1996). Identification of opioid receptor-like (ORL1) peptide-stimulated [35S]GTP gamma S binding in rat brain. Neuroreport 7, 729-33.

Simon EJ (1986). Recent studies on opioid receptors: heterogeneity and purification. Ann N Y Acad Sci 463, 31-45.

Simon EJ (1991). Opioid receptors and endogenous opioid peptides. Med Res Rev 11, 357-74.

Simon EJ, Hiller JM, Edelman I (1973). Stereospecific binding of the potent narcotic analgesic (3H) Etorphine to rat-brain homogenate. Proc Natl Acad Sci U S A 70, 1947-9.

Sirkin DW, Precht W, Courjon JH (1984). Initial, rapid phase of recovery from unilateral vestibular lesion in rat not dependent on survival of central portion of vestibular nerve. Brain Res 302, 245-56.

Smith PF, Curthoys IS (1988a). Neuronal activity in the contralateral medial vestibular nucleus of the guinea pig following unilateral labyrinthectomy. Brain Res 444, 295-307.

Smith PF, Curthoys IS (1988b). Neuronal activity in the ipsilateral medial vestibular nucleus of the guinea pig following unilateral labyrinthectomy. Brain Res 444, 308-19.

Smith PF, Curthoys IS (1988c). Recovery of resting activity in the ipsilateral vestibular nucleus following unilateral labyrinthectomy: noncommissural influences. Adv Otorhinolaryngol 42, 177-9.

Smith PF, Curthoys IS (1989). Mechanisms of recovery following unilateral labyrinthectomy: a review. Brain Res Brain Res Rev 14, 155-80.

Smith PF, Darlington CL (1988). The NMDA antagonists MK801 and CPP disrupt compensation for unilateral labyrinthectomy in the guinea pig. Neurosci Lett 94, 309-13.

Smith PF, Darlington CL (1991). Neurochemical mechanisms of recovery from peripheral vestibular lesions (vestibular compensation) [published erratum appears in Brain Res Brain Res Rev 1992 May-Aug;17(2):183]. Brain Res Brain Res Rev 16, 117-33.

Smith PF, Darlington CL (1992). Comparison of the effects of NMDA antagonists on medial vestibular nucleus neurons in brainstem slices from labyrinthine-intact and chronically labyrinthectomized guinea pigs. Brain Res 590, 345-9.

Smith PF, Darlington CL, Curthoys IS (1986a). The effect of visual deprivation on vestibular compensation in the guinea pig. Brain Res 364, 195-8.

Smith PF, Darlington CL, Curthoys IS (1986b). Vestibular compensation without brainstem commissures in the guinea pig. Neurosci Lett 65, 209-13.

Smith PF, Darlington CL, Hubbard JI (1990). Evidence that NMDA receptors contribute to synaptic function in the guinea pig medial vestibular nucleus. Brain Res 513, 149-51.

Smith PF, Darlington CL, Hubbard JI (1991). Evidence for inhibitory amino acid receptors on guinea pig medial vestibular nucleus neurons in vitro. Neurosci Lett 121, 244-6.

Sobko A, Peretz A, Attali B (1998). Constitutive activation of delayed-rectifier potassium channels by a src family tyrosine kinase in Schwann cells. Embo J 17, 4723-34.

Stahl JS, Simpson JI (1995). Dynamics of rabbit vestibular nucleus neurons and the influence of the flocculus. J Neurophysiol 73, 1396-413.

Stein B, Carpenter MB (1967). Central projections of portion of the vestibular ganglia innervating specific parts of the labyrinth in the rhesus monkey. Am. J. Anat. 120, 281-318.

Steinbusch HW (1991). Distribution of histaminergic neurons and fibers in rat brain. Comparison with noradrenergic and serotonergic innervation of the vestibular system. Acta Otolaryngol Suppl 479, 12-23.

Sulaiman MR, Dutia MB (1998). Opioid inhibition of rat medial vestibular nucleus neurones in vitro and its dependence on age. Exp Brain Res 122, 196-202.

Surprenant A, Shen KZ, North RA, Tatsumi H (1990). Inhibition of calcium currents by noradrenaline, somatostatin and opioids in guinea-pig submucosal neurones. J Physiol (Lond) 431, 585-608.

T

Tallent M, Dichter MA, Bell GI, Reisine T (1994). The cloned kappa opioid receptor couples to an N-type calcium current in undifferentiated PC-12 cells. Neuroscience 63, 1033-40.

Tarlov E (1969). The rostral projections of the primate vestibular nuclei: an experimental study in macaque, baboon and chimpanzee. J Comp Neurol 135, 27-56.

Tarlov E (1970a). Organization of vestibulo-oculomotor projections in the cat. Brain Res 20, 159-79.

Tarlov E (1970b). Vestibulo-oculomotor organization: anatomical basis for certain vestibular influences on coordinated eye movements. Trans Am Neurol Assoc 95, 320-2.

Tarlov E, Tarlov SR (1971). The representation of extraocular muscles in the oculomotor nuclei: experimental studies in the cat. Brain Res 34, 36-52.

Tatsumi H, Costa M, Schimerlik M, North RA (1990). Potassium conductance increased by noradrenaline, opioids, somatostatin, and G-proteins: whole-cell recording from guinea pig submucous neurons. J Neurosci 10, 1675-82.

Tempel A, Zukin RS (1987). Neuroanatomical patterns of the mu, delta, and kappa opioid receptors of rat brain as determined by quantitative in vitro autoradiography. Proc Natl Acad Sci U S A 84, 4308-12.

Terenius L (1973). Stereospecific interaction between narcotic analgesics and a synaptic plasm a membrane fraction of rat cerebral cortex. Acta Pharmacol Toxicol 32, 317-20.

Terenius L, Wahlstrom A (1975). Search for an endogenous ligand for the opiate receptor. Acta Physiol Scand 94(1), 74-81.

The nuclei of origin of brainstem enkephalin and cholecystokinin projections to the spinal trigeminal nucleus of the rat. Neuroscience 20, 409-25.

Thompson RC, Mansour A, Akil H, Watson SJ (1993). Cloning and pharmacological characterization of a rat mu opioid receptor. Neuron 11, 903-13.

Tighilet B, Lacour M (1996). Distribution of histaminergic axonal fibres in the vestibular nuclei of the cat. Neuroreport 7, 873-8.

Tighilet B, Lacour M (1997). Histamine immunoreactivity changes in vestibular-lesioned and histaminergic-treated cats. Eur J Pharmacol 330, 65-77.

Traber J, Fischer K, Latzin S, Hamprecht B (1975). Morphine antagonises action of prostaglandin in neuroblastoma and neuroblastoma times glioma hybrid cells. Nature 253, 120-2.

Travagli RA, Dunwiddie TV, Williams JT (1995). Opioid inhibition in locus coeruleus. J Neurophysiol 74, 518-28.

Traynor JR, Elliott J (1993). delta-Opioid receptor subtypes and cross-talk with mu-receptors. Trends Pharmacol Sci 14, 84-6.

U

Ueda H, Nozaki M, Satoh M (1991). Multiple opioid receptors and GTP-binding proteins. Comp Biochem Physiol C 98, 157-69.

Ujihara H, Akaike A, Sasa M, Takaori S (1988). Electrophysiological evidence for cholinoceptive neurons in the medial vestibular nucleus: studies on rat brain stem in vitro. Neurosci Lett 93, 231-5.

Ujihara H, Akaike A, Sasa M, Takaori S (1989). Muscarinic regulation of spontaneously active medial vestibular neurons in vitro. Neurosci Lett 106, 205-10.

Ulas J, Monaghan DT, Cotman CW (1990). Plastic response of hippocampal excitatory amino acid receptors to deafferentation and reinnervation. Neuroscience 34, 9-17.

Umetani T (1992). Efferent projections from the flocculus in the albino rat as revealed by an autoradiographic orthograde tracing method. Brain Res 586, 91-103.

V

Vaughan CW, Christie MJ (1996). Increase by the ORL1 receptor (opioid receptor-like1) ligand, nociceptin, of inwardly rectifying K conductance in dorsal raphe nucleus neurones. Br J Pharmacol 117, 1609-11.

Vaughan CW, Christie MJ (1997). Presynaptic inhibitory action of opioids on synaptic transmission in the rat periaqueductal grey in vitro. J Physiol (Lond) 498, 463-72.

Vaughan CW, Ingram SL, Christie MJ (1997). Actions of the ORL1 receptor ligand nociceptin on membrane properties of rat periaqueductal gray neurons in vitro. J Neurosci 17, 996-1003.

Vibert N, De Waele C, Serafin M, Babalian A, Muhlethaler M, Vidal PP (1997). The vestibular system as a model of sensorimotor transformations. A combined in vivo and in vitro approach to study the cellular mechanisms of gaze and posture stabilization in mammals. Prog Neurobiol 51, 243-86.

Vibert N, Serafin M, Crambes O, Vidal PP, Muhlethaler M (1995a). Dopaminergic agonists have both presynaptic and postsynaptic effects on the guinea-pig's medial vestibular nucleus neurons. Eur J Neurosci 7, 555-62.

Vibert N, Serafin M, Khateb A, Vidal PP, Muhlethaler M (1992). Effects of amino acids on medial vestibular neurones in guinea pig. Soc. Neurosci. *Abstr* 18, 509.

Vibert N, Serafin M, Vidal PP, Muhlethaler M (1995b). Direct and indirect effects of muscimol on medial vestibular nucleus neurones in guinea-pig brainstem slices. Exp Brain Res 104, 351-6.

Vibert N, Serafin M, Vidal PP, Muhlethaler M (1995c). Effects of baclofen on medial vestibular nucleus neurones in guinea-pig brainstem slices. Neurosci Lett 183, 193-7.

Von Kugelgen I, Illes P, Wolf D, Starke K (1985). Presynaptic inhibitory opioid delta- and kappa-receptors in a branch of the rabbit ileocolic artery. Eur J Pharmacol 118, 97-105.

W

Wagner EJ, Ronnekleiv OK, Grandy DK, Kelly MJ (1998). The peptide orphanin FQ inhibits beta-endorphin neurons and neurosecretory cells in the hypothalamic arcuate nucleus by activating an inwardly-rectifying K+ conductance. Neuroendocrinology 67, 73-82.

Wall PD, Devor M (1981). The effect of peripheral nerve injury on dorsal root potentials and on transmission of afferent signals into the spinal cord. Brain Res 209, 95-111.

Wamsley JK (1983). Opioid receptors: autoradiography. Pharmacol Rev 35, 69-83.

Wang JB, Imai Y, Eppler CM, Gregor P, Spivak CE, Uhl GR (1993). mu opiate receptor: cDNA cloning and expression. Proc Natl Acad Sci U S A 90, 10230-4.

Wang JB, Johnson PS, Imai Y, Persico AM, Ozenberger BA, Eppler CM, et al. (1994). cDNA cloning of an orphan opiate receptor gene family member and its splice variant. FEBS Lett 348, 75-9.

Wang JJ, Dutia MB (1995). Effects of histamine and betahistine on rat medial vestibular nucleus neurones: possible mechanism of action of anti-histaminergic drugs in vertigo and motion sickness. Exp Brain Res 105, 18-24.

Watson SJ, Khachaturian H, Akil H, Coy DH, Goldstein A (1982a). Comparison of the distribution of dynorphin systems and enkephalin systems in brain. Science 218, 1134-6.

Watson SJ, Khachaturian H, Coy D, Taylor L, Akil H (1982b). Dynorphin is located throughout the CNS and is often co-localized with alpha-neo-endorphin. Life Sci 31, 1773-6.

Watson SJ, Khachaturian H, Taylor L, Fischli W, Goldstein A, Akil H (1983). Pro-dynorphin peptides are found in the same neurons throughout rat brain: immunocytochemical study. Proc Natl Acad Sci U S A 80, 891-4.

Weber E, Evans CJ, Barchas JD (1983). Multiple endogenous ligands for opioid receptors. Trends Neurosci. 12, 333-337.

Wick MJ, Minnerath SR, Lin X, Elde R, Law PY, Loh HH (1994). Isolation of a novel cDNA encoding a putative membrane receptor with high homology to the cloned mu, delta, and kappa opioid receptors. Brain Res Mol Brain Res 27, 37-44.

Williams JT, Egan TM, North RA (1982). Enkephalin opens potassium channels on mammalian central neurones. Nature 299, 74-7.

Williams JT, North RA (1984). Opiate-receptor interactions on single locus coeruleus neurones. Mol Pharmacol 26, 489-97.

Wilson VJ, Wylie RM, Marco LA (1967). Projection to the spinal cord from the medial and descending vestibular nuclei of the cat. Nature 215, 429-30.

Wilson, V.J. and Melvill Jones, G. (1979). Mammalian Vestibular Physiology New York: Plenum Press.

Wilson VJ, Boyle R, Fukushima K, Rose PK, Shinoda Y, Sugiuchi Y, et al. (1995). The vestibulocollic reflex. J Vestib Res 5, 147-70.

Wimpey TL, Chavkin C (1991). Opioids activate both an inward rectifier and a novel voltage-gated potassium conductance in the hippocampal formation. Neuron 6, 281-9.

Wohltmann M, Roth BL, Coscia CJ (1982). Differential postnatal development of mu and delta opiate receptors. Brain Res 255, 679-84.

Wolfe GI, Taylor CL, Flamm ES, Gray LG, Raps EC, Galetta SL (1993). Ocular tilt reaction resulting from vestibuloacoustic nerve surgery. Neurosurgery 32, 417-20; discussion 420-1.

Wuster M, Rubini P, Schulz R (1981). The preference of putative pro-enkephalins for different types of opiate receptors. Life Sci 29, 1219-27.

Wuster M, Schulz R, Herz A (1979). Specificity of opioids towards the mu-, delta- and epsilon-opiate receptors. Neurosci Lett 15, 193-8.

X

Xerri C, Lacour M (1980). [Compensation deficits in posture and kinetics following unilateral vestibular neurectomy in cats. The role of sensorimotor activity]. Acta Otolaryngol (Stockh) 90, 414-24.

Y

Yamanaka T, Sasa M, Matsunaga T (1997). Glutamate as a primary afferent neurotransmitter in the medial vestibular nucleus as detected by in vivo microdialysis. Brain Res 762, 243-6.

Yasuda K, Raynor K, Kong H, Breder CD, Takeda J, Reisine T, et al. (1993). Cloning and functional comparison of kappa and delta opioid receptors from mouse brain. Proc Natl Acad Sci U S A 90, 6736-40.

Yoshikawa K, Williams C, Sabol SL (1984). Rat brain preproenkephalin mRNA. cDNA cloning, primary structure, and distribution in the central nervous system. J Biol Chem 259, 14301-8.

Yoshimura M, North RA (1983). Substantia gelatinosa neurones hyperpolarized in vitro by enkephalin. Nature 305, 529-30.

Z

Zagon IS, Gibo DM, McLaughlin PJ (1991). Zeta (zeta), a growth-related opioid receptor in developing rat cerebellum: identification and characterization. Brain Res 551, 28-35.

Zaki PA, Bilsky EJ, Vanderah TW, Lai J, Evans CJ, Porreca F (1996). Opioid receptor types and subtypes: the delta receptor as a model. Annu Rev Pharmacol Toxicol 36, 379-401.

Zanni M, Giardino L, Toschi L, Galetti G, Calza L (1995). Distribution of neurotransmitters, neuropeptides, and receptors in the vestibular nuclei complex of the rat: an immunocytochemical, in situ hybridization and quantitative receptor autoradiographic study. Brain Res Bull 36, 443-52.

Zhang S, Yu L (1995). Identification of dynorphins as endogenous ligands for an opioid receptor-like orphan receptor. J Biol Chem 270, 22772-6.